# Gene Expression Profiling of CD23$^{+}$ t(14;18)-Negative Follicular Lymphoma Demonstrates Activation of the IL4/JAK/STAT6 Pathway and a Role in Its Pathogenesis

**Dissertation**

der Mathematisch-Naturwissenschaftlichen Fakultät

der Eberhard Karls Universität Tübingen

zur Erlangung des Grades eines

Doktors der Naturwissenschaften

(Dr. rer. nat.)

vorgelegt von

Tim-Colin Schade

aus Ulm

Tübingen

2025

Gedruckt mit Genehmigung der Mathematisch-Naturwissenschaftlichen Fakultät der
Eberhard Karls Universität Tübingen.

| | |
|---|---|
| Tag der mündlichen Qualifikation: | 08.04.2026 |
| Dekan: | Prof. Dr. Thilo Stehle |
| 1. Berichterstatter/-in | Prof. Dr. Leticia Quintanilla-Martinez de Fend |
| 2. Berichterstatter/-in | Prof. Dr. Alexander Weber |

Erklärung:

Hiermit erkläre ich,

- dass ich diese Arbeit selbst verfasst habe.

- dass ich keine anderen als die angegebenen Quellen benutzt und dass ich alle wörtlich oder sinngemäß aus anderen Werken übernommenen Aussagen als solche gekennzeichnet habe.

- dass die eingereichte Arbeit weder vollständig noch in wesentlichen Teilen Gegenstand eines anderen Prüfungsverfahrens gewesen ist.

Tübingen, den 19.12.2025

# Acknowledgements

I would like to take this opportunity to thank the following people, without whose support the work would not have been possible:

Prof. Dr. Leticia Quintanilla-Martinez de Fend, who made this work possible.

Prof. Dr. Alexander Weber, who supported me during the decisive phases of my thesis.

Prof. Dr. Klaus Harter, without whose support this thesis could not have been completed in this way.

Dr. Irina Bonzheim for scientific support.

Dr. Aylin Schneider, Lejla Mahmutovic, Franziska Otto, Dr. Sinja Kieninger, Vanessa Borgmann and Achim Rau for their support in mutation analysis.

Dr. Dominik Nann, Dr. Sven Mattern, Dr. Antonio Vogelsberg, Dr. Leonie Frauenfeld, Dr. Ivonne Aidee Montes Mojarro and Dr. Massimo Granai for their support in (hemato)pathology.

Franziska Mihalik, Rebecca Braun, Esther Kohler, Barbara Mankel, Seba Colak and Ria Knittel for lab support.

Dr. Hannah Gierer, Hannes Armbruster and Anna-Lisa Wilhelmi for making my workdays even more enjoyable and for our funny conversations.

Christiane Stoffregen and IHC team for their great support in IHC.

Vanessa, ma bae.

Mark, Dr. Alex, Dr. Ulrich (Ulle), Franzi, Ivan, Aykon, Schayan and Nicolas for their unconditional support.

Lukas, who sadly cannot witness this historical moment but will forever remain in my heart.

And my family, for their unwavering love and support.

# Acronyms

| Acronym | Description |
|---|---|
| **AB** | Antibody |
| **ABC** | Activated B-cell-like |
| **ADCC** | Antibody-dependent Cellular Cytotoxicity |
| **AID** | Activation-induced Cytidine Deaminase |
| **AP-1** | Activator Protein 1 |
| **APC** | Antigen-presenting Cell |
| **ASC** | Antibody-secreting Cells |
| **Asn** | Asparagine |
| ***BCL2*** | B-cell Lymphoma 2 |
| ***BCL6*** | B-cell Lymphoma 6 |
| **BCR** | B-cell Receptor |
| **BM** | Bone Marrow |
| ***BTLA*** | B- and T-Lymphocyte Attenuator |
| ***CCL17*** | C-C Motif Chemokine Ligand 17 |
| ***CCL22*** | C-C Motif Chemokine Ligand 22 |
| **CD** | Cluster of Differentiation |
| **cDNA** | Complementary DNA |
| **CHIP** | Clonal Hematopoiesis of Indeterminate Potential |
| **COO** | Cell of Origin |
| **COSMIC** | Catalogue of Somatic Mutations in Cancer |
| ***CREBBP*** | cAMP Response Element-Binding Protein Binding Protein |
| **CSR** | Class-Switch Recombination |
| **CTL** | Cytotoxic T Lymphocyte |
| **DAMP** | Damage-associated Molecular Pattern |
| **dbSNP** | Database of Single Nucleotide Polymorphisms |
| **DC-SIGN** | Dendritic Cell-Specific Intercellular Adhesion Molecule-3-grabbing non-integrin |
| **DFL** | Duodenal-Type Follicular Lymphoma |
| **DLBCL** | Diffuse Large B-cell Lymphoma |
| **DNA** | Deoxyribonucleic Acid |

| | |
|---|---|
| **DZ** | Dark Zone |
| ***E2A*** | E Protein 2A (TCF3) |
| ***EP300*** | Enhancer of Zeste Homologue 2 |
| ***EZH2*** | E1A Binding Protein p300 |
| **FC** | Fold Change |
| ***FCER2*** | Fc Epsilon Receptor II (CD23) |
| **FDC** | Follicular Dendritic Cell |
| **FDR** | False Discovery Rate |
| **FFPE** | Formalin-fixed paraffin-embedded |
| **FL** | Follicular Lymphoma |
| **FLneg** | t(14;18)-negative Follicular Lymphoma |
| **FLneg$^{m}$** | FLneg *STAT6/SOCS1* mutated |
| **FLneg$^{wt}$** | FLneg *STAT6/SOCS1* wild-type |
| **FLpos** | Follicular Lymphoma t(14;18)-positive |
| **FRC** | Fibroblastic Reticular Cell |
| **GC** | Germinal Center |
| **GCB** | Germinal Center B cell |
| **GEP** | Gene Expression Profiling |
| **GRCh37/hg19** | Genome Reference Consortium Human Build 37 |
| **GSEA** | Gene Set Enrichment Analysis |
| **H&E** | Hematoxylin and Eosin |
| **H3K27m3** | Trimethylation of Lysine 27 on histone H3 |
| **H3K4** | Histone H3 Lysine 4 |
| ***HIST1H1*** | Histone H1 |
| **HLA** | Human Leukocyte Antigen |
| **HPF** | High Power Field |
| **HSC** | Hematopoietic Stem Cell |
| **ICC** | International Consensus Classification |
| **Ig** | Immunoglobulin |
| **IgH** | Immunoglobulin Heavy Chain |
| **IGV** | Integrated Genomics Viewer |
| **IHC** | Immunohistochemistry |
| **IL** | Interleukin |
| ***IL4R*** | Interleukin 4 Receptor |

| | |
|---|---|
| **IRF** | Interferon Regulatory Factor |
| **ISFN** | *In situ* Follicular Neoplasia |
| **JAK** | Janus Kinase |
| ***KMT2D*** | Lysine Methyltransferase 2D |
| **LN** | Lymph Node |
| **LZ** | Light Zone |
| **MAMP** | Microbe-associated Molecular Pattern |
| ***MAP2K1*** | Mitogen-activated Protein Kinase Kinase 1 |
| ***MEF2B*** | Myocyte Enhancer Factor 2B |
| **MHC** | Main Histocompatibility Complex |
| **MIB1** | Mindbomb E3 Ubiquitin Protein Ligase 1 |
| **MSC** | Mesenchymal Stromal Cells |
| ***MYC*** | MYC Proto-Oncogene |
| **NCCT** | NGS Competence Center Tübingen |
| **NET** | Neutrophil Extracellular Trap |
| **NFκB** | Nuclear Factor Kappa-Light-Chain Enhancer of Activated B cells |
| **NGS** | Next-Generation Sequencing |
| **NHL** | Non-Hodgkin Lymphoma |
| **NK cell** | Natural Killer Cell |
| **NLR** | NOD-like Receptor |
| **P53** | Tumor Protein P53 |
| **PAMP** | Pathogen-associated Molecular Pattern |
| ***PAX5*** | Paired Box 5 |
| **PCA** | Principle Component Analysis |
| **PCFCL** | Primary Cutaneous Follicle Center Lymphoma |
| **PCR** | Polymerase Chain Reaction |
| **PIAS** | Protein Inhibitor of activated STAT |
| **PID** | Pathway Interaction Database |
| **PMBCL** | Primary Mediastinal Large B-cell Lymphoma |
| **PRC2** | Polycomb Repressive Complex 2 |
| **PRR** | Pattern Recognition Receptor |
| **PTFL** | Pediatric-Type Follicular Lymphoma |
| **PTP** | Protein Tyrosine Phosphatase |
| **RAG** | Recombination-activated Genes |

| | |
|---|---|
| **REAL** | Revised European American Lymphoma |
| **RLF** | Reporter Library File |
| **RLR** | RIG-I-like Receptor |
| **RNA** | Ribonucleic Acid |
| **ROS** | Reactive Oxygen Species |
| **SHM** | Somatic Hypermutation |
| ***SOCS1*** | Suppressor of Cytokine Signaling 1 |
| ***STAT6*** | Signal Transducer and Activator of Transcription 6 |
| **TAM** | Tumor-associated Macrophages |
| **$T_{FH}$** | T Follicular Helper Cells |
| **tFL** | Transformed Follicular lymphoma |
| **$T_{FR}$** | T Follicular Regulatory Cells |
| **TLR** | Toll-like Receptor |
| **TMAP** | Torrent Mapping Alignment Program |
| **$T_{Reg}$** | T Regulatory Cells |
| ***TYK2*** | Tyrosine Kinase 2 |
| **WHO** | World Health Organization |

# Table of Contents

# Abstract

Follicular Lymphoma (FL) is a genetically and transcriptionally heterogeneous disease. Classic FL is characterized by t(14;18) (FLpos), while the pathogenesis of t(14;18)-negative FL (FLneg) remains less defined. Recent studies have shown that FLneg could be divided in those with *STAT6/SOCS1* mutations and a group of FLneg without recurrent mutations. While these genetic differences are well described, their functional and transcriptional consequences in FLneg remain poorly understood. Therefore, we performed comprehensive gene expression profiling (GEP) using HTG and NanoString platforms to investigate the impact of *STAT6/SOCS1* mutations on the transcriptional profile of FLneg. Our cohort represents the largest to date for FLneg GEP and was divided into 37 FLneg$^{m}$ (*STAT6/SOCS1* mutated), 14 FLneg$^{wt}$ (wild-type) and 8 FLpos$^{m}$ (*BCL2* rearranged and *STAT6/SOCS1* mutated). We confirmed the strong association between *STAT6/SOCS1* mutations and CD23 expression in FLneg, underlining IL4/JAK/STAT6 pathway activation as key driver of CD23 upregulation. Here, FLpos showed a difference and appeared to be driven primarily by paracrine IL4 signaling from the tumor microenvironment. Using differential gene expression analyses, we found a distinct transcriptional program in FLneg$^{m}$, characterized by persistent germinal center markers, *STAT6* target genes, and immune modulation signatures, which suggest a post-activated germinal center phenotype. On the other hand, signatures of terminal B-cell differentiation and an immunologically active microenvironment in FLneg$^{wt}$ were identified, which included upregulation of *IRF4* and *SLAMF7*. Unsupervised clustering revealed transcriptional subgroups within FLneg$^{m}$, suggesting heterogeneity in STAT6 pathway activation. Different pathway activation is likely caused by mutational burden and co-mutations. Also, FLneg$^{wt}$ showed heterogeneous expression profiles, including cases with high *SLAMF7* and *FCRLA* expression. These cases are probably linked to a more differentiated B-cell state. Finally, our findings support a model in which constitutive *STAT6* pathway activation in FLneg$^{m}$ impairs terminal differentiation and sustains a GC-like phenotype, whereas FLneg$^{wt}$ retains the ability to differentiate. Our findings refine the current understanding of FLneg molecular stratification and propose a differentiation-based model of pathogenesis driven by IL4/JAK/STAT6 signaling. Extended subtype groups and functional validation are needed for further investigation.

# Zusammenfassung

Das follikuläre Lymphom (FL) ist eine genetisch und transkriptionell heterogene Erkrankung. Während das klassische FL mit einer t(14;18) Translokation (FLpos) assoziiert ist, bleibt die Pathogenese des t(14;18)-negativen FL (FLneg) bislang weniger verstanden. Aktuelle Studien zeigten, dass FLneg in eine Gruppe mit *STAT6/SOCS1*-Mutationen sowie eine Wildtyp-Gruppe aufgeteilt werden kann. Auch wenn diese genetischen Unterschiede bereits beschrieben wurden, blieben die funktionellen und transkriptionellen Auswirkungen dieser Mutationen bei FLneg unklar. In dieser Studie wurde daher eine umfassende Genexpressionsanalyse mit HTG EdgeSeq und NanoString durchgeführt. Dabei sollte die Auswirkung von *STAT6/SOCS1*-Mutationen auf das Transkriptom von FLneg untersucht werden. Die untersuchte FLneg Kohorte stellt die Größte dar, bei welcher eine Genexpressionsanalyse durchgeführt wurde. Sie wurde in 37 FLneg$^{m}$ (mit *STAT6/SOCS1*-Mutationen), 14 FLneg$^{wt}$ (Wildtyp) und 8 FLpos$^{m}$ (*BCL2*-transloziert und *STAT6/SOCS1*-mutiert) unterteilt. Wir konnten einen Zusammenhang zwischen *STAT6/SOCS1*-Mutationen und CD23-Expression in FLneg bestätigen. Dies weist auf eine konstitutive Aktivierung des IL4/JAK/STAT6-Signalwegs als zentralen Treiber der CD23-Expression hin. Im Gegensatz dazu scheint die CD23-Expression in FLpos primär durch parakrine IL4-Signale aus dem Tumormikromilieu induziert zu werden. Die Genexpressionsanalysen zeigten ein spezifisches Transkriptionsmuster in FLneg$^{m}$, welches durch persistente Keimzentrumsmarker, STAT6-Zielgene und immunmodulatorische Signaturen gekennzeichnet ist. Dies weist auf einen aktivierten Keimzentrumstyp der FLneg$^{m}$ B-Zellen hin. Im Gegensatz dazu zeigte FLneg$^{wt}$ Signaturen von B-Zell-Differenzierung und einem immunologisch aktiven Tumormikromilieu, passend zur Hochregulierung von *IRF4* und *SLAMF7*. Das Unsupervised Clustering zeigte transkriptionelle Untergruppen innerhalb von FLneg$^{m}$, was auf eine Heterogenität der STAT6-Pathway-Aktivierung hindeutete, vermutlich beeinflusst durch Mutationslast und Co-Mutationen. FLneg$^{wt}$ zeigte ebenfalls heterogene Expressionsprofile, mit Fällen, welche durch hohe *SLAMF7* und *FCRLA* Expression auffielen und damit mit einem eher differenzierten B-Zell-Status assoziiert waren. Letztlich stützen unsere Erkenntnisse das Modell, bei welcher ein konstitutiv aktivierter STAT6-Pathway in FLneg$^{m}$ die terminale Differenzierung von B-Zellen stört und einen Keimzentrumsähnlichen Phänotyp erhalten, während FLneg$^{wt}$ weiter differenzieren kann. Die Studie bietet Einblicke in die molekulare Unterteilung von FLneg and schlägt ein Differenzierungs-basiertes Modell der Pathogenese, verursacht durch den IL4/JAK/STAT6 Signalweg, vor. Eine Erweiterung der Kollektive um weitere FL Fälle sowie die funktionelle Testung der Ergebnisse werden benötigt, um das Modell zu validieren.

# List of Figures

# List of Tables

# 1. Introduction

## 1.1 The Human Immune System

The human immune system is essential for the prevention of infections, the recognition and elimination of extrinsic and intrinsic factors, and ultimately the formation of immunological memory to enable a rapid response in case of re-exposure. Extrinsic factors are bacteria, parasites, and viruses, intrinsic factors are associated to altered and cancer cells. It is composed of three lines of defense: barriers, the innate immune system and the adaptive immune system [1].

### 1.1.1 Barriers

The barriers of the immune system consist of physical (skin, mucosa, tight junctions, saliva, urine), chemical (pH, enzymes, antimicrobial peptides, gastric acid), and microbial barriers (commensal microorganisms). Together, these mechanisms reduce pathogen entry, promote pathogen control and maintain tissue homeostasis [2-4].

### 1.1.2 The Innate Immune System

The central function of the innate immune system is the early detection and elimination of pathogens, as well as the activation of adaptive immunity. It is characterized by a very rapid response and reacts within minutes to hours. Furthermore, unlike the adaptive immune system, which will be discussed in a later chapter, it does not exhibit immunological memory toward specific epitopes. Nevertheless, through "trained immunity", it can enhance the speed and magnitude of the immune response upon re-exposure. The recognition of pathogens occurs through specific structures known as pattern recognition receptors (PRRs). In addition to PRRs, the innate immune system includes the complement system, phagocytes (macrophages, neutrophils), natural killer (NK) cells, and soluble mediators (cytokines, chemokines, interferons). Finally, the innate immune system determines the activation of the adaptive immune response [5-7].

### 1.1.3 The Adaptive Immune System

The adaptive immune system exhibits high specificity and enables the formation of long-lasting immunological memory. However, the activation of this system requires antigen presentation as well as co-stimulatory signals from antigen-presenting cells (APCs). Activated naïve $CD4^+$ T cells differentiate into specialized subsets, whereas the cytokine milieu plays a crucial role. T follicular helper ($T_{FH}$) cells for example, are essential for B-cell activation. Within germinal centers, $T_{FH}$ cells support B cells through CD40L, IL-4, and IL-21. $CD8^+$ T cells, in turn, recognize antigens presented on MHC class I and exert cytotoxic effects on infected or malignant cells. B cells, another key cell type of the adaptive immune response, can recognize antigens through their B-cell receptor (BCR) but require T-cell signals for full activation. Here, the interaction of CD80/CD86 with CD28 on T cells takes place (**Figure 1**). Also, CD40-CD40L interaction is required for B-cell activation. The main function of B cells is the production of highly specific antibodies (immunoglobulins), which are produced after plasma cell differentiation. Antibodies have several functions, including direct neutralization of pathogens such as viruses, opsonization (facilitating pathogen recognition by phagocytes), complement activation, and antibody-dependent cellular cytotoxicity (ADCC), which involves apoptotic destruction of the target cells [8]. The development of B cells from early progenitor to differentiated plasma cells is discussed in the following chapter.

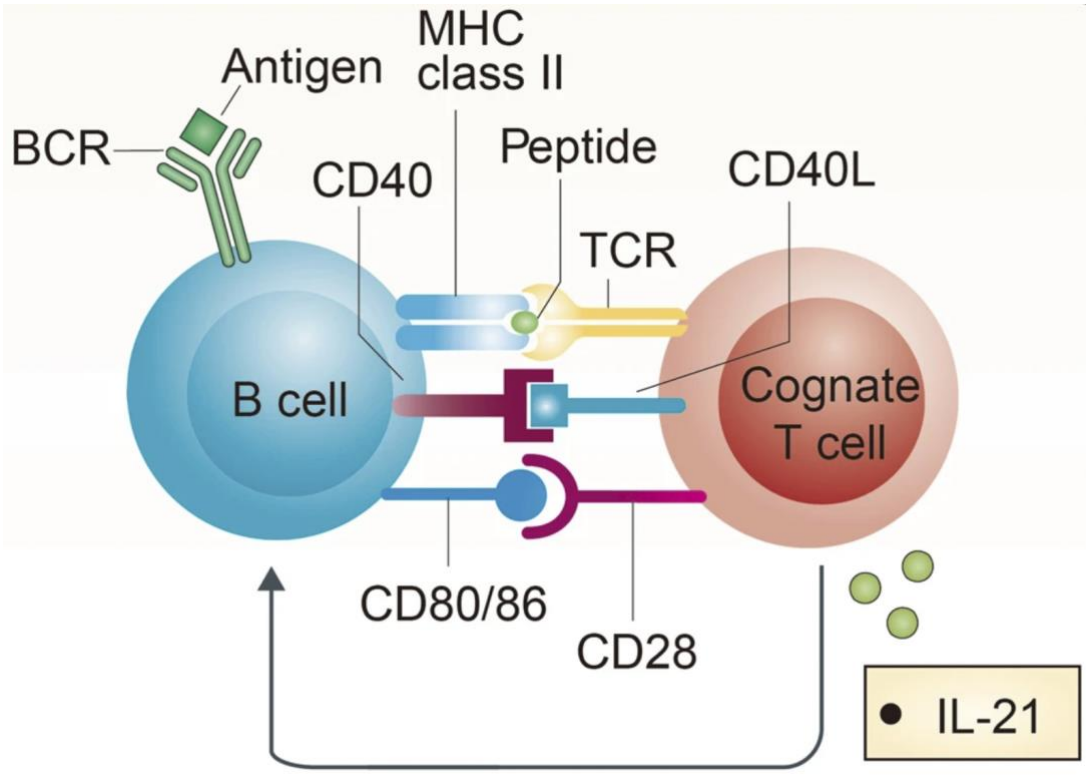


**Figure 1: Illustration of B- and T-cell interaction.**
B cells and T cells interact using different mechanisms, such as CD80/86 and CD28, CD40 and CD40L, and T-cell receptor (TCR) and peptide-loaded MHC II (modified from Peng *et al.* 2018 [9]).

## 1.2 B-Cell Development and Transcriptional Programs

B-cell maturation represents a complex interaction of cellular programs that allows B cells to develop from early progenitors to fully differentiated and specialized cells [10]. In the following subchapters an overview of the developmental stages and relevant markers is provided.

### 1.2.1 Overview of B-Cell Development

The development from hematopoietic stem cells (HSC) to fully differentiated plasma and memory cells occurs through tightly regulated mechanisms. Briefly, a multipotent hematopoietic stem cell in the bone marrow (BM) is the starting point for B-cell maturation. It differentiates into a pro-B cell. During this process, VDJ rearrangement occurs, which enables BCR diversity. Through successful rearrangement, the cell differentiates into a pre-B cell and forms the pre-BCR. After light chain gene rearrangement, the complete BCR, immunoglobulin M (IgM), is formed. To eliminate autoreactive cells, a negative selection process takes place. This stage is referred to as the immature B cell. Immature B cells leave the bone marrow and migrate to the spleen. There, the maturation is completed as they progress through T1 and T2 stages. Mature naïve B cells, which

express IgM and IgD BCRs, then circulate in the peripheral lymphoid organs. These cells are activated through antigen contact and T helper cells resulting in proliferation and differentiation. Activated B cells undergo somatic hypermutation and class-switch recombination in germinal centers and are called germinal center B cells (GCB). In the next step, they differentiate into a post-GCB, from which memory B cells and eventually plasma cells arise (**Figure 2**) [11].

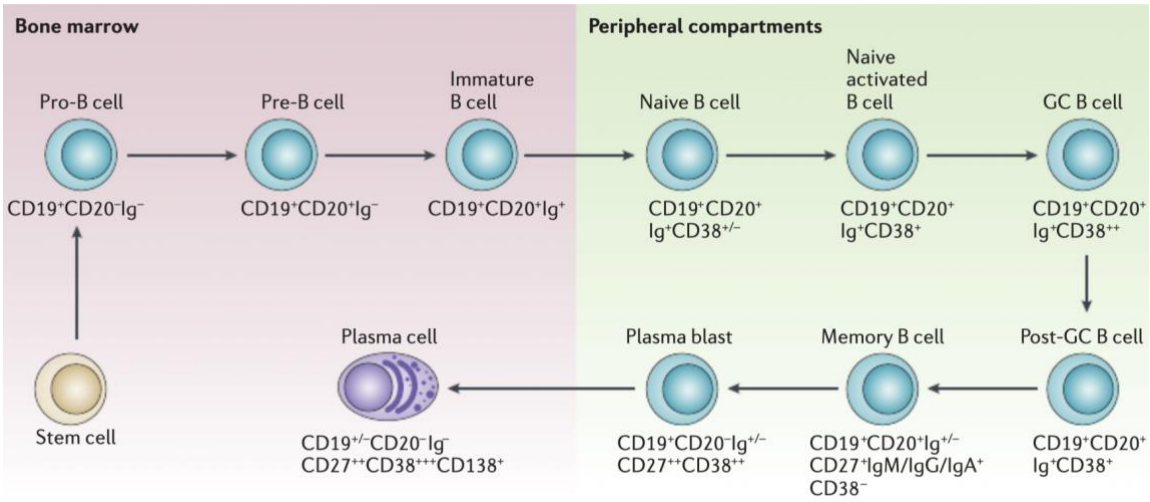


**Figure 2: Schematic representation of B-cell development.**
B-cell maturation starts in the BM and continues in the periphery from naïve B-cell stage on. During the maturation molecular changes lead to the expression of different cell surface markers which are distinct for the respective B-cell stage (reproduced from Edwards *et al.* 2006 [12].

### 1.2.2 Transcriptional Profiles

During B-cell maturation, distinct genetic programs are activated, resulting in the stage-specific expression of certain genes that play crucial roles at each step. Focusing on the germinal center reaction, the transcription factors *IRF4*, *IRF8*, and *MEF2B* play an important role in the early stages, as they induce *BCL6*. Furthermore, *BOB.1/OBF.1* is associated with the initiation of *BCL6* expression, and regulates *MEF2B*. *IRF4* in turn, appears to be involved in the regulation of *BOB.1/OBF.1*. Somatic hypermutation in the dark zone is induced by paired box 5 (*PAX5)*, E protein 2a (*E2A*), and *IRF8*, as they positively regulate activation-induced cytidine deaminase (*AID*). The expression of *IRF4* is initially suppressed to prevent premature plasma cell differentiation. In the light zone, the expression of *IRF4*, *PAX5*, and *E2A* promotes *AID* expression, leading to affinity maturation and class-switch recombination. *BCL6* is inhibited during this process. Subsequently, *IRF4* and *BOB.1/OBF.1* induce the expression of *BLIMP-1*, which inhibits e.g. *BCL6*, *AID*, *PAX5*, and MYC proto-oncogene (*MYC*) (**Figure 3**) [13].

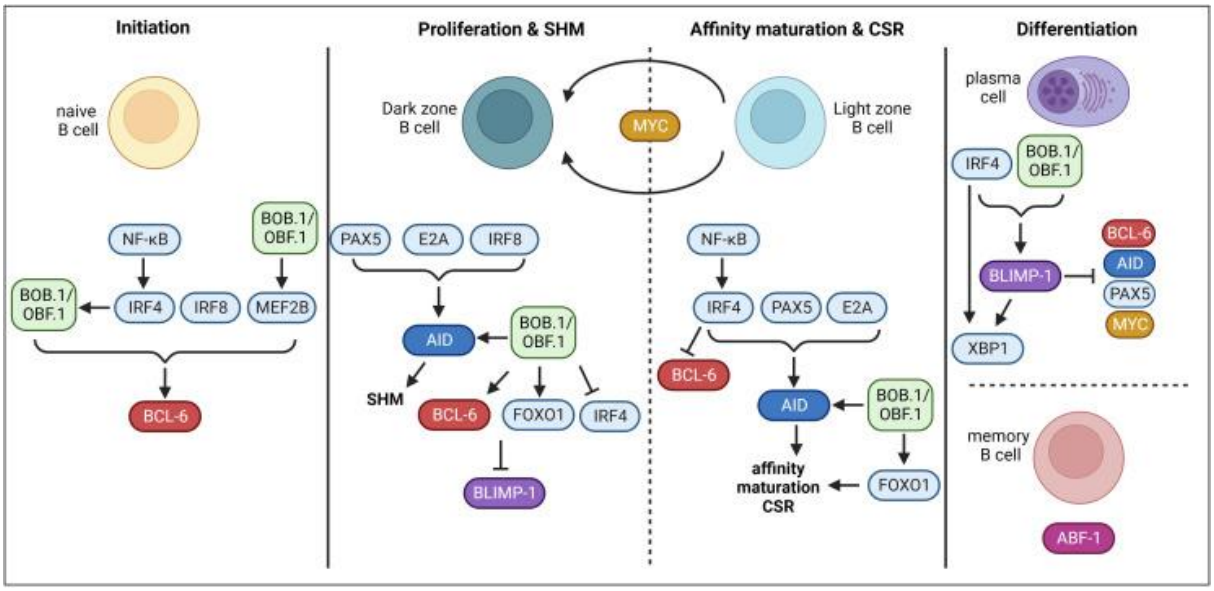


**Figure 3: Transcriptional program during germinal center reaction.**
Reproduced from Betzler *et al.* 2023 [13].

## 1.3 Classification of B-Cell Lymphomas

The malignant counterpart of functional B-cell development is called B-cell lymphoma, which represents a group of hematological malignancies originating from different stages of B-cell development and differentiation. Due to the various clinical presentations, molecular characteristics and treatment responses, classification systems are necessary for guidance of diagnosis, prognosis and treatment selection [14]. In 1966, Rappaport *et al.* introduced a lymphoma classification system that organized subtypes according to their morphological characteristics [15]. Later, newly created Kiel classification by Lennert *et al.* discussed the differential state of the cells [16] and was updated in 1988 [17]. Revised European American Lymphoma (REAL) classification suggested categorization of lymphoma considering morphologic, immunologic and genetics, which provided the fundament for World Health Organization (WHO) classification published in 2017 [14] and International Consensus Classification (ICC) introduced in 2022 [18]. Both classifications concentrate on immunophenotyping and molecular analysis. However, ICC integrates unique

molecular pattern even more compared to WHO. In general, B-cell lymphomas are classified by the differentiation state of the malignant B cell. Due to various molecular characteristics, further subtyping is necessary. By using continuously improved classifications, B-cell lymphoma diagnosis, treatment and prognosis will be improved. One B-cell lymphoma, which plays an important role in classification, is follicular lymphoma (FL).

## 1.4 Follicular Lymphoma

FL is an indolent B-cell lymphoma that was first described in 1925 as two patients presented with lymphadenopathy and splenomegaly [19]. It belongs to one of the most common subtypes of non-Hodgkin lymphoma (NHL) occurring in 20 – 30%. FL mostly affects people above 60y, typically shows an indolent clinical course and is known for a slow disease progression. However, histological transformation may lead to a more aggressive form with worse prognosis, called diffuse large B-cell lymphoma (DLBCL) [20].

The hallmark of FL, t(14;18)(q32;q21), is the result from aberrant recombination-activated genes (RAG)-mediated V(D)J rearrangement during pre-B cell stage in the BM [21]. It occurs in 85 – 90% of all FL cases (FLpos) [18]. The translocation leads to the constitutive expression of BCL2 preventing cells from apoptosis. A small subset of approx. 15% of FL cases lacks this translocation (FLneg) [22]. Apart from the translocation, epigenetic molecular alterations are present. FL represents a heterogeneous entity and can be further subtyped. FLpos includes early lesions such as FL-like cells located in the peripheral blood, in situ follicular neoplasia and duodenal-type follicular lymphoma. Additional subtypes are follicular lymphoma grade 1-3A and transformed follicular lymphoma.

FLneg, in turn, is subdivided into nodal FLneg, which can be further classified into subgroups characterized by C23 positivity, BCL6 rearrangements and an "others" group. Also, extranodal and pediatric type FL represent FLneg subgroups.

### 1.4.1 Histopathology

Healthy lymph nodes (LN) typically show an organized structure containing cortex, paracortex and medulla [23]. The cortex contains follicles, where germinal centers (GC) are located (**Figure 4**) [24]. In the GC, B-cell proliferation, selection and maturation take place. GCs are divided into two zones: dark zone (DZ) and light zone (LZ). The DZ contains centroblasts, which are large

proliferating B cells and associated to somatic hypermutation. Here, AID randomly mutates the variable region of the antibody (AB) leading to an altered affinity of the AB to its antigen. Depending on the affinity from antibody to antigen, B-cells either go through apoptosis (low affinity) or proceed to the LZ (high affinity) [24].

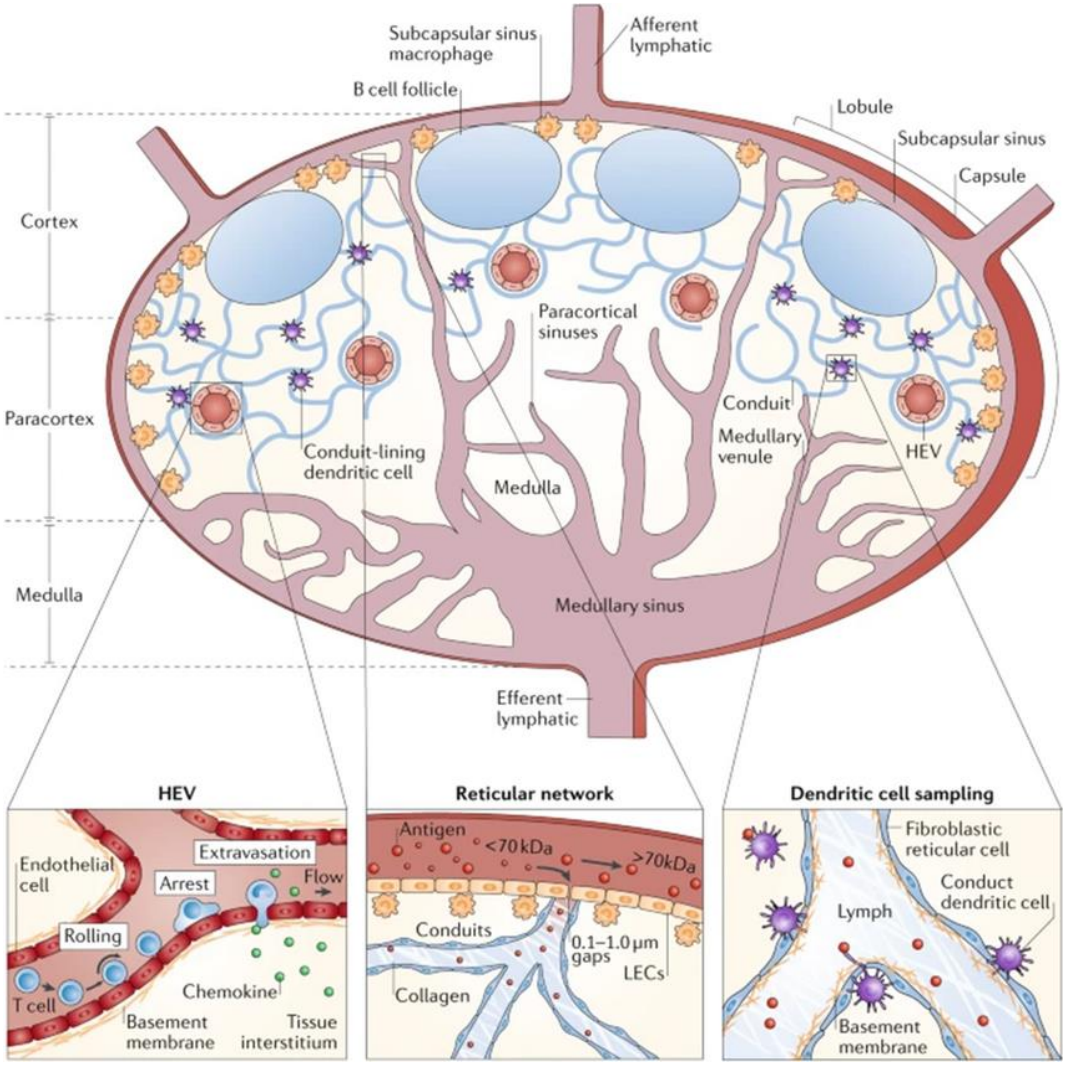


**Figure 4: Schematic representation of a human LN.**
Within the cortex, GCs located in follicles are responsible for maturation and proliferation of B cells (reproduced from He *et al.* 2023 [24]).

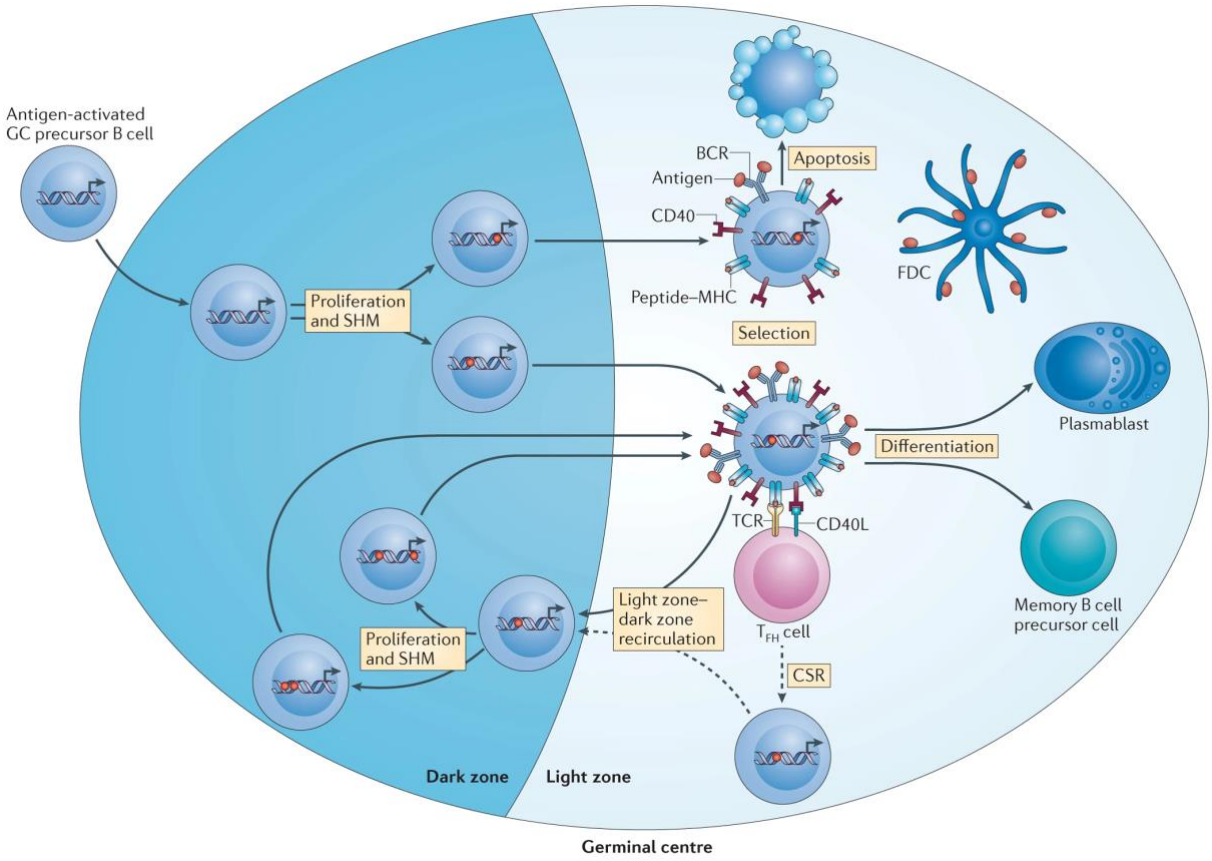


**Figure 5: Processes occurring within the germinal center of a LN.**
In DZ, B cells undergo proliferation and somatic hypermutation followed by selection and class-switch recombination (CSR) in the LZ (reproduced from De Silva *et al.* 2015 [25]).

In the LZ B cells are called centrocytes. Centrocytes are smaller, non-proliferating B cells that undergo affinity maturation. During this process they interact with $T_{FH}$ and follicular dendritic cells (FDC) to undergo positive selection based on antigen affinity. After positive selection of a GCB three cell fates are possible. GCBs can either differentiate into plasma cells for antibody production, develop into memory B cells for long-term immunity or return to the DZ for further proliferation and mutation, depending on molecular signals during the process (**Figure 5**) [25].

Taken together, LNs are physiologically highly regulated and organized structures. In contrast, FL presents significant histopathological changes (**Figure 6**) [26]:

a) The zonal architecture described above is lost leading to closely packed follicles without clear zonal polarization. Due to the disruption of interactions between neoplastic B cells and stromal elements, DZ/LZ disappeared [26].
b) Cell composition changes. FL follicles consist of centrocytes and centroblasts. The grading of FL is dependent on the ratio of both: Grade 1 contains < 5 centroblasts per high power field (HPF, the field of view of the pathologist using 400x magnification), Grade 2 shows

6 – 15 centroblasts/HPF and Grade 3 with > 15 centroblasts/HPF. Grade 3A still shows centrocytes while Grade 3B lacks centrocytes [26]

c) In advanced stages, nodular pattern of FL can evolve to diffuse pattern, where progression or transformation of neoplastic cells leads to infiltration of surrounding tissues resulting in a more aggressive disease course. Therefore, grading is crucial in FL diagnosis [26].

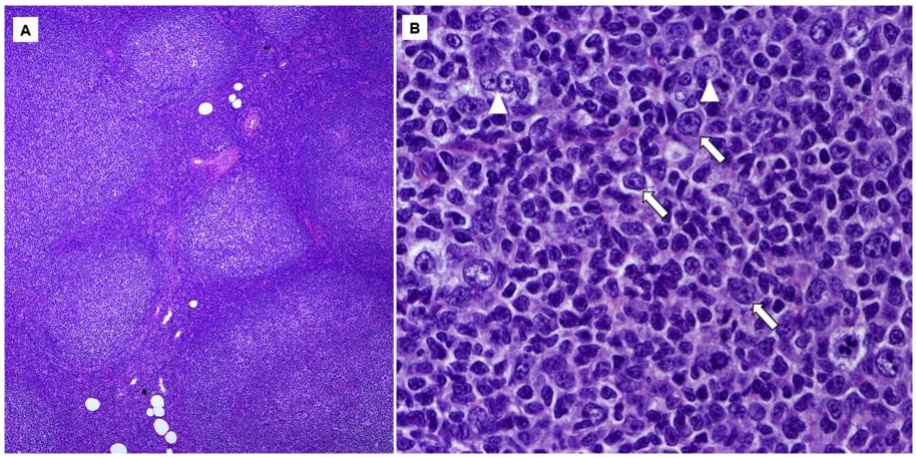


**Figure 6: H&E staining showing histopathological changes in FL.**
A: Irregular follicles, B: Irregular shaped centrocytes, centroblasts (arrows) and follicular dendritic cells (FDC, arrowheads). Magnification na, (reproduced from Randall *et al.* 2020 [26]).

Apart from histopathological features, FL is characterized by specific expression of proteins associated with cell type lineage, cell of origin and neoplastic cells, which can be detected via immunohistochemical staining.

### 1.4.2 Immunohistochemistry Phenotype

Immunohistochemistry is a useful tool for FL diagnosis (**Figure 7**). For B-cell lineage confirmation, cluster of differentiation (CD) 20 and CD79a are stained. Both markers are typically expressed on B-cells. To confirm GCB origin, CD10 and B-cell Lymphoma 6 (BCL6) staining are used. The FDC network, which can be disrupted in FL, is then detected using CD21 or CD23. This staining also helps differentiating to lymphoma such as DLBCL. Ki-67 is used to assess proliferation, where low grade FL shows lower Ki-67 index and high-grade FL shows higher proliferation index [27]. In healthy/reactive GCs BCL2 is not expressed. Therefore, BCL2 staining supports to differentiate FL cells from reactive LN cells. Immunohistochemical analysis helps to provide insights into the phenotype and cellular origin of FL as well as differentiation to other hematological entities. The impact of molecular alterations on FL will be presented in the next chapter.

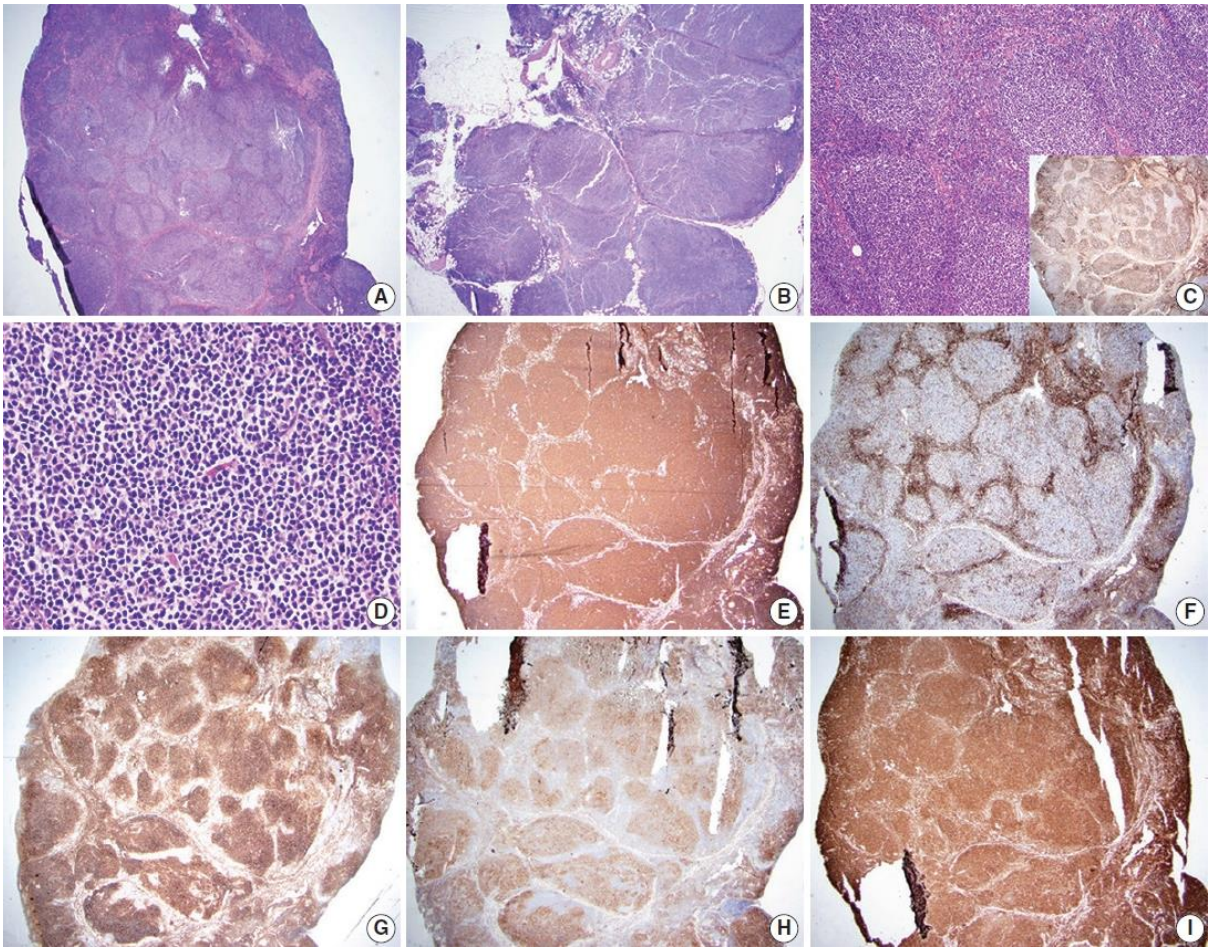


**Figure 7: Exemplary representation of a low-grade FL case with different immunohistochemical (IHC) staining.**
A – D: Hematoxylin & eosin (H&E) staining, C = CD21 immunostaining for follicular dendritic cell meshwork to identify follicles, E = CD20 immunostaining for highlighting B cells, F = CD3 immunostaining for reactive T cells, G = CD10 immunostaining to prove GCB origin of neoplastic B cells, H = BCL6 immunostaining to prove GCB origin of neoplastic B cells, I = Immunostaining for BCL2 to differentiate reactive from neoplastic B cells (reproduced from Khanlari *et al.* 2022 [27]). Magnification na.

### 1.4.3 Pathogenesis

The pathogenesis of FL appears as a complex interplay of various molecular mechanisms and alterations:

**Epigenetic regulators**

FL often harbors mutations in epigenetic regulators involved in posttranslational modification, including N-methyltransferase 2D (*KMT2D*), cAMP response element-binding protein binding protein (*CREBBP*), enhancer of zeste homologue 2 (*EZH2*), and E1A binding protein P300 (*EP300*) [28, 29]. Most of these mutations reduce transcriptional activity, with *EZH2* being a notable exception [30]. Mutations in *KMT2D* disrupt H3K4 methylation. The disruption results in dysfunctional enhancers, which in turn decreases gene expression of genes associated to cell differentiation and development [31]. Histone acetyltransferases *CREBBP* and *EP300* normally allow histone acetylation leading to better accessibility for transcription. Up on mutational events,

loss of function occurs followed by chromatin condensation and transcriptional repression of e.g. tumor protein p53 (*p53*), *BCL6*, *CDKN1A* and *IRF4*. Suppression of these genes promotes cell survival, proliferation and immune escape mechanisms [32, 33]. Gain of function of *EZH2*, which encodes for catalytic component of polycomb repressive complex 2 (PRC2), results in aberrant histone H3 lysine 27 trimethylation (H3K27m3), which is associated with terminal differentiation block and MHC downregulation [33-35] (**Figure 8**).

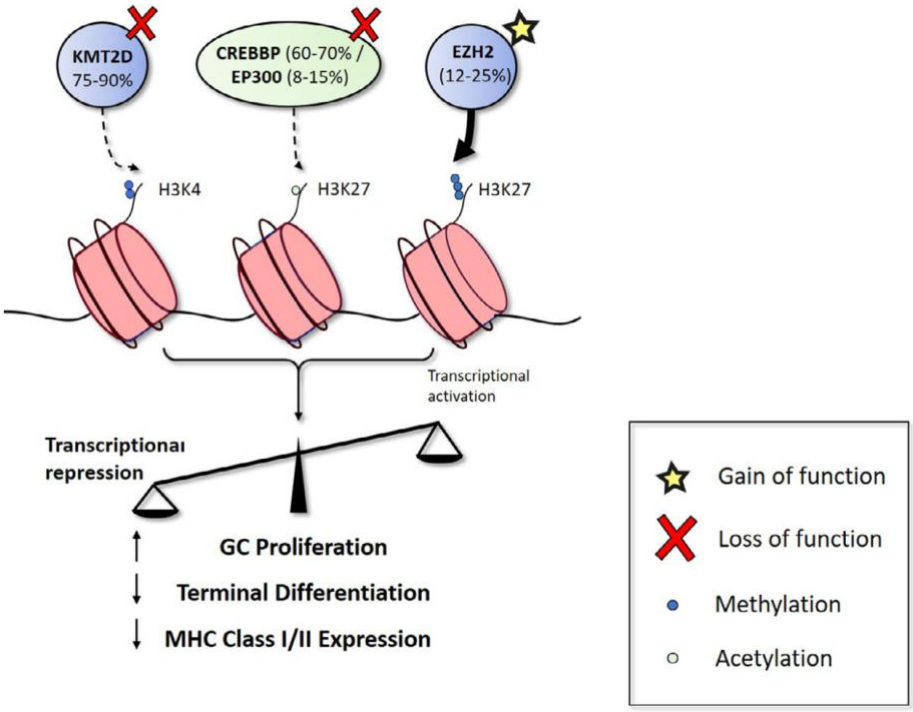


**Figure 8: Epigenetic modulators altered in FL.**
Loss of function mutations in *KMT2D*, *CREBBP* and *EP300* cause transcriptional repression. Gain of function of *EZH2* increases repressive methylation (reproduced from Kumar *et al.* 2021 [36]).

Furthermore, histone H1 (*HIST1H1*) mutations play a role in the pathogenesis of follicular lymphoma [37]. *HIST1H1* is generally involved in the stabilization of desoxyribonucleic acid (DNA) [38]. Mutations in *HIST1H1* disrupt chromatin organization and alter epigenetic mechanisms [39].

### Tumor microenvironment

It is already known that FL is highly dependent on the tumor microenvironment. By influencing tumor-associated macrophages (TAMs), FDCs, mesenchymal stromal cells (MSCs), fibroblastic reticular cells (FRCs), as well as T follicular regulatory ($T_{FR}$) cells, $T_{FH}$ cells, $CD4^+$ T regulatory ($T_{REG}$) cells, and $CD8^+$ cytotoxic T cells (CTLs), immune evasion and tumor survival is facilitated [40].

**N-Glycosylation**

N-glycosylation can occur during somatic hypermutation (SHM) of FL cells. 79% of FL cases were found to harbor N-glycosylation motifs, whereas only 9% of healthy B cells were affected [41]. In this process, additional N-glycosylation motifs are added to the immunoglobulin variable (IgV) regions of the BCR. The N-glycosylation motif consists of the following amino acids: Asparagine (Asn), any amino acid (X, except proline) and Serine (Ser) or Threonine (Thr). FL cells with N-glycosylation motifs often carry high-mannose glycans. It has already been observed that these glycans can interact with mannose-binding lectins. One study showed that the glycans interacted with dendritic cell-specific intercellular adhesion molecule-3-grabbing non-integrin (DC-SIGN), which is expressed by macrophages and dendritic cells in the tumor microenvironment [42]. The addition of N-glycosylation motifs contributes to antigen-independent survival and proliferation signals, as neighboring BCRs can interact with each other. This so-called "autonomous receptor clustering" contributes to survival of FL cells [43].

In summary, the pathogenesis of FL is the result of a complex interplay of mechanisms, including epigenetic regulation, alterations in signaling pathways, and interactions with its tumor microenvironment.

### 1.4.4 Precursor/early Lesion of FL

In 2002, Cong *et al.* first described the "in situ localization of follicular lymphoma" (ISFN). In this context, BCL2-positive B cells were found within the germinal center of a reactive (inconspicuous) lymph node, which was associated with early precursors of follicular lymphoma [44]. Years later, the prevalence of ISFN was investigated as part of a large-scale analysis. Of the 1,294 reactive lymph nodes examined, 22 lymph nodes (in 3 out of 132 patients) showed evidence of ISFN [45]. Schmidt *et al.*, in a comparison of unpaired and paired ISFN cases, found that additional genetic alterations occur between ISFN and manifested FL. While ISFN carried the t(14;18) translocation, it exhibited few other genetic changes [46]. The paired ISFN cases were used in a subsequent study for mutation analysis. It was demonstrated that the ISFN cases already harbored mutations in *CREBBP*, *EZH2*, Tumor Necrosis Factor Receptor Superfamily Member 14 (*TNFRSF14*), and *KMT2D* [47]. ISFN can also progress directly to DLBCL, even in the absence of FL [48]. Another subtype of t(14;18)-positive FL is duodenal-type FL (DFL). DFL shows an overlap with ISFN, as both do not form a tumor mass and exhibit a low risk of disease progression [14, 49-51]. One study was able to identify a clonal relationship between ISFN and DFL [52]. Another type of early lesion

are FL-like B cells, which circulate in the peripheral blood showing FL-typical genotypic and phenotypic features [53].

### 1.4.5 t(14;18)-negative FL

15% of FL cases lack t(14;18). In addition to cryptic/complex rearrangements and a variability in *BCL2* breakpoint sites, there are also true FLneg, which show distinct histological features [54-56] (**Figure 9**). Within the FLneg entity, additional important subtypes could be identified, such as nodal, extranodal and pediatric.

**Nodal FLneg**

The comparison of gene expression between nodal FLneg and FLpos cases revealed distinct profiles. While FLpos was associated with a B-cell germinal center profile, FLneg was linked to activated B-cell like characteristics, NFκB signaling, proliferation, and bystander cell signatures. Furthermore, copy number alterations were found [57]. A subsequent study identified a micro ribonucleic acid (RNA) profile in FLneg that was associated with proliferation and a late-germinal center B-cell phenotype [58]. Katzenberger *et al.* identified a specific subtype within FLneg, which was associated with a predominantly diffuse pattern, absence of t(14;18), deletion of 1p36, grade 1 and 2, frequent expression of CD23, and large localized inguinal tumors [59].

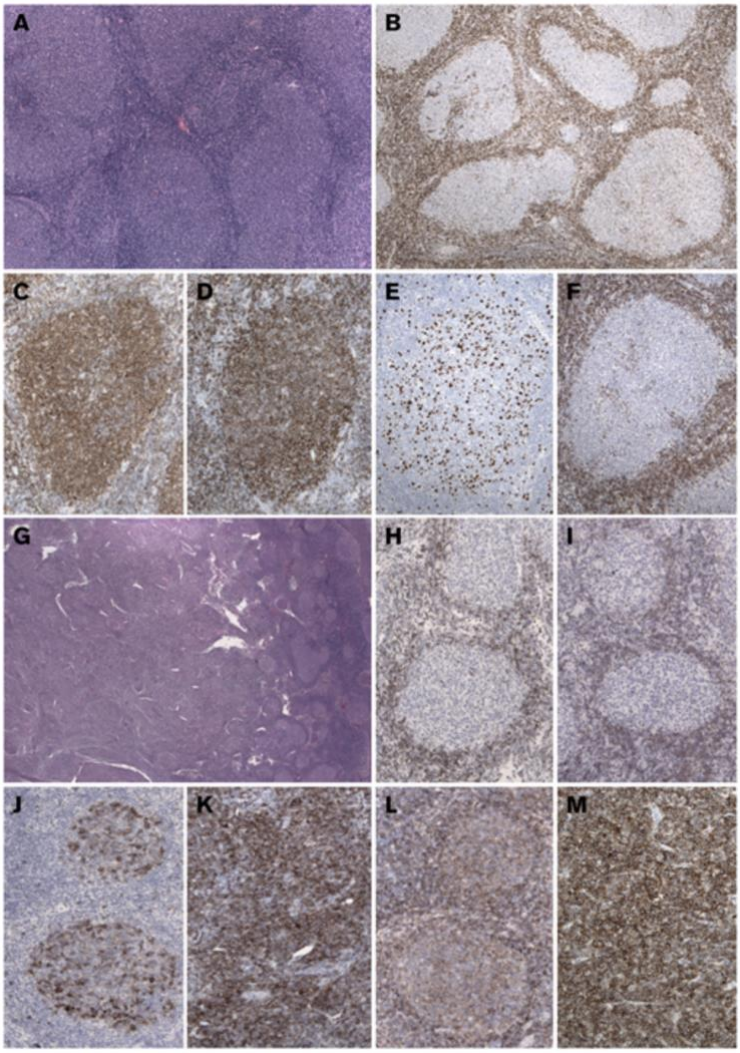


**Figure 9: Morphological characteristics of FLneg.**
A – F represent IHC staining from Case FL7 (group B2). A: H&E staining showing follicular growth pattern without clear mantle zones(50x). B: Follicles are BCL2-negative (100/D5 clone, 50x). C: CD20-positive staining (100x). D: CD23-positive staining (100x). E: MIB1 (mindbomb E3 ubiquitin protein ligase 1 (Ki-67)) depicting low proliferation (100x). F: BCL2-negative (E17, 100x). G – M: Case FL11 from group A1. G: H&E staining showing follicular and diffuse infiltration (25x). H: BCL2-negative (E17, 100x), I: BCL2-negative (100/D5 clone, 100x). J: CD10-positive in follicular area (100x). K: CD10-positive in diffuse area (100x). L: CD23-positive in follicular area (100x). M: CD23-positive in diffuse area (100x) (reproduced from Nann *et al.* 2020) [60].

Years later, molecular analyses were conducted on cases with similar features. Within this study, it was found that signal transducer and activator of transcription 6 (*STAT6*) mutations occur significantly more frequently in FLneg compared to FLpos. The authors hypothesized an involvement of the Interleukin (IL) 4/Janus kinase (JAK)/STAT6 pathway in this context, which further needs to be investigated [61]. Further studies have shown differences in N-glycosylation sites between FLneg and FLpos. In this context, FLneg exhibited significantly fewer N-glycosylation sites in immunoglobulin genes compared to FLpos [62]. Using an even larger cohort, the cases were further categorized into early-stage (I/II), advanced-stage (III/IV), treatment naïve, and relapsed groups. While stage I/II showed no differences between FLneg and FLpos cases, stage III/IV t(14;18) negative cohort showed reduced N-glycosylation sites compared to t(14;18)-positive FL [63]. A study analyzed a larger cohort of FLneg cases to investigate molecular

characteristics. The cases exhibited copy number alterations and mutations analogous to FLpos but with different occurrences. Gene mutations with the highest occurrence included *STAT6* (57%), *CREBBP* (49%), *TNFRSF14* (39%), and *KMT2D* (27%). Based on the molecular profile, three distinct groups were identified. Group 1 consisted of CD23$^+$ FLneg cases, Group 2 exhibited *BCL6* translocations, and the remaining cases were classified as group 3 [60].

CD23$^+$ FLneg, which was identified in group 1 of the previous study, was also suggested as an interim new entity in the ICC [18, 64, 65] due to its phenotype with CD23$^+$, genotype with *STAT6* mutations and distinct clinical features [59, 61, 66]. Due to the strong correlation between *STAT6* mutations and CD23 expression, CD23 was suggested as a surrogate marker in routine diagnostics [60]. It has already been shown in a FL collective without subtype classification that *STAT6* mutations led to the upregulation of IL4/JAK/STAT target genes, including Fc epsilon receptor II (*FCER2* (CD23)), C-C motif chemokine ligand 11 (*CCL17*), and C-C motif chemokine ligand 22 (*CCL22*) [67, 68]. In addition to *STAT6* mutations, this subtype can also harbor suppressor of cytokine signaling (SOCS) 1 mutations, which likewise contribute to *STAT6* activation [60]. However, the activation of the *STAT6* pathway alone does not appear to be sufficient for lymphomagenesis [67]. Since *STAT6*-mutated FLneg often harbor *CREBBP* and /or tumor necrosis factor receptor superfamily member 14 (*TNFRSR14*) mutations, these mutations may interact with *STAT6* in the process of lymphomagenesis [61, 69, 70]. While *CREBBP* mutations support immune evasion and prevent apoptosis by inhibiting *CREBBP* target genes [71, 72], *TNFRSF14* mutations promote re-education of the tumor microenvironment by altering B- and T-lymphocyte attenuator (BTLA)-TNFRSF14 pathway [73]. Currently, comprehensive GEP datasets investigating the impact on cellular pathways and biological effects of these mutations are limited.

**Extranodal FLneg**

FL is mainly seen as disease affecting nodal sites, where extranodal infiltration can occur during disease progression. However, there are extranodal FL seen as distinct entity by ICC, such as primary cutaneous follicle center lymphoma (PCFCL), which is localized in the skin [18]. It shows distinct clinicopathological features such as reduced CD10 and lack of *BCL2* translocation. Compared to classic FL, *KMT2D*, *CREBBP* and *BCL2* were less mutated in PCFCL [74]. The overall survival of PCFCL was found to be superior compared to gastrointestinal FL [75].

**Pediatric FLneg**

FL can also occur in children and young adults, called pediatric-type FL (PTFL). This form of FL is characterized by the absence of t(14;18), a high proliferation index, and high-grade cytology. The disease is localized and shows a superior prognosis. At the molecular level, PTFL shows no mutations in *KMT2D*, *EZH2*, or *CREBBP*. The biallelic inactivation of *TNFRSF14* represents an overlap with FLneg. In addition, mutations affecting the *IRF8* and mitogen-activated protein kinase kinase 1 (*MAP2K1*) genes are characteristic molecular alterations that distinguish PTFL from other forms of FL [76-80].

### *BCL6* rearranged FLneg

Another subgroup, which plays an important role, is FLneg with *BCL6* rearrangement (FLneg$^{BCL6\text{-}R}$), which is characterized by overexpressed *BCL6*. *BCL6*-R in FLneg are more frequent in FL3B compared to FL1-3A. [81-83]. This was confirmed by another study, which found *BCL6*-R in 22% of FLneg cases [60]. FLneg$^{BCL6\text{-}R}$ typically presented in more advanced clinical stages (III/IV), showed a follicular growth pattern and a more complex genetic profile, which resembled FLpos, which was similarly reported by another study, where 65% of FLneg$^{BCL6\text{-}R}$ presented in stage III/IV. Interestingly, the cases showed fewer *CREBBP* (45%) and *STAT6* (9%) mutations [84]. Both studies demonstrated that FLneg stage I/II is more *STAT6*-driven, while in stage III/IV *BCL6* played an important role.

### Comparison of FL subtypes

Recently, a review by Salaverria *et al.* compared the genetic profiles of FL subtypes. The FL subtypes showed significant differences in their genetic profiles, highlighting the substantial heterogeneity of FL (**Figure 10**) [85].

| Entity | *BCL2*-pos FL | DTFL | Nodal *BCL2*-neg FL all | *STAT6* mut + *BCL2*-neg FL | *STAT6 mut*– *BCL2*-neg FL | PCFCL *BCL2*-neg FL | LFGT FL | Thyroid *BCL2*-neg FL | PTFL | LBCL-*IRF4* |
|---|---|---|---|---|---|---|---|---|---|---|
| No. cases | n = 100 | n = 31 | n = 74 | n = 52 | n = 22 | n = 31 | n = 10 | n = 4 | n = 81 | n = 17 |
| *STAT6* | 12 | 3 | 70 | 100 | 0 | 10 | n.a. | n.a. | 4 | 0 |
| *KMT2D* | 82 | 52 | 36 | 42 | 23 | 10 | 0 | 25 | 9 | 6 |
| *CREBBP* | 64 | 68 | 62 | 71 | 41 | 13 | 0 | 25 | 3 | 0 |
| *TNFRSF14* | 35 | 32 | 45 | 50 | 33 | 26 | 60 | 75 | 42 | 0 |
| *EZH2* | 20 | 16 | 22 | 23 | 18 | 7 | 20 | 0 | 4 | 0 |
| *MEF2B* | 18 | 16 | 3 | 4 | 0 | 0 | 0 | n.a. | 0 | 0 |
| *HIST1H1E* | 17 | 0 | 11 | 13 | 5 | 4 | n.a. | n.a. | 8 | 0 |
| *TNFAIP3* | 11 | 0 | 5 | 4 | 9 | 12 | 10 | 0 | 4 | 0 |
| *EP300* | 10 | 3 | 8 | 10 | 5 | 14 | 0 | 0 | 4 | 0 |
| *FOXO1* | 10 | 6 | 20 | 21 | 18 | 7 | 0 | 0 | 3 | 0 |
| *SOCS1* | 8 | n.a. | 12 | 13 | 9 | 11 | 20 | 0 | 11 | 0 |
| *MAP2K1* | 0 | n.a. | 0 | 0 | 0 | 0 | 0 | 0 | 44 | 12 |
| *IRF8* | 10 | 6 | 14 | 12 | 33 | 4 | n.a. | n.a. | 23 | 0 |
| *IRF4* | 0 | 0 | 3 | 4 | 0 | 8 | 0 | n.a. | 0 | 76 |

**Figure 10: Comparison of FL subtype genetic profiles.**
FL subtypes show distinct genetic features (reproduced from Salaverria *et al.* 2023 [85]).

## 1.5 Gene Expression Profiling

Gene expression profiling (GEP) is a powerful tool which helps understanding biological mechanisms and processes, advancing disease research and diagnosis and guiding therapeutic strategies and drug development [86-88]. GEP can be performed using various methods which are based on the quantitation or specific counting of transcripts. It includes classical approaches such as next-generation sequencing (NGS) of complementary DNA (cDNA) libraries (HTG Edgeseq, HTG Molecular Diagnostics), or alternative techniques like RNA counting using an automated fluorescence microscope (NanoString, Bruker Spatial Biology Inc.). The methods can be performed both as whole transcriptome and panel-specific approach. HTG Edgeseq provides extraction-free RNA isolation followed by a nuclease protection assay. In this process, gene-specific DNA protection probes with wings bind to the target RNA and wingmen. Subsequently, unbound RNA molecular and probes are digested using S1 nuclease. This results in a 1:1 ratio of probes to target RNA. Using molecular barcoding, the probes are labeled for later differentiation between samples. Additionally, adapters are added to facilitate ion sphere particle binding during emulsion polymerase chain reaction (PCR), which occurs prior to Ion Torrent sequencing. In a final step, the probes are quantified and pooled, followed by Ion Torrent sequencing (**Figure 11**). HTG Edgeseq allows the use of specific panels with up to 2,500 genes. The panels are typically assigned to distinct functions or research areas, such as the Precision Immuno-Oncology Panel including 1,392 genes [89-92]. NanoString is based on RNA molecule counting by an automated fluorescence microscope. Briefly, two probes bind to the RNA molecule of interest: capture and reporter probe. Both probes contain 50 nucleotides. The capture probe is conjugated with biotin and allows immobilization of RNA molecules onto a streptavidin-modified cartridge. The reporter probe is conjugated with a unique fluorescence barcode, a barcode, which is read by an automated fluorescence microscope (**Figure 12**). PanCancer NanoString also offers specialized panels, such as the Immune Profiling Panel, which includes 770 genes [93, 94]. The Precision Immuno-Oncology Panel from HTG and the nCounter Immune Profiling Panel from NanoString have already been compared in a study using formalin-fixed paraffin-embedded (FFPE) material. The two panels showed largely consistent results in terms of significantly correlated genes. Shared genes that were differentially expressed primarily belonged to the chemokine family and the interleukin (IL) family [95]. To generate a robust data set, the use of both methods, where feasible, could provide more reliable and comprehensive results.

GEP has already provided important insights in cancer research. In 2000, GEP allowed classification of DLBCL into subtypes with different developmental states of malignant B-cells:

GCB, activated B-cell-like (ABC) and an unclassifiable subtype [96]. The subtypes were discovered during investigation of DLBCL gene expression data. Until now, the determination of the cell of origin (COO) has no huge impact in therapy. Nonetheless, it reveals different mechanisms and important insights into the biology of lymphomagenesis.

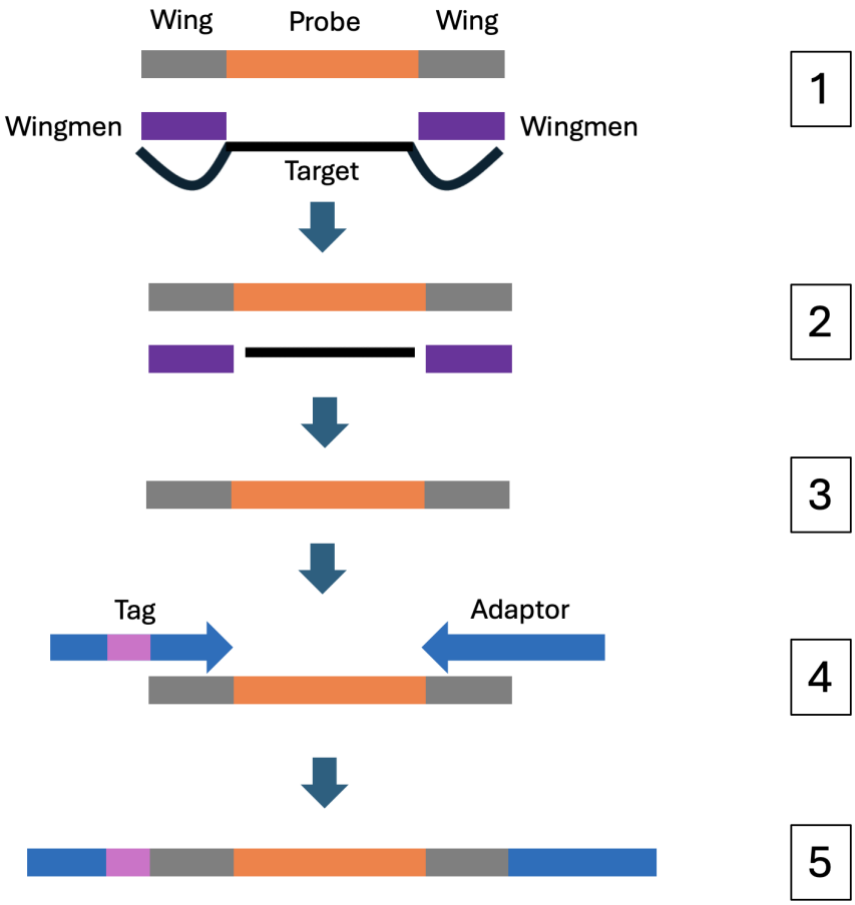


**Figure 11: Schematic representation of HTG Edgeseq principle.**
During nuclease protection assay, protection probes bind to complementary RNA, followed by S1 nuclease digestion and target RNA elimination (step 1 – 3). Samples were tagged using molecular barcoding (step 4), then quantified, pooled and sequenced (step 5). Modified and redrawn based on HTG Molecular Diagnostics manual.

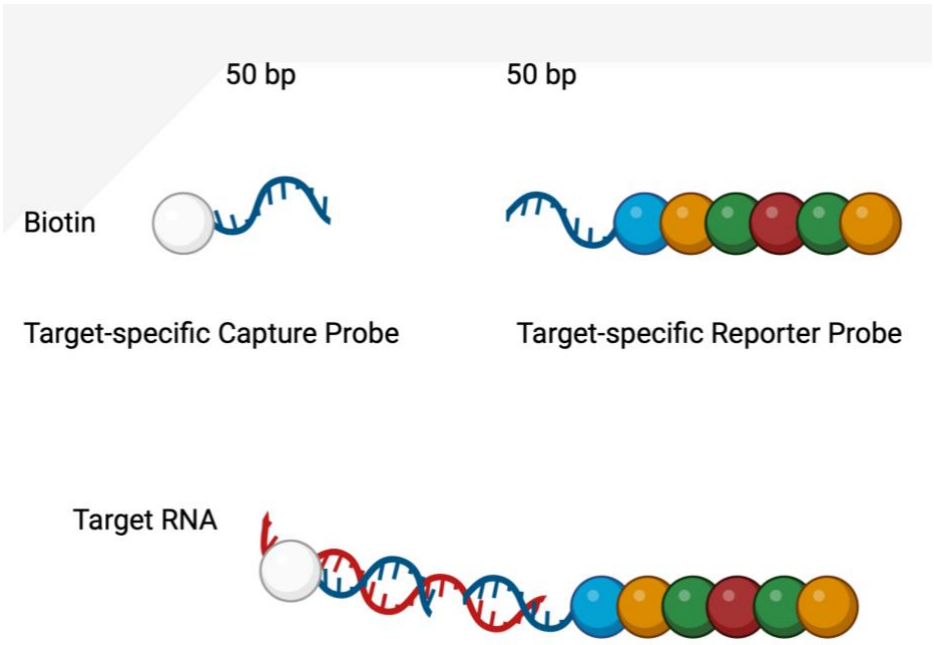


**Figure 12: Schematic representation of NanoString principle.**
Biotin-conjugated capture probe and fluorophore-barcode labeled reporter probe bind to target RNA, allowing washing steps and RNA counting by an automated fluorescence microscope. Each barcode is assigned to a specific gene. Created with BioRender.com. Modified and redrawn based on NanoString nCounter manual.

# 2. Hypothesis and Objectives

FL represents a molecularly and clinically heterogeneous disease comprising distinct genetic subgroups as demonstrated in previous studies [46-48, 60, 78, 97]. Our recent study showed that FLneg harboring *STAT6* and *SOCS1* mutations and expressing CD23 form a distinct biological entity suggesting that the IL4/JAK/STAT6 pathway plays a crucial role.

**Hypothesis**

We hypothesize that activating mutations in the IL4/JAK/STAT6 pathway of FLneg lead to intrinsic activation of STAT6-mediated transcription. This leads to altered gene expression patterns, affecting B-cell differentiation and the tumor microenvironment. Accordingly, FLneg *STAT6/SOCS1* wild-type cases are expected to display different molecular profiles and microenvironmental interactions.

**Objectives**

The aim of this study is to systematically investigate the impact of *STAT6/SOCS1* mutations on gene expression profiles and tumor microenvironment in FLneg and FLpos. The genetic landscape of these subgroups will be extended by mutation analysis of additional lymphoma-associated and IL4/JAK/STAT6-related genes.

The objectives are divided into the following parts:

1. Mutation analysis of FLneg and FLpos cases with and without *STAT6/SOCS1* mutations using an IL4/JAK/STAT6-associated gene panel as well as an extended lymphoma gene panel to detect additional genetic drivers
2. GEP of FLneg and FLpos cases to identify differentially expressed genes and altered pathways between mutated and wild-type groups
3. Bioinformatic analysis of GEP data using DESeq2, ClusterProfiler and Gene Set Enrichment Analysis (GSEA) to uncover activated molecular networks and biological processes

# 3. Materials and Methods

## 3.1 Materials

### 3.1.1 Patient Material

FFPE material used for this work was obtained from the archives of the Institute of Pathology Tübingen and following collaborating institutes:

- Institute of Pathology and Microbiology, Wilhelminenspital Vienna (Andreas Chott)
- Institute of Medical Genetics and Pathology, University Hospital Basel (Thomas Menter)
- Section of Pathology, Department of Medical Biotechnology, University of Siena (Lorenzo Leoncini)
- Hematopathology Unit, Hospital Clínic, Institut d'Ínvestigacions Biomèdiques August Pi I Sunyer (IDIBAPS) Barcelona (Itziar Salaverria and Elias Campo)
- Centro de Investigacíon Biomédica en Red de Cáncer (CIBERONC) Madrid (Itziar Salaverria and Elias Campo)
- Hematopathology Section, Laboratory of Pathology, National Cancer Institute Bethesda (Elaine S Jaffe)

Nodal FL cases were reclassified by hematopathologists using WHO classification from 2017 [98], 2022 [51] and ICC from 2022 [18]. To support lymphoma diagnosis, clonality analysis, IHC staining and FISH analysis were conducted as part of routine diagnostics. For gene expression profiling, FL cases were selected based on *BCL2* translocation state ((t14;18)(q32;q21)), *STAT6* and/or *SOCS1* mutations and CD23 protein expression (via immunohistochemistry).
The study was approved by ethics committee of the University Hospital Tübingen by following positive ethics approvals:

- 211/2021BO2
- 348/2020BO

### 3.1.2 Instruments

Instruments used in this study are summarized in the following table (**Table 1**).

**Table 1: Instruments used in this study**

| **Instrument** | **Provider** |
|---|---|
| BenchMark ULTRA IHC/ISH | Roche |
| Ependorf 100 – 1000 µL pipette | Eppendorf |
| Eppendorf 0.5 – 10 µL pipette | Eppendorf |
| Eppendorf 10 – 100 µL pipette | Eppendorf |
| Eppendorf 20 – 200 µL pipette | Eppendorf |
| Eppendorf Multipette plus | Eppendorf |
| Gilson P20 | Gilson |
| Gilson P200 | Gilson |
| Heizblock Thriller | Peqlab |
| Heraeus Multifuge 1L-R Centrifuge | Thermo Fisher Scientific |
| HTG Edgeseq processor | HTG Molecular Diagnostics, Inc. |
| Ion Chef System | Thermo Fisher Scientific |
| Ion Gene Studio S5 Prime | Thermo Fisher Scientific |
| LightCycler 480 II | Roche |
| Maxwell® RSC | Promega |
| NanoDrop | ThermoFisher Scientific |
| NanoString nCounter® Sprint Profiler | nanoString Technologies |
| Perfect Spin Mini Zentrifuge for 2x8 PCR | Peqlab |
| Qubit Fluorometer 3.0 | Thermo Fisher Scientific |
| Thermocycler | Eppendorf |
| Thermocycler nexusGX2e | Eppendorf |
| Thermomixer comfort | Eppendorf |

### 3.1.3 Kits

Kits used in this study are summarized in the following table (**Table 2**).

**Table 2: Kits used in this study**

| **Kit** | **Provider** |
|---|---|
| Agencourt® AMPure XP-Kit | Beckman Coulter |
| HighPrep PCR | Biozym |
| HTG Edgeseq Precision Immuno-Oncology Panel | HTG Molecular Diagnostics, Inc. |
| Ion 530 Chip Kit | Thermo Fisher Scientific |
| Ion 530 Kit – Chef | Thermo Fisher Scientific |
| Ion AmpliSeq Library Kit v2.0 | Thermo Fisher Scientific |
| Ion Express Barcode Adapters 1-16 Kit | Thermo Fisher Scientific |
| Ion Library TaqMan Quantitation Kit | Thermo Fisher Scientific |
| KAPA Library Quantification Kit (Ion Torrent) | Roche |
| Maxwell RSC FFPE Plus DNA Purification Kit Custom AX4920 | Promega Corporation |
| Maxwell RSC RNA FFPE Kit | Promega Corporation |
| nCounter® PanCancer Immune Profiling | nanoString Technologies |
| Qubit® dsDNA BR Assay Kit | Thermo Fisher Scientific |
| Qubit® dsDNA HS Assay Kit | Thermo Fisher Scientific |

### 3.1.4 Primer and NGS-Panels

For mutation analysis four customized Ampliseq panels (ThermoFisher Scientific) were used: IL4R, FLneg, FLpos and Oncomine Lymphoma III. FLneg and FLpos were already used in a previous study [60]. 98.24% of all exons of *FOXO1*, *EP300*, *MEF2B*, *HIST1H1B-E, TNFRSF14*, *KMT2D*, *GNA13* and hot spot regions of *CREBBP EZH2*, were covered in FLneg panel. In FLpos, 93.89% of all exons of *STAT6*, *SOCS1, TNFAIP3*, and hot spot regions of *NOTCH1*, *NOTCH2*, *MAP2K1*, *MYD88* and *XPO1* were covered. The newly designed Il4R custom panel covered complete coding DNA (CDS) sequence of *IL4R*, *PTPN1*, *IL13RA1*, Tyrosine Kinase 2 (*TYK2*), *JAK1*, *JAK2*, *JAK3*, *DUSP2*, *PTPRD*, *STAT3* and *SOCS3*. Oncomine Lymphoma III panel covered CDS or CDS of hotspot regions of 78 lymphoma-related genes. Tables with further information can be found in the appendix (**Table 27**, **Table 28**, **Table 29** and **Table 30**).

### 3.1.5 Chemicals

Chemicals used in this study are summarized in the following table (**Table 3**).

**Table 3: Chemicals used in this study**

| **Chemicals** | **Provider** |
|---|---|
| 40% PEG 8000 | Carl Roth |
| 500mM Tris-HCl pH 8.0 | Archer |
| Ethanol p.a. | Merck |
| NaOH | Sigma-Aldrich |
| Tween 20 | Sigma-Aldrich |
| Xylol p.a. | VWR |

### 3.1.6 Antibodies

The antibody used in immunohistochemistry (IHC) in this study is summarized in the following table (**Table 4**).

**Table 4: Antibodies used in immunohistochemistry**

| **Antibody/Clone** | **Dilution** | **Provider** |
|---|---|---|
| CD23/SP23 | stock | Roche |

### 3.1.7 Buffer

The buffers used in this study are summarized in the following table (**Table 5**).

**Table 5: Buffer used in this study**

| **Buffer** | **Ingredients (per sample)** | **Method** |
|---|---|---|
| Library Clean-up buffer | 39 µL 5M NaOH<br>31.25 µL 40% PEG 8000<br>29.75 µL $ddH_2O$ | HTG Edgeseq |
| Library Dilution Buffer | 297 µL 10 mM Tris-HCl | HTG Edgeseq |
| Master Mix Library Quantitation | 12 µL 2x Master Mix<br>4 µL $ddH_2O$ | HTG Edgeseq |
| Master Mix Molecular Barcoding | 30 µL OneTaq HotStart 2x Master Mix<br>14 µL $ddH_2O$<br>6 µL specific forward primer | HTG Edgeseq |
| NanoString Hybridization Mix | 8 µL Master mix<br>8 µL RNA sample | NanoString |

| | | |
|---|---|---|
| | 2 µL Capture Probe | |
| Qubit Working Solution | 1 µL Qubit dsDNA HS reagent<br>199 µL Qubit dsDNA HS buffer | Qubit |

### 3.1.8 Software

The software used in this study is summarized in the following table (**Table 6**).

**Table 6: Software used for this study**

| Software | Version | Provider |
|---|---|---|
| ClusterProfiler | 3.20 | [99] |
| DESeq2 | 3.20 | [100] |
| Endnote™ | 21.5 | Clarivate |
| Gene Set Enrichment Analysis | 4.3.3 | Broad Institute Cambridge<br>[101, 102] |
| GraphPad Prism | 10.6.1 | GraphPad Software, LLC. |
| Integrated Genomics Viewer | 2.16.2 | Broad Institute Cambridge |
| Ion Ampliseq Designer | 7.49 | Thermo Fisher Scientific |
| Ion Reporter™ | 5.20.2.0 | Thermo Fisher Scientific |
| Ion Torrent Suite™ | 5.16.1 | Thermo Fisher Scientific |
| Nf-core/NanoString | 1.3.0 | Peltzer, A. & Mohr, C. |
| RStudio | 2023.06.0+421 | Posit Software, PBC |

### 3.1.9 Consumables

Consumables were used from following companies: Beckman Coulter, Becton Dickinson, Biozym, Carl Roth GmbH, Corning Inc., Eppendorf, Falcon, Greiner Bio-One, Neolab, Sarstedt and Zeiss.

## 3.2 Methods

### 3.2.1 Immunohistochemical Staining

IHC of CD23 was performed on 2.5 µm FFPE sections of FL cases, CD23 antibody was used in stock concentration. The protocol that was used to perform IHC staining on a BenchMark ULTRA IHC/ISH Staining Module using U Optiview DAB IHC v5 (v1.00.0117) is listed in the appendix.

### 3.2.2 Deparaffinization for DNA/RNA Extraction

To deparaffinize tissue sections for DNA extraction two cuvettes with inlays were prepared with xylol under a fume hood. 1 – 10 blank sections (5 µm) on silanized slides (prepared by IHC laboratory) without cover slips were incubated in cuvette No. 1 for 5 min followed by incubation in cuvette No. 2 for 5 min. Afterwards, the inlays which contained the sections were dried on a paper towel. If a special area was marked on H&E section before for macrodissection, blank section was scratched only on the specific area using a scalpel. This process was facilitated by moistening the scalpel tip with incubation buffer. Scratched material was transferred into a reaction tube containing 180 µL incubation buffer and vortexed.

### 3.2.3 DNA Extraction

20 µL proteinase K were added to the reaction tube. The samples were incubated at 70 °C on a Thermoshaker with closed lid overnight. If digestion wasn't completed after incubation, 10 µL proteinase K were added followed by 1 h additional incubation at 70 °C. After incubation 400 µL lysis buffer were added and vortexed.

Next, required number of cartridges, RSC plungers and elution tubes were placed into Maxwell RC Cartridge Rack. Cartridges were pushed into the rack and foils removed. If less than 8 samples were purified, cartridges were placed in the middle of the rack. Elution tubes were placed into the designated holders and lids were turned into opposite direction of the cartridges. In well No. 8 (next to elution tube) of each cartridge a plunger was placed. 60 – 100 µL nuclease-free water were added to elution tubes dependent on amount of tissue. Samples are then transferred into the cartridges, one sample per cartridge. To start the Maxwells RSC instrument, power was turned on and tablet booted. After a self-test program "cell DNA" was selected. Barcode and expiration date

of the kit were entered and confirmed. In sample overview, sample fields were selected and sample names entered. Maxwell RSC Cartridge Rack was placed into the instrument and the program started. Isolation required approx. 24 min. After the program had finished, elution tubes were closed, shortly centrifuged and placed on a magnetic rack. The elutes then were transferred into a new 1.5 mL tube and stored at 4 – 7 °C.

### 3.2.4 RNA Extraction

The experiment was performed under a fume hood. Blank sections were placed into a rack and incubated in xylol for 5 min. During incubation two thermocyclers were prepared and heated to 80 °C and 56 °C. After incubation racks were incubated in a second xylol container for 5 min. During incubation 1.5 mL tubes containing 225 µL lysis buffer and paper towels for the blank section rack were prepared. Blank sections were dried on the paper towel. If macrodissection was necessary, H&E slides were used as template for scratching of the blank sections. Otherwise, complete blank section was scratched. Scratching was performed using a scalpel. Scratched material was transferred into lysis buffer. Afterwards, 25 µL Proteinase K per sample were added. Solution was mixed and incubated at 56 °C for 15 min. Then samples were incubated at 80 °C for 1 h. Samples were cooled down at RT for 15 min. Racks were prepared as in 3.2.3 using "FFPE RNA" program. After cooling down, 50 µL master mix 2 were added per sample and incubated at RT for 15 min. Afterwards, samples were centrifuged in a table centrifuge at max g for 2 min. Samples were transferred into the cartridges as in 3.2.3 and run was started, which lasted approx. 40 min. Elutes were transferred into new tubes as in 3.2.3 and either stored at -20 °C or a RNA measurement was performed.

### 3.2.5 Determination of Nucleic Acid Concentration with NanoDrop Spectrophotometer

Usually, nucleic acid measurement was performed directly after extraction. Absorption was measured at 260 nm. First, NanoDrop instrument and computer software were started followed by wavelength verification. "DNA" or "RNA" was selected, depending on measurement. Instrument was blanked using 1 µL dd$H_2O$. Afterwards, 1 µL of DNA/RNA was added on the NanoDrop cuvette and measurement was started. Between each measurement the instrument was cleaned using a lint-free towel. To exclude potential contamination during measurements, last measurement was dd$H_2O$ again.

### 3.2.6 Determination of DNA Concentration using Qubit

Qubit technology allows specific measurement of double stranded DNA using intercalating fluorophore, which leads to a more precise measurement. The experiments were conducted with Qubit® dsDNA HS/BR Assay Kit. First, Qubit fluorometer was calibrated using "Standard 1" and "Standard 2". Standards were prepared using Qubit dsDNA HS reagent, which was thawed protected from light. Working solution was prepared by diluting reagent 1:200 in Qubit dsDNA HS buffer as following: For each sample (+ two standards and one additional sample) 199 µL buffer and 1 µL HS reagent were transferred into a 50 mL Falcon and vortexed. For Standard 1 and 2, 190 µL of working solution were transferred into reaction tubes, 10 µL of Standard 1 and Standard 2 were then added and mixed. For sample preparation, 199 µL working solution and 1 µL sample were mixed and vortexed. Standards and samples were incubated at RT for 2 min. During incubation Qubit device was started. Program "DNA" and "dsDNA High Sensitivity" (HS) was selected. After incubation, calibration was performed using program "Standards lesen". First, Standard 1 was measured followed by Standard 2. Then samples were measured by placing the sample tubes into the slot of the Qubit Fluorometer and selecting "Proben analysieren" and the amount of sample used (1 µL). If sample concentration was too high to display, repetition of the experiment using BR kit was indicated. Concentrations below 1 ng/µL were below limit of detection, in this case it was indicated to perform a vacuum concentration step and repeat experiment.

While NanoDrop provides insight into the purity and total amount of nucleic acid present, Qubit delivers more precise values for DNA or RNA by measuring only intact nucleic acid strands. This facilitates the preparation of NGS libraries and contributes to successful NGS runs.

### 3.2.7 Determination of DV200 Value for NanoString

DV200 analysis (capillary gel electrophoresis) was kindly performed by NGS Competence Center Tübingen (NCCT).

DV200 determined RNA quality and integrity. The value indicated the percentage of RNA fragments that are larger than 200 nucleotides. DV200 in the range of 50 – 80 % were considered as adequate values for the following analyses, < 30 % typically showed a more fragmented RNA, which was not suitable for analysis. The value was used for NanoString to prefilter samples, since FFPE process led to RNA degradation. 5 µL/sample were prepared in a 96 well plate and transported to NCCT on dry ice. Analysis was performed and data provided by NCCT.

### 3.2.8 Mutation Analysis with Ion Torrent

Mutation analysis consisted of library preparation, quantification, pooling, template preparation using the Ion Chef, and sequencing on the Ion GeneStudio S5. Detailed procedure is shown in the appendix.

Mutation analyses were performed using Ion AmpliSeq Custom Panels and next-generation sequencing (Ion GeneStudio S5 Prime System, Thermo Fisher Scientific). Raw data obtained through next-generation sequencing were processed and analyzed using the Ion Torrent Software Suite (Thermo Fisher Scientific). Read alignment was performed against Genome Reference Consortium Human Build 37 (GRCh37/hg19) reference genome using Torrent Mapping Alignment Program (TMAP) aligner integrated into the Torrent Suite (Thermo Fisher Scientific). Variants affecting non-interrogated regions and common polymorphisms with more than 0.1% frequency in normal population were excluded. Furthermore, variants located in regions with low coverage (below 50 reads) were removed. Variants called by the Ion Reporter Software were visually inspected using the Integrative Genomics Viewer (IGV, Broad Institute) to exclude artifacts related to panel and fixation. The allele frequency threshold was set at 5% depending on sample quality. Variant annotation and filtering were performed using Database of Single Nucleotide Polymorphisms (dbSNP) and Catalogue of Somatic Mutations in Cancer (COSMIC) databases within a workflow implemented in the Ion Reporter Software. The prediction of mutation effects was performed using SIFT (http://sift.jcvi.org/) and Polyphen-2 (http://genetics.bwh.harvard.edu/pph2/). These tools allowed the prediction of functional consequences on protein structure and function caused by amino acid substitution. After quality and frequency filtering, all remaining variants, including those of uncertain significance, were retained for further analysis.

### 3.2.9 Gene Expression Profiling with HTG Edgeseq

HTG Edgeseq is a robust GEP method using predefined gene panels such as HTG Edgeseq Precision Immuno-Oncology Panel, which covered 1,392 genes associated with immunology and oncology. Experiments were performed according to mRNA-FFPE-IonTorrentS5-V2 protocol from HTG Molecular Diagnostics, Inc.

**RNA isolation**

RNA isolation of FFPE material was performed using a HTG-specific isolation process, in which the cells were lysed. Here, 5 µm blank sections of FL cases were scratched and transferred into a 1.5 mL reaction tube containing 35 µL lysis buffer/6 $mm^2$ FFPE material. 300 µL denaturation oil/tube were added by carefully pipetting on the wall of the tubes. Tubes were spun down in a table centrifuge at max g for 1 min followed by incubation at 95 °C on a Thermoshaker for 15 min without shaking. Samples were then cooled down at RT for 5 – 10 min. 1/20 of the volume of lysis buffer corresponded to the volume of required Proteinase K. Proteinase K was pipetted directly into the lysis buffer and mixed by pipetting up and down. Samples were incubated at 50 °C on a Thermoshaker at 300 rpm for 3 h. After incubation samples were either stored at -20 °C or directly processed in nuclease protection assay.

**Nuclease protection assay**

In this assay, extracted RNA was transcribed into DNA using gene-specific probes followed by the nuclease protection assay (step 1, 2, 3 **Figure 11**). The assay was performed automatically in the HTG instrument. First, HTG EdgeSeq Assay Reagent pack was removed from the freezer and thawed at RT for at least 80 min. If samples were stored in the freezer, reaction tubes were thawed at 50 °C for at least 45 min without agitation. During thawing steps HTG instrument was cleaned using RNase. Samples and assay were entered into the instrument software. Plate map was created, and barcode of sample plate was scanned. 35 µL per sample were transferred into the predefined well in the 96-well sample plate. Since for the experiments 8-sample kits were used, usually A1 – H1 was occupied. Sample plate, stop plate, disposable tip pack and HTG EdgeSeq Assay Reagent Pack were placed into the HTG processor. Lids were removed and program was started. This process ran for approx. 20 h. Afterwards, stopping plate was stored at – 20 °C or directly used for molecular barcoding (step 4 **Figure 11**).

**Molecular barcoding**

PCR-based molecular barcoding (HTG Edgeseq sequencing Tag Pack IT, 8Fx1R/24Fx1R) allowed binding to ion sphere particles during emulsion PCR as well as identification of samples during sequencing on the Ion GeneStudio S5 Prime. Master mix for one sample contained 30 µL OneTaq HotStart 2x Mastermix in GC Buffer (NEB), 14 µL PCR-grade $H_2O$ and 6 µL reverse primer (TR). Master mix was prepared in an adequate reaction tube and dispensed into PCR tubes. Each tube represented one sample, which obtained 6 µL of specific forward primer (T1 – T24). Stopping plate was thawed at RT for 5 min. 4 µL/sample were removed from stopping plate, transferred to PCR tubes and mixed. PCR tubes were spun down shortly and transferred to thermocycler using following program (**Table 7**):

**Table 7: PCR program of HTG molecular barcoding**

| Temperature [°C] | Duration | Cycles |
|---|---|---|
| 95 | 4 min | 1 |
| 95 | 15 sec | 19 |
| 56 | 45 sec | |
| 68 | 45 sec | |
| 68 | 10 min | 1 |
| 4 | Hold | - |

After program has finished PCR tubes were stored at -20 °C or directly processed for library clean up.

**Library clean up**

Library clean up preparation was performed as follows: 100 µL clean up buffer/sample were prepared in a 15 mL Falcon tube using 39 µL NaOH, 31.25 µL 40% PEG 8000 and 29.75 µL dd$H_2O$. Scale-up was performed according to sample size (+ 2 additional samples). 80% ethanol was prepared using 0.8 mL 100% ethanol and 0.2 mL dd$H_2O$. Scale-up was performed according to sample size (+ 2 additional samples). AMPure XP Magnetic beads were brought to RT for 30 min and vortexed to allow complete resuspension. For each sample a new PCR tube was prepared. 37.5 µL magnetic beads/sample were pipetted into new PCR tubes. 100 µL clean up buffer/sample were added and mixed. 55 µL PCR product/sample were added to the magnetic bead solution. PCR tubes were mixed using a multichannel pipette set to 100 µL. Tubes were incubated at RT for 5 min. After incubation tubes were placed into a magnetic rack and incubated at RT for 5 min. Afterwards, supernatant was removed and 200 µL 80% ethanol/sample were added, followed by incubation at RT for 1 min. Supernatant was removed and step repeated. After removing supernatant, magnetic bead pellets were dried on the magnetic rack at RT for 5 – 10 min (avoid cracks in the pellet). PCR tubes were removed from magnetic rack, 40 µL 10 mM Tris-HCL pH 8.0/sample were added and mixed. Samples were incubated at RT for 5 min. After incubation, samples were placed on the magnetic rack and incubated at RT for 5 min. 30 µL of cleaned sample were then transferred into new PCR tubes.

**Library quantitation**

Libraries were quantified using KAPA Library Quantification Kit, which was thawed at RT for 30 min. During thawing dilution series was prepared. 1:100 and 1:10,000-fold dilutions were prepared

in an Axygen 96-well plate as follows: 297 µL 10 mM Tris/0.05% Tween 20 were dispensed, 2x for each sample (1:100 and 1:10,000 dilution). 3 µL cleaned-up library sample were pipetted into 1:100 dilution and mixed. 3 µL 1:100 solution were transferred into 1:10,000 solution and mixed. 2X Master Mix was prepared by adding 1 mL 10X Primer Premix to KAPA SYBR FAST qPCR Master mix. 1x qPCR reaction contained 12 µL 2xMaster mix and 4 µL dd$H_2O$. Master mix was prepared for 3 replicates/sample, 6 Standards (3 replicates/standard), one negative control (no template control, as triplicate) and 3 extra reactions. After preparation, 16 µL Master mix/sample were dispensed in a MicroAmp qPCR reaction plate. 4 µL dd$H_2O$ were added to negative controls, 4 µL of each DNA standard were added to the respective Standard and 4 µL of 1:10,000 library to each sample replicate. Afterwards, qPCR plate was sealed using MicroAmp Optical Adhesive Film and centrifuged down. Quantitation was performed on a Light Cycler 480 II using following program (**Table 8**):

**Table 8: Light Cycler 480 II qPCR program for library quantitation**

| Step | Temperature [°C] | Duration | Cycles |
|---|---|---|---|
| Initial Denaturation | 95 | 5 min | 1 |
| Denaturation | 95 | 30 sec | 30 |
| Annealing/Extension | 60 | 45 sec | |

### Library Pooling and Normalization

PCR data (concentration in pM) from previous step were exported from Light Cycler and transferred into HTG Input Template. This template was then loaded into HTG Library Calculator. Program "mRNA" and sequencer "ION Torrent" were selected. By default, HTG Library Calculator set pooling concentration to 100 pM. The software automatically calculated the required volumes of the samples to be sequenced. Samples without dilution factor were marked as "use neat" compared to the samples with dilution factors. These samples were diluted by using 5 µL sample and the calculated volume of 10 mM Tris pH 8.0. After preparing required sample dilutions samples were pooled in a reaction tube using the indicated sample volumes. The library then was adjusted to a volume of 100 µL by adding 10 mM Tris pH 8.0. The pooled library was vortexed and spun down in a microcentrifuge. The library was either stored at -20 °C or directly processed.

### Next-Generation Sequencing

45 min before starting the run, ION Chef reagents were thawed at RT for 45 min. During thawing run was created in Ion Torrent Suite Software. Run Plan name was entered as well as number of

barcodes present in the library and sample tube barcode. The sample sheet, which was created during nuclease protection assay on HTG instrument, was uploaded using "load samples table". Then it was checked if the correct instrument was selected as well as template kit, sequencing kit and chip type match. Either Ion 530 chip or 540 chip were used. HTG Precision Immune-Oncology Panel allowed sequencing of 8 samples on 530 chip or 48 samples on 540 chip. 25 µL of diluted libraries were transferred into the barcoded Library Sample Tube. The tube was briefly spun down and placed back in the Ion Chef Reagents Cartridge. Ion Chef run was performed according to Ion Chef User Manual.

After sequencing, FASTQ files were prepared by Ion Torrent suite file exporter, downloaded from Ion Torrent suite and parsed using HTG EdgeSeq Parser software. Data analysis was performed using DESeq2 package in RStudio.

### 3.2.10 Gene Expression Profiling with NanoString

NanoString method allows quick determination of gene expression in FFPE material.

**Hybridization**

First, thermocycler was heated to 65 °C. RNA samples were thawed on ice, while Reporter CodeSet and Capture ProbeSet were thawed at RT. 70 µL hybridization buffer were transferred to Reporter CodeSet to create a Master Mix, followed by mixing with a pipette. 8 µL Master Mix were dispensed in each of 12 PCR-tubes. Afterwards, 8 µL sample were added and mixed. 2 µL Capture ProbeSet were added to each tube and mixed. PCR-tubes were directly placed in pre-heated thermocycler. 65 °C for 24 h and ramp down to 4 °C were set.

**Creating NanoString Run**

During hybridization NanoString run on nCounter instrument was prepared. The run plan was created either by direct input into the screen of the machine, or by accessing via IP. Run name was set and samples (1 – 12) were entered. Each panel was linked to a specific reporter library file (RLF) where barcodes were assigned to genes. The RLF file for Immune Profiling panel was uploaded and the run was saved.

**NanoString Run**

NanoString cartridge was thawed for 30 min at RT before usage. After 24 h hybridization, samples were removed from thermocycler and processed. The sample volume was adjusted to a volume

between 30 – 35 µL. Then the cartridge was removed from its package, oriented with barcode on the bottom and NanoString symbol at the top. Using a 100 µL or 200 µL pipette 30 µL/sample were injected into the respective loading port, which was assigned to a sample in the run plan. After pipetting all 12 samples into the 12 loading ports. Excessive liquid was removed from the cartridge surface using a lint-free wipe. A seal was applied on the sample ports. Reagent port coverage seal was removed. The drawer of nCounter was opened by selecting "initiate run", the cartridge positioned, and the drawer closed by selecting "close drawer". After cartridge was loaded, the run created before was selected in "run selection". Finally, "review run" allowed verification of correct sample assignment, "Start processing" started the RNA counting process. During run, nCounter performed several magnetic bead-based washing steps to remove unbound probes. After washing steps, automated RNA counting started. The whole process took approx. 6h. The instrument created reporter code count (RCC) files, which were downloaded directly from the instrument. RCC files were processed via nf-core/nanostring pipeline followed by DESeq2 package in RStudio.

### 3.2.11 Gene Set Enrichment Analysis & ClusterProfiler

GSEA was performed on HTG and NanoString Data ($FLneg^{m}$ vs. $FLneg^{wt}$). Data was normalized during GEP (via DESeq2). GCT and CLS files were prepared as indicated by Broad Institute. For this analysis Pathway interaction database (PID) *IL4* pathway gene set was used and obtained from Broad Institute. Number of permutations preset, 1000, was used. Collapse was set to "no collapse" to keep initial data. Permutation type was set to "phenotype". Sample size was equal to gene expression profiling. Enrichment plot and *IL4* pathway heatmap were extracted from index. Enrichment score, normalized enrichment score and false discovery rate (FDR) q-value were obtained from GSEA Results Summary. ClusterProfiler analysis was performed during DESeq2 analysis using Reactome database.

### 3.2.12 Statistics

The statistical analyses were performed using GraphPad Prism 10 (GraphPad Software, Boston, MA, USA) and R (Posit Software, PBC, Boston, MA, USA). Within R software, DESeq2 package was used for differential gene expression analysis, ClusterProfiler for enrichment analysis. In general, statistical significance was defined as $p < 0.05$, unless stated otherwise. For multiple hypothesis testing during DESeq2 analysis, adjusted p-values (false discovery rate, FDR via Benjamini-Hochberg) were used.

### Chi-square ($\chi^2$) Test of Independence

To assess associations between two categorical variables (e.g. mutation status vs. CD23 expression), chi-square test was applied. Here, observed frequencies in each category were compared with the frequencies expected under the null hypothesis of independence.

### Fisher's exact test

Unlike the chi-square test, it calculated the exact probability of obtaining the observed values under the null hypothesis of independence. The probability model was the hypergeometric distribution. Due to its exact significance level, it was recommended for small sample sizes. The test was also applied for comparison of mutation status and CD23 expression.

### Odds ratio (OR) and 95% Confidence Intervals

OR and 95% Confidence Intervals provided the quantification of strength as well as the direction of association between categorical variables. OR > 1 showed a positive association, OR < 1 a negative association. Baptista-Pike method was used by GraphPad Prism to allow more stable estimates when using small sample settings. Using CI intervals, the determination of the strength and uncertainty of an effect was possible, since the p-value alone only indicated the likeliness of an effect to exist.

### Binary Logistic Regression

This test was used to investigate the effect of combined genetic variables (mutations) on CD23 expression. The significance of this model was calculated using the Likelihood-Ratio-Test.

### Differential Gene Expression Analysis with DESeq2

This method allowed the analysis of gene expression data generated with HTG and NanoString platforms. Briefly, read counts with a negative binomial distribution were modeled and fold changes (FC) between experimental groups were estimated. Multiple testing using Benjamini-Hochberg false discovery rate to adjust statistical significance was included into analysis. Genes with p-adj. < 0.05 and FC +1.5/-1.5 were considered as significant, if not stated differently.

Raw read counts were normalized within DESeq2 using median-of-ratios method, correcting for library size and RNA composition between samples. Normalized counts were then processed in GSEA [100].

**Principle Component Analysis (PCA)**

This analysis was included into DESeq2 package and used to visualize sample-to-sample relationships. Thus, batch effects, biological clustering, and outliers could be determined. It was based on the transformation of many gene expression variables into so-called principal components and helped to identify the greatest variance across samples. PCA was applied to assess the relation between gene expression of FL subgroups.

**Gene Set Enrichment Analysis (GSEA)**

GSEA allowed the identification of enriched biological pathways. Normalized gene reads during DESeq2 were compared to specific gene sets, in this study the IL4/JAK/STAT6 pathway gene set. By comparing two groups (e.g. $FLneg^{m}$ vs. $FLneg^{wt}$) it was possible to assess the enrichment of the IL4 pathway in those groups. GSEA is based on a weighted Kolmogorov-Smirnov-like statistic to a ranked gene list. Here, an enrichment score based on the maximum deviation sum from zero is calculated to assess non-random gene set enrichment. The statistical significance was assessed by permutation testing and multiple testing correction (FDR). FDR < 0.25 was defined as significant (as recommended by the Broad Institute guidelines) [101, 102].

**ClusterProfiler**

This R package also allowed the identification of enriched pathways. It implemented GSEA together with other enrichment methods. Furthermore, the package allowed the generation of enrichment plots and pathway maps [99].

# 4. Results

## 4.1 Determination of the Study Cohort

FL study cohort was assembled by combining 35 FLneg cases from our previous study [60] and 16 new FLneg cases. Nann *et al.* already observed a correlation between *STAT6/SOCS1* mutations and positive CD23 IHC staining. Therefore, this knowledge was applied as a selection criterion by including CD23-positive FLneg cases when assembling the cohort. Including CD23-positive FLneg cases drastically increased the probability of obtaining *STAT6/SOCS1* cases, which was the primary goal of the cohort expansion. Additionally, 25 new FLpos cases were included. For the cohort of the previous study, mutation analysis data for FLneg panel and FLpos panel were already available. The 16 new FLneg cases as well as the 25 new FLpos cases were analyzed unless this had already been done as part of routine diagnostics. Characteristics of all FL cases are provided in **Table 9**. During the reclassification of FL cases by a hematopathologist, FLneg13, FLneg39 and FLneg40 were assigned to the FLpos group, as they showed increased levels of *BCL2* transcripts during preliminary experiments using HTG and NanoString gene expression profiling. Since FLpos13 already existed, FLneg13 was renamed to FLpos13.2. *BCL6*-R cases (FLneg3, FLneg5, FLneg18, FLneg37, FLneg38, FLneg69) were not separated from FLneg subgroups and included into analysis.

**Table 9: Key characteristics of FLneg and FLpos cohort**
BCL2, BCL6, CD10 and CD23 were stained using IHC. *BCL6-R* was determined using FISH. Growth pattern either reflects Fo (follicular), D (diffuse) or F/D (follicular/diffuse). + indicates positive straining/presence of rearrangement, - shows absence of staining/rearrangement. Cytological grading, growth pattern and stage was determined by an experienced hematopathologist, NA = not available (modified from Nann *et. al* 2020 [60])

| Case | Sex | Age, y | Biopsy Site | Cytological grading | Growth pattern | *BCL6-R* | BCL2 | BCL6 | CD10 | CD23 | Ki67, % | Stage |
|---|---|---|---|---|---|---|---|---|---|---|---|---|
| FLneg1 | M | 61 | Cervical LN | 1-2 | Fo | - | - | + | + | - | 20 | $II_{EB}$ |
| FLneg2 | F | 73 | Axillary LN | 3A | Fo | - | - | + | - | - | 70 | NA |
| FLneg3 | M | 49 | Submandibular LN | 1-2 | Fo | + | - | + | + | - | 25 | IA |
| FLneg4 | F | 50 | Inguinal LN | 3A | F/D | | - | + | + | + | 50 | IA |
| FLneg5 | F | 62 | Axillary LN | 1-2 | Fo | + | - | + | + | - | 15 | IIIA |
| FLneg7 | F | 72 | Axillary LN | 1-2 | Fo | - | - | + | + | + | 10 | IIIA |
| FLneg8 | F | 53 | Inguinal LN | 1-2 | F/D | - | - | + | + | + | 10 | IA |
| FLneg9 | F | 79 | LN | 1-2 | Fo | - | - | + | - | - | 10 | NA |
| FLneg10 | M | 72 | Axillary LN | 1-2 | D | - | - | + | + | + | 30 | IIIA |
| FLneg11 | F | 65 | Inguinal LN | 1-2 | Fo | - | - | + | + | + | 30 | IA |
| FLneg14 | M | 49 | Left Inguinal LN | 1-2 | Fo | - | - | + | + | + | 10 | II |
| FLneg16 | M | 60 | LN | 1-2 | Fo | - | (+) | + | + | - | 60 | IA |
| FLneg17 | F | 56 | Inguinal LN | 1-2 | D | - | - | + | + | + | 30 | IA |
| FLneg18 | F | 65 | Intraabdominal LN | 1-2 | Fo | + | - | + | + | - | 20 | IV |
| FLneg25 | F | 46 | Inguinal LN | 1-2 | D | - | - | + | + | + | 10 | IA |
| FLneg26 | F | 77 | Cervical LN | 1-2 | Fo | - | - | + | - | - | 15 | IA |
| FLneg27 | F | 79 | Axillary LN | 1-2 | Fo | - | - | + | + | + | 70 | IA |
| FLneg28 | F | 72 | Right axilla LN | 1-2 | Fo | - | - | + | + | + | 30 | NA |
| FLneg29 | F | 52 | Left inguinal LN | 1-2 | F/D | - | - | + | + | + | 30 | NA |
| FLneg30 | M | 42 | Right cervical LN | 3A | Fo | - | - | + | (+) | - | 75 | NA |
| FLneg32 | M | 80 | Inguinal LN | 3A | F/D | - | - | (+) | - | - | 30 | NA |
| FLneg33 | F | 78 | Right axilla LN | 1-2 | Fo | - | - | + | + | - | 20 | NA |
| FLneg35 | M | 69 | Right cervical LN | 3A | Fo | - | - | + | - | - | 60 | NA |
| FLneg36 | F | 77 | Right cervical LN | 1-2 | Fo | - | - | + | + | - | 20 | NA |
| FLneg37 | F | 60 | Left inguinal LN | 1-2 | Fo | + | - | + | + | + | 10 | IA |
| FLneg38 | F | 53 | Axillary LN | 1-2 | Fo | + | - | + | + | + | 30-35 | II |
| FLneg41 | F | 53 | Inguinal LN | 1-2 | F/D | - | - | + | + | + | 20 | IA |
| FLneg42 | F | 74 | Inguinal LN | 1-2 | Fo | NA | - | + | + | - | 80 | IVA |
| FLneg44 | F | 49 | Inguinal LN | 1-2 | D | - | - | + | + | + | 45 | IA |
| FLneg45 | F | 42 | Inguinal LN | 1-2 | Fo | - | - | + | + | + | 35 | IA |
| FLneg46 | F | 81 | Inguinal LN | 1-2 | Fo | - | (+) | + | + | + | 35 | IA |
| FLneg63 | F | 56 | Inguinal LN | 1-2 | D | - | + | + | + | (+) | 40 | $III_E$ |
| FLneg65 | M | 63 | Inguinal LN | 1-2 | D | - | - | + | + | + | 15-20 | IA |
| FLneg66 | F | 51 | Inguinal LN | 1-2 | D | - | - | + | + | + | 20 | NA |
| FLneg67 | F | 61 | Inguinal LN | 1-2 | D | - | - | + | + | + | 10 | IA |
| FLneg68 | F | 58 | Inguinal LN | 3A | D | NA | - | + | + | (+) | NA | NA |
| FLneg69 | M | 52 | Inguinal LN | 1-2 | D | + | | + | - | + | Increased | NA |
| FLneg70 | F | 69 | Left inguinal LN | 1-2 | Fo | NA | - | + | + | + | NA | NA |

| | | | | | | | | | | | |
|---|---|---|---|---|---|---|---|---|---|---|---|
| FLneg71 | M | 62 | Neck LN | NA | NA | NA | (+) | NA | (+) | NA | NA | NA |
| FLneg73 | F | 59 | Axillary LN | 1-2 | D | NA | + | + | + | + | NA | NA |
| FLneg74 | F | 57 | Inguinal LN | 1-2 | F/D | NA | (+) | + | + | (+) | NA | NA |
| FLneg75 | F | 61 | Inguinal LN | 1-2 | NA | NA | + | NA | + | (+) | NA | NA |
| FLneg76 | F | 54 | Inguinal LN | 1-2/3A | NA | NA | - | + | + | + | NA | NA |
| FLneg77 | M | 40 | Inguinal LN | NA | D | NA | + | + | + | + | NA | NA |
| FLneg78 | NA | 59 | Inguinal LN | 1-2 | NA | NA | + | + | + | + | NA | NA |
| FLneg79 | NA | 68 | Axillary LN | 1-2 | NA | NA | + | + | + | + | NA | NA |
| FLneg80 | NA | 43 | Axillary LN | 1-2 | NA | NA | + | NA | + | + | NA | NA |
| FLneg81 | NA | 35 | Inguinal LN | 1-2 | NA | NA | + | NA | + | + | NA | NA |
| FLneg82 | NA | 57 | Inguinal LN | 1-2 | NA | NA | + | NA | + | + | NA | NA |
| FLneg83 | M | 53 | NA | 1-2 | NA | NA | + | NA | + | + | NA | NA |
| FLneg84 | F | 53 | NA | 1-2 | NA | NA | + | NA | + | + | NA | NA |
| | | | | | | | | | | | | |
| FLpos1 | M | 78 | Iliacal LN | 1-2 | NA | NA | + | + | + | - | NA | NA |
| FLpos2 | F | 59 | Tonsillar fossa | 1-2 | NA | NA | + | + | + | (+) | NA | NA |
| FLpos3 | F | 49 | Cervical LN | 1-2 | NA | NA | + | + | + | - | NA | NA |
| FLpos4 | F | 63 | Inguinal LN | 1-2 | NA | NA | + | + | + | NA | NA | NA |
| FLpos5 | F | 47 | Cervical LN | 1-2 | NA | NA | + | + | + | - | NA | NA |
| FLpos6 | M | 69 | Axillary LN | 3 | NA | NA | + | + | + | - | NA | NA |
| FLpos7 | F | 68 | Cervical LN | 1-2 | NA | NA | + | NA | + | - | 0 | NA |
| FLpos8 | M | 69 | Axillary LN | 1-2 | NA | NA | + | + | + | - | NA | NA |
| FLpos9 | F | 67 | Inguinal LN | 2/3A | F/D | NA | + | + | + | - | NA | NA |
| FLpos10 | NA | 65 | Axillary LN | 1-2 | NA | NA | + | NA | + | + | NA | NA |
| FLpos11 | NA | 66 | Submandibular LN | 1-2 | NA | NA | + | NA | + | + | NA | NA |
| FLpos12 | NA | 73 | Inguinal LN | 1-2 | NA | NA | + | NA | + | + | NA | NA |
| FLpos13 | NA | 47 | Left inguinal LN | 1-2 | NA | NA | + | NA | + | + | NA | NA |
| FLpos13.2 | F | 61 | LN | 1-2 | Fo | NA | - | + | + | - | 10 | IV |
| FLpos14 | NA | 68 | Left axillary LN | 1-2 | NA | NA | + | NA | + | + | NA | NA |
| FLpos15 | NA | 39 | Left cervical LN | 1-2 | NA | NA | + | NA | + | + | NA | NA |
| FLpos16 | NA | 57 | Intestine LN | 1-2 | NA | NA | + | NA | NA | + | NA | NA |
| FLpos17 | NA | 58 | Inguinal LN | 1-2 | NA | NA | + | NA | + | + | NA | NA |
| FLpos18 | NA | 49 | Cervical LN | 1-2 | NA | NA | + | NA | + | + | NA | NA |
| FLpos19 | NA | 72 | Inguinal LN | 1-2 | NA | NA | + | NA | + | + | NA | NA |
| FLpos20 | NA | 73 | NA | 1-2 | NA | NA | + | NA | + | + | NA | NA |
| FLpos21 | F | 78 | NA | 1-2 | NA | NA | + | NA | + | + | NA | NA |
| FLpos22 | M | 67 | NA | 3A | NA | NA | + | NA | + | + | NA | NA |
| FLpos23 | M | 36 | NA | 1-2 | NA | NA | + | + | + | + | NA | NA |
| FLpos24 | F | 32 | NA | 1-2 | NA | NA | + | NA | - | + | NA | NA |
| FLpos25 | M | 66 | NA | 1-2 | NA | NA | + | NA | + | + | NA | NA |
| FLpos39 | M | 68 | Inguinal LN | 1-2 | Fo | NA | - | + | + | + | 30 | IA |
| FLpos40 | F | 68 | Axillary LN | 1-2 | Fo | NA | - | + | + | - | 20 | IA |

### 4.1.1 FLneg-typical Gene Mutation Analysis

FLneg panel mutation analysis (*TNFAIP*, *STAT6*, *SOCS1*, *XPO1*, *NOTCH1*, *MYD88*, *MAP2K1*, *NOTCH2*) was performed on FLneg and FLpos cohort. Apart from the cases already characterized as part of the study from Nann et. al [60] (FLneg1 – FLneg67, 35 FLneg cases), 16 additional FLneg cases (FLneg68 – FLneg84) and 25 FLpos cases were included into the analysis. In the total cohort of 51 FLneg cases, *STAT6* represented as the most frequent mutated gene (33/51, 65%), followed by *SOCS1* (12/51, 24%). *TNFAIP3* (4/51, 8%), *NOTCH1* (2/51, 4%) and *NOTCH2* (1/51, 2%) were rather rarely mutated, while *XPO1*, *MYD88* and *MAP2K1* mutations were not found at all (**Figure 13**). No abnormalities were observed in the other genes. Specific mutations are listed in appendix (**Table 31**, **Table 32**).

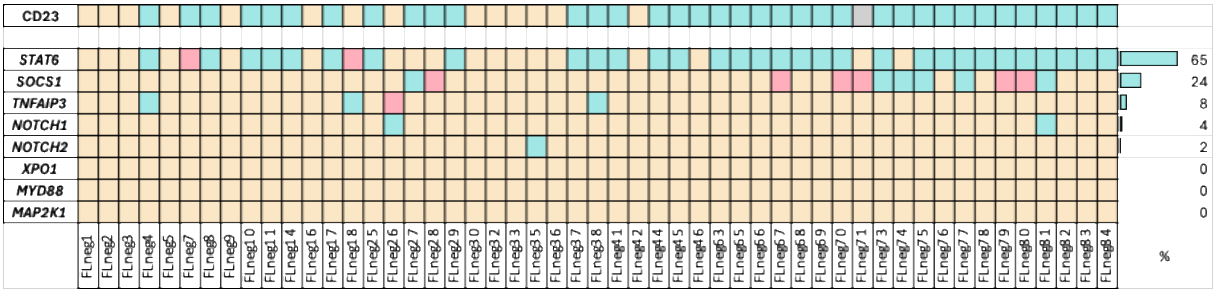


**Figure 13: Mutation matrix of FLneg cohort analyzed via FLneg panel.**
CD23 IHC was added for comparison.FLneg1 – Flneg67 were already characterized in [60], FLneg68 – FLneg84 were analyzed as part of this thesis. In total, *STAT6* was the most frequent mutation (33/51, 65%). Light yellow = wild-type, aqua = mutation (IHC: positive), rose = > 1 mutation, n=51.

Next, the correlation between *STAT6*/*SOCS1* mutations and CD23 IHC was examined. 35/37 *STAT6*/*SOCS1*-mutated FL cases demonstrated CD23 positivity. In only one case (FLneg18) CD23 positivity could not be detected despite a *STAT6* mutation. In contrast, FLneg46 exhibited CD23 positivity despite the absence of *STAT6*/*SOCS1* mutations. For FLneg71, a *SOCS1*-mutated case, CD23 staining was not done due to lack of material. The three outliers were nonetheless included in the following GEP to investigate their behavior at the transcriptional level. Chi-square test showed a highly significant association, which was confirmed by Fisher's exact test. Odds ratio was 455 with 95% CI ≈ 25.88 – 4767 indicating a very strong association (**Table 10**).

**Table 10: Distribution of FLneg$^{m}$ vs. wt across CD23 status, with statistical tests and effect sizes**
$\chi^2(1) = 40.57$, $p < 0.0001$. Fisher's exact test (two-sided) $p < 0.0001$. Odds Ratio (OR) = 455, 95% CI ≈ 25.88 – 4767. FLneg71 was excluded from analysis due to missing CD23 data, n =50. Statistics were calculated using GraphPad Prism 10.

| ***STAT6/SOCS1*** | **CD23$^{+}$** | **CD23$^{-}$** |
|---|---|---|
| m | 35 | 1 |
| wt | 1 | 13 |
| total | 36 | 14 |

The characterization of different FL subtypes also required the molecular analysis of FLpos cases using the FLneg panel. The data were either already available from routine diagnostics or obtained through new analyses. *STAT6* was the most frequently mutated gene at 40% (10/25), followed by *SOCS1* at 24% (6/25). One case showed a mutation in *MAP2K1* (1/25, 4%). *TNFAIP3*, *XPO1*, *NOTCH1*, *MYD88* and *NOTCH2* were exclusively wild-type (**Figure 14**). Here, preference was also given to searching for CD23-positive FLpos cases. Compared to FLneg cohort, *STAT6* showed a significant difference in mutational frequency (**Figure 15**).

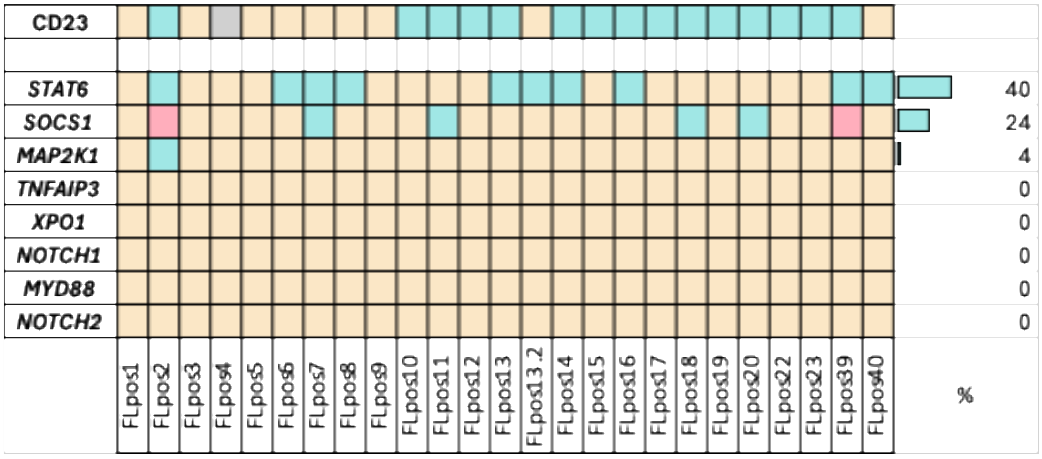


**Figure 14: Mutation matrix of FLpos cohort analyzed via FLneg panel.**
*STAT6* was the most frequent mutation (10/25, 40%). CD23 IHC was added for comparison. Light yellow = wild-type, aqua = mutation (IHC: positive), rose = > 1 mutation, grey = no information available, n=25.

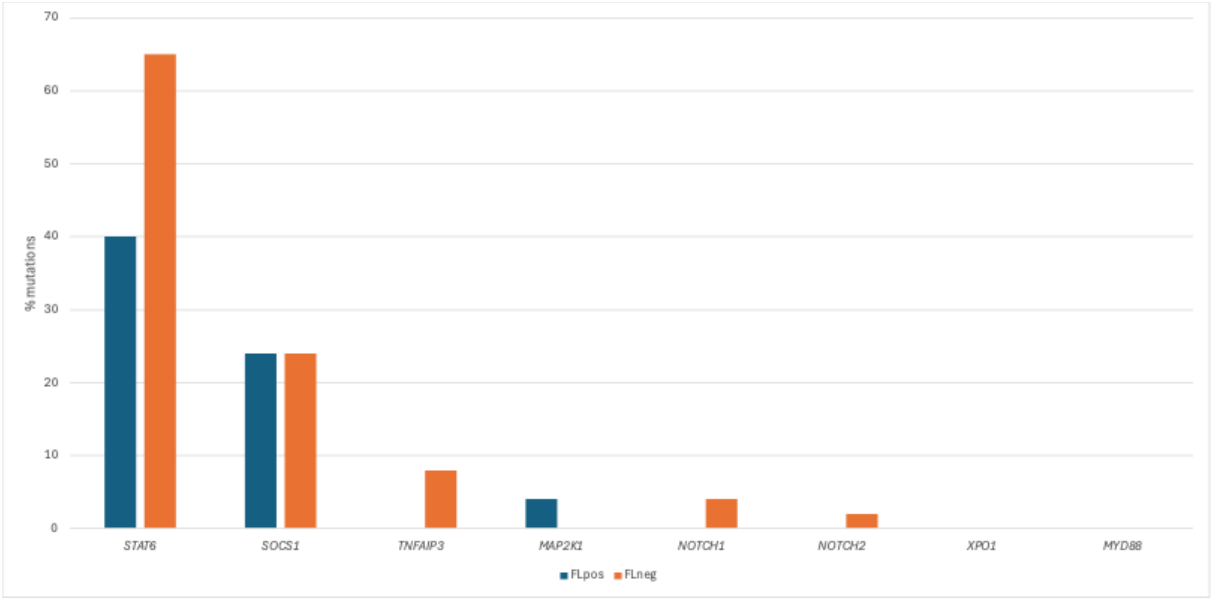


**Figure 15: Comparison of FLneg panel results between FLpos and FLneg cohort.**
*STAT6* is the only gene which shows statistically significant difference between FLneg and FLpos. $\chi^2(1) = 8.316$, $p \approx 0.004$. Fisher's exact test, $p = 0.01$; OR = 4.5, 95% CI = 1.5 – 13.5. Genes with $p < 0.05$ were considered as significant. The remaining genes showed $p > 0.05$ and were not considered as significant. Statistics were calculated using GraphPad Prism 10.

Regarding the FLpos cohort, the correlation between *STAT6/SOCS1* mutations and CD23 positivity was also examined. Interestingly, there was no statistically significant difference or association between *STAT6/SOCS1* mutated/wild-type FLpos and CD23 positivity (**Table 11**). 13/25 FLpos cases carried *STAT6/SOCS1* mutations. 8 of these cases were $CD23^+$, while 5 were $CD23^-$. 7 *STAT6/SOCS1*$^{wt}$ cases were $CD23^+$, and 4 cases were $CD23^-$.

**Table 11: Distribution of FLpos$^m$ vs. wt across CD23 status, with statistical tests and effect sizes**
$\chi^2(1) = 0.011$, $p \approx 0.92$. Fisher's exact test: (two-sided) $p \approx 1$. Odds Ratio (OR) = 0.91, 95% CI = 0.2 – 4.3. Significance level $p < 0.05$ was considered as significant. FLpos4 was removed from analysis due to missing CD23 data. Statistics were calculated using GraphPad Prism 10

| ***STAT6/SOCS1*** | **$CD23^+$** | **$CD23^-$** |
|---|---|---|
| **m** | 8 | 5 |
| **wt** | 7 | 4 |
| **total** | 15 | 9 |

Ultimately, a difference in the correlation between *STAT6/SOCS1*$^m$ FL cases and CD23 was observed. While almost all mutated FLneg cases were $CD23^+$, only 8 out of 13 mutated FLpos cases showed $CD23^+$.

### 4.1.2 FL-typical Gene Mutation Analysis

FLpos panel analysis was performed on FLneg and FLpos cohorts, unless it had already been conducted as part of routine diagnostics or the Nann *et al.* study [60]. 44/51 FLneg cases provided data by routine diagnostics or new analysis. In FLneg cohort, FLneg28, FLneg63, FLneg65 and FL66 were not suitable for analysis due to insufficient DNA quality. FLneg73, FLneg76 and FLneg77 lacked material. *CREBBP* and *TNFRSF14* were the most frequently mutated genes (20/44, 45%), followed by *KMT2D* (12/44, 27%), *FOXO1* (12/44, 27%), *EZH2* (6/44, 14%), *EP300* (4/44, 9%), *HIST1H1E* (4/44, 9%), *HIST1H1C* (3/44, 7%), *HIST1H1B* (2/44, 5%), *HIST1H1D* (2/44, 5%), *GNA13* (2/44, 5%) and *MEF2B* (1/44, 2%) (**Figure 16**). In FLpos cohort, FLpos2, FLpos6, FLpos7, FLpos9, and FLpos20 were excluded after analysis due to excessive fixation artifacts. *CREBBP* was the most frequently mutated gene (15/20, 75%), followed by *TNFRSF14* (9/20, 45%), *KMT2D* (9/20, 45%), *EZH2* (6/20, 30%), *FOXO1* (3/20, 15%), *MEF2B* (2/20, 10%), *GNA13* (2/20, 10%), *HIST1H1E* (2/20, 10%), *HIST1H1B* (1/20, 5%), *HIST1H1D* (1/20, 5%) and *EP300* (1/20, 5%). *HIST1H1C* showed no mutations (**Figure 17**). Only *CREBBP* showed statistically significant differences between the two cohorts (20/44, 45% in FLneg vs. 15/20, 75% in FLpos, **Figure 18**).

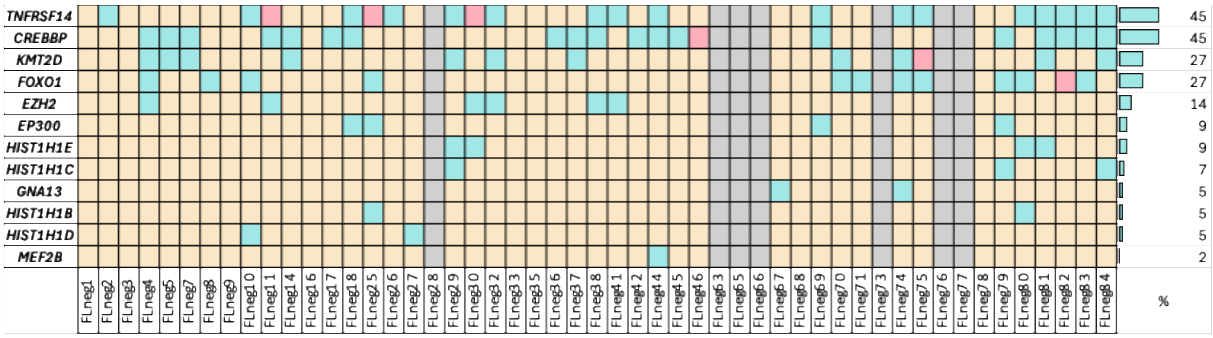


**Figure 16: Mutation matrix of FLneg cohort analyzed via FLpos panel.**
FLneg1 – Flneg67 were already characterized in [60], FLneg68 – Flneg84 were analyzed as part of this thesis. *CREBBP* and *TNFRSF14* were the most frequent mutations (20/44, 45%). Light yellow = wild-type, aqua = mutation, rose = > 1 mutation, grey = not done due to missing material/low DNA quality, 7 cases were excluded due to missing material/low DNA quality, n=44.

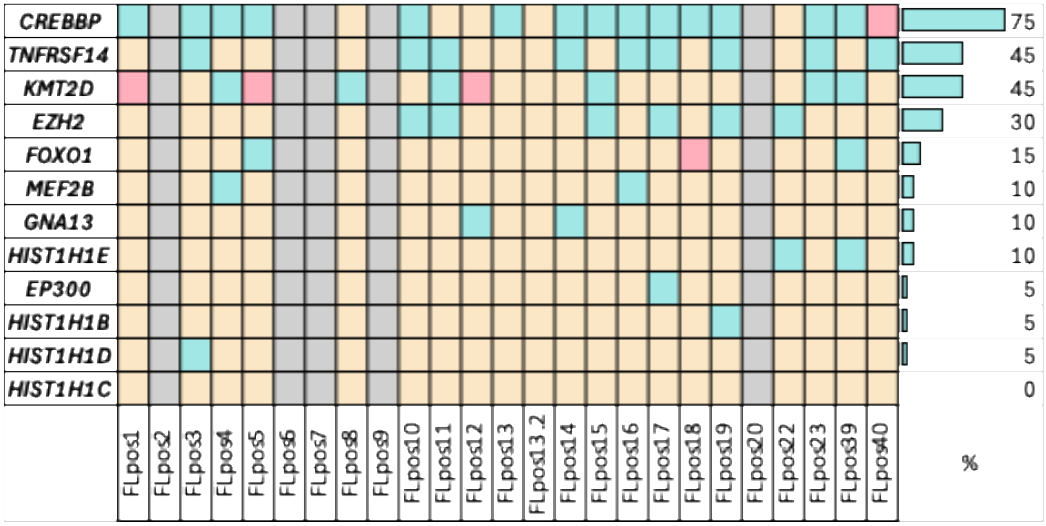


**Figure 17: Mutation matrix of FLpos cohort analyzed via FLpos panel.**
*CREBBP* was the most frequent mutation (15/20, 75%). Light yellow = wild-type, aqua = mutation, rose = > 1 mutation, grey = not done due to missing material/fixation artifacts, 5 cases were excluded due to missing material/fixation artifacts, n=20.

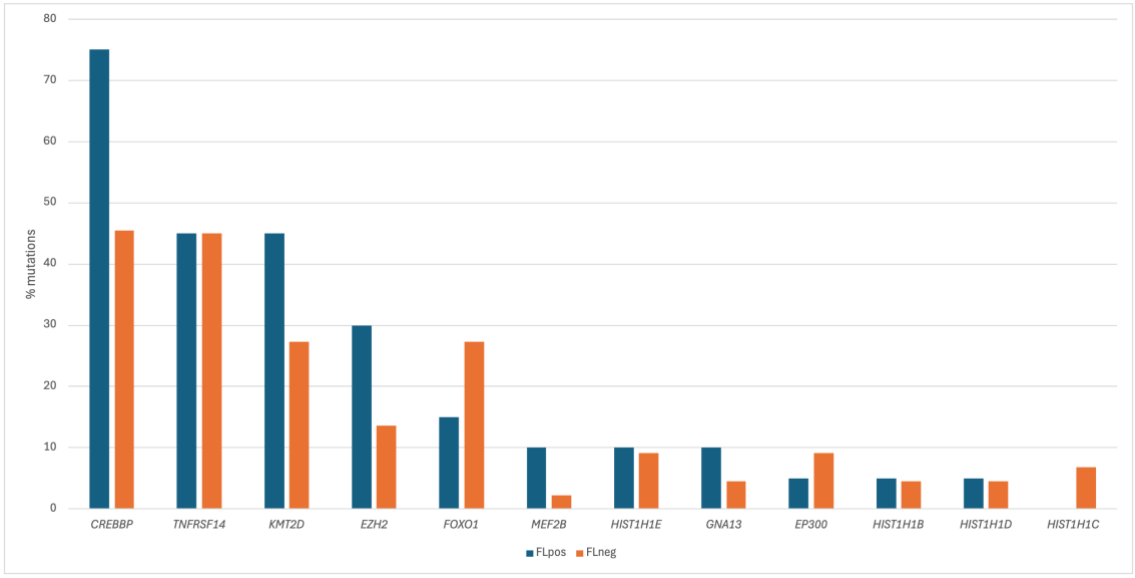


**Figure 18: Comparison of FLpos panel results between FLpos and FLneg cohort.**
*CREBBP* is the only gene which shows a statistically significant difference between FLneg and FLpos. $\chi^2(1) = 7.260$, $p \approx 0.01$. Fisher's exact test, $p = 0.01$; OR = 4.7, 95% CI = 1.5 – 13.0. Genes with $p < 0.05$ were considered as significant. The remaining genes showed $p > 0.05$ and were not considered as significant. Statistics were calculated using GraphPad Prism 10.

### 4.1.3 Oncomine Lymphoma III Analysis

During the analysis of the FLneg cohort using the FLneg panel, 14 FLneg cases were identified that lacked mutations in *STAT6/SOCS1* (**Figure 13**).

To identify additional potential drivers for tumorigenesis and pathway associated gene mutations, a mutation analysis on these cases using the Oncomine Lymphoma III panel was performed. This panel included an extended number of 78 lymphoma-associated genes (**Table 29**). 14 cases were analyzed. Due to restricted DNA integrity and quality which resulted in numerous panel artifacts, FLneg2 and FLneg16 could not be evaluated. In 10/12 cases, additional mutations were identified. Only FLneg3 and FLneg46 remained wild-type for all examined genes. The most frequently mutated genes were *ATM*, *TMSB4X*, and *TET2* (3/12, each 25%). Notably, all three genes exhibited multiple mutations in at least one case (**Figure 19**).

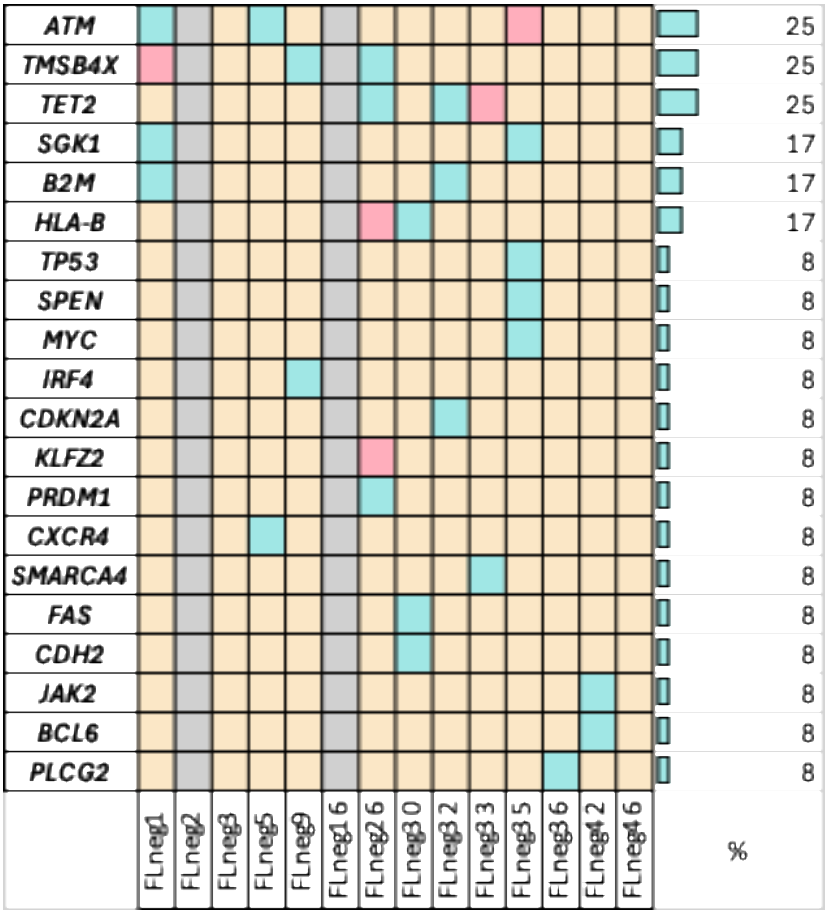


**Figure 19: Mutation matrix of *STAT6/SOCS1*$^{wt}$ FLneg cohort analyzed via Oncomine Lymphoma III panel.**
Additional mutations were found in 10/12 cases, except for FLneg3 and FLneg46. Light yellow = wild-type, aqua = mutation, rose = > 1 mutation, grey = not done due to excessive fixation artifacts, n = 12.

### 4.1.4 Group Formation

FL cases were grouped by presence of t(14;18) and mutational state of *STAT6* and/or *SOCS1* (**Table 12**). CD23 IHC was checked for each case since it was considered as surrogate marker for *STAT6*/*SOCS1* mutations and pathway activation. If not already stained in routine diagnostics and material was available, staining was performed subsequently. Based on mutation status FL subgroups were assigned to: "FLneg$^{m}$", which referred to t(14;18)-negative *STAT6* and/or *SOCS1* mutated FL and "FLpos$^{m}$", which referred to t(14;18)-positive *STAT6* and/or *SOCS1* mutated FL. The same principle was applied for *STAT6*/*SOCS1*$^{wt}$ cases.

**Table 12: Group formation of FL cases**
FL cases were grouped by t(14;18) presence and mutational status of *STAT6*/*SOCS1*

| Cohort | ***STAT6/SOCS1*$^{m}$** | ***STAT6/SOCS1*$^{wt}$** |
|---|---|---|
| FLneg | 37 | 14 |
| FLpos | 13 | 15 |

Regarding FLneg$^{BCL6\text{-}R}$ no additional separations were performed.

## 4.2 *IL4R* Pathway Mutation Analysis

*STAT6* and *SOCS1* belong to the IL4R signaling pathway [103]. Due to the increasing frequency of *STAT6* and *SOCS1* mutations in FLneg, further genes associated to IL4R pathway were investigated. For that reason, a customized panel covering the following genes was developed: *IL4R*, *PTPN1*, *IL13RA1*, *TYK2*, *JAK1*, *JAK2*, *JAK3*, *DUSP2*, *PTPRD*, *STAT3* and *SOCS3*. 19 FLneg$^{m}$, 11 FLneg$^{wt}$, 9 FLpos$^{m}$ and 7 FLpos$^{wt}$ were included into analysis. Among the FLneg cases, only FLneg27$^{m}$, FLneg46$^{wt}$, and FLneg79$^{m}$ displayed additional IL4R pathway-associated mutations. FLneg27$^{m}$ and FLneg46$^{wt}$ each presented a *STAT3* mutation, while FLneg79$^{m}$ carried a *JAK1* mutation (**Figure 20**). In the FLpos cohort, two cases, FLpos18$^{m}$ and FLpos23$^{wt}$, demonstrated additional mutations. FLpos18$^{m}$ presented one mutation in *TYK2* and three mutations in *SOCS3*, while FLpos23$^{wt}$ exhibited a mutation in *PTPRD* (**Figure 21**).

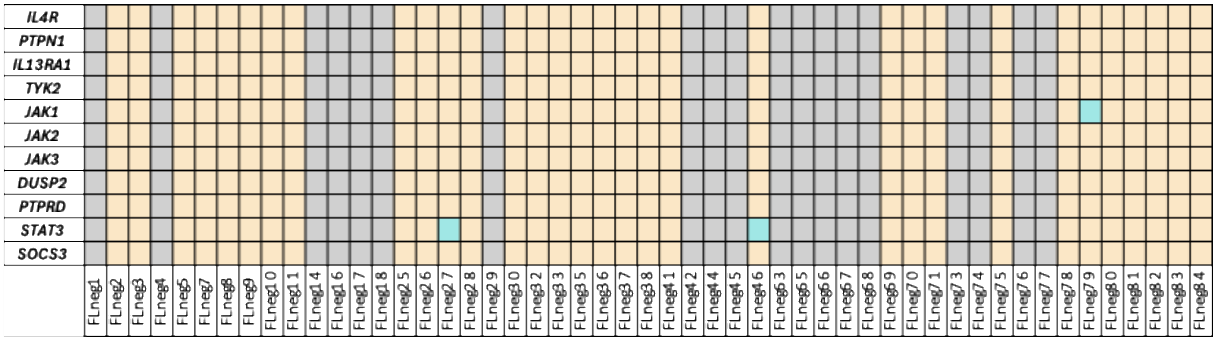


**Figure 20: Mutation analysis of FLneg using customized IL4R panel.**
3/30 cases showed additional mutations. FLneg27$^{m}$ and FLneg46$^{wt}$ harbored an additional *STAT3* mutation, while FLneg79$^{m}$ carried a *JAK1* mutation. Light yellow = wild-type, aqua = mutation, grey = not done due to excessive fixation artifacts, n = 30.

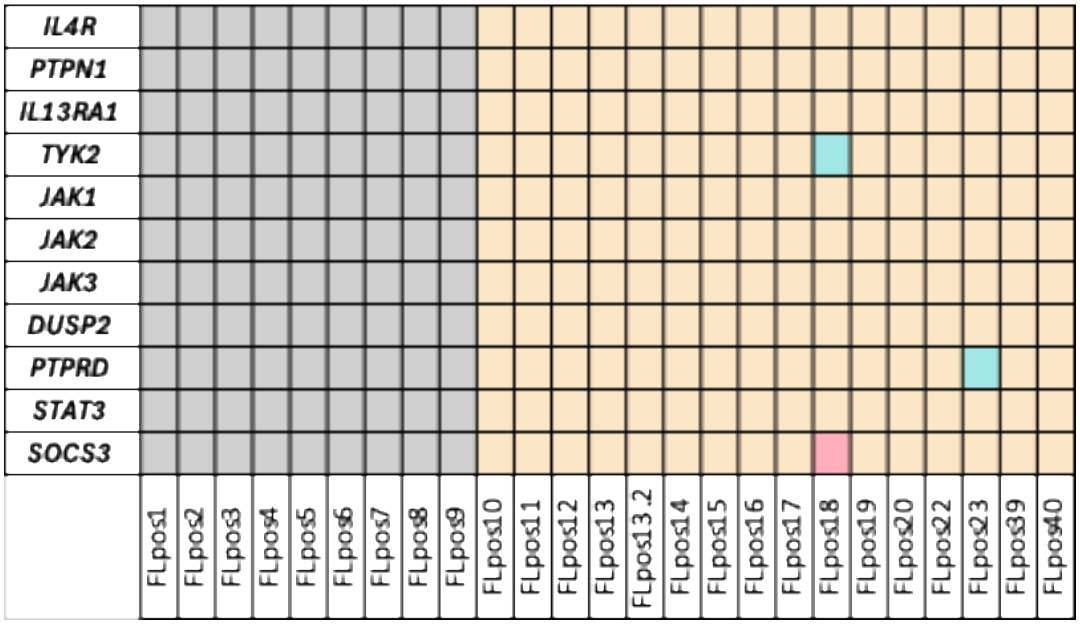


**Figure 21: Mutation analysis of FLpos using customized IL4R panel.**
2/16 cases showed additional mutations. FLpos18$^{m}$ harbored an additional *TYK2* mutation as well as three *SOCS3* mutations, FLpos23$^{wt}$ carried a *PTPRD* mutation. Light yellow = wild-type, aqua = mutation, rose = < 1 mutation, grey = not done due to excessive fixation artifacts, n = 16

In summary, IL4R pathway-associated mutations were found in 5/46 FL cases.

## 4.3 Gene Expression Profiling of FLneg and FLpos

GEP was conducted to investigate previously determined FL subgroups at the transcriptional level. For this approach, two GEP methods were employed: HTG and NanoString. The panels used for experiments (HTG Precision Immuno-Oncology and NanoString Immune Profiling) showed 607 overlapping genes. 783 genes were specific for HTG, 123 for NanoString (Appendix **Table 33**). The different number of unique genes between the two panels results from the fact that the HTG panel covers twice as many genes as the NanoString panel. Whenever possible, the same FLneg and FLpos cases were used. Due to material scarcity and method-specific QC failures, the number of cases analyzed per method varied: In HTG analysis, 4 FL cases (FLneg63$^{m}$, FLpos13$^{m}$, FLpos16m and FLpos18$^{m}$) were excluded. In NanoString analysis, 12 FL cases (FL18$^{m}$, FL35$^{wt}$, FL67$^{m}$, FL69$^{m}$, FL73$^{m}$, FL78$^{m}$, FL82$^{m}$, FL83$^{m}$, FLpos2$^{m}$, FLpos8$^{m}$, FLpos11$^{m}$ and FLpos40$^{m}$) were excluded (**Figure 22**).

| Case | HTG | NanoString |
|---|---|---|
| FLneg1wt | | |
| FLneg2wt | | |
| FLneg3wt | | |
| FLneg4m | | |
| FLneg5wt | | |
| FLneg7m | | |
| FLneg8m | | |
| FLneg9wt | | |
| FLneg10m | | |
| FLneg11m | | |
| FLneg14m | | |
| FLneg16wt | | |
| FLneg17m | | |
| FLneg18m | | |
| FLneg25m | | |
| FLneg26wt | | |
| FLneg27m | | |
| FLneg28m | | |
| FLneg29m | | |
| FLneg30wt | | |
| FLneg32wt | | |
| FLneg33wt | | |
| FLneg35wt | | |
| FLneg36wt | | |
| FLneg37m | | |
| FLneg38m | | |
| FLneg41m | | |
| FLneg42wt | | |
| FLneg44m | | |
| FLneg45m | | |
| FLneg46m | | |
| FLneg63m | | |
| FLneg67m | | |
| FLneg68m | | |
| FLneg69m | | |
| FLneg70m | | |
| FLneg71m | | |
| FLneg73m | | |
| FLneg74m | | |
| FLneg75m | | |
| FLneg76m | | |
| FLneg77m | | |
| FLneg78m | | |
| FLneg80m | | |
| FLneg81m | | |
| FLneg82m | | |
| FLneg83m | | |
| FLneg84m | | |
| | | |
| FLpos2m | | |
| FLpos8m | | |
| FLpos11m | | |
| FLpos13m | | |
| FLpos13.2m | | |
| FLpos14m | | |
| FLpos16m | | |
| FLpos18m | | |
| FLpos20m | | |
| FLpos39m | | |
| FLpos40m | | |

**Figure 22: FLneg and FLpos cases used in gene expression profiling with either HTG, NanoString or both.**
43 cases were used in both methods, 12 cases only in HTG and 4 cases only in NanoString. Cases excluded for both analyses not shown. Green = used, orange = not included due to low RNA concentration or RNA integrity.

### 4.3.1 HTG Analysis

HTG method was applied to perform GEP on FLneg and FLpos cases using the Precision Immuno-Oncology Panel, encompassing 1,392 genes. A total of 34 FLneg$^{m}$ and 13 FLneg$^{wt}$ cases were analyzed. FLneg79$^{m}$ and FLneg63$^{m}$ could not be used due to insufficient material and were excluded from the analysis. The generated FASTQ files were processed using HTG parser software to extract raw gene counts, facilitating their analysis with DESeq2 algorithm. A total of 40 differentially expressed genes (DEGs) were identified (**Figure 23**). From the perspective of FLneg$^{m}$, 26 genes were upregulated compared to FLneg$^{wt}$, while 14 genes were downregulated. The top upregulated genes included *FCER2* (CD23), *IL4R*, *CCL17*, *CD83*, *ALOX5*, *IL17RB*, *MME* (CD10), *ELL3*, *CD40*, and *GPR18*. Conversely, the top downregulated genes represented *SLAMF7*, *FCRLA*, *TNFRSF13B* (TACI), *FCGR2B*, *C1QB*, *CXCL10*, *FCGR1A_FCGR1B, MNDA*, *IRF4*, and *LAG3* (**Table 13**). Whole DEG list can be found in appendix (**Table 34**).

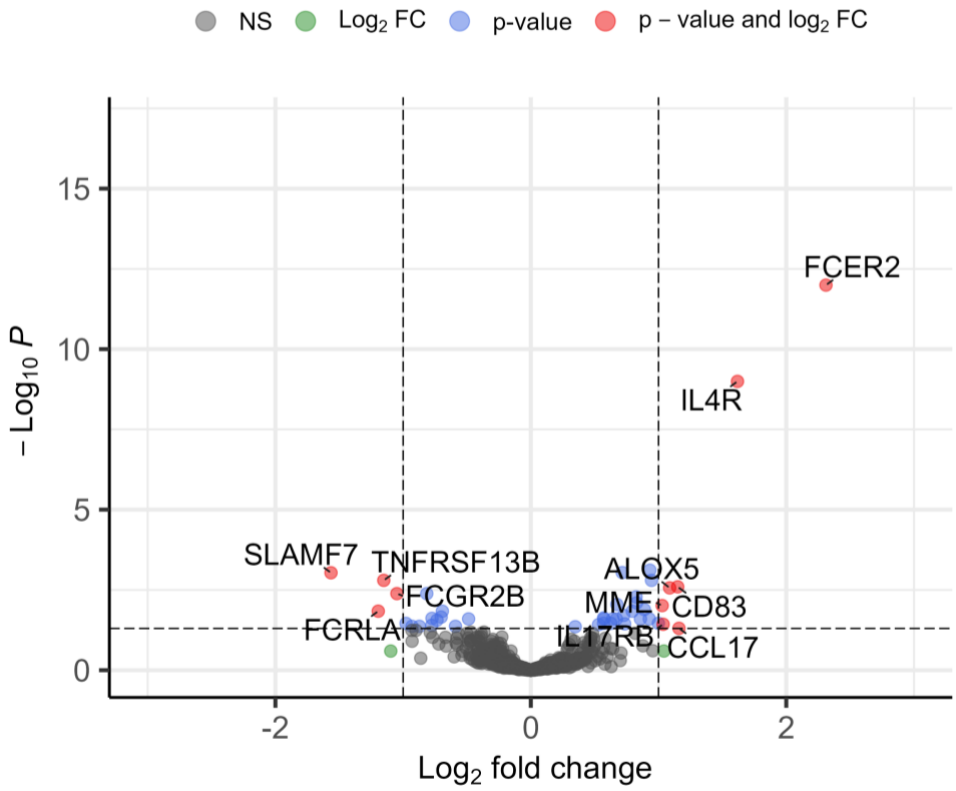


**Figure 23: Volcano Plot depicting differential gene expression analysis comparing FLneg$^{m}$ against FLneg$^{wt}$ using HTG technology.**
The x-axis represents $log_2$ fold change, the y-axis $-log_{10}$ p-adj-value. Genes with p-adj. ≤ 0.05 and FC -1.5/+1.5 were considered as significant. Volcano plot was created using DESeq2 package in R, n = 47.

**Table 13: Top 10 up- and downregulated genes after gene expression analysis from the perspective of FLneg$^{m}$ vs. FLneg$^{wt}$ using HTG technology**
FC threshold +1.5/-1.5 and p-adj. ≤ 0.05 were considered as significant

| Genes | Description | FC | padj |
|---|---|---|---|
| *FCER2* (CD23) | Fc Fragment of IgE Receptor II | 5.0 | 0.00 |
| *IL4R* | Interleukin 4 Receptor | 3.1 | 0.00 |
| *CCL17* | C-C Motif Chemokine ligand 17 | 2.2 | 0.05 |
| *CD83* | CD83 | 2.2 | 0.00 |
| *ALOX5* | Arachidonate 5-Lipoxygenase | 2.1 | 0.00 |
| *IL17RB* | Interleukin 17 Receptor B | 2.1 | 0.04 |
| *MME* (CD10) | Membrane Metalloendoproteinase | 2.0 | 0.01 |
| *ELL3* | Elongation Factor for RNA Polymerase II-like 3 | 2.0 | 0.03 |
| *CD40* (TNFRSF5) | Tumor Necrosis Factor Receptor Superfamily Member 5 | 1.9 | 0.00 |
| *GPR18* | G Protein-coupled Receptor 18 | 1.9 | 0.00 |
| *LAG3* | Lymphocyte activation gene 3 | -1.7 | 0.02 |
| *IRF4* | Interferon Regulatory Factor 4 | -1.7 | 0.04 |
| *MNDA* | Myeloid Cell Nuclear Differentiation Antigen | -1.8 | 0.00 |
| *FCGR1A_FCGR1B* | Fc Fragment of IgG Receptor IA and IB | -1.8 | 0.04 |
| *CXCL10* | C-X-C Motif Chemokine Ligand 10 | -1.9 | 0.04 |
| *C1QB* | Complement C1q B Chain | -2.0 | 0.03 |
| *FCGR2B* | Fc Fragment of IgG Receptor IIB | -2.1 | 0.00 |
| *TNFRSF13B* (TACI) | Tumor Necrosis Factor Receptor Superfamily Member 13B | -2.2 | 0.00 |
| *FCRLA* | Fc Receptor-like A | -2.3 | 0.01 |
| *SLAMF7* (CD319) | SLAM family member 7 | -3.0 | 0.00 |

To verify whether both groups could be distinguished based on the DEGs, hierarchical clustering was performed (**Figure 24**). Here, samples were grouped automatically based on expression similarity and co-expression patterns. This approach allowed the identification of clear differences in gene expression between FLneg$^{m}$ and FLneg$^{wt}$. All cases, except for FLneg16$^{wt}$, clustered within their respective group. Furthermore, additional peculiarities were observed within the FLneg$^{m}$ cluster: FLneg80$^{m}$ and FLneg84$^{m}$ were each clustered at the margins. FLneg80$^{m}$ exhibited relatively low *TNFRSF13B* expression compared to the other cases but showed high expression of *FCER2* (CD23), *IL4R*, and *CD83*, along with a markedly increased *CCL17* expression. In contrast, FLneg84$^{m}$ displayed strong *IL4R* and *FCER2* (CD23) expression but had noticeably lower *CD83* and *CCL17* expression. Within FLneg$^{wt}$ group, FLneg2$^{wt}$ displayed exceptionally high expression levels of *FCRLA* and *SLAMF7*. Interestingly, subclusters appeared within the FLneg$^{m}$ cluster. In general, three subclusters could be identified. Cluster 1 (left) and Cluster 2 (center) were characterized by strong expression of *IL4R*, *FCER2*, and *CD83*. In Cluster 2, a higher expression of *ALOX5* and *FCRLA* was found in comparison. Cluster 3 (right) exhibited an overall weaker pattern of *IL4R*, *FCER2*, and *CD83* expression. It appeared that *STAT6* pathway activation decreases from Cluster 1 to Cluster 3, while the expression level of differentiation genes increased. To identify possible correlation with gene mutations, the results of the mutation analysis (FLneg,

FLpos and IL4R panel) were examined in the context of the subclusters. It was noted that the mutational burden steadily decreased from Cluster 1 to the wild-type group. The cases in Cluster 1 showed 4.1 mutations/case, in Cluster 2 3.3 mutations/case, in cluster 3 2.8 mutations/case and in wild-type group 1.3 mutations/case. When examining the most frequently mutated genes within the clusters, it became evident that *STAT6* and *SOCS1* exhibited different mutation frequencies. In Cluster 1, 91% (10/11) of cases exhibited a *STAT6* mutation, while 64% (7/11) carried a *SOCS1* mutation, 55% (6/11) were both *STAT6* and *SOCS1* mutated. In Cluster 2, 100% (9/9) of cases had a *STAT6* mutation and one of this case showed an additional *SOCS1* mutation (1/9, 11%). In Cluster 3, 67% (10/15) of cases showed a *STAT6* mutation, while 20% (3/15) were *SOCS1* mutated. None of the cases had concurrent *STAT6* and *SOCS1* mutations. In summary, clustering of both entities was successfully achieved using HTG data.

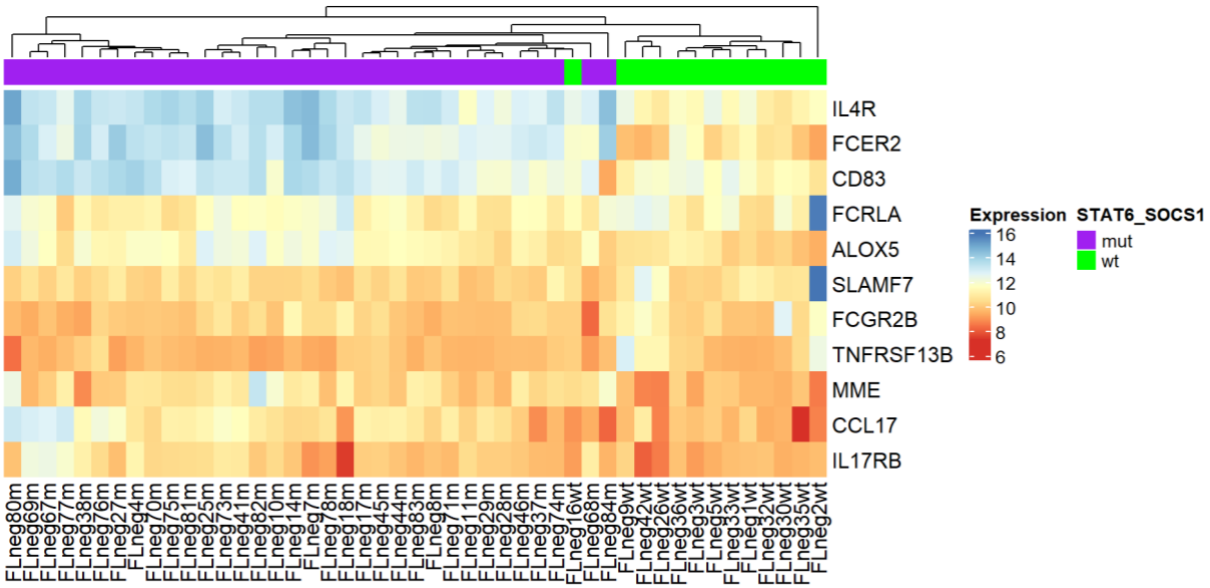


**Figure 24: Heatmap of GEP FLneg$^{m}$ vs. FLneg$^{wt}$ using HTG technology.**
Hierarchical clustering of significant DEGs (FC: +/- 1.5, p-adj. < 0.05), n = 47. Expression indicates normalized expression values, from low (red) to high (blue). The purple cases represent FLneg$^{m}$ while the green cases represent FLneg$^{wt}$. In both groups cases cluster together according to their gene expression profiles. FLneg16$^{wt}$ is the only group outlier, which was slightly shifted towards FLneg$^{m}$ group. Heatmap was created using DESeq2 package in R.

Next, FLneg$^{m}$ and FLpos$^{m}$ were evaluated on exhibiting different transcriptional activities. For that reason, GEP of FLneg$^{m}$ vs. FLpos$^{m}$ was performed. 34 FLneg$^{m}$ cases from the previous analysis were compared to 8 FLpos$^{m}$ from the FLpos collective, which provided sufficient RNA quality. 6 DEGs were identified (**Table 14**, **Figure 25**). It appeared that both *BCL2* and, to some extent, *GZMK* influenced clustering of the two groups (**Figure 26**). FLneg67$^{m}$ was identified as outlier, which was in the FLpos$^{m}$ cluster.

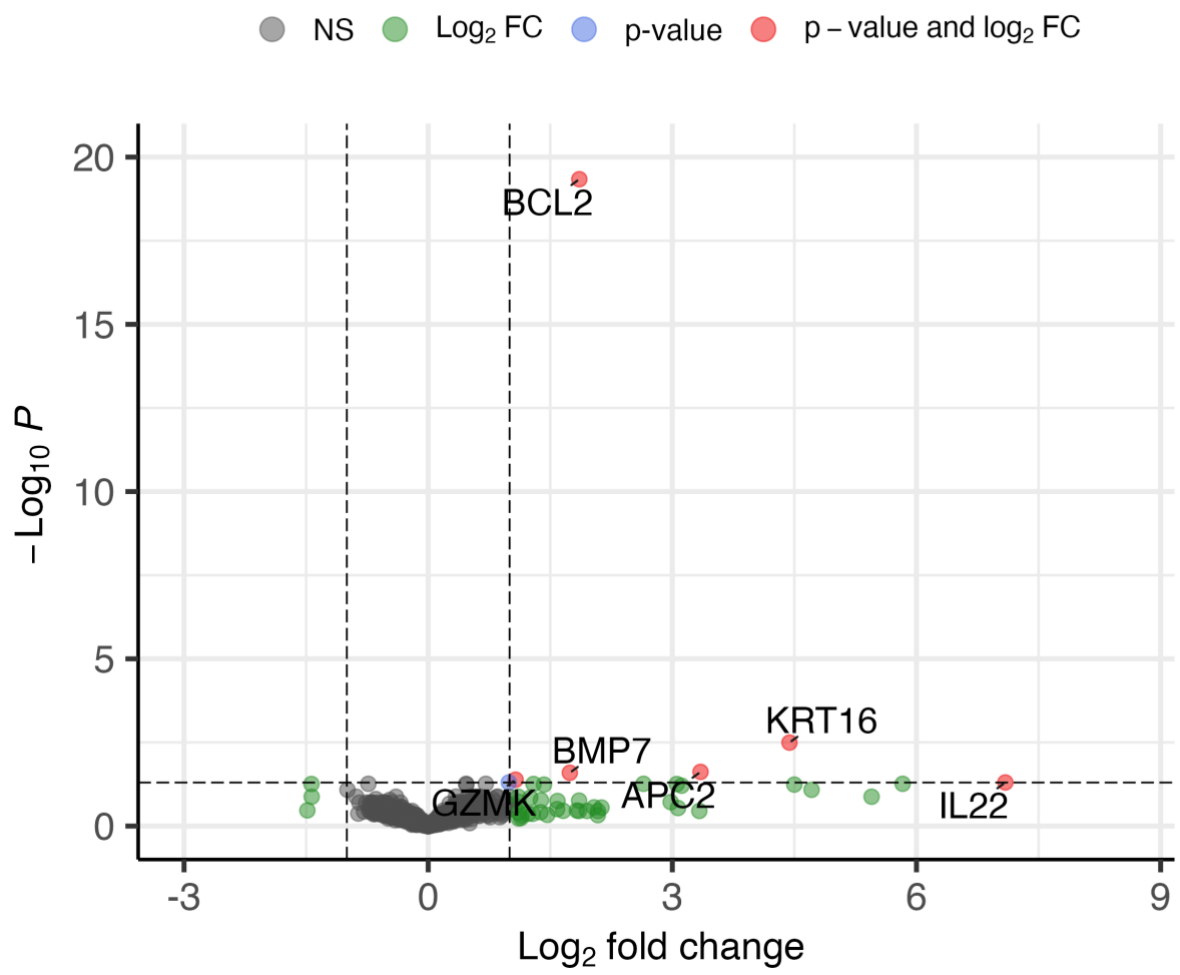


**Figure 25: Volcano Plot depicting differential gene expression analysis comparing FLpos$^{m}$ against FLneg$^{m}$ using HTG technology**
The x-axis represents $log_2$ fold change, the y-axis $-log_{10}$ p-adj-value. Genes with p-adj. ≤ 0.05 and FC -1.5/+1.5 were considered as significant. Volcano plot was created using DESeq2 package in R, n = 42.

**Table 14: Up- and downregulated genes after gene expression analysis from the perspective of FLpos$^{m}$ vs. FLneg$^{m}$ (HTG)**
FC threshold +1.5/-1.5 and p-adj. ≤ 0.05 were considered as significant

| Genes | Description | FC | padj |
|---|---|---|---|
| *IL22* | Interleukin 22 | 136 | 0.05 |
| *KRT16* | Keratin 16 | 22 | 0.00 |
| *APC2* | APC Regulator of WNT Signaling Pathway 2 | 10 | 0.02 |
| *BCL2* | B-Cell Lymphoma 2 | 4 | 0.00 |
| *BMP7* | Bone Morphogentic Protein 7 | 3 | 0.03 |
| *GZMK* | Granzyme K | 2 | 0.04 |

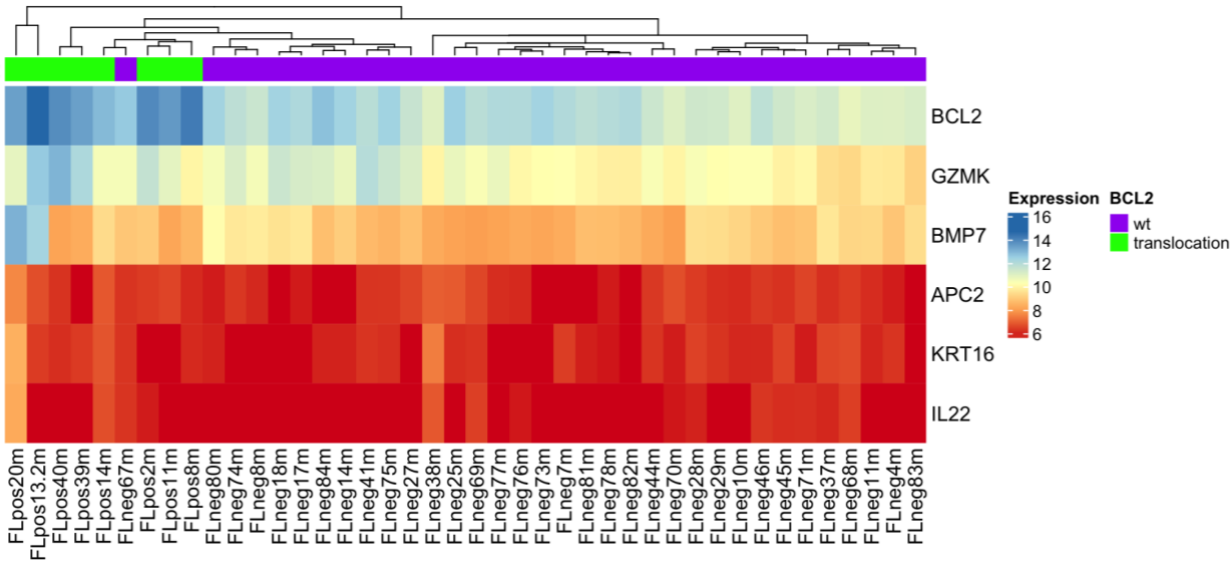


**Figure 26: Heatmap of GEP FLpos$^{m}$ vs. FLneg$^{m}$ using HTG technology.**
Hierarchical clustering of significant DEGs (FC: +/- 1.5, p-adj. ≤ 0.05), n = 42. Expression indicates normalized expression values, from low (red) to high (blue). The purple cases represent FLneg$^{m}$, while the green cases represent FLpos$^{m}$. In both groups cases cluster together according to their gene expression profiles. FLneg67$^{m}$ is the only outlier, which was located within FLpos$^{m}$ group. Heatmap was created using DESeq2 package in R.

### 4.3.2 NanoString Analysis

To generate a more robust dataset, another GEP method using the nCounter NanoString Immune Profiling panel was conducted, comparing gene expression of FLneg$^{m}$ to FLneg$^{wt}$. For this purpose, 28 FLneg$^{m}$ cases and 12 FLneg$^{wt}$ cases were successfully analyzed. 11 cases were excluded from the analysis: Seven cases exhibited a DV200 value below 25% and/or an insufficient RNA concentration (unable to achieve the required 50 ng input RNA). These cases included FLneg18$^{m}$, FLneg35$^{wt}$, FLneg65$^{m}$, FLneg66$^{m}$, FLneg78$^{m}$, FLneg79$^{m}$, FLneg82$^{m}$ and FLneg83$^{m}$. One case showed a housekeeping gene error (below 50 counts) and was therefore excluded from the analysis (FLneg67$^{m}$). This case was already identified as outlier in HTG analysis FLneg$^{m}$ vs. FLpos$^{m}$, where FLneg67$^{m}$ clustered within the FLpos$^{m}$ group. Additionally, two cases had no remaining material available (FLneg69$^{m}$ and FLneg73$^{m}$). RCC files generated using NanoString technology were processed with nf-core/nanostring software and subsequently analyzed using DESeq2 algorithm. 74 DEGs were identified. The top 10 upregulated genes included *LTF*, *FCER2* (CD23), *CCL17*, *IL17RB*, *IL4R*, *MME* (CD10), *LY86*, *C3*, *TNFRSF17* and *CLEC4A*. *CEACAM6*, *CHIT1, FCGR2B, FCGR3A* (CD16A), *SLC11A1* (NRAMP1), *TNFRSF13B* (TACI), *C1QB*, *IFNG, LILRB3* and *CXCL11* were found to be top 10 downregulated genes (**Table 15**). Whole DEG list can be found in appendix (**Table 35**).

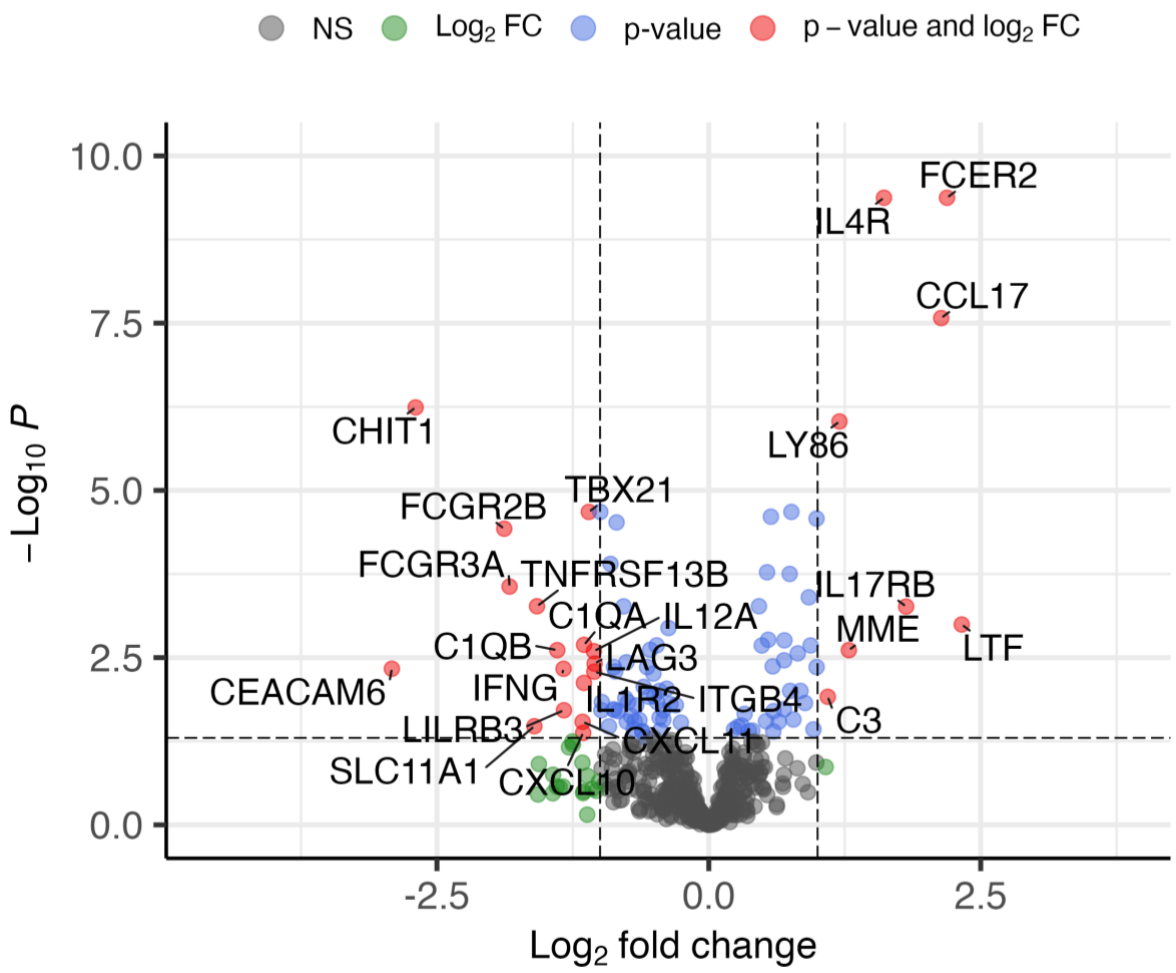


**Figure 27: Volcano Plot depicting differential gene expression analysis comparing FLneg$^{m}$ to FLneg$^{wt}$ using NanoString.** The x-axis represents $log_2$ fold change, the y-axis $-log_{10}$ p-adj-value. Genes with p-adj. < 0.05 and FC -1.5/+1.5 were considered as significant. Volcano plot was created using DESeq2 package in R, n = 40.

**Table 15: Top 10 up- and downregulated genes after gene expression analysis from the perspective of FLneg$^{m}$ vs. FLneg$^{wt}$ using NanoString technology**
FC threshold +1.5/-1.5 and p-adj. < 0.05 were considered as significant

| Genes | Description | FC | padj |
|---|---|---|---|
| *LTF* | Lactotransferrin | 5.0 | 0.00 |
| *FCER2 (CD23)* | Fc Fragment of IgE Receptor II | 4.6 | 0.00 |
| *CCL17* | C-C Motif Chemokine Ligand 17 | 4.4 | 0.00 |
| *IL17RB* | Interleukin 17 Receptor B | 3.5 | 0.00 |
| *IL4R* | Interleukin 4 Receptor | 3.1 | 0.00 |
| *MME* (CD10) | Membrane Metalloproteinase | 2.4 | 0.00 |
| *LY86* | Lymphocyte Antigen 86 | 2.3 | 0.00 |
| *C3* | Complement component C3 | 2.1 | 0.01 |
| *TNFRSF17* | Tumor Necrosis Factor Receptor Superfamily Member 17 | 2.0 | 0.00 |
| *CLEC4A* | C-Type Lectin Domain Family 4 Member A | 2.0 | 0.00 |
| *CXCL11* | C-X-C Motif Chemokine Ligand 11 | -2.2 | 0.02 |
| *LILRB3* | Leukocyte Immunoglobulin-Like Receptor Subfamily B Member 3 | -2.5 | 0.02 |
| *IFNG* | Interferon Gamma | -2.5 | 0.01 |
| *C1QB* | Complement C1q B Chain | -2.6 | 0.00 |
| *TNFRSF13B* (TACI) | Tumor Necrosis Factor Receptor Superfamily Member 13B | -3.0 | 0.00 |
| *SLC11A1* (NRAMP1) | Solute Carrier Family 11 Member 1 | -3.0 | 0.04 |
| *FCGR3A* (CD16) | Fc Fragment of IgG Receptor IIIA | -3.6 | 0.00 |
| *FCGR2B* | Fc Fragment of IgG Receptor IIB | -3.7 | 0.00 |
| *CHIT1* | Chitinase 1 | -6.5 | 0.00 |
| *CEACAM6* | Carcinoembryonic Antigen-Related Cell Adhesion Molecule 6 | -7.5 | 0.01 |

Here, it was also assessed whether FLneg$^{m}$ and FLneg$^{wt}$ cohorts could be distinguished based on the DEGs. Samples were grouped considering expression similarity and co-expression patterns. It was found that FLneg$^{m}$ and FLneg$^{wt}$ cohorts can be distinguished based on DEGs identified with NanoString. Interestingly, there were two FLneg$^{wt}$ clusters. A small cluster, which included FLneg42$^{wt}$, FLneg2$^{wt}$ and FLneg26$^{wt}$, and a larger cluster containing the remaining FLneg$^{wt}$ cases. Except for one case, FLneg16$^{wt}$ which was in the FLneg$^{m}$ cluster, the cases showed cluster according to their group (**Figure 28**).

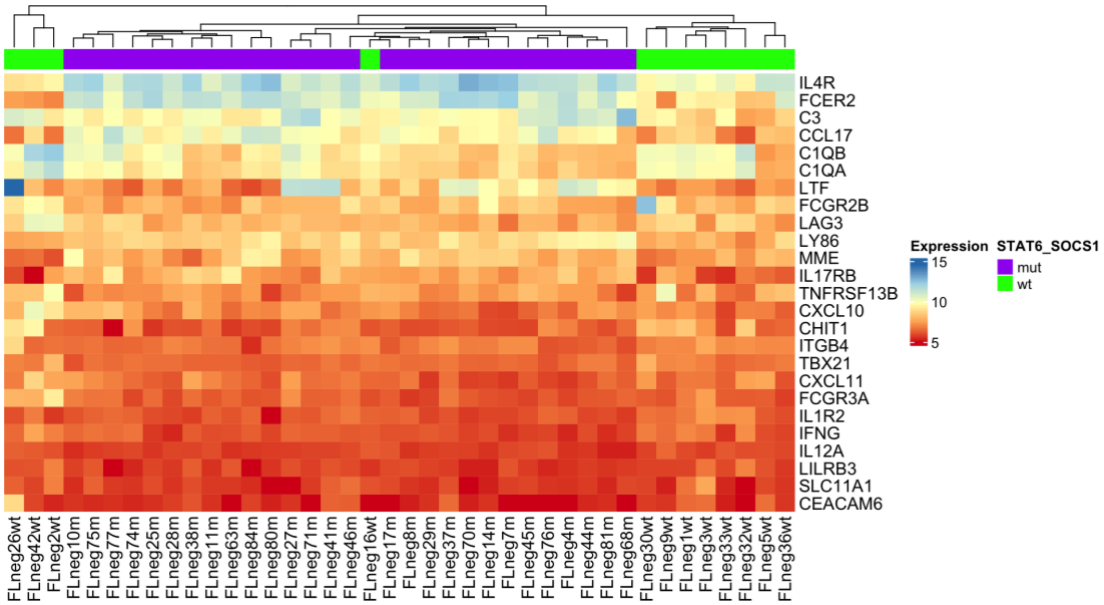


**Figure 28: Heatmap of GEP FLneg$^{m}$ vs. FLneg$^{wt}$ using NanoString technology.**
Hierarchical clustering of significant DEGs (FC: +/- 1.5, p-adj. < 0.05), n = 40. Expression indicates normalized expression values, from low (red) to high (blue). The purple cases represent FLneg$^{m}$, while the green cases represent FLneg$^{wt}$. Both groups cluster together according to their gene expression profiles except for FLneg16$^{wt}$. FLneg$^{wt}$ showed two clusters. Heatmap was created using DESeq2 package in R.

Additionally, GEP for FLpos$^{m}$ vs. FLneg$^{m}$ using NanoString technology was performed. 7 FLpos$^{m}$ were compared to 28 FLneg$^{m}$. 11 DEGs were identified (**Figure 29**, **Table 16**). FLpos$^{m}$ and FLneg$^{m}$ could be divided into distinct clusters based on the DEGs (**Figure 30**).

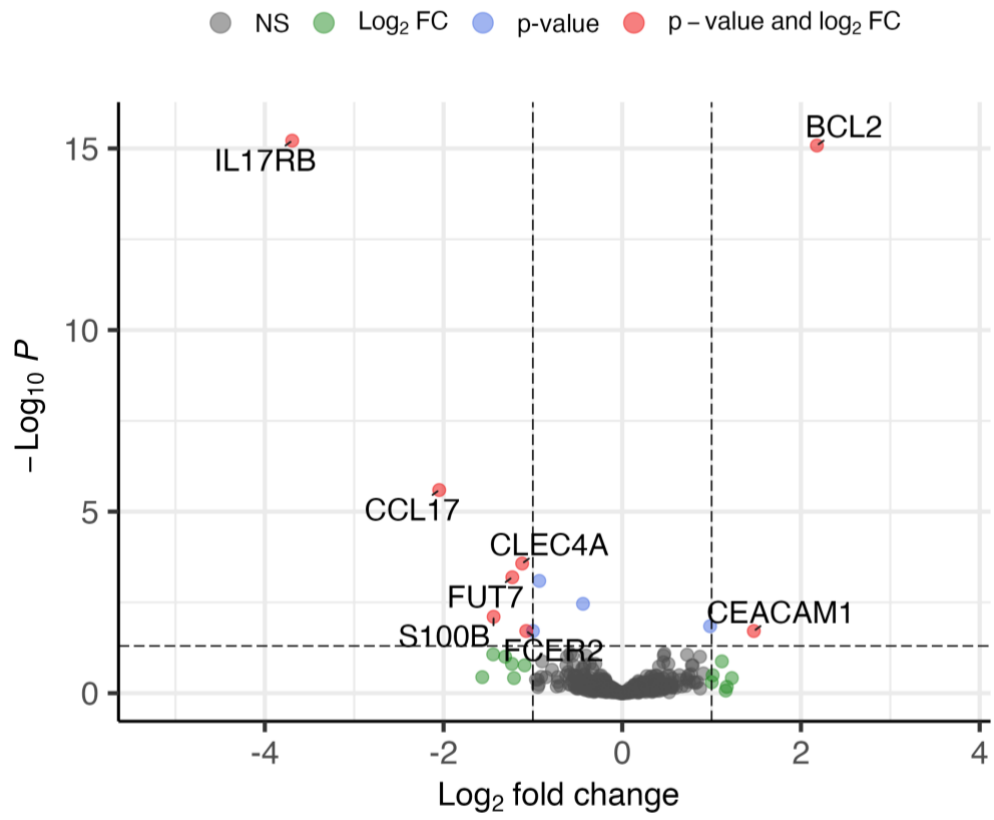


**Figure 29: Volcano Plot displaying differential gene expression analysis comparing FLpos$^{m}$ against FLneg$^{m}$ using NanoString technology**
The x-axis represents $log_2$ fold change, the y-axis $-log_{10}$ p-adj-value. Genes with p-adj. < 0.05 and FC -1.5/+1.5 were considered as significant. Volcano plot was created using DESeq2 package in R, n = 35.

**Table 16: Up- and downregulated genes after gene expression analysis using NanoString from the perspective of FLpos$^{m}$ vs. FLneg$^{m}$.**
FC threshold +1.5/-1.5 and p-adj. < 0.05 were considered as significant

| Genes | Description | FC | padj |
|---|---|---|---|
| *BCL2* | B-cell Lymphoma 2 | 4.5 | 0.00 |
| *CEACAM1* | Carcinoembryonic Antigen-Related Cell Adhesion Molecule 1 | 2.8 | 0.02 |
| *CCL3* | C-C Motif Chemokine Ligand 3 | 2.0 | 0.01 |
| *SELL* | Selectin L | -1.9 | 0.00 |
| *IL21* | Interleukin 21 | -2.0 | 0.02 |
| *FCER2* (CD23) | Fc Fragment of IgE Receptor II | -2.1 | 0.02 |
| *CLEC4A* | C-Type Lectin Domain Family 4 Member A | -2.2 | 0.00 |
| *FUT7* | Fucosyltransferase 7 | -2.3 | 0.00 |
| *S100B* | S100 Calcium Binding Protein B | -2.7 | 0.01 |
| *CCL17* | C-C Motif Chemokine Ligand 17 | -4.1 | 0.00 |
| *IL17RB* | Interleukin 17 Receptor B | -12.9 | 0.00 |

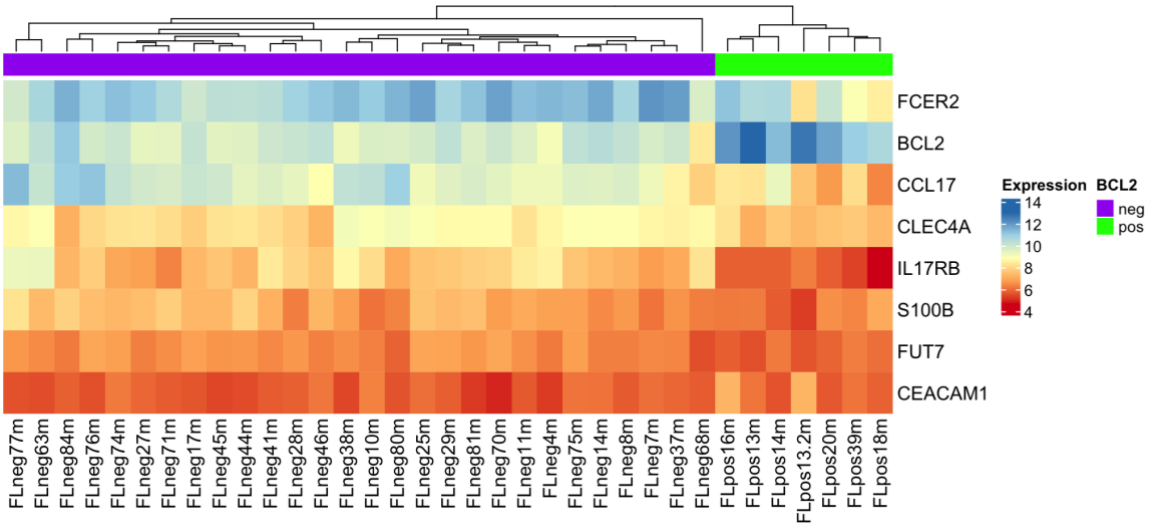


**Figure 30: Heatmap of GEP FLpos$^{m}$ vs. FLneg$^{m}$ using NanoString technology**
Hierarchical clustering of significant DEGs (FC: +/- 1.5, p-adj. < 0.05), n = 35. Expression indicates normalized expression values, from low (red) to high (blue). The purple cases represent FLneg$^{m}$, while the green cases represent FLpos$^{m}$. In both groups cases cluster together according to their gene expression profiles.

### 4.3.3 Comparison of HTG and NanoString Data

Using HTG and NanoString technologies, GEP of FLneg and FLpos subtypes was performed. This allowed the identification of DEGs that were significant across both panels, as well as DEGs that were detected exclusively by one of the panels.

First, the aim was to compare the results of GEP methods HTG and NanoString comparing FLneg$^{m}$ against FLneg$^{wt}$. Using HTG, 40 DEGs were detected, while NanoString identified 71 DEGs. 22 common DEGs were identified using both HTG and NanoString (**Figure 31**, **Figure 32**). The top upregulated genes included *FCER2* (CD23), *IL4R* and *CCL17*. Overall, the fold changes observed were generally very similar. However, *CCL17* and *IL17RB* exhibited an approx. twofold higher fold change with NanoString compared to HTG, while *SLAMF7* showed also differences in fold change (**Figure 33**).

18 DEGs were detected exclusively with HTG. Of these, 11 were not included in the NanoString panel, while 7 were present but did not reach significance, since 6 genes did not reach p-adj. and FC, one gene did not reach p-adj. (**Table 17**).

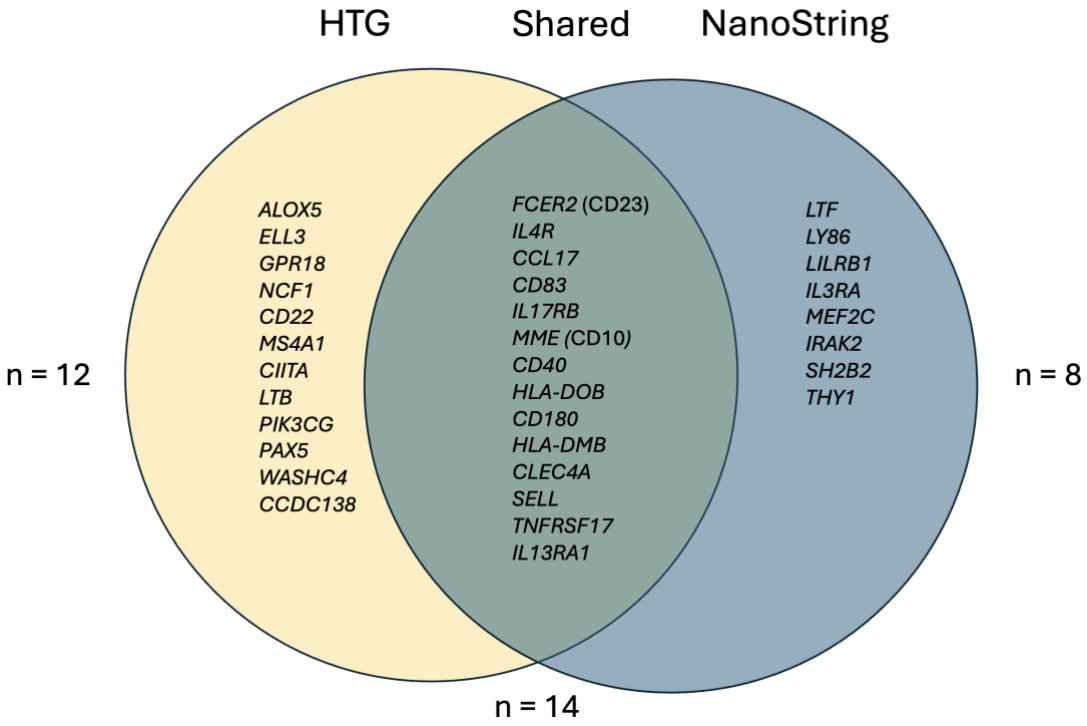


**Figure 31: Upregulated genes in both HTG and NanoString FLneg$^{m}$.**
HTG and NanoString shared 14 upregulated genes, while 12 genes were only upregulated in HTG and 8 in NanoString.

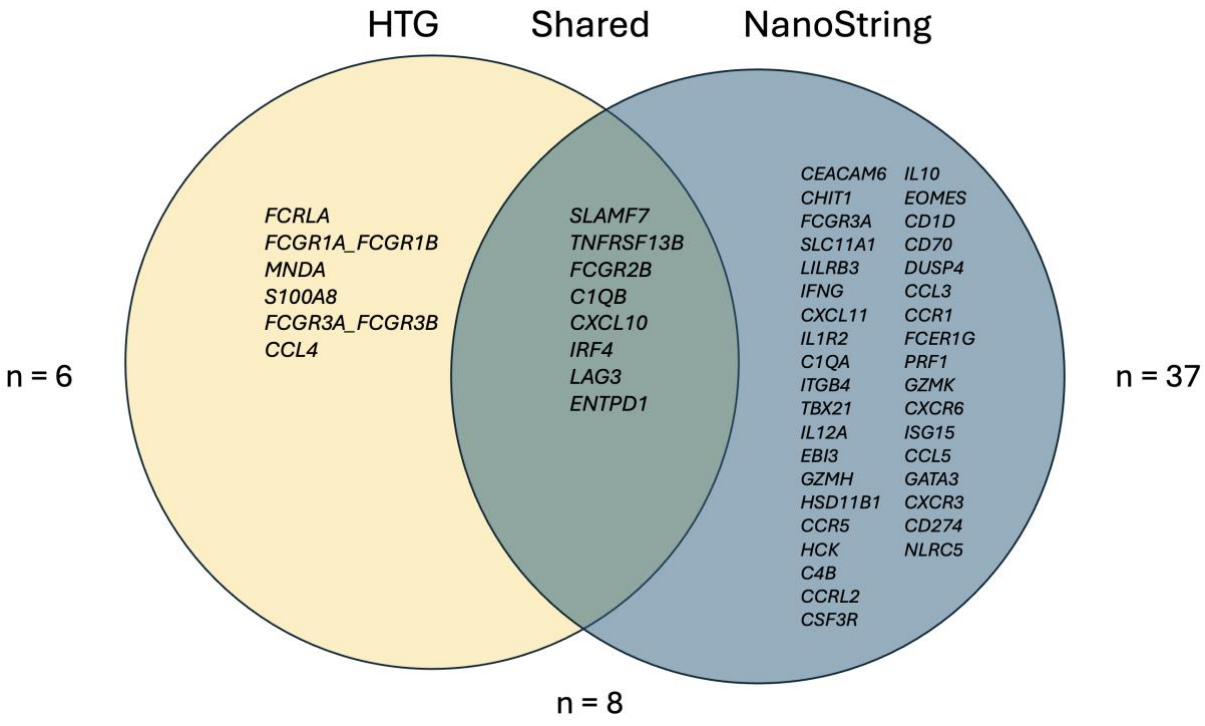


**Figure 32: Upregulated genes in both HTG and NanoString FLneg$^{wt}$.**
HTG and NanoString shared 8 upregulated genes, while 6 genes were only upregulated in HTG and 37 in NanoString.

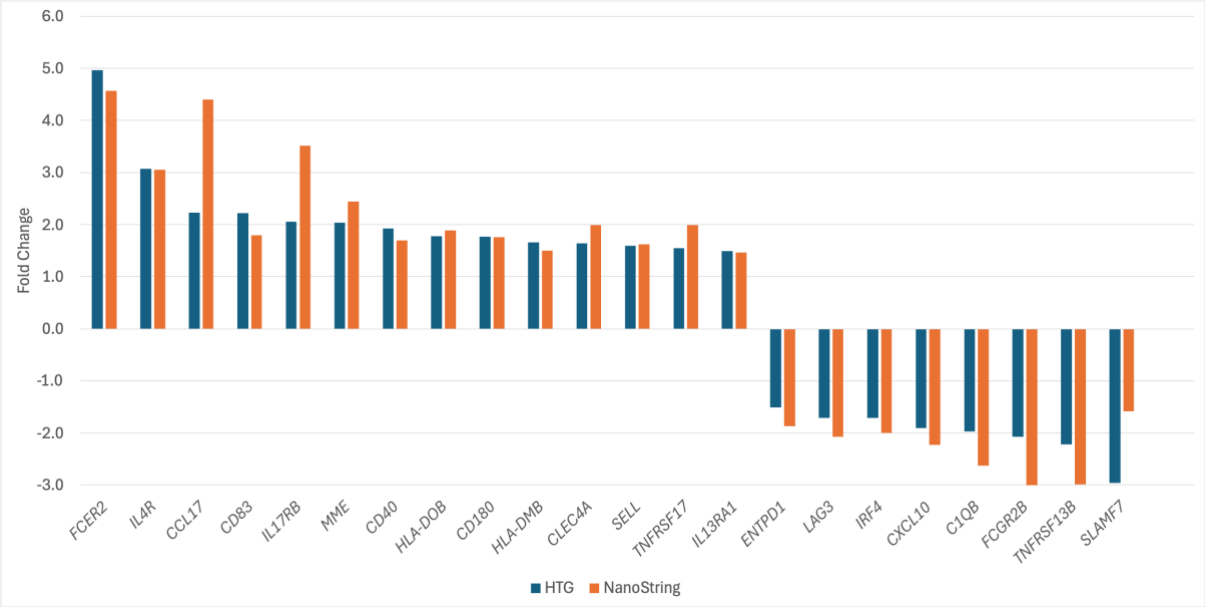


**Figure 33: Comparison of shared significant DEGs obtained from HTG and NanoString analysis.**
Perspective from FLneg$^{m}$ vs. FLneg$^{wt}$, n = 22.

Regarding NanoString DEGs only, 52 unique genes were found, of which 31 did not meet the p-adj. and FC criteria, 3 genes lacked FC threshold, and 12 genes did not reach p-adj. threshold (**Table 18**).

**Table 17: Comparison of DEGs identified with HTG panel only**
Availability of genes in the NanoString panel was assessed. Cells were highlighted in red, if the gene was unavailable. If available, the corresponding values (FC and p-adj.) were added. Values leading to exclusion were marked in red. The threshold criteria for significance were set to p-adj. < 0.05 and FC -1.5/+1.5, n = 18

| HTG only | | NanoString panel | | |
|---|---|---|---|---|
| **Genes** | **FC** | **available** | **FC** | **padj** |
| *ALOX5* | 2.1 | | | |
| *CCDC138* | 1.5 | | | |
| *CCL4* | -1.6 | yes | -1.6 | 0.06 |
| *CD22* | 1.9 | yes | 1.3 | 0.42 |
| *CIITA* | 1.7 | | | |
| *ELL3* | 2.0 | | | |
| *FCGR1A_FCGR1B* | -1.8 | | | |
| *FCGR3A_3B* | -1.6 | | | |
| *FCRLA* | -2.3 | | | |
| *GPR18* | 1.9 | | | |
| *LTB* | 1.7 | yes | 1.1 | 0.66 |
| *MNDA* | -1.8 | | | |
| *MS4A1* | 1.8 | yes | 1.3 | 0.30 |
| *NCF1* | 1.9 | | | |
| *PAX5* | 1.6 | yes | 1.3 | 0.22 |
| *PIK3CG* | 1.6 | yes | 1.2 | 0.23 |
| *S100A8* | -1.7 | yes | -2.3 | 0.14 |
| *WASHC4* | 1.5 | | | |

**Table 18: Comparison of DEGs identified with NanoString panel only**
Availability of genes in the HTG panel was assessed. Cells were highlighted in red, if the gene was unavailable. If available, the corresponding values (FC and p-adj.) were added. Values leading to exclusion were marked in red. The threshold criteria regarding significance were set to p-adj. < 0.05 and FC -1.5/+1.5, na = not applicable, no calculation possible, n = 52

| NanoString only | | HTG panel | | |
|---|---|---|---|---|
| Genes | FC | available | FC | padj |
| *C1QA* | -2.2 | yes | -1.6 | 0.15 |
| *C3* | 2.1 | yes | 1.8 | 0.17 |
| *C4B* | -1.5 | yes | -1.2 | 0.59 |
| *CCL19* | 1.5 | yes | 1.3 | 0.29 |
| *CCL3* | -1.7 | yes | -1.0 | na |
| *CCL5* | -1.5 | yes | -1.3 | 0.32 |
| *CCR1* | -1.7 | yes | -1.2 | 0.29 |
| *CCR5* | -1.8 | yes | -1.3 | 0.21 |
| *CCRL2* | -1.5 | yes | -1.1 | na |
| *CD1D* | -1.8 | yes | -1.1 | na |
| *CD274* | -1.5 | yes | -1.2 | 0.25 |
| *CD70* | -1.8 | yes | -1.5 | na |
| *CD9* | 1.6 | | | |
| *CEACAM6* | -7.5 | yes | -1.2 | na |
| *CHIT1* | -6.5 | yes | -1.9 | na |
| *CSF3R* | -1.5 | yes | -1.2 | 0.29 |
| *CXCL11* | -2.2 | yes | -1.1 | na |
| *CXCR3* | -1.5 | yes | -1.1 | 0.78 |
| *CXCR6* | -1.6 | yes | -1.4 | 0.12 |
| *DUSP4* | -1.7 | yes | -1.3 | 0.42 |
| *EBI3* | -2.0 | yes | -1.4 | 0.31 |
| *EOMES* | -1.8 | yes | -1.4 | 0.03 |
| *FCER1G* | -1.7 | yes | -1.4 | 0.12 |
| *FCGR3A* | -3.6 | | | |
| *GATA3* | -1.6 | yes | 1.1 | 0.84 |
| *GZMH* | -2.0 | yes | -1.4 | na |
| *GZMK* | -1.6 | yes | -1.6 | 0.18 |
| *HCK* | -1.8 | | | |
| *HSD11B1* | -1.9 | yes | -1.3 | 0.37 |
| *IFNG* | -2.5 | yes | -1.4 | 0.10 |
| *IL10* | -1.8 | yes | -1.3 | 0.07 |
| *IL12A* | -2.1 | yes | -1.6 | na |
| *IL1R2* | -2.2 | yes | -1.2 | na |
| *IL3RA* | 1.8 | yes | 1.5 | na |
| *IRAK2* | 1.7 | yes | -1.0 | 0.94 |
| *IRF8* | 1.5 | yes | 1.3 | 0.41 |
| *ISG15* | -1.6 | yes | -1.3 | 0.26 |
| *ITGB4* | -2.1 | yes | -1.9 | na |
| *LILRB1* | 1.9 | yes | 1.0 | 0.92 |
| *LILRB3* | -2.5 | | | |
| *LTF* | 5.0 | | | |
| *LY86* | 2.3 | yes | 1.4 | 0.19 |
| *MAP2K1* | 1.5 | yes | 1.3 | 0.04 |
| *MEF2C* | 1.6 | yes | 1.5 | 0.10 |
| *NLRC5* | -1.5 | yes | -1.3 | 0.25 |
| *PRF1* | -1.7 | yes | -1.9 | 0.06 |
| *S100B* | 1.7 | yes | 1.1 | 0.68 |
| *SH2B2* | 1.6 | | | |
| *SLC11A1* | -3.0 | yes | -1.5 | na |
| *SYT17* | 1.9 | yes | 1.4 | 0.2 |
| *TBX21* | -2.1 | yes | -1.4 | na |
| *THY1* | 1.7 | yes | 1.0 | 0.04 |

### 4.3.4 Gene Set Enrichment Analysis and ClusterProfiler

In addition to the identification of DEGs between FLneg$^{m}$ and FLneg$^{wt}$, GSEA (Broad Institute) was performed. This method allowed the detection of more subtle changes within a gene set compared to the stringent DESeq2 algorithm. Data was compared using an *IL4* pathway gene set from PID.

The analysis of HTG data revealed clear and significant differences in the expression of *IL4* pathway-associated genes between the groups (**Figure 34**A). Notably, the top six genes *FCER2* (CD23), *IL4R*, *IL4*, *CCL26*, *THY1*, and *CCL17* were significantly less expressed in the FLneg$^{wt}$ group compared to the FLneg$^{m}$ group (**Figure 35**A). Like the HTG data, a significant difference in the expression of *IL4*-associated genes was observed when comparing FLneg$^{m}$ und FLneg$^{wt}$ in NanoString analysis (**Figure 34**B). The top four genes included *FCER2* (CD23), *CCL17*, *IL4R*, *IL13RA1* (**Figure 35**B). In FLneg36$^{wt}$ case, it was noticeable that this case exhibited a slightly elevated expression of *FCER2* (CD23) compared to the other FLneg$^{wt}$ cases. This minor deviation is also observable in the HTG data. Furthermore, ClusterProfiler package in R was employed to screen for pathway enrichments in HTG data. The most significantly enriched pathways included "Interleukin-4 and Interleukin-13 Signaling" and "Signaling by Interleukins" and (**Figure 36**, **Figure 37**).

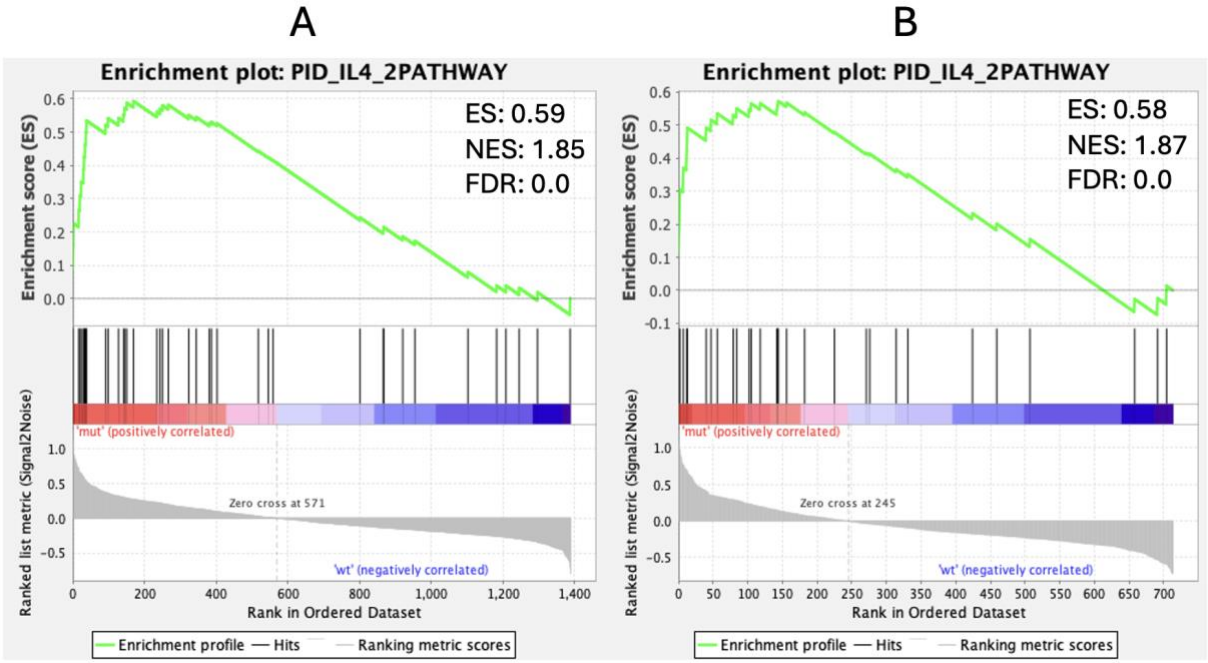


**Figure 34: GSEA enrichment plot of HTG data FLneg$^{m}$ vs. FLneg$^{wt}$.**
A: HTG gene set normalized during DESeq2 analysis was compared to PID *IL4* pathway. FDR < 25% indicates significant result, enrichment score (ES) = 0.59, normalized enrichment score (NES) = 1.85, n = 47. B: GSEA enrichment plot of NanoString data FLneg$^{m}$ vs. FLneg$^{wt}$.HTG gene set normalized during DESeq2 analysis was compared to PID *IL4* pathway. FDR < 25% indicates significant result, enrichment score (ES) = 0.58, normalized enrichment score (NES) = 1.87, n = 40. Enrichment plots were created using GSEA software (Broad Institute).

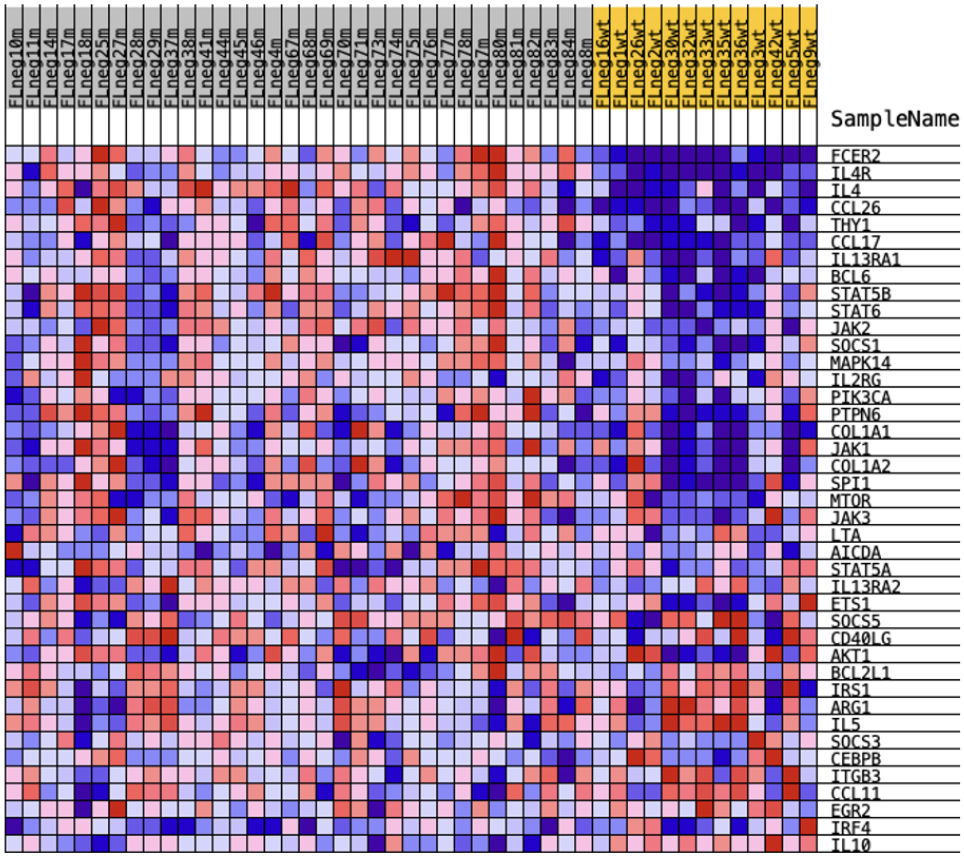


A

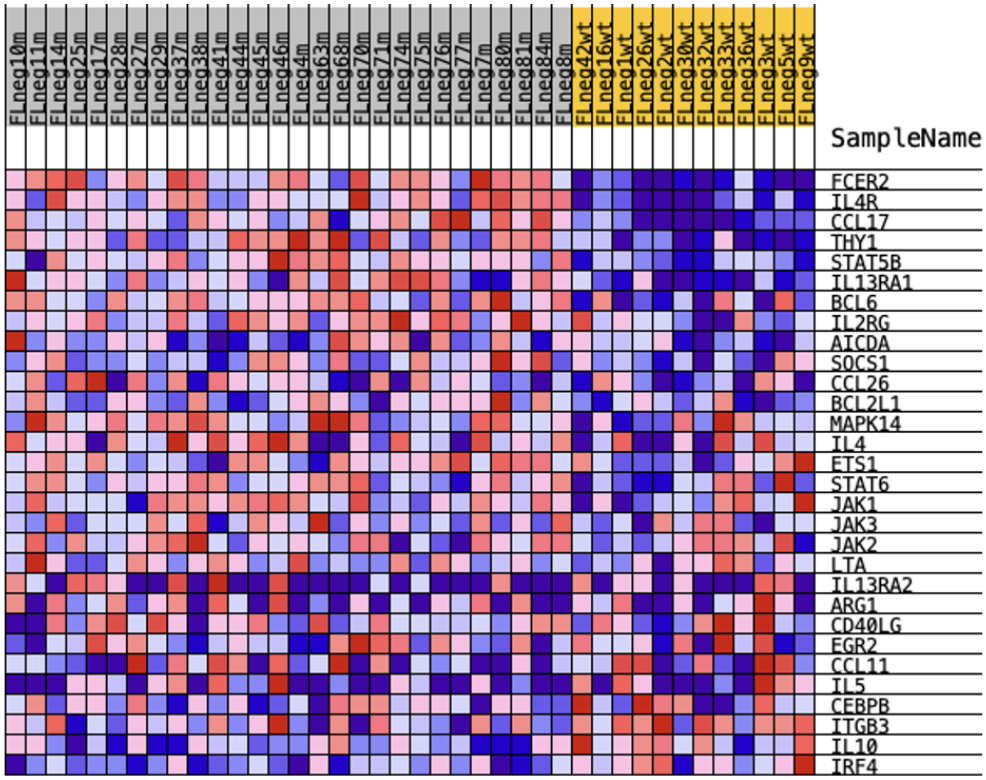


B

**Figure 35: Blue-Pink O'Grams of HTG and NanoString data FLneg$^{m}$ vs. FLneg$^{wt}$.**
A: HTG data FLneg$^{m}$ vs. FLneg$^{wt}$. HTG gene set normalized during DESeq2 analysis was compared to PID *IL4* pathway, n = 47. B: NanoString data FLneg$^{m}$ vs. FLneg$^{wt}$.NanoString gene set normalized during DESeq2 analysis was compared to PID *IL4* pathway, n = 40. Colors indicate deviations from the gene-specific mean expression. Red = relatively higher expression, blue = relatively lower expression. Both HTG and NanoString revealed stronger upregulation in IL4-pathway associated genes in FLneg$^{m}$. Figures were created using GSEA software (Broad Institute).

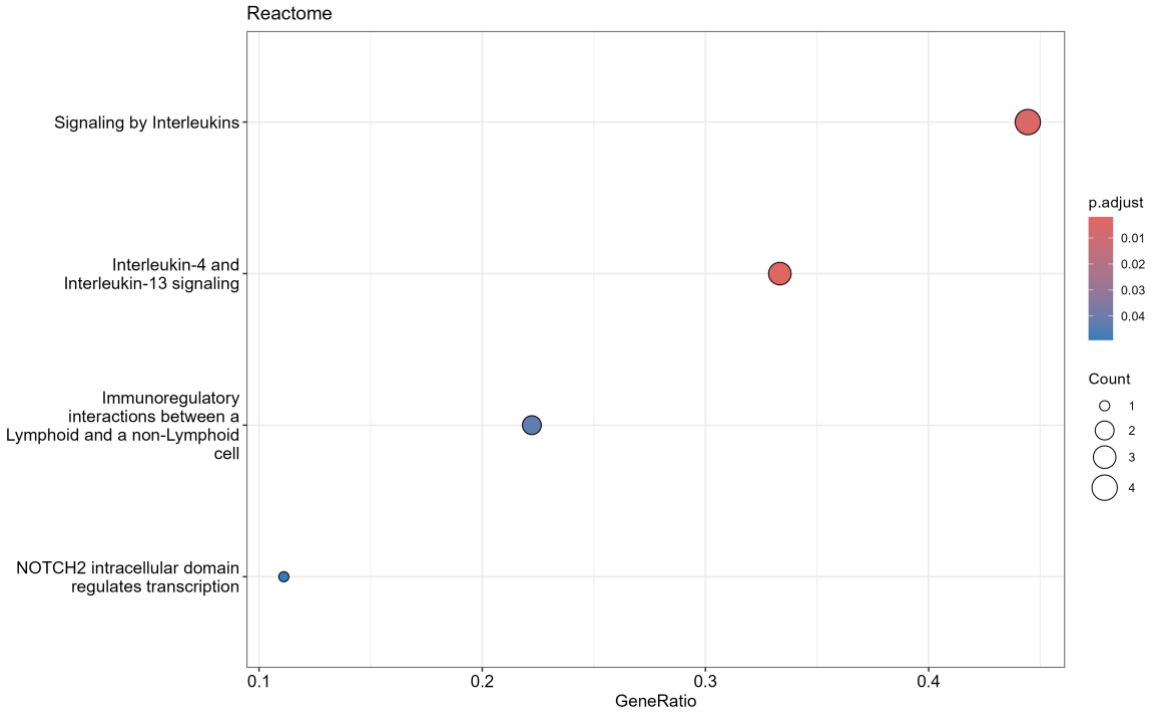


**Figure 36: Cluster Profiler analysis dot plot of HTG data FLneg$^{m}$ vs. FLneg$^{wt}$ using Reactome database.**
Interleukin signaling, especially Interleukin-4 and Interleukin-13 signaling, belong to the top enriched pathways. Dot plot was created using ClusterProfiler package in R.

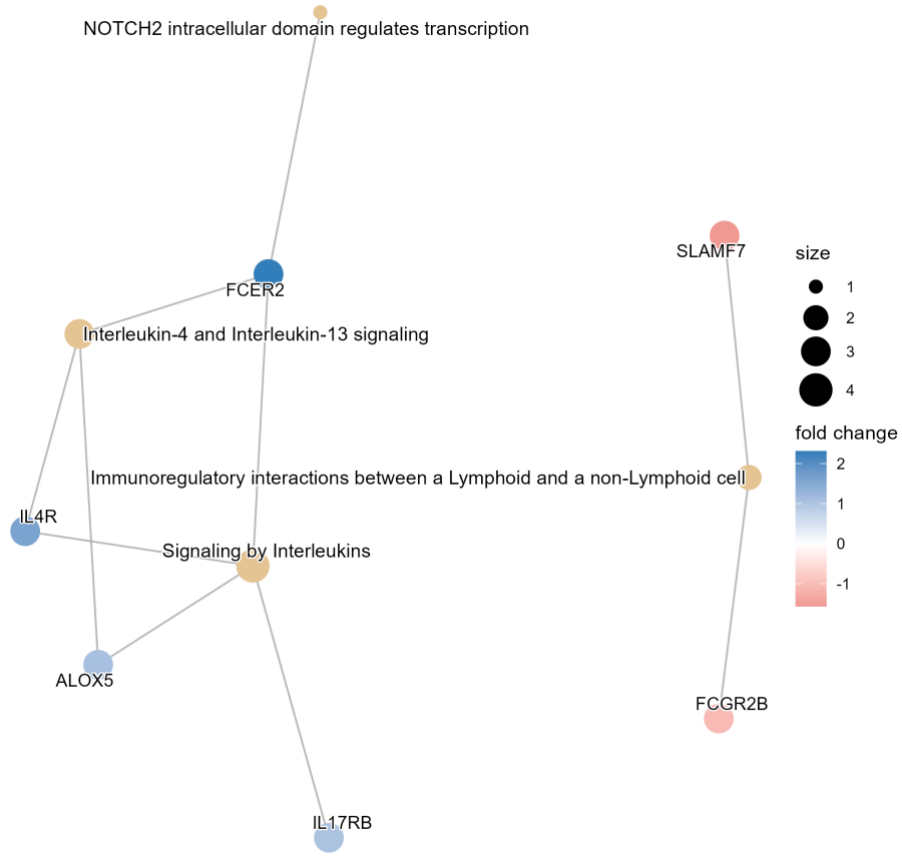


**Figure 37: Cluster Profiler analysis Reactome network plot of HTG data FLneg$^{m}$ vs. FLneg$^{wt}$.**
Interleukin signaling, especially Interleukin-4 and Interleukin-13 signaling, belong to the top enriched pathways. Reactome network plot was created using ClusterProfiler package in R.

### 4.3.5 Influence of *CREBBP/TNFRSF14* Co-Mutations

Next, we wanted to examine a potential influence of *CREBBP* and *TNFRSF14* co-mutations on gene transcription. FLneg$^{m}$ cohort was stratified into *CREBBP*$^{m}$, *CREBBP*$^{wt}$, *TNFRSF14*$^{m}$, *TNFRSF14*$^{wt}$, and GEP using available HTG data was conducted. DESeq2 was applied to identify differentially expressed genes between *CREBBP*$^{m/wt}$ and *TNFRSF14*$^{m/wt}$ groups.

First, 16 *CREBBP*$^{m}$ cases were analyzed against 10 *CREBBP*$^{wt}$ cases. No DEGs were identified in this comparison. The principal component analysis (PCA) further confirmed that the samples did not show significant separation. Notably, two outliers were observed: FLneg80$^{m}$ and FLneg18$^{m}$. These cases deviated from the main clustering pattern (**Figure 38**).

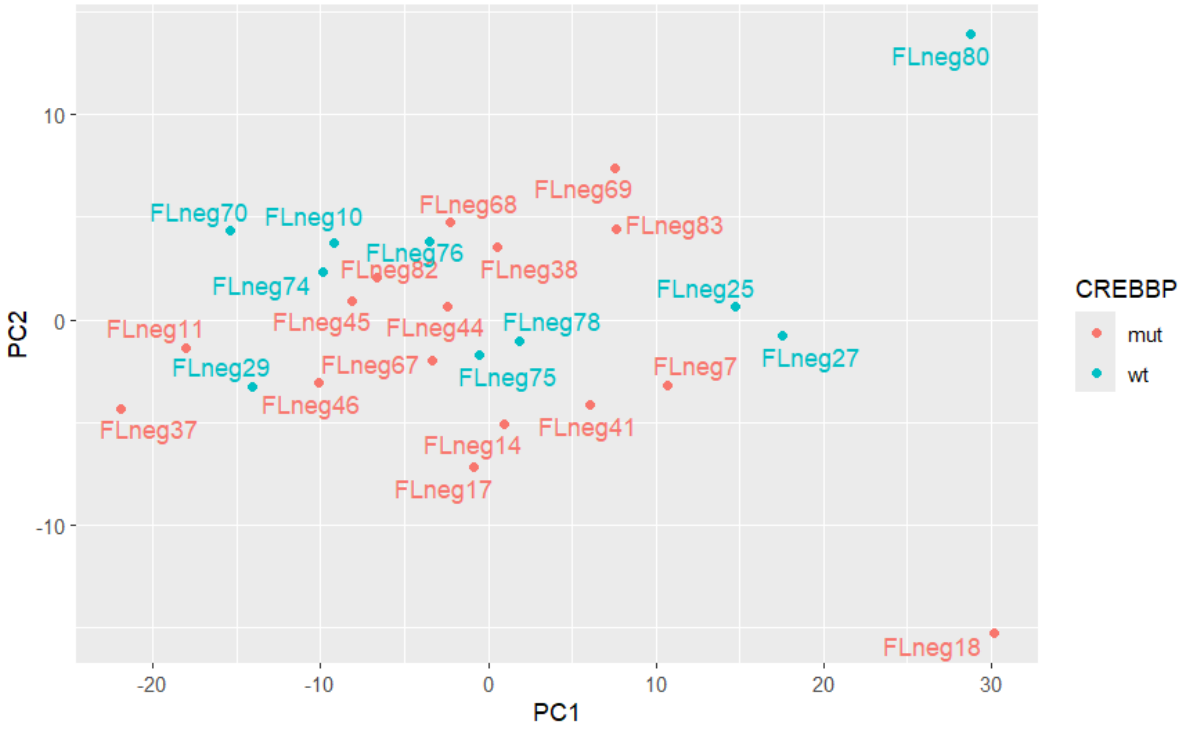


**Figure 38: PCA of *CREBBP*$^{m}$ and *CREBBP*$^{wt}$ FLneg cases with *STAT6/SOCS1* mutation.**
The groups did not show significant separation. Two outliers were identified, FLneg80$^{m}$ and FLneg18$^{m}$, n = 26. PCA was created using DESeq2 package in R.

Since no DEGs were identified, a heatmap of the entire panel was generated to explore potential patterns or associations within the dataset. *CREBBP* groups did not exhibit distinct clustering in the heatmap, indicating that there were no clear transcriptional differences detectable using the actual approach (**Figure 39**).

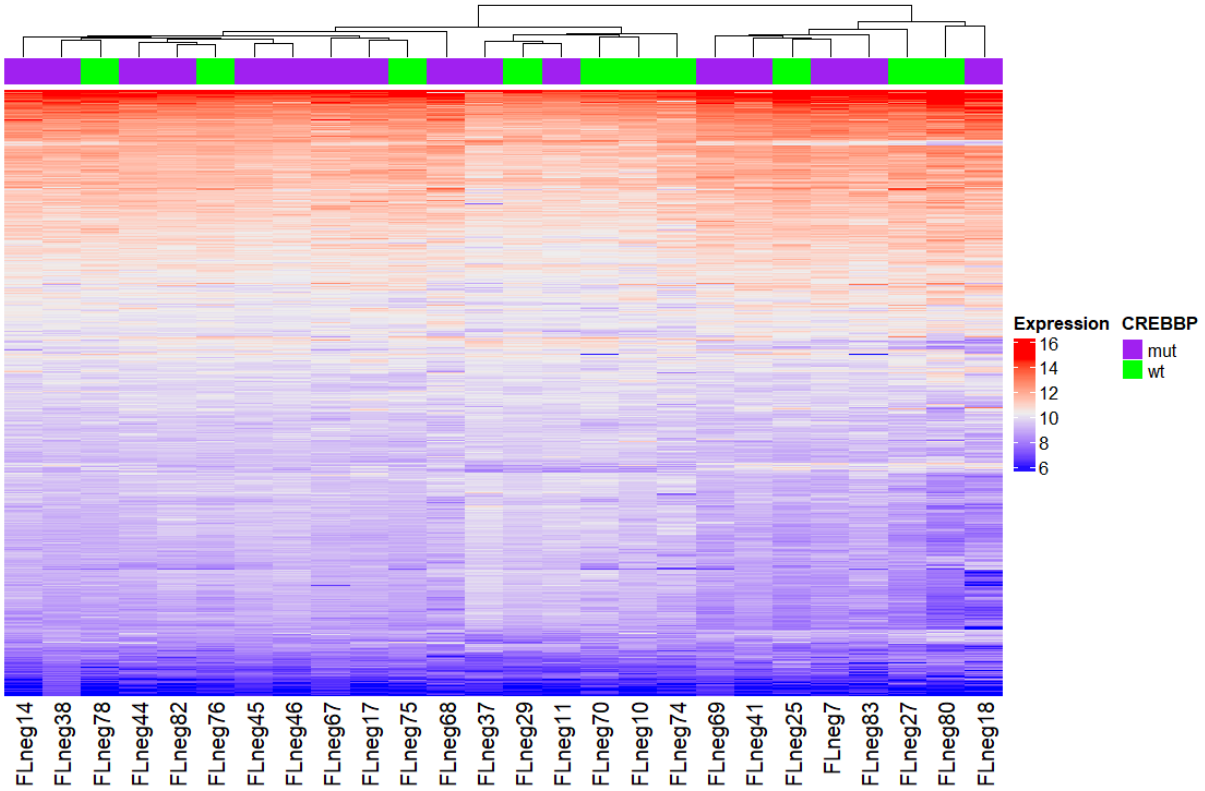


**Figure 39: Heatmap of GEP of FLneg$^{m}$ *CREBBP*$^{m}$ and *CREBBP*$^{wt}$ cases using HTG technology**
Hierarchical clustering of normalized counts. Expression indicates normalized expression values, from low (blue) to high (red). The purple cases represent FLneg$^{m}$ *CREBBP*$^{m}$, while the green cases represent FLneg$^{m}$ *CREBBP*$^{wt}$. No clustering between both groups detected, n = 26. Heatmap was created using DESeq2 package in R.

Next, it was aimed to investigate whether *TNFRSF14* as co-mutation alongside *STAT6/SOCS1* has an impact on gene expression. For this purpose, a DESeq2 analysis comparing 15 FLneg$^{m}$ *TNFRSF14*$^{m}$ cases against 12 FLneg$^{m}$ *TNFRSF14*$^{wt}$ cases was conducted. Similarly, no significant DEGs were identified in this analysis. PCA did not reveal any clear separation between the groups (**Figure 40**). Accordingly, a heatmap was generated using normalized counts of all genes. No distinct clustering between the groups was observed (**Figure 41**).

In summary, under the current testing conditions, no impact on gene expression could be detected for both *CREBBP* and *TNFRSF14* co-mutations.

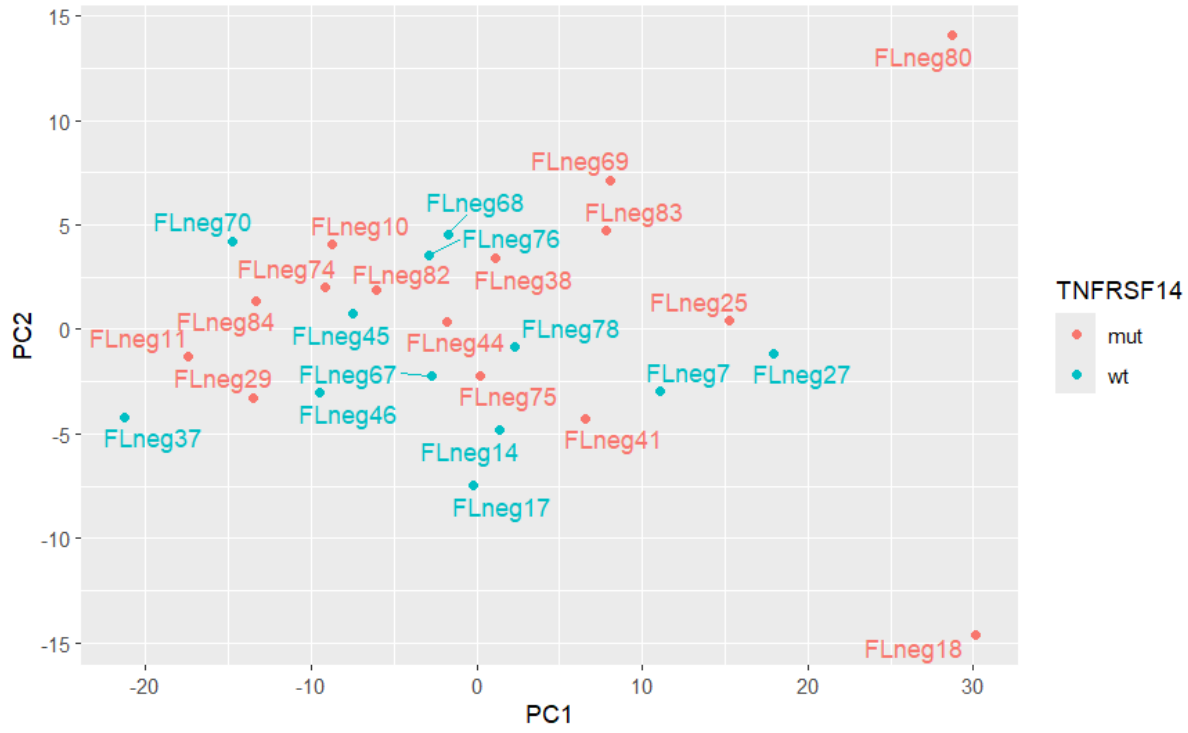


**Figure 40: PCA of *TNFRSF14*$^{m}$ and *TNFRSF14*$^{wt}$ FLneg cases with *STAT6/SOCS1* mutation.**
The groups did not show significant separation. Two outliers were identified, FLneg80$^{m}$ and FLneg18$^{m}$, n = 27. PCA was created using DESeq2 package in R.

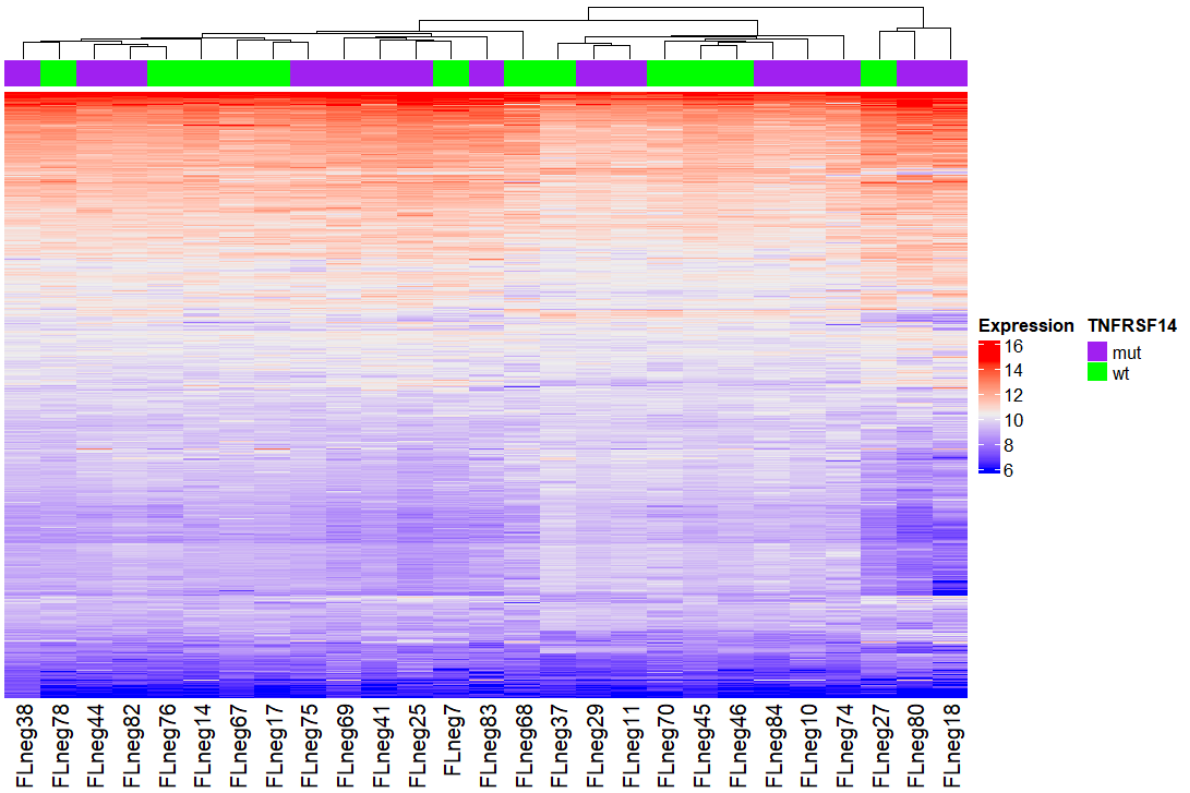


**Figure 41: Heatmap of GEP of FLneg$^{m}$ *TNFRSF14*$^{m}$ and *TNFRSF14*$^{wt}$ cases using HTG technology**
Hierarchical clustering of normalized counts. Expression indicates normalized expression values, from low (blue) to high (red). The purple cases represent FLneg$^{m}$ *TNFRSF14*$^{m}$, while the green cases represent FLneg$^{m}$ *TNFRSF14*$^{wt}$. No clustering between both groups detected, n = 27. Heatmap was created using DESeq2 package in R.

### 4.3.6 Correlation of CD23, *CREBBP* and *STAT6/SOCS1*

A recent study suggested that *CREBBP* co-mutations negatively regulate STAT6 and mTOR pathway in FL (without subtype classification) [71]. It was aimed to apply that finding to our FLpos cohort, which represented the classic FL, and check for *CREBBP* status. *CREBBP* status was available for 20 cases, with 15/20 showing mutations. Assuming that intact *CREBBP* is crucial for the IL4 pathway, such as described in the study, odds ratio, p-value (Fisher's exact test) and binary logistic regression to evaluate dependencies were calculated between *CREBBP*, *STAT6/SOCS1* and CD23 IHC in FLpos. Since CD23 data was missing for one case, the following analyses were conducted with the remaining 19 FLpos cases. In the comparison of *CREBBP* status and CD23 expression, an observed odds ratio of 1.67 and a p-value of 1.0 was calculated. Accordingly, no significant difference between *CREBBP* alterations and CD23 expression could be detected (**Table 19**).

**Table 19: *CREBBP* mutations vs. CD23 expression in FLpos**
Fisher's exact test: The odds ratio of 1.67 indicates that *CREBBP*$^{m}$ cases possess slightly higher likelihood of being CD23$^{+}$ compared to *CREBBP*$^{wt}$. However, the p-value of 1.0 shows that this association was not statistically significant, significance level $p < 0.05$. Statistics were calculated using GraphPad Prism 10

| | **CD23$^{+}$** | **CD23$^{-}$** | **Total** |
|---|---|---|---|
| ***CREBBP*$^{m}$** | 10 | 4 | 14 |
| ***CREBBP*$^{wt}$** | 3 | 2 | 5 |
| **Total** | 13 | 6 | 19 |

Subsequently, the correlation between *CREBBP* alterations and *STAT6/SOCS1* co-mutations was investigated. For this comparison, the case with missing CD23 status was included, as the information was not required for the analysis. The calculated odds ratio was 2.25, with a p-value of 0.62. The values indicated that *CREBBP* and *STAT6/SOCS1* mutations did not correlate in this setting (**Table 20**).

**Table 20: *CREBBP* vs *STAT6/SOCS1* co-mutations in FLpos**
Fisher's exact test: The odds ratio of 2.25 indicates that *CREBBP*$^{m}$ cases possess higher likelihood of carrying *STAT6/SOCS1* co-mutations compared to *CREBBP*$^{wt}$. However, the p-value of 0.62 shows that this association was not statistically significant, significance level $p < 0.05$. Statistics were calculated using GraphPad Prism 10

| | ***CREBBP*$^{m}$** | ***CREBBP*$^{wt}$** | **Total** |
|---|---|---|---|
| ***STAT6/SOCS1*$^{m}$** | 3 | 2 | 5 |
| ***STAT6/SOCS1*$^{wt}$** | 6 | 9 | 15 |
| **Total** | 9 | 11 | 20 |

Finally, a significant association between CD23 positivity and *CREBBP* status was investigated, after accounting whether *STAT6/SOCS1* is mutated (and vice versa). This assumption was evaluated by performing a binary logistic regression (**Table 21**). The Log-Likelihood Ratio (LLR) p-value of 0.89 indicated that there was no significant combined effect of *CREBBP* and *STAT6/SOCS1* mutations on CD23 expression in this dataset.

**Table 21: Overview of comparisons and binary logistic regression in FLpos**
LLR p-value (0.8938) indicates that there was no significant combined effect of *CREBBP* and *STAT6/SOCS1* mutations on CD23 in this dataset, Fisher's exact test and Multiple Logistic Regression were used, $p < 0.05$ was considered as significant. Statistics were calculated using GraphPad Prism 10

| Comparison | Odds Ratio | 95% CI | P-Value | Test/Model |
|---|---|---|---|---|
| ***CREBBP* vs. CD23** | 1.67 | 0.17 – 16.6 | 1.0 | Fisher's exact |
| ***STAT6/SOCS1* vs. CD23** | 0.86 | 0.13 – 5.7 | 1.0 | Fisher's exact |
| ***CREBBP* vs. *STAT6/SOCS1*** | 2.25 | 0.29 – 17.7 | 0.62 | Fisher's exact |
| **Binary Logistic Regression (CD23 ~ *CREBBP* + *STAT6/SOCS1*** | na | na | 0.89 | Likelihood-ratio test (model) |

Regarding the mutation data of the five FLpos$^{m}$ CD23$^{-}$ cases, no specific abnormalities were identified.

Next, same calculations were performed using FLneg mutation data. Neither *CREBBP* and CD23 expression nor *STAT6/SOCS1* mutations and *CREBBP* mutations showed a correlation (**Table 22**, **Table 23**). Interestingly, when calculating correlation between *STAT6/SOCS1* and CD23 expression using *CREBBP* as further variable, the result was still significant (**Table 24**).

**Table 22: *CREBBP* mutations vs. CD23 expression in FLneg**
$\chi^2(1) = 2.686$, $p \approx 0.101$. Fisher's exact test: (two-sided) $p = 0.2$. Odds Ratio (OR) = 3.08, 95% CI = 0.82 – 10.28. The odds ratio of 3.08 indicates that *CREBBP*$^{m}$ cases possess slightly higher likelihood of being CD23$^{+}$ compared to *CREBBP*$^{wt}$. However, the p-value of 0.2 shows that this association was not statistically significant. Significance level $p < 0.05$ was considered as significant. FLpos4 was removed from analysis due to missing CD23 data. Statistics were calculated using GraphPad Prism 10

| | CD23$^{+}$ | CD23$^{-}$ | Total |
|---|---|---|---|
| ***CREBBP*$^{m}$** | 16 | 4 | 20 |
| ***CREBBP*$^{wt}$** | 13 | 10 | 23 |
| **Total** | 29 | 14 | 43 |

**Table 23: *CREBBP* vs. *STAT6/SOCS1* co-mutations in FLneg**

$\chi^2(1) = 2.361$, $p \approx 0.12$. Fisher's exact test: (two-sided) p = 0.2. Odds Ratio (OR) = 2.86, 95% CI = 0.77 – 9.51.
The odds ratio of 2.86 indicates that *CREBBP*$^{m}$ cases possess higher likelihood of carrying *STAT6/SOCS1* co-mutations compared to *CREBBP*$^{wt}$. However, the p-value of 0.2 shows that this association was not statistically significant. Significance level $p < 0.05$ was considered as significant. Statistics were calculated using GraphPad Prism 10

| | ***CREBBP*$^{m}$** | ***CREBBP*$^{wt}$** | **Total** |
|---|---|---|---|
| ***STAT6/SOCS1*$^{m}$** | 16 | 14 | 30 |
| ***STAT6/SOCS1*$^{wt}$** | 4 | 10 | 14 |
| **Total** | 20 | 24 | 44 |

**Table 24: Overview of comparisons and binary logistic regression in FLneg**

LLR p-value (< 0.0001) indicates that there was a significant effect of *STAT6/SOCS1* mutations despite *CREBBP* mutations on CD23 in this dataset. Fisher's exact test and Multiple Logistic Regression were used, $p < 0.05$ was considered as significant. Statistics were calculated using GraphPad Prism 10

| **Comparison** | **Odds Ratio** | **95% CI** | **P-Value** | **Test/Model** |
|---|---|---|---|---|
| ***CREBBP* vs. CD23** | 3.08 | 0.82 – 10.28 | 0.12 | Fisher's exact |
| ***STAT6/SOCS1* vs. CD23** | 455.0 | 25.88 - 4767 | < 0.0001 | Fisher's exact |
| ***CREBBP* vs. *STAT6/SOCS1*** | 2.86 | 0.77 – 9.51 | 0.195 | Fisher's exact |
| **Binary Logistic Regression (CD23 ~ *CREBBP* + *STAT6/SOCS1*** | na | na | < 0.0001 | Likelihood-ratio test (model) |

# 5. Discussion

## 5.1 Study Cohort and Rationale for Group Selection

The cohort for this study was assembled by merging 35 FLneg cases from the Nann cohort with 16 newly included FLneg cases. This resulted in the largest FLneg cohort to date for GEP (n = 51). To better characterize *STAT6/SOCS1* mutated FLneg, $CD23^{+}$ cases were predominantly added to the cohort, assuming that features are associated. Based on the *STAT6/SOCS1* mutational profile, our cohort was classified into $FLneg^{m}$, $FLneg^{wt}$, and $FLpos^{m}$.

During the mutation analysis of FLneg and FLpos cases using the FL-typical panel, differences in *CREBBP* mutation frequencies were observed. While 45% (20/44) of FLneg cases harbored a *CREBBP* mutation, the frequency was 75% (15/20) in FLpos cohort. The mutation frequency observed in FLneg cohort aligns with the original cohort used by Nann *et al.* (22/45, 49%) [60]. Our results are also well aligned with those of Zamò *et al.*, who, despite using a smaller cohort of 13 FLneg and 28 FLpos, reported differences in *CREBBP* mutation frequencies (FLneg: 5/13, 38%, FLpos 17/28, 61%) [62]. To date, no data exist confirming a direct biological association between *CREBBP* and t(14;18). Hence, further research is needed in this field.

Regarding methodology, the deliberate inclusion of CD23-positive cases increased the probability of obtaining *STAT6/SOCS1* mutated cases. At the same time, a selection bias was introduced leading to a potential overestimation compared to an unselected cohort.

## 5.2 *STAT6/SOCS1* Mutations and CD23 Expression in FLneg vs. FLpos

Recent studies have identified a strong association between activating *STAT6* mutations and increased CD23 expression in FL [60, 68]. Therefore, during group formation, the relation between *STAT6/SOCS1* mutations and CD23 expression was examined across subgroups, to determine if this association could be reproduced, particularly in FLneg. Indeed, it was possible to validate the results of previous studies with our data, displaying that not only *STAT6* but also *SOCS1* mutations in FLneg showed a strong significant association to CD23 expression. This implies that CD23 expression in FLneg is primarily and directly driven by genetic alterations, namely activating

mutations in the IL4/STAT6 pathway. In contrast, FLpos cases exhibited CD23 expression less frequently and without statistical significance, where CD23 expression is not exclusively driven by genetic alterations but may also origin from external signals within the TME. This concept is consistent with the model proposed by Salaverria *et al.* (2023), which revealed the TME as key difference between FLneg and FLpos [85]. While FLneg was primarily characterized by intrinsic mutations in epigenetic modifiers and genes associated with the STAT6 pathway (e.g. *STAT6*, *SOCS1*), FLpos appeared to exhibit an increased dependence on the TME. Here, paracrine activation of STAT6 by IL4-secrected from $T_{FH}$ cells may induce CD23 expression even in the absence of *STAT6* mutations. Pangault et al (2010) further support this mechanism by demonstrating that $T_{FH}$ cells are the main source of IL4 in classic FL, which resulted in STAT6 phosphorylation in neoplastic B cells, following upregulation of STAT6 target genes, including *FCER2* (CD23) [104]. Furthermore, $FLneg^{m}$ often co-harbored *CREBBP*/and or *TNFRSF14* mutations, which may act synergistically in FL pathogenesis [61, 69, 70]. *CREBBP* alterations in the HAT domain were associated to MHCII complex downregulation, impairing recognition of B cells through T cells [105]. Loss of *CREBBP* acetyltransferase activity interfered with B-cell differentiation and leads to decreased p53 activity [47, 72, 106]. *TNFRSF14* mutations led to expansion of $T_{FH}$ cells and activation of tumor stroma, which promotes paracrine IL4 signaling [73]. There may be further mechanisms that modulate CD23 expression, such as involvement of CCAAT-enhancer-binding proteins beta (C/EBPß) and NF-κB [107]. This could explain lacking CD23 expression in $FLneg^{m}$ despite *STAT6*/*SOCS1* mutations. Epigenetic modulations may also play a role in CD23 expression but require further research.

The strong link between *STAT6*/*SOCS1* mutations and CD23 expression raises several questions. It remains to be clarified, if CD23 serves as surrogate marker or if CD23 expression also leads to direct functional alterations within FLneg signaling. However, an improved overall survival in $CD23^{+}$ FL could be observed [108]. Furthermore, activation of STAT6 should be evaluated via phospho-STAT6 using IHC, as well as primary FLneg cells, which, through IL4 stimulation, allow a functional validation of the data generated in this study. Siddiqi *et. al.*, which found and described FLneg characteristics, discovered increased phospho-STAT6 in *STAT6* mutated cases using IHC [61]. The antibody used in this study could help to assess phospho-STAT6 in our FL cohort. Ultimately, testing for *STAT6*/*SOCS1* and CD23 by IHC would be well suited as an integral component of routine FL diagnostics.

## 5.3 Alternative Oncogenic Drivers in FLneg and FLpos

In 2018, Viganò *et al.* investigated primary mediastinal large B-cell lymphoma (PMBCL) for mutations in the Interleukin 4 Receptor (IL4R) pathway, which represents an important signaling axis in this entity. Briefly, the IL4R pathway consists of either Type I IL4Rα and a gamma chain, which are membrane-bound, or Type II IL4Rα, which forms a membrane-associated receptor together with IL13Rα. Upon activation through IL4 and IL13, janus tyrosine kinases (JAK) or tyrosine kinase 2 (TYK2) are phosphorylated leading to activation of downstream signaling and expression of target genes such as *CD23*, *CCL17* and MHCII [109-116].

As in FL, *STAT6* and *SOCS1* mutations were identified, as well as an activated IL4/JAK/STAT6 pathway. Here, Vigano *et al.* investigated a cohort of 30 PMBCL patients and found *SOCS1* mutations in 53% (16/30) and *STAT6* mutations in 43% (13/30) of cases. Interestingly, a gain/amplification of *JAK2* was detected in 41% (11/27) of cases, *PTPN1* mutations in 27% (8/30), and *IL4R* mutations in 20% (6/30) of the patients. In the analysis of downstream targets such as phospho-STAT6, CD23, and CCL17, a correlation with JAK-STAT pathway mutations was observed, particularly in cases with multiple hits.

In another study investigating molecular alterations in FL and transformed FL (tFL), JAK-STAT-associated genes such as *STAT6* and *SOCS1*, as well as *IL4R* and *STAT3*, were analyzed. Using a combined dataset of 42 tFL, two cases exhibited an *IL4R* mutation, while another two cases harbored a *STAT3* mutation [117-119]. The studies show that the IL4/JAK/STAT6 pathway plays an important role across B-cell lymphomas.

The observations by previous studies suggest that the activation of the IL4/JAK/STAT6 pathway can be mediated by mutations affecting transcription factors, as well as by genetic alterations at the receptor and kinase level. Based on the parallels to PMBCL and tFL, we designed a customized IL4R-associated gene panel to investigate whether FLneg and FLpos cases harbor additional mutations affecting the IL4R pathway.

To date, no study has comprehensively analyzed a larger cohort on *STAT6* associated mutations in FLneg. In the current study, apart from *STAT6* and *SOCS1*, no additional mutations in the IL4R pathway were detected, except for a very small number of cases. There was also no difference

between *STAT6/SOCS1*-mutated cases and wild-type cases, as well as in relation to the presence of t(14;18). This result suggests that in FL *STAT6* and *SOCS1* are the predominantly IL4/JAK/STAT6 associated drivers contributing to FL pathogenesis. Here, the TME might play an important role. While FL shows two altered genes (*STAT6*, *SOCS1*) associated with IL4/JAK/STAT6 and an IL4-rich TME supported by $T_{FH}$ cells secreting IL4, PMBCL showed more altered genes (*STAT6*, *SOCS1*, *JAK2*, *PTPN1*, *IL4R*) but a IL4 poor TME [110, 120]. PMBCL might compensate the lacking paracrine activity by inducing additional mutations such as *JAK2*.

Next, we considered the subtypes FLneg$^{wt}$ and FLneg$^{BCL6\text{-}R}$. Without constitutive *BCL2* expression and activating *STAT6/SOCS1* mutations, additional genetic alterations must be responsible for lymphomagenesis in FLneg$^{wt}$. Therefore, the Oncomine Lymphoma III panel was used to identify additional lymphoma-associated mutations. In addition to FL-typical mutations such as *CREBBP* and *KMT2D*, *ATM*, *TMSB4X*, and *TET2* mutations were identified in 25% of cases (n=12). Notably, multiple hits were observed for each of these mutations. Furthermore, two cases were wild- type for the entire panel. Ataxia-Telangiectasia mutated (*ATM*) plays a vital role in DNA damage activating cell cycle arrest and apoptosis. *ATM* mutations have been found in larger numbers in mantle cell lymphoma (MCL) but also been detected at lower frequencies in DLBCL and FL [121, 122]. Thymosin Beta-4 (*TMSB4X*) is involved in actin cytoskeleton organization and cell migration leading to changes in cancer behavior [123]. A *TMSB4X* mutation has already been identified in a DLBCL case [124]. The three cases with *TMSB4X* mutations were analyzed and it was found that 2/3 cases exhibited disease progression. FLneg1$^{wt}$ presented disease progression at 70 and 144 months, with last follow-up after 242 months. This case was the only one among the three to exhibit multiple hits in *TMSB4X*. FLneg9$^{wt}$ showed disease progression after 60 months. In FLneg26$^{wt}$, no further disease progression was observed at the last follow-up after 42 months. So far, there are no larger targeted studies on FLneg disease progression with a focus on *TMSB4X*, making it impossible to draw definitive conclusions at this point. The data on *TET2* mutations carried by three cases and FL is very limited. In a DLBCL study, *TET2* mutations were found in 10% of cases suggesting that *TET2* mutations may also play an important role in FL which can act as DLBCL precursor [125]. It could also be associated to clonal hematopoiesis of indeterminate potential (CHIP). A recent study investigated a potential link between CHIP and lymphoid malignancies, namely DLBCL, FL and others. Whole exome analysis was performed on CHIP-associated genes such as *DNMT3A*, TET2 and *ASXL1*. Patients with CHIP mutations revealed a higher risk for developing malignancies and are known to occur in acute myeloid leukemia (AML) [126] but also in non-Hodgkin lymphoma [127]. Further analysis of the entire FLneg and FLpos

cohort using the Oncomine Lymphoma III panel could provide insights into a potential association. Our data indicate that additional genetic drivers such as *ATM*, *TMSB4X* and *TET2* might contribute to lymphomagenesis and remain to be functionally verified. Whole exome sequencing and inclusion of paired non-tumor samples to address CHIP and consideration of clinical relevance are required to allow better characterization of additional genetic drivers.

A subset of FLneg characterized by *BCL6*-R has been discussed in recent literature and was summarized by Salaverria et al [64]. In our cohort, 6/51 FLneg cases harbored *BCL6*-R. During gene expression profiling, these cases were evaluated regarding abnormalities. However, the cases were located within their respective subgroups (FLneg$^{m}$ or FLneg$^{wt}$) and did not form a distinct transcriptional cluster. Based on our data, there was no separate *BCL6*-R associated phenotype observed. Since the groups were created based on presence and absence of *STAT6*/*SOCS1* mutations, potential transcriptional changes induced by *BCL6*-R may be covered by the transcriptional differences of FLneg$^{m}$ and FLneg$^{wt}$. The separation of FLneg by *BCL6*-R might show differences in their transcriptional profile.

Furthermore, it was aimed to investigate differences in gene expression between FLneg$^{m}$ and FLpos$^{m}$ cases. The number of differentially expressed genes using HTG platform was very low, suggesting that the separation was likely based solely on *BCL2* upregulation. In NanoString, the number of differentially expressed genes was also low with a focus on *BCL2* but also on IL4/JAK/STAT6 target genes. Due to the limited number of FLpos$^{m}$ cases, the interpretability of these findings remains restricted. Larger scale studies on this topic could provide new insights into the differences between FLneg$^{m}$ and FLpos$^{m}$ subgroups.

## 5.4 *STAT6* Pathway Activation and B-Cell Differentiation State in FLneg

### 5.4.1 Molecular Background of JAK/STAT signaling

JAK/STAT pathways are important for cell signaling and comprise over 50 cytokines and growth factors [128]. They are involved in adipogenesis, apoptosis, inflammation, immune fitness, hematopoiesis, and tissue repair [129]. The activation is induced by various upstream membrane receptors. Ligands bind to these receptors, leading to receptor dimerization. There are also receptors that form inactive dimers [130-136]. Through the ligand-receptor interaction, JAK

undergoes transphosphorylation and activation. The activation of JAK promotes tyrosine phosphorylation of the receptor leading to docking sites for STAT proteins. The binding of STAT to the docking site allows JAK to phosphorylate and activate STAT. Activated STAT then dissociates and forms homodimers or heterodimers. This occurs through SH2-domain-phosphotyrosine interactions. The dimers migrate into the nucleus and regulate transcription via several mechanisms either through direct binding to the target gene or by forming transcriptional complexes with STAT and non-STAT transcription factors [137, 138].

Negative regulation of the JAK/STAT pathways occurs through protein inhibitor of activated STAT (PIAS), protein tyrosine phosphatases (PTPs), and SOCS. PTPs inhibit JAK/STAT signal transduction by dephosphorylating STAT proteins [139]. The inhibition by PIAS occurs exclusively through interaction with active STAT dimers, by either impeding DNA-binding activity, supporting the sumoylation of transcription factors, recruiting other co-factors, or chelating other transcription factors, which leads to the formation of repressor complexes [140-144]. SOCS proteins show several inhibition mechanisms of JAK/STAT pathway. They either block the phosphotyrosine of the membrane receptor, preventing the formation of the docking site for STAT, inhibit JAK activation by binding to JAK or the receptor, or participate in the formation of an E3 ubiquitin ligase complex, leading to the degradation of JAK and STAT [145-148]. In general, there are four known JAK family members, JAK1, JAK2, TYK2, and JAK3, which differ in their tissue expression and function. Except for JAK3, which is specifically expressed in the BM, lymphatic tissue, endothelial cells, and cardia muscle cells [149, 150], all other JAK family member expression comprises many different tissue types [151-157]. STAT protein family consists of STAT1, STAT2, STAT3, STAT4, STAT5a, STAT5b, and STAT6 [158-161].

### 5.4.2 Role of IL4/JAK/STAT6 Signaling in Germinal Center B-cell Maturation

IL4 activates the IL4/JAK/STAT6 pathway. A pathway that plays an important role in B cells [116, 162, 163]. IL4 as ligand is considered as an important regulator of the immune system due to involvement in T-helper 2 responses, polarization of M2 macrophages, tissue repair and parasitic helminths defense [164-166]. Furthermore, IL4 is involved in the co-stimulation of B cells as well as in immunoglobulin E (IgE) class switching [167, 168]. It has been shown that IL4 activates the IL4/JAK/STAT6 pathway, promoting the expression of target genes such as MHCII genes, *FCER2* (CD23), and *IL4R*, *CD83*, *CD80* and *CD86*. *CD22*, *FCGRII*, and *PDL1*, which have inhibitory properties, showed reduced expression [169-177].

Interestingly, IL4 is associated with B-cell differentiation. In stimulated B cells, IL4 led to a reduced expression of Syndecan-1 (CD138), which is linked to antibody-secreting cells (ASCs) [178]. In addition, IL4 was shown to negatively regulate Blimp-1 (*PRDM1*) [179-181]. *STAT6* also plays an important role in shaping B-cell differentiation states acting as regulator of GCB cell fate. Here, by responding to IL4 signaling from $T_{FH}$ cells [182]. Pignarre *et al.* found that the IL4/STAT6 pathway is fundamental for B-cell activation and differentiation within the GC. They identified distinct features between $CD23^+$ and $CD23^-$ germinal center B-cells revealing post-activated GC phenotype ($CD23^+$) and pre-plasmablast phenotype ($CD23^-$). Using *STAT6* knockout mice they found reduced CD23 expression in pre-plasmablast phenotype. These cells exhibited elevated IRF4 protein levels matching with a previous study that showed *IRF4* as important regulator in B-cell differentiation. Low IRF4 concentrations led to the expression of germinal center B-cell-associated genes such as *BCL6*. Higher concentrations, on the other hand, promoted increased differentiation into plasma cells [183, 184]. Ultimately, they were able to demonstrate the relevance of the *STAT6* pathway in B-cell differentiation, showing that differentiation was not possible without downregulation of the *STAT6* pathway.

### 5.4.3 Study Design and Platform Comparison

So far, there is no study that has examined the impact of *STAT6/SOCS1* mutations on the STAT6 pathway in FLneg on larger scale. We therefore supplemented the cases from the Nann *et al.* paper ([60]) with new cases, characterized them, and analyzed them using two different gene expression methods, HTG and NanoString. The use of these two different gene expression methods aimed to create a robust dataset and identify genes that showed particular significance. To investigate the impact of *STAT6/SOCS1* mutations in FLneg, the FLneg cases were divided into $FLneg^m$ (*STAT6/SOCS1*$^m$) and $FLneg^{wt}$ (*STAT6/SOCS1*$^{wt}$). Using HTG technology, 40 differentially expression genes between the groups were identified. NanoString showed 37 differentially expressed genes.

Before differentially expressed genes identified by HTG and NanoString are being discussed, the discrepancies between both methods should be considered. Several factors could explain these differences: 1) Platform-specific panel coverage. As demonstrated in the Results section, some genes were only covered by one of the two methods 2) Differences in sensitivity and detection range. HTG and NanoString rely on different technologies. HTG is a sequencing-based approach, whereas NanoString uses a direct RNA counting method through hybridization and molecular

barcodes. The sequencing-based nature of HTG allows for higher detection sensitivity and a broader dynamic range. In contrast, NanoString, which relies on a hybridization-based RNA counting method, may struggle with extremely low or high transcript counts. Low-expressed genes might be below the limit of detection due to weaker hybridization signals. Signal saturation in highly expressed genes may limit the ability to quantify large expression differences accurately. 3) Sample processing and RNA integrity. HTG and NanoString both have difference RNA extraction methods. HTG directly processes FFPE samples without RNA lysis extraction, whereas NanoString requires this step. This may lead to RNA loss, especially in degraded samples. For NanoString samples were filtered based on RNA integrity (DV200), which induced slight cohort differences 4) Batch effects and platform-specific variability. Both methods are subject to different sources of batch effects, instrumental and protocol-related differences can lead to platform-specific biases, e.g. during normalization and background correction. 5) Biological variability and tissue heterogeneity. Expression profiles may be influenced by differences in tissue composition. Zhang *et al.* (2023) compared HTG and NanoString panels and found that there were differences in the expression of genes encoding interleukins, chemokines and chemokine receptors. The authors assumed that these differences are caused by tissue heterogeneity rather than probe design or assay chemistry [95]. In summary, both biological and technical factors may contribute to the observed differences in gene expression profiles between HTG and NanoString. Therefore, significant DEGs identified by both methods represent a robust dataset, whereas discordant genes should be considered carefully. Since STAT6 pathway activation was deduced from mutational and transcriptional data, and phospho-STAT6 as well as additional IHC and functional assays are lacking, this represents an important limitation of this study.

### 5.4.4 Functional Interpretation: STAT6 Activation, GC Retention, and Differentiation

Using HTG and NanoString technologies to compare FLneg$^{m}$ and FLneg$^{wt}$, most of the differentially expressed genes were associated with changes in the tumor microenvironment, including inflammation, immune modulation, migration, and further adaptions. However, a striking observation was the upregulation of STAT6 pathway-associated and germinal center retention markers in FLneg$^{m}$, whereas FLneg$^{wt}$ showed enrichment of B-cell differentiation markers and immune effector genes.

Several genes strongly upregulated in FLneg$^{m}$, including *FCER2* (CD23), *IL4R*, *IL13RA1* and *CCL17*, are well-established targets of IL4/JAK/STAT6 signaling. *FCER2* and *IL4R* are

characteristic markers of IL4 stimulation in B cells [185, 186]. Previously, they were linked to post-activated GCB [183]. It was already shown that upregulation of the Chemokine *CCL17*, leads to attraction of regulatory T cells, which favor an immunosuppressive microenvironment [187]. The expression of *CCL17* further supports enhanced *STAT6* activation in FLneg$^{m}$.

The transcriptional program was further characterized by simultaneous upregulation of *CD83* and *CD40* indicating persistent B-cell activation [188-190]. In addition, *ALOX5* (5-lipoxygenase), an enzyme that is linked to immunosuppressive signaling via leukotriene biosynthesis and $T_{reg}$-mediated tolerance in FL, was also upregulated [191]. It was already found to be expressed in follicular lymphoma but not in non-neoplastic germinal centers. Remarkably, DLBCL (both GBC and non-GCB type) were negative for *ALOX5* in a total of 25 cases [192]. However, data on the impact of *ALOX5* in FL is limited, especially on the finding of upregulated *ALOX5* in FLneg$^{m}$. *PIK3CG* is involved in BCR signaling and represents an important target in cancer therapy. BCR signaling in FL is known to be altered compared to nonmalignant B cells [193]. Furthermore, it was already demonstrated that IL4R activation promotes PI3K/Akt signaling, which could explain the upregulation in FLneg$^{m}$ [194]. Further GC-associated genes, including *PAX5*, *MS4A1* (CD20), *CD22* and *CIITA*, were also upregulated in FLneg$^{m}$. *PAX5* is associated to plasma cell differentiation. Here, *PAX5* is important for regulation of terminal B-cell differentiation. Downregulation of *PAX5* leads to plasma cell differentiation, while enforced expression prevented differentiation [195, 196]. Regarding *CD20*, a study showed a link between IL4/JAK/STAT6 and *CD20* in chronic lymphocytic leukemia, where the activation of this pathway lead to expression of *CD20* [197]. Constitutive activation of *STAT6* could have influenced *CD20* expression in FLneg$^{m}$. The upregulation of the inhibitory molecule *CD22* seems contradictory in activated B cells. *CD22* expression may stem from less-activated B-cell populations or serve as compensatory mechanism against constitutively activated STAT6 pathway.

*CIITA* is known as master trans activator of MHC class II genes. This gene may be upregulated as countermeasure against *CREBBP* mutations [32]. Interestingly, human leucocyte antigen (*HLA*)-*DOB*, *HLA-DMB* were both upregulated in FLneg$^{m}$. Physiologically, HLA-DMB$^{high}$ and HLA-DOB$^{low}$ allow optimal antigen presentation, since HLA-DOB shows an inhibitory function on HLA-DMB [198-200]. However, the upregulation of both genes is contradictory to GCB physiology. Upregulation of both genes could represent the result of an impaired antigen presentation caused by *CREBBP* mutations as already demonstrated by another study [201].

In contrast, *IRF4*, *SLAMF7*, and *TNFRSF13B*, which were upregulated in FLneg$^{wt}$ suggest a more differentiated B-cell state. IRF4 is a master regulator of plasma cell differentiation functionally interacting with BCL6. Low levels maintain the GC state through BCL6. High levels of IRF4 lead to decreased BCL6 levels and promote plasmablast transition [184, 202]. *SLAMF7* and *TNFRSF13B* are both associated with antibody-secreting cell stages and plasma cell lineage commitment [203, 204]. Physiologically, SLAMF7 is induced by IL21 and IFN-γ in B cells [205]. Notably, *IFNG* was also differentially expressed, which may contribute to *SLAMF7* activation. In other cancers, such as clear cell renal cell carcinoma, *SLAMF7* has been linked to T cell exhaustion leading to poor survival [206]. Another gene upregulated in FLneg$^{wt}$ is *CXCL11*. The CXCL11/CXCR4 axis is associated with tumor growth and tumor inhibition and an active immune tumor environment [207]. Perforin 1 (*PRF1*) is a cytotoxic molecule secreted by NK cells and cytotoxic T cells and promotes antitumor effects [208]. *ISG15* shows both pro and anti-tumorigenic effects [209]. Taken together, these molecules reflect an immune active environment in FLneg$^{wt}$.

*ENTPD1* (CD39) and *LAG3* were significantly upregulated in FLneg$^{wt}$. *ENTPD1* is involved in ATP hydrolysis and promotes immunosuppressive adenosine production, especially in synergy with CD73. Blocking CD39 was shown to improve T-cell responses [210-214]. *LAG3* is a key transmembrane checkpoint molecule that suppresses T-cell function through interaction with MHCII [215]. The expression of *ENTPD1* and *LAG3* might indicate a distinct TME shaping in FLneg$^{wt}$, possibly reflecting increased infiltration be regulatory cells.

The upregulation of *CD180* in FLneg$^{m}$ is also notable. CD180 is involved in innate immunity signaling via TLR2 and promotes B-cell activation [216, 217]. An unexpected finding is the upregulation of *TNFRSF17* (B-cell maturation antigen, BCMA), which is typical for late differentiation B cells and would not be expected in FLneg$^{m}$. It is involved in growth, proliferation and survival of differentiating B cells and plays an important role in the pathogenesis of multiple myeloma [218, 219]. Despite a potential stall in B-cell maturation through IL4/JAK/STAT6 pathway, differentiation programs might partly be upregulated.

In summary, transcriptional data supports a constitutive activation of the IL4/JAK/STAT pathway in FLneg$^{m}$, accompanied by persistent GC-like programs and immunosuppressive TME features. FLneg$^{wt}$ showed hallmarks of a later B-cell differentiation stage and an immunologically active TME.

### 5.4.5 Integration into a Germinal Center Differentiation Model

Gene set enrichment analysis was performed using both HTG and NanoString data to allow further biological interpretations. Both datasets revealed significant differences in *STAT6*-associated genes between FLneg$^{m}$ and FLneg$^{wt}$. The analysis of the HTG data using Cluster Profiler further confirmed an enrichment of *STAT6*-associated genes.

The significantly increased expression of *FCER2* (CD23), *IL4R*, *IL13RA1* and *CCL17* in FLneg$^{m}$ strongly supports the model of a constantly active IL4/JAK/STAT6 signaling axis. This pathway is directly linked to CD23 expression and other activation-associated genes in GCBs [183]. As these genes are typically downregulated during terminal B-cell differentiation, their constant upregulation suggests that FLneg$^{m}$ cases maintain a post-activated GC phenotype, instead of progressing towards plasmablast differentiation. This concept is shown in **Figure 42**, which depicts the normal physiological pathway of GCB differentiation and the proposed mechanism in FLneg$^{m}$. The figure was adapted from Pignarre *et al.* to reflect our specific findings: Normally, naïve B cells encounter an antigen and upregulate CD23 upon IL4 stimulation. Activated CD23$^{+}$ B cells then migrate into the germinal center, where proliferation, somatic hypermutation and selection occurs. IL4/JAK/STAT6 signaling is naturally attenuated during this process, leading to CD23 downregulation. At the same time, transcriptional regulators such as IRF4 are induced, resulting in the transition to a plasmablast state, germinal center exit and terminal differentiation. [183]. In contrast, it seems like this differentiation pathway is disrupted in FLneg$^{m}$. The constitutive activation of the STAT6 pathway promotes expression of IL4R, CD23 and downstream target genes, preventing IRF4-mediated differentiation. Hence, B cells remain trapped in a post-activated GC-like state, unable to exit the germinal center (**Figure 42** left). This assumption is supported by additional plasmablast-associated genes upregulated in FLneg$^{wt}$. *SLAMF7* [203], *TNFRSF13B* [204], *IRF4* [220] and *LAG3* [221] are linked to terminal differentiation and immunoregulatory activity, which is consistent with a more differentiated phenotype.

Together, these findings support the hypothesis proposed by Pignarre *et al.* and we extend it to FLneg: Wild-type FLneg cases can pursue physiological B-cell differentiation, while *STAT6*/*SOCS1*-mutated FLneg remain trapped within the germinal center, characterized by a post-activated transcriptional program under constant STAT6 pathway activation. Further studies using primary FL cells and *in vivo* models are needed to validate our model. Here, it would be interesting to determine whether the STAT6 pathway can be modulated by drugs and whether the distinctive differentiation stages, if confirmed, can also be influenced.

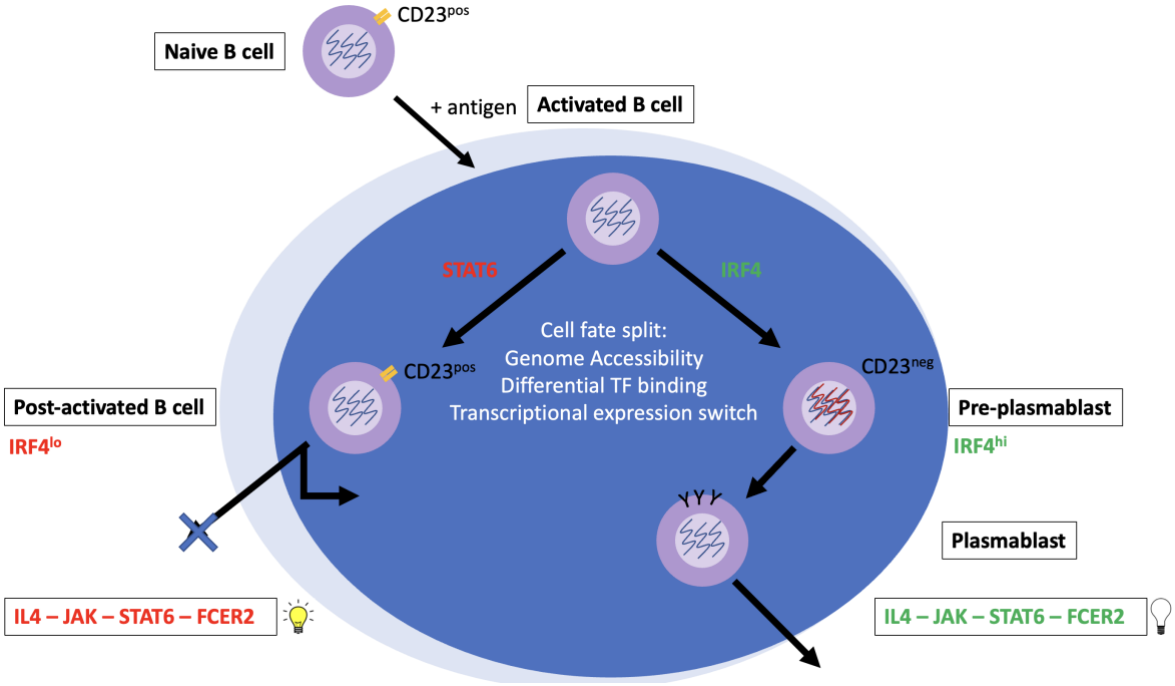


**Figure 42: Hypothesis of B-cell differentiation between FLneg$^{m}$ and FLneg$^{wt}$.**
*STAT6/SOCS1* mutated cases could be trapped within the germinal center by constitutive *STAT6* pathway activation preventing *IRF4* upregulation, showing a post-activated B-cell type, while *STAT6/SOCS1* wild-type cases could upregulate *IRF4*, further differentiate and exit the germinal center (modified from Pignarre *et al.* 2021[183]).

## 5.5 Molecular Heterogeneity and Outlier in FLneg$^{m}$ and FLneg$^{wt}$

### 5.5.1 Outliers in HTG and NanoString Clustering

**HTG**

Apart from one outlier, FL16$^{wt}$, which, despite being a *STAT6/SOCS1* wild-type case, was positioned at the edge of the FLneg$^{m}$ cluster, two FLneg$^{m}$ cases that were located at the periphery of the cluster, and another FLneg$^{wt}$ case (FLneg2$^{wt}$) that was placed at the edge of the FLneg$^{wt}$ cluster, it was possible to separate the two entities using GEP of HTG data. The outlier and the notable cases displayed altered gene expression for specific genes in the heatmap. FLneg16$^{wt}$ showed a slightly elevated gene expression of *IL4R* and *CD83* compared to the other wild-type cases. Interestingly, this case did not exhibit mutations in either the FL-typical or FLneg-typical panel; it was wild-type for all genes. Due to excessive artifacts, the Oncomine Lymphoma III panel could not provide further insights into the mutational landscape of FLneg16$^{wt}$. Nevertheless, this case appeared to differ from the other FLneg$^{wt}$ cases and the finding that it was characterized as outlier in both platforms suggest a reanalysis and a reclassification by a hematopathologist to provide new insights.

The peripheral location of FLneg80$^{m}$ may originate from its distinct gene expression compared to other FLneg$^{m}$ cases, particularly in *IL17RB* and *TNFRSF13B*, which showed lower gene expression and higher *CD83*, *FCER2* (CD23) and *IL4R* expression. Here, the combination of a *STAT6* mutation and multiple *SOCS1* mutations in this case could lead to a stronger expression of *STAT6*-associated genes. The location of FLneg84$^{m}$ at the edge of the FLneg$^{m}$ cluster, transitioning toward FLneg$^{wt}$, is likely due to its weaker expression of *CD83* and *CCL17*. Due to limited genetic information, no definitive conclusion can be drawn at this point. It is also important to consider biological variability between patient samples.

The evaluation of FLneg$^{m}$ vs. FLpos$^{m}$ heatmap data was limited due to low case numbers. As expected, *BCL2* showed stronger upregulation in FLpos$^{m}$. FLneg67$^{m}$, which clustered within FLpos$^{m}$ cluster, did not show any clear defining features, except for slightly elevated *BCL2* expression. Further cases are needed to increase reliability of GEP.

**NanoString**

Interestingly, FLneg16$^{wt}$, represented as outlier in NanoString FLneg$^{m}$ vs. FLneg$^{wt}$ as well. This case will be discussed in 5.5.3. The identification of the same outlier using both platforms underscores the robustness of our approaches.

### 5.5.2 Transcriptional Subclusters within FLneg$^{m}$

In HTG data, a further interesting observation was the stratification of the FLneg$^{m}$ cluster into three transcriptionally distinct subclusters, which occurred after hierarchical clustering of FLneg$^{m}$ vs. FLneg$^{wt}$. These subclusters showed differences in the expression intensity of STAT6 target genes such as *IL4R*, *FCER2*, and *CD83*. From Cluster 1 to Cluster 3, these genes showed gradual decrease in gene expression. At the same time, gene expression of genes associated with late B-cell differentiation increased, supporting the hypothesis, that these genes reflect differentiation state of the malignant FL cells. It was found that the subcluster distribution also correlated with mutational burden and composition. Cluster 1 showed the highest number of mutations per case accompanied by a high proportion of double-mutated cases (*STAT6* + *SOCS1*). In contrast, Cluster 3 was characterized by fewer mutations and lower frequency of co-mutations. Additive or synergistic effects through *STAT6* gain of function and simultaneous loss of function in *SOCS1* may lead to enhanced and sustained pathway activation [222]. This finding indicates that FLneg$^{m}$ is not a transcriptionally uniform entity but instead comprises a spectrum of subtypes with variable STAT6 pathway activity and mutational load. The biological stability and correlation with clinical or histological features remain to be further investigated. However, the data show that molecular stratification within FLneg$^{m}$ may refine current classification and help to find functionally distinct subtypes.

### 5.5.3 Heterogeneity in FLneg$^{wt}$

Within the FLneg$^{wt}$ group, one notable case was FLneg2$^{wt}$. This case exhibited very strong *FCRLA* and *SLAMF7* expression. The case was Grade IIIA, had a high Ki-67 index, and, apart from a *TNFRSF14* mutation, showed no other mutations in FL, FLneg and IL4R panels. Unfortunately, due to artifacts, an evaluation of the Oncomine Lymphoma III panel was not possible, which could have provided information on additional gene mutations. In a later analysis, where MUM1 (*IRF4*) staining was performed on FL cases (data not shown), this case showed a positive result. Combined with the strong expression of *SLAMF7*, which is associated to plasma cells ([203]), this suggests that the B cells in this case are in a more differentiated state. Regarding *FCRLA*, which also was

highly expressed in this case, a study found elevated *FCRLA* levels in a subset of terminally differentiated B cells [223]. Therefore, the high *FCRLA* expression could be related to the high expression of *SLAMF7*.

Using NanoString data, the FLneg$^{m}$ and FLneg$^{wt}$ could be separated from each other except for one outlier, FLneg16$^{wt}$, a wild-type case located within the FLneg$^{m}$ cluster. The case was likely assigned to the FLneg$^{m}$ cluster because *STAT6*-associated genes, such as *IL4R*, *FCER2*, and *CCL17*, showed an overall higher expression. The outlier was also detected in the HTG heatmap and had already been discussed in that context. Since it was identified by both methods, we do not assume a technical cause but rather a biological one, which could be further investigated through additional mutation analyses. Also, a misdiagnosis cannot be excluded. Hematopathology reevaluation and expanded sequencing would be required to clarify this case.

Next, the separation of FLneg$^{wt}$ into two subgroups was investigated. Three cases formed an additional cluster. The mutational landscape of the cases was unremarkable. The comparison of case characteristics could not provide any similarities except for the expression profile, which showed lower expression of *STAT6*-associated genes compared to the other FLneg$^{wt}$ cluster. Thus, the two groups could also be separated using NanoString technology.

Ultimately, our data support that FLneg$^{m}$ and FLneg$^{wt}$ are molecularly diverse entities showing heterogeneity within their group, leading to differences in TME composition, mutational patterns, or differentiation stage. Since the subgroupings were deduced exclusively from transcriptional clustering, histology, microdissection and single-cell data would be needed to confirm these clusters as true biological subtypes or intratumoral heterogeneity.

## 5.6 *CREBBP* and *TNFRSF14* Co-Mutations in FLneg and their Impact on Gene Expression

*STAT6/SOCS1*-mutated FLneg cases often exhibited co-mutations in *CREBBP* and *TNFRSF14* [60]. To investigate whether these co-mutations influence gene expression, the subset of our FLneg$^{m}$ cohort with known *CREBBP* and *TNFRSF14* mutation status using HTG data was analyzed. PCA plots could not differentiate the groups. Furthermore, no differentially expressed genes were found between *CREBBP*-mutated and wild-type cases, nor between *TNFRSF14*-mutated and wild-type cases. Therefore, it is currently not possible to determine whether there is a connection between these co-mutations and gene expression. The negative result must be

considered with caution, since *CREBBP* as chromatin regulator influences much more genes than covered by our panels. Therefore, whole exome analysis would be recommended. Also, genes influenced by *TNFRSF14* are not completely covered by our panel. Ultimately, mutational status alone cannot reflect functional activity, since allelic imbalances, domain involvement and co-occurring mutations should also be considered.

A recent study suggested that intact *CREBBP* is required for IL4/JAK/STAT6 pathway activation and mutated *CREBBP* weakens pathway activation in FL [71]. In the current study, FLpos was used for statistical analysis to investigate a potential link between *CREBBP* mutations, *STAT6/SOCS1* mutations and CD23 expression. In 2/5 cases information on FL-positive mutations were missing, preventing any definitive conclusions for these cases. The small sample number, possible interference with CD23 regulating mechanisms and compensation of *STAT6/SOCS1* for *CREBBP* mutations could explain this result. Based on the available data, it is not possible to determine whether epigenetic alterations influence CD23 expression. An expansion of the cohort and the use of larger gene panels, up to whole exome sequencing, could provide further insights.

Multivariate analysis of all FLneg cases using binary logistic regression (including *CREBBP* and *STAT6/SOCS1* mutation status) showed a highly significant association to CD23 expression. This effect almost exclusively resulted from strong correlation between *STAT6/SOCS1* mutations and CD23 expression. *CREBBP* status could not show any effect, neither in single analysis nor in multivariate model. This result emphasized that in FLneg CD23 expression is predominantly induced by genetic alterations of IL4/JAK/STAT6 pathway and epigenetic changes such as *CREBBP* mutations might not contribute in a significant way. Using the multivariate model we could underline the dominant role of *STAT6/SOCS1* as predictors for CD23 positivity in this collective. Nevertheless, limited gene panel coverage and small group sizes prevent from drawing definitive conclusions. Expanded cohorts and broader sequencing approaches will be required to determine the influence of *CREBBP* and *TNFRSF14* co-mutations.

## 5.7 Limitations

This chapter discussed the key limitations discussed previously.

### 5.7.1 Cohort-related Limitations

The enrichment of $CD23^+$ FLneg cases improved the detection of $FLneg^m$ cases but introduced a selection bias which influenced the prevalence of $FLneg^m$. Furthermore, the number of $FLpos^m$ cases was very small, limiting comparisons between $FLneg^m$ and $FLpos^m$. Also, some cases lacked complete sequencing data due to technical artifacts leading to incomplete mutational characterization.

### 5.7.2 Biological Limitations

The functional consequences of mutations found using Oncomine Lymphoma III panel (e.g. *ATM*, *TET2*, *TMSB4X*) remain unknown. The subclusters identified within $FLneg^m$ and $FLneg^{wt}$ still require clinical correlation. Last, outlier cases could reflect biological subgroups or misclassification but could not fully be resolved.

Taken together, the limitations mentioned suggest the consideration of additional approaches, such as functional assays, broader genomic profiling and spatial analysis to further explore STAT6-driven biology in FLneg. They do not invalidate the findings but define the boundaries of interpretation and underline the need for integrative multi-omics approaches.

# 6. Summary and Outlook

## 6.1.1 Summary

In this thesis, the transcriptional consequences of activating *STAT6* and loss of function *SOCS1* mutations in FLneg and FLpos were systematically investigated. Using two independent HTG EdgeSeq and NanoString gene expression profiling platforms, distinct transcriptional signatures in mutated cases were identified, characterized by elevated expression of *IL4R*, *FCER2* (CD23), *IL13RA1*, and *CCL17*. The upregulation of these genes is associated with IL4/JAK/STAT6 activation [183]. Additionally, upregulated *CD83*, *ALOX5*, and *PIK3CG* suggested persistent B-cell activation and a retention of post-germinal center B-cell phenotype.

By contrast, FLneg wild-type cases were characterized by an upregulation of *IRF4*, *SLAMF7* and *TNFRSF13B* as well as immune effectors, which leads to the assumption of a more differentiated and immunologically active microenvironment. These findings support the model introduced by Pignarre *et al.* and extended by our data to FLneg, proposing that FLneg$^{m}$ cases might be transcriptionally trapped in a post-activated germinal center state caused by consistent *STAT6* activation, while FLneg$^{wt}$ can further differentiate and exit the germinal center.

Importantly, subclustering within FLneg$^{m}$ revealed transcriptional heterogeneity, which was associated with different *STAT6* activity and mutational load. This variability within FLneg$^{m}$ may reflect different degrees of pathway activation, potentially defining biologically meaningful subgroups. Transcriptionally defined subtypes in other lymphomas with JAK/STAT involvement have already been identified in classic Hodgkin lymphoma [224].

## 6.1.2 Future Directions

Key differentially expressed genes such as *IRF4* should be validated at the protein level using MUM1 immunohistochemistry. Next, functional validation on STAT6-driven B-cell differentiation blockade should be performed *in vitro* or *ex vivo* using either primary FLneg$^{m}$ samples or CRISPR-modified models such as in a study from Reddy *et al.* (2017), which applied CRISPR to evaluate functional impact of previously identified genetic drivers [225]. This approach could help to

confirm the causative role of *STAT6* gain-of-function mutations in preventing IRF4 induction and terminal differentiation.

Since the present thesis investigated bulk FL samples, integration of spatial transcriptomics and single-cell analyses would expand the knowledge regarding cell-type specific expression patterns and TME interactions. Extending this STAT6-focused paradigm to other GC-derived lymphomas (pediatric-type FL, MZL) could help determine whether STAT6-mediated GC retention is a broader mechanism of lymphomagenesis. Regarding clinical implications, CD23 and selected STAT6 target genes might serve as biomarker panel to recognize FLneg$^{m}$ patients. These patients might be susceptible to inhibition of JAK/STAT and PI3K signaling. JAK and PI3K inhibitors have already shown effects in related B-cell malignancies [226, 227]. Using preclinical models and clinical studies, these agents might be effective in STAT6-driven FLneg subsets.

The differences in TME between FLneg$^{m}$ (immunosuppressive signature) and FLneg$^{wt}$ (immunologically active signature) gene expression data raise the question if these subgroups may respond differently to immunomodulatory therapies. In a first step, TME differences should be confirmed using spatial transcriptomics followed by functional testing. Ultimately, differently shaped TMEs, if confirmed, would allow specific treatment of FLneg$^{m}$ and FLneg$^{wt}$ patients, elevating therapeutic success.

In summary, this thesis found FLneg$^{m}$ as distinct molecular subset. It was characterized by constitutive IL4/JAK/STAT6 pathway activation, GC retention and specific TME signature. Our mutational, transcriptional and conceptual data delivers the basis for future functional studies, biomarker-driven subclassification and therapeutic targeting in FLneg and related GC-derived lymphomas.

# 7. Author's contribution

In the following table the experiments and analyses in this thesis as well as their contributors are listed (**Table 25**):

**Table 25: Experiments/analyses performed in this thesis with corresponding contributors**

| **Experiment/Analysis** | **Contributor** |
|---|---|
| CD23 IHC staining | IHC department |
| Deparaffinization for DNA/RNA Extraction | Molecular Tumor Diagnostics Lab |
| DNA Extraction | Molecular Tumor Diagnostics Lab |
| RNA Extraction | Molecular Tumor Diagnostics Lab |
| Determination of nucleic acid concentration with NanoDrop spectrophotometer | Molecular Tumor Diagnostics Lab |
| Determination of DNA concentration using Qbit | Molecular Tumor Diagnostics Lab |
| Determination of DV200 for NanoString | NGS Competence Center Tübingen |
| Mutation Analysis with Ion Torrent | Experimental: mainly Molecular Tumor Diagnostics Lab during research runs<br>Data Analysis: Author + validation by experienced member of the molecular pathology department |
| Gene Expression Profiling with HTG | Experimental: Author<br>Data Analysis: Author<br>Later validated by a bioinformatician |
| Gene Expression Profiling with NanoString | Experimental: Author<br>Data Analysis: Author<br>Later validated by a bioinformatician |
| Gene Set Enrichment Analysis & ClusterProfiler | Author, later validated by a bioinformatician |
| Statistical Analyses | Author |

# 8. References


1. Carpenter, S. and L.A.J. O'Neill, From periphery to center stage: 50 years of advancements in innate immunity. Cell, 2024. **187**(9): p. 2030-2051.

2. Kalló, G., et al., Chemical barrier proteins in human body fluids. Biomedicines, 2022. **10**(7): p. 1472.

3. Lee, H.-J. and M. Kim, Skin barrier function and the microbiome. International journal of molecular sciences, 2022. **23**(21): p. 13071.

4. Wertz, P.W. and S. de Szalay, Innate antimicrobial defense of skin and oral mucosa. 2020, MDPI. p. 159.

5. Amarante-Mendes, G.P., et al., Pattern Recognition Receptors and the Host Cell Death Molecular Machinery. Front Immunol, 2018. **9**: p. 2379.

6. Netea, M.G. and L.A.B. Joosten, Trained innate immunity: Concept, nomenclature, and future perspectives. Journal of Allergy and Clinical Immunology, 2024. **154**(5): p. 1079-1084.

7. Pradeu, T., et al., The conceptual foundations of innate immunity: Taking stock 30 years later. Immunity, 2024. **57**(4): p. 613-631.

8. Chi, H., M. Pepper, and P.G. Thomas, Principles and therapeutic applications of adaptive immunity. Cell, 2024. **187**(9): p. 2052-2078.

9. Peng, B., Y. Ming, and C. Yang, Regulatory B cells: the cutting edge of immune tolerance in kidney transplantation. Cell Death & Disease, 2018. **9**(2): p. 109.

10. Hardy, R.R. and K. Hayakawa, B cell development pathways. Annu Rev Immunol, 2001. **19**: p. 595-621.

11. Pieper, K., B. Grimbacher, and H. Eibel, B-cell biology and development. J Allergy Clin Immunol, 2013. **131**(4): p. 959-71.

12. Edwards, J.C.W. and G. Cambridge, B-cell targeting in rheumatoid arthritis and other autoimmune diseases. Nature Reviews Immunology, 2006. **6**(5): p. 394-403.

13. Betzler, A.C., A. Ushmorov, and C. Brunner, The transcriptional program during germinal center reaction - a close view at GC B cells, Tfh cells and Tfr cells. Front Immunol, 2023. **14**: p. 1125503.

14. Swerdlow, S.H., O. World Health, and C. International Agency for Research on, WHO classification of tumours of haematopoietic and lymphoid tissues. Revised fourth edition. ed. World Health Organization classification of tumours. 2017, Lyon: International Agency for Research on Cancer. 585 pages : illustrations.

15. Rappaport, H. and P. National Research Council . Committee on, Tumors of the hematopoietic system. Atlas of tumor pathology 2nd ser. fasc. 8. 1966, Washington, D.C: Armed Forces Institute of Pathology. 442 p. : ill.

16. Bennett, M., et al., CLASSIFICATION OF NON-HODGKIN'S LYMPHOMAS. The Lancet, 1974. **304**(7877): p. 405-408.

17. Stansfeld, A.G., et al., Updated Kiel classification for lymphomas. Lancet, 1988. **1**(8580): p. 292-3.

18. Campo, E., et al., The International Consensus Classification of Mature Lymphoid Neoplasms: a report from the Clinical Advisory Committee. Blood, 2022. **140**(11): p. 1229-1253.

19. Brill, N.E., G. Baehr, and N. Rosenthal, Generalized giant lymph follicle hyperplasia of lymph nodes and spleen; a hitherto undescribed type. Am J Med, 1952. **13**(5): p. 570-4.

20. Swerdlow, S.H., et al., World Health Organization classification of tumours of haematopoietic and lymphoid tissues. 2008, Lyon: IARC press.

21. Vaandrager, J.W., et al., V(D)J recombinase-mediated transposition of the BCL2 gene to the IGH locus in follicular lymphoma. Blood, 2000. **96**(5): p. 1947-52.

22. Yunis, J.J., et al., Distinctive chromosomal abnormalities in histologic subtypes of non-Hodgkin's lymphoma. N Engl J Med, 1982. **307**(20): p. 1231-6.

23. Bujoreanu, I. and V. Gupta, Anatomy, Lymph Nodes, in *StatPearls*. 2024, StatPearls Publishing: Treasure Island (FL).

24. He, A., et al., Nanovaccine-based strategies for lymph node targeted delivery and imaging in tumor immunotherapy. Journal of Nanobiotechnology, 2023. **21**.

25. De Silva, N.S. and U. Klein, Dynamics of B cells in germinal centres. Nature Reviews Immunology, 2015. **15**(3): p. 137-148.

26. Randall, C. and Y. Fedoriw, Pathology and diagnosis of follicular lymphoma and related entities. Pathology, 2020. **52**(1): p. 30-39.

27. Khanlari, M. and J.R. Chapman, Follicular lymphoma: updates for pathologists. J Pathol Transl Med, 2022. **56**(1): p. 1-15.

28. Okosun, J., et al., Integrated genomic analysis identifies recurrent mutations and evolution patterns driving the initiation and progression of follicular lymphoma. Nature Genetics, 2014. **46**(2): p. 176-181.

29. Pasqualucci, L., et al., Inactivating mutations of acetyltransferase genes in B-cell lymphoma. Nature, 2011. **471**(7337): p. 189-195.

30. Béguelin, W., et al., EZH2 Is Required for Germinal Center Formation and Somatic EZH2 Mutations Promote Lymphoid Transformation. Cancer Cell, 2013. **23**(5): p. 677-692.

31. Zhang, J., et al., Disruption of KMT2D perturbs germinal center B cell development and promotes lymphomagenesis. Nat Med, 2015. **21**(10): p. 1190-8.

32. Li, J., et al., Loss of CREBBP and KMT2D cooperate to accelerate lymphomagenesis and shape the lymphoma immune microenvironment. Nature Communications, 2024. **15**(1): p. 2879.

33. Zhu, Y., et al. The Role of CREBBP/EP300 and Its Therapeutic Implications in Hematological Malignancies. Cancers, 2023. **15**, DOI: 10.3390/cancers15041219.

34. Huet, S., et al., EZH2 alterations in follicular lymphoma: biological and clinical correlations. Blood Cancer J, 2017. **7**(4): p. e555.

35. Morin, R.D., et al., Somatic mutations altering EZH2 (Tyr641) in follicular and diffuse large B-cell lymphomas of germinal-center origin. Nat Genet, 2010. **42**(2): p. 181-5.

36. Kumar, E., L. Pickard, and J. Okosun, Pathogenesis of follicular lymphoma: genetics to the microenvironment to clinical translation. British Journal of Haematology, 2021. **194**(5): p. 810-821.

37. Li, H., et al., Mutations in linker histone genes HIST1H1 B, C, D, and E; OCT2 (POU2F2); IRF8; and ARID1A underlying the pathogenesis of follicular lymphoma. Blood, 2014. **123**(10): p. 1487-1498.

38. Kalashnikova, A.A., R.A. Rogge, and J.C. Hansen, Linker histone H1 and protein-protein interactions. Biochim Biophys Acta, 2016. **1859**(3): p. 455-61.

39. Soshnev, A.A., et al., Histone H1 Mutations in Lymphoma: A Link(er) between Chromatin Organization, Developmental Reprogramming, and Cancer. Cancer Res, 2021. **81**(24): p. 6061-6070.

40. Dobaño-López, C., et al., Follicular Lymphoma Microenvironment: An Intricate Network Ready for Therapeutic Intervention. Cancers, 2021. **13**(4): p. 641.

41. Zhu, D., et al., Acquisition of potential N-glycosylation sites in the immunoglobulin variable region by somatic mutation is a distinctive feature of follicular lymphoma. Blood, 2002. **99**(7): p. 2562-8.

42. Valle-Argos, B., et al., DC-SIGN binding to mannosylated B-cell receptors in follicular lymphoma down-modulates receptor signaling capacity. Scientific Reports, 2021. **11**(1): p. 11676.

43. McCann, K.J., et al., Remarkable selective glycosylation of the immunoglobulin variable region in follicular lymphoma. Mol Immunol, 2008. **45**(6): p. 1567-72.

44. Cong, P., et al., In situ localization of follicular lymphoma: description and analysis by laser capture microdissection. Blood, 2002. **99**(9): p. 3376-3382.

45. Henopp, T., et al., Prevalence of follicular lymphoma in situ in consecutively analysed reactive lymph nodes. Histopathology, 2011. **59**(1): p. 139-142.

46. Schmidt, J., et al., Increasing genomic and epigenomic complexity in the clonal evolution from in situ to manifest t(14;18)-positive follicular lymphoma. Leukemia, 2014. **28**(5): p. 1103-1112.

47. Schmidt, J., et al., CREBBP gene mutations are frequently detected in in situ follicular neoplasia. Blood, 2018. **132**(25): p. 2687-2690.

48. Antonio, V., et al., Genetic evolution of in situ follicular neoplasia to aggressive B-cell lymphoma of germinal center subtype. Haematologica, 2021. **106**(10): p. 2673-2681.

49. Mamessier, E., et al., Nature and importance of follicular lymphoma precursors. Haematologica, 2014. **99**(5): p. 802.

50. Hellmuth, J.C., et al., Duodenal-type and nodal follicular lymphomas differ by their immune microenvironment rather than their mutation profiles. Blood, The Journal of the American Society of Hematology, 2018. **132**(16): p. 1695-1702.

51. Alaggio, R., et al., The 5th edition of the World Health Organization Classification of Haematolymphoid Tumours: Lymphoid Neoplasms. Leukemia, 2022. **36**(7): p. 1720-1748.

52. Dominik, N., et al., Clonally related duodenal-type follicular lymphoma and in situ follicular neoplasia. Haematologica, 2019. **104**(11): p. e537-e539.

53. Roulland, S., et al., Follicular Lymphoma-Like B Cells In Healthy Individuals Are Released From Pretumoral Niches Established In Secondary Lymphoid Tissues. Blood, 2010. **116**(21): p. 466-466.

54. Vaandrager, J.-W., et al., Interphase FISH detection of rearrangement in follicular lymphoma using breakpoint-flanking probes. Genes, Chromosomes and Cancer, 2000. **27**(1): p. 85-94.

55. Albinger-Hegyi, A., et al., High Frequency of t(14;18)-Translocation Breakpoints Outside of Major Breakpoint and Minor Cluster Regions in Follicular Lymphomas: Improved Polymerase Chain Reaction Protocols for Their Detection. The American Journal of Pathology, 2002. **160**(3): p. 823-832.

56. Aster, J.C. and J.A. Longtine, Detection of BCL2 rearrangements in follicular lymphoma. Am J Pathol, 2002. **160**(3): p. 759-63.

57. Leich, E., et al., Follicular lymphomas with and without translocation t(14;18) differ in gene expression profiles and genetic alterations. Blood, 2009. **114**(4): p. 826-834.

58. Leich, E., et al., MicroRNA profiles of t(14;18)–negative follicular lymphoma support a late germinal center B-cell phenotype. Blood, 2011. **118**(20): p. 5550-5558.

59. Katzenberger, T., et al., A distinctive subtype of t(14;18)-negative nodal follicular non-Hodgkin lymphoma characterized by a predominantly diffuse growth pattern and deletions in the chromosomal region 1p36. Blood, 2009. **113**(5): p. 1053-61.

60. Nann, D., et al., Follicular lymphoma t(14;18)-negative is genetically a heterogeneous disease. Blood Adv, 2020. **4**(22): p. 5652-5665.

61. Siddiqi, I.N., et al., Characterization of a variant of t(14;18) negative nodal diffuse follicular lymphoma with CD23 expression, 1p36/TNFRSF14 abnormalities, and STAT6 mutations. Mod Pathol, 2016. **29**(6): p. 570-81.

62. Zamò, A., et al., Differences between BCL2-break positive and negative follicular lymphoma unraveled by whole-exome sequencing. Leukemia, 2018. **32**(3): p. 685-693.

63. Leich, E., et al., Follicular lymphoma subgroups with and without t(14;18) differ in their N-glycosylation pattern and IGHV usage. Blood Advances, 2021. **5**(23): p. 4890-4900.

64. Salaverria, I., O. Weigert, and L. Quintanilla-Martinez, The clinical and molecular taxonomy of t(14;18)-negative follicular lymphomas. Blood Adv, 2023. **7**(18): p. 5258-5271.

65. Jaffe, E.S. and A. Carbone, B- and T-/NK-Cell Lymphomas in the 2022 International Consensus Classification of Mature Lymphoid Neoplasms and Comparison with the WHO Fifth Edition. Hemato, 2024. **5**(2): p. 157-170.

66. Zamò, A., et al., The exomic landscape of t(14;18)-negative diffuse follicular lymphoma with 1p36 deletion. British Journal of Haematology, 2018. **180**(3): p. 391-394.

67. Mentz, M., et al., PARP14 is a novel target in STAT6 mutant follicular lymphoma. Leukemia, 2022. **36**(9): p. 2281-2292.

68. Yildiz, M., et al., Activating STAT6 mutations in follicular lymphoma. Blood, 2015. **125**(4): p. 668-679.

69. Nann, D., et al., Clonally related duodenal-type follicular lymphoma and in situ follicular neoplasia. Haematologica, 2019. **104**(11): p. e537-e539.

70. Xian, R.R., et al., CREBBP and STAT6 co-mutation and 16p13 and 1p36 loss define the t(14;18)-negative diffuse variant of follicular lymphoma. Blood Cancer J, 2020. **10**(6): p. 69.

71. Shao, Q., et al., STAT6 mutations compensate for CREBBP mutations and hyperactivate IL4/STAT6/RRAGD/mTOR signaling in follicular lymphoma. Leukemia, 2025.

72. Zhang, J., et al., The CREBBP Acetyltransferase Is a Haploinsufficient Tumor Suppressor in B-cell Lymphoma. Cancer Discov, 2017. **7**(3): p. 322-337.

73. Boice, M., et al., Loss of the HVEM Tumor Suppressor in Lymphoma and Restoration by Modified CAR-T Cells. Cell, 2016. **167**(2): p. 405-418.e13.

74. Barasch, N.J.K., et al., The molecular landscape and other distinctive features of primary cutaneous follicle center lymphoma. Hum Pathol, 2020. **106**: p. 93-105.

75. Conconi, A., et al., Primary Extranodal Follicular Lymphoma: A Retrospective Survey of the International Extranodal Lymphoma Study Group (IELSG). Hematological Oncology, 2025. **43**(4): p. e70111.

76. Ozawa, M.G., et al., A study of the mutational landscape of pediatric-type follicular lymphoma and pediatric nodal marginal zone lymphoma. Modern Pathology, 2016. **29**(10): p. 1212-1220.

77. Martin-Guerrero, I., et al., Recurrent loss of heterozygosity in 1p36 associated with TNFRSF14 mutations in IRF4 translocation negative pediatric follicular lymphomas. haematologica, 2013. **98**(8): p. 1237.

78. Schmidt, J., et al., Genome-wide analysis of pediatric-type follicular lymphoma reveals low genetic complexity and recurrent alterations of TNFRSF14 gene. Blood, The Journal of the American Society of Hematology, 2016. **128**(8): p. 1101-1111.

79. Louissaint Jr, A., et al., Pediatric-type nodal follicular lymphoma: a biologically distinct lymphoma with frequent MAPK pathway mutations. Blood, The Journal of the American Society of Hematology, 2016. **128**(8): p. 1093-1100.

80. Schmidt, J., et al., Mutations of MAP2K1 are frequent in pediatric-type follicular lymphoma and result in ERK pathway activation. Blood, 2017. **130**(3): p. 323-327.

81. Baron, B.W., et al., Identification of the gene associated with the recurring chromosomal translocations t (3; 14)(q27; q32) and t (3; 22)(q27; q11) in B-cell lymphomas. Proceedings of the National Academy of Sciences, 1993. **90**(11): p. 5262-5266.

82. Horsman, D.E., et al., Follicular lymphoma lacking the t (14; 18)(q32; q21): identification of two disease subtypes. British journal of haematology, 2003. **120**(3): p. 424-433.

83. Jardin, F., et al., Follicular lymphoma without t (14; 18) and with BCL-6 rearrangement: a lymphoma subtype with distinct pathological, molecular and clinical characteristics. Leukemia, 2002. **16**(11): p. 2309-2317.

84. Vries, L.-d., et al., Genomic and microenvironmental landscape of stage I follicular lymphoma, compared with stage III/IV. 2022.

85. Salaverria, I., O. Weigert, and L. Quintanilla-Martinez, The clinical and molecular taxonomy of t(14;18)-negative follicular lymphomas. Blood Advances, 2023. **7**(18): p. 5258-5271.

86. Beard, R.E., et al., Gene expression profiling using nanostring digital RNA counting to identify potential target antigens for melanoma immunotherapy. Clin Cancer Res, 2013. **19**(18): p. 4941-50.

87. Melero, I., et al., Therapeutic vaccines for cancer: an overview of clinical trials. Nat Rev Clin Oncol, 2014. **11**(9): p. 509-24.

88. Gajewski, T.F., et al., Molecular profiling to identify relevant immune resistance mechanisms in the tumor microenvironment. Curr Opin Immunol, 2011. **23**(2): p. 286-92.

89. Jaramillo, M.C., et al., Gene expression profiling signatures for immunophenotyping of tumor microenvironment using HTG EdgeSeq Precision Immuno-Oncology Panel. Journal of Clinical Oncology, 2021. **39**(15_suppl): p. e14528-e14528.

90. Ran, D., et al., Platform comparison of HTG EdgeSeq and RNA-Seq for gene expression profiling of tumor tissue specimens. Journal of Clinical Oncology, 2020. **38**(15_suppl): p. 3566-3566.

91. O'Rourke, D., et al., Abstract 2016: Comparison of HTG-edge targeted RNA sequencing platform with whole transcriptome RNA sequencing for clinical biomarker studies. Cancer Research, 2020. **80**(16_Supplement): p. 2016-2016.

92. Borchert, S., et al., Transcriptome-Wide Gene Expression Profiles from FFPE Materials Based on a Nuclease Protection Assay Reveals Significantly Different Patterns between Synovial Sarcomas and Morphologic Mimickers. Cancers, 2022. **14**(19): p. 4737.

93. Cesano, A., nCounter® PanCancer Immune Profiling Panel (NanoString Technologies, Inc., Seattle, WA). Journal for ImmunoTherapy of Cancer, 2015. **3**(1): p. 42.

94. Kolhe, R., et al., Nanostring-Based Identification of the Gene Expression Profile in Trigger Finger Samples. Healthcare, 2021. **9**(11): p. 1592.

95. Zhang, L., et al., Cross-platform comparison of immune-related gene expression to assess intratumor immune responses following cancer immunotherapy. Journal of Immunological Methods, 2021. **494**: p. 113041.

96. Alizadeh, A.A., et al., Distinct types of diffuse large B-cell lymphoma identified by gene expression profiling. Nature, 2000. **403**(6769): p. 503-11.

97. Schmidt, J., et al., Mutations of MAP2K1 are frequent in pediatric-type follicular lymphoma and result in ERK pathway activation. Blood, The Journal of the American Society of Hematology, 2017. **130**(3): p. 323-327.

98. Arber, D.A., et al., The 2016 revision to the World Health Organization classification of myeloid neoplasms and acute leukemia. Blood, 2016. **127**(20): p. 2391-2405.

99. Yu, G., et al., clusterProfiler: an R package for comparing biological themes among gene clusters. Omics, 2012. **16**(5): p. 284-7.

100. Love, M.I., W. Huber, and S. Anders, Moderated estimation of fold change and dispersion for RNA-seq data with DESeq2. Genome Biology, 2014. **15**(12): p. 550.

101. Mootha, V.K., et al., PGC-1α-responsive genes involved in oxidative phosphorylation are coordinately downregulated in human diabetes. Nature Genetics, 2003. **34**(3): p. 267-273.

102. Subramanian, A., et al., Gene set enrichment analysis: A knowledge-based approach for interpreting genome-wide expression profiles. Proceedings of the National Academy of Sciences, 2005. **102**(43): p. 15545-15550.

103. Losman, J.A., et al., Cutting edge: SOCS-1 is a potent inhibitor of IL-4 signal transduction. J Immunol, 1999. **162**(7): p. 3770-4.

104. Pangault, C., et al., Follicular lymphoma cell niche: identification of a preeminent IL-4-dependent TFH–B cell axis. Leukemia, 2010. **24**(12): p. 2080-2089.

105. Jiang, Y., et al., CREBBP inactivation promotes the development of HDAC3-dependent lymphomas. Cancer discovery, 2017. **7**(1): p. 38-53.

106. Schroers-Martin, J.G., et al., Tracing founder mutations in circulating and tissue-resident follicular lymphoma precursors. Cancer discovery, 2023. **13**(6): p. 1310-1323.

107. Tinnell, S.B., et al., STAT6, NF-kappaB and C/EBP in CD23 expression and IgE production. International Immunology, 1998. **10**(10): p. 1529-1538.

108. Olteanu, H., et al., CD23 Expression in Follicular Lymphoma: Clinicopathologic Correlations. American Journal of Clinical Pathology, 2011. **135**(1): p. 46-53.

109. Shi, J., et al., Involvement of IL-4, IL-13 and Their Receptors in Pancreatic Cancer. International Journal of Molecular Sciences, 2021. **22**(6): p. 2998.

110. Viganò, E., et al., Somatic IL4R mutations in primary mediastinal large B-cell lymphoma lead to constitutive JAK-STAT signaling activation. Blood, 2018. **131**(18): p. 2036-2046.

111. Witthuhn, B.A., et al., Involvement of the Jak-3 Janus kinase in signalling by interleukins 2 and 4 in lymphoid and myeloid cells. Nature, 1994. **370**(6485): p. 153-7.

112. Murata, T., P.D. Noguchi, and R.K. Puri, IL-13 induces phosphorylation and activation of JAK2 Janus kinase in human colon carcinoma cell lines: similarities between IL-4 and IL-13 signaling. J Immunol, 1996. **156**(8): p. 2972-8.

113. Smerz-Bertling, C. and A. Duschl, Both interleukin 4 and interleukin 13 induce tyrosine phosphorylation of the 140-kDa subunit of the interleukin 4 receptor. J Biol Chem, 1995. **270**(2): p. 966-70.

114. Wang, H.Y., J. Zamorano, and A.D. Keegan, A role for the insulin-interleukin (IL)-4 receptor motif of the IL-4 receptor alpha-chain in regulating activation of the insulin receptor substrate 2 and signal transducer and activator of transcription 6 pathways. Analysis by mutagenesis. J Biol Chem, 1998. **273**(16): p. 9898-905.

115. Millward-Sadler, S.J., et al., Roles for the interleukin-4 receptor and associated JAK/STAT proteins in human articular chondrocyte mechanotransduction. Osteoarthritis Cartilage, 2006. **14**(10): p. 991-1001.

116. Takeda, K., et al., Essential role of Stat6 in IL-4 signalling. Nature, 1996. **380**(6575): p. 627-630.

117. Bouska, A., et al., Combined copy number and mutation analysis identifies oncogenic pathways associated with transformation of follicular lymphoma. Leukemia, 2017. **31**(1): p. 83-91.

118. Okosun, J., et al., Integrated genomic analysis identifies recurrent mutations and evolution patterns driving the initiation and progression of follicular lymphoma. Nat Genet, 2014. **46**(2): p. 176-181.

119. Pasqualucci, L., et al., Genetics of follicular lymphoma transformation. Cell Rep, 2014. **6**(1): p. 130-40.

120. Guiter, C., et al., Constitutive STAT6 activation in primary mediastinal large B-cell lymphoma. Blood, 2004. **104**(2): p. 543-549.

121. Ma, M.C.J., et al., Subtype-specific and co-occurring genetic alterations in B-cell non-Hodgkin lymphoma. Haematologica, 2022. **107**(3): p. 690-701.

122. Grønbæk, K., et al., ATM mutations are associated with inactivation of theARF-TP53 tumor suppressor pathway in diffuse large B-cell lymphoma. Blood, 2002. **100**(4): p. 1430-1437.

123. Morita, T. and K.i. Hayashi, Tumor Progression Is Mediated by Thymosin-β4 through a TGFβ/MRTF Signaling Axis. Molecular Cancer Research, 2018. **16**(5): p. 880-893.

124. Quintanilla-Martinez, L., et al., Emerging entities: high-grade/large B-cell lymphoma with 11q aberration, large B-cell lymphoma with IRF4 rearrangement, and new molecular subgroups in large B-cell lymphomas. A report of the 2022 EA4HP/SH lymphoma workshop. Virchows Archiv, 2023. **483**(3): p. 281-298.

125. Dominguez, P.M., et al., TET2 Deficiency Causes Germinal Center Hyperplasia, Impairs Plasma Cell Differentiation, and Promotes B-cell Lymphomagenesis. Cancer Discovery, 2018. **8**(12): p. 1632-1653.

126. Young, A.L., et al., Clonal hematopoiesis and risk of acute myeloid leukemia. Haematologica, 2019. **104**(12): p. 2410-2417.

127. Liu, M., et al., Clonal hematopoiesis of indeterminate potential (CHIP) and risk of non-Hodgkin lymphoma: A community-based cohort study. Hemasphere, 2025. **9**(7): p. e70187.

128. Darnell Jr, J.E., STATs and gene regulation. Science, 1997. **277**(5332): p. 1630-1635.

129. Owen, K.L., N.K. Brockwell, and B.S. Parker, JAK-STAT signaling: a double-edged sword of immune regulation and cancer progression. Cancers, 2019. **11**(12): p. 2002.

130. Brooks, A.J., et al., Mechanism of activation of protein kinase JAK2 by the growth hormone receptor. Science, 2014. **344**(6185): p. 1249783.

131. Krause, C.D., et al., Interactions among the components of the interleukin-10 receptor complex. Biochemical and biophysical research communications, 2006. **340**(2): p. 377-385.

132. Kramer, J.M., et al., Cutting edge: evidence for ligand-independent multimerization of the IL-17 receptor. The Journal of Immunology, 2006. **176**(2): p. 711-715.

133. Naismith, J.H., et al., Crystallographic Evidence for Dimerization of Unliganded Tumor Necrosis Factor Receptor∗. Journal of Biological Chemistry, 1995. **270**(22): p. 13303-13307.

134. Remy, I., I.A. Wilson, and S.W. Michnick, Erythropoietin receptor activation by a ligand-induced conformation change. Science, 1999. **283**(5404): p. 990-993.

135. Livnah, O., et al., Crystallographic evidence for preformed dimers of erythropoietin receptor before ligand activation. Science, 1999. **283**(5404): p. 987-990.

136. Tenhumberg, S., et al., gp130 dimerization in the absence of ligand: preformed cytokine receptor complexes. Biochemical and biophysical research communications, 2006. **346**(3): p. 649-657.

137. Durham, G.A., et al., Targeting SOCS proteins to control JAK-STAT signalling in disease. Trends in pharmacological sciences, 2019. **40**(5): p. 298-308.

138. O'Shea, J.J., et al., The JAK-STAT pathway: impact on human disease and therapeutic intervention. Annual review of medicine, 2015. **66**(1): p. 311-328.

139. Ram, P.A. and D.J. Waxman, Interaction of growth hormone-activated STATs with SH2-containing phosphotyrosine phosphatase SHP-1 and nuclear JAK2 tyrosine kinase. Journal of Biological Chemistry, 1997. **272**(28): p. 17694-17702.

140. Sachdev, S., et al., PIASy, a nuclear matrix–associated SUMO E3 ligase, represses LEF1 activity by sequestration into nuclear bodies. Genes & development, 2001. **15**(23): p. 3088-3103.

141. Tussié-Luna, M.I., et al., Physical and functional interactions of histone deacetylase 3 with TFII-I family proteins and PIASxβ. Proceedings of the National Academy of Sciences, 2002. **99**(20): p. 12807-12812.

142. Rogers, R.S., C.M. Horvath, and M.J. Matunis, SUMO modification of STAT1 and its role in PIAS-mediated inhibition of gene activation. Journal of Biological Chemistry, 2003. **278**(32): p. 30091-30097.

143. Sonnenblick, A., C. Levy, and E. Razin, Interplay between MITF, PIAS3, and STAT3 in mast cells and melanocytes. Molecular and cellular biology, 2004. **24**(24): p. 10584-10592.

144. Wu, H., et al., Generation of committed erythroid BFU-E and CFU-E progenitors does not require erythropoietin or the erythropoietin receptor. Cell, 1995. **83**(1): p. 59-67.

145. Okumura, F., et al., The role of cullin 5-containing ubiquitin ligases. Cell division, 2016. **11**: p. 1-16.

146. Yasukawa, H., et al., The JAK-binding protein JAB inhibits Janus tyrosine kinase activity through binding in the activation loop. The EMBO journal, 1999.

147. Kershaw, N.J., et al., SOCS3 binds specific receptor–JAK complexes to control cytokine signaling by direct kinase inhibition. Nature structural & molecular biology, 2013. **20**(4): p. 469-476.

148. Yoshimura, A., et al., A novel cytokine-inducible gene CIS encodes an SH2-containing protein that binds to tyrosine-phosphorylated interleukin 3 and erythropoietin receptors. The EMBO journal, 1995. **14**(12): p. 2816-2826.

149. Verbsky, J.W., et al., Expression of Janus kinase 3 in human endothelial and other non-lymphoid and non-myeloid cells. Journal of Biological Chemistry, 1996. **271**(24): p. 13976-13980.

150. Lai, K.S., et al., A kinase-deficient splice variant of the human JAK3 is expressed in hematopoietic and epithelial cancer cells (∗). Journal of Biological Chemistry, 1995. **270**(42): p. 25028-25036.

151. Takahashi, T. and T. Shirasaw, Molecular cloning of rat JAK3, a novel member of the JAK family of protein tyrosine kinases. FEBS letters, 1994. **342**(2): p. 124-128.

152. Rane, S.G. and E.P. Reddy, JAK3: a novel JAK kinase associated with terminal differentiation of hematopoietic cells. Oncogene, 1994. **9**(8): p. 2415-2423.

153. Kawamura, M., et al., Molecular cloning of L-JAK, a Janus family protein-tyrosine kinase expressed in natural killer cells and activated leukocytes. Proceedings of the National Academy of Sciences, 1994. **91**(14): p. 6374-6378.

154. Harpur, A., et al., JAK2, a third member of the JAK family of protein tyrosine kinases. Oncogene, 1992. **7**(7): p. 1347-1353.

155. Gurniak, C.B. and L.J. Berg, Murine JAK3 is preferentially expressed in hematopoietic tissues and lymphocyte precursor cells. 1996.

156. Krolewski, J., et al., Identification and chromosomal mapping of new human tyrosine kinase genes. Oncogene, 1990. **5**(3): p. 277-282.

157. Wilks, A.F., et al., Two novel protein-tyrosine kinases, each with a second phosphotransferase-related catalytic domain, define a new class of protein kinase. Molecular and cellular biology, 1991. **11**(4): p. 2057-2065.

158. Hou, J., et al., An interleukin-4-induced transcription factor: IL-4 Stat. Science, 1994. **265**(5179): p. 1701-1706.

159. LIu, X., et al., Cloning and expression of Stat5 and an additional homologue (Stat5b) involved in prolactin signal transduction in mouse mammary tissue. Proceedings of the National Academy of Sciences, 1995. **92**(19): p. 8831-8835.

160. Zhong, Z., Z. Wen, and J.E. Darnell, Jr., Stat3 and Stat4: members of the family of signal transducers and activators of transcription. Proc Natl Acad Sci U S A, 1994. **91**(11): p. 4806-10.

161. Shuai, K., et al., A single phosphotyrosine residue of Stat91 required for gene activation by interferon-γ. Science, 1993. **261**(5129): p. 1744-1746.

162. Takeda, K., T. Kishimoto, and S. Akira, STAT6: its role in interleukin 4-mediated biological functions. J Mol Med (Berl), 1997. **75**(5): p. 317-26.

163. Kaplan, M.H., et al., Stat6 is required for mediating responses to IL-4 and for development of Th2 cells. Immunity, 1996. **4**(3): p. 313-9.

164. Luzina, I.G., et al., Regulation of inflammation by interleukin-4: a review of "alternatives". J Leukoc Biol, 2012. **92**(4): p. 753-64.

165. Finkelman, F.D., et al., Suppression of in vivo polyclonal IgE responses by monoclonal antibody to the lymphokine B-cell stimulatory factor 1. Proceedings of the National Academy of Sciences, 1986. **83**(24): p. 9675-9678.

166. Swain, S.L., et al., IL-4 directs the development of Th2-like helper effectors. J Immunol, 1990. **145**(11): p. 3796-806.

167. Lebman, D.A. and R.L. Coffman, Interleukin 4 causes isotype switching to IgE in T cell-stimulated clonal B cell cultures. J Exp Med, 1988. **168**(3): p. 853-62.

168. Hofman, F.M., et al., IL-4 regulates differentiation and proliferation of human precursor B cells. J Immunol, 1988. **141**(4): p. 1185-90.

169. Nelms, K., et al., The IL-4 receptor: signaling mechanisms and biologic functions. Annu Rev Immunol, 1999. **17**: p. 701-38.

170. Mokada-Gopal, L., et al., Identification of Novel STAT6-Regulated Proteins in Mouse B Cells by Comparative Transcriptome and Proteome Analysis. J Immunol, 2017. **198**(9): p. 3737-3745.

171. Schroder, A.J., et al., Cutting edge: STAT6 serves as a positive and negative regulator of gene expression in IL-4-stimulated B lymphocytes. J Immunol, 2002. **168**(3): p. 996-1000.

172. Stack, R.M., et al., IL-4 treatment of small splenic B cells induces costimulatory molecules B7-1 and B7-2. J Immunol, 1994. **152**(12): p. 5723-33.

173. Vallé, A., et al., IL-4 and IL-2 upregulate the expression of antigen B7, the B cell counterstructure to T cell CD28: an amplification mechanism for T-B cell interactions. Int Immunol, 1991. **3**(3): p. 229-35.

174. Defrance, T., et al., Human recombinant interleukin 4 induces Fc epsilon receptors (CD23) on normal human B lymphocytes. J Exp Med, 1987. **165**(6): p. 1459-67.

175. Noelle, R., et al., Increased expression of Ia antigens on resting B cells: an additional role for B-cell growth factor. Proceedings of the National Academy of Sciences, 1984. **81**(19): p. 6149-6153.

176. Clark, E.A., et al., Activation of human B cells. Comparison of the signal transduced by IL-4 to four different competence signals. J Immunol, 1989. **143**(12): p. 3873-80.

177. King, I.L. and M. Mohrs, IL-4-producing CD4+ T cells in reactive lymph nodes during helminth infection are T follicular helper cells. J Exp Med, 2009. **206**(5): p. 1001-7.

178. Acosta Rodriguez, E.V., et al., Interleukin-4 biases differentiation of B cells from Trypanosoma cruzi-infected mice and restrains their fratricide: role of Fas ligand down-regulation and MHC class II-transactivator up-regulation. J Leukoc Biol, 2003. **73**(1): p. 127-36.

179. Acosta-Rodríguez, E.V., et al., Galectin-3 mediates IL-4-induced survival and differentiation of B cells: functional cross-talk and implications during Trypanosoma cruzi infection. J Immunol, 2004. **172**(1): p. 493-502.

180. Knödel, M., et al., Blimp-1 over-expression abrogates IL-4- and CD40-mediated suppression of terminal B cell differentiation but arrests isotype switching. Eur J Immunol, 2001. **31**(7): p. 1972-80.

181. Bryant, V.L., et al., Cytokine-mediated regulation of human B cell differentiation into Ig-secreting cells: predominant role of IL-21 produced by CXCR5+ T follicular helper cells. J Immunol, 2007. **179**(12): p. 8180-90.

182. Turqueti-Neves, A., et al., B-cell-intrinsic STAT6 signaling controls germinal center formation. European Journal of Immunology, 2014. **44**(7): p. 2130-2138.

183. Pignarre, A., et al., Plasmablasts derive from CD23– activated B cells after the extinction of IL-4/STAT6 signaling and IRF4 induction. Blood, 2021. **137**(9): p. 1166-1180.

184. Ochiai, K., et al., Transcriptional Regulation of Germinal Center B and Plasma Cell Fates by Dynamical Control of IRF4. Immunity, 2013. **38**(5): p. 918-929.

185. Murata, T., J. Taguchi, and R.K. Puri, Interleukin-13 receptor alpha' but not alpha chain: a functional component of interleukin-4 receptors. Blood, 1998. **91**(10): p. 3884-91.

186. Passerini, V., et al., PARP14 Is a Novel Therapeutic Target in STAT6 mutant Follicular Lymphoma. Blood, 2018. **132**: p. 2842.

187. Rawal, S., et al., Role of IL-4 in Inducing Immunosuppressive Tumor Microenvironment in Follicular Lymphoma. Blood, 2011. **118**(21): p. 771.

188. Krzyzak, L., et al., CD83 Modulates B Cell Activation and Germinal Center Responses. J Immunol, 2016. **196**(9): p. 3581-94.

189. Li, Z., et al., CD83: Activation Marker for Antigen Presenting Cells and Its Therapeutic Potential. Frontiers in Immunology, 2019. **Volume 10 - 2019**.

190. Elgueta, R., et al., Molecular mechanism and function of CD40/CD40L engagement in the immune system. Immunol Rev, 2009. **229**(1): p. 152-72.

191. Marques, R.M., et al., Loss of 15-lipoxygenase disrupts Treg differentiation altering their pro-resolving functions. Cell Death & Differentiation, 2021. **28**(11): p. 3140-3160.

192. Kubo, T., et al., Immunohistochemical analysis of arachidonate 5-lipoxygenase expression in B-cell lymphomas: Implication for B cell differentiation and its analogy with lymphomagenesis. Pathol Res Pract, 2023. **242**: p. 154328.

193. Irish, J.M., et al., Altered B-cell receptor signaling kinetics distinguish human follicular lymphoma B cells from tumor-infiltrating nonmalignant B cells. Blood, 2006. **108**(9): p. 3135-3142.

194. Han, Y., et al., Interleukin-4 activates the PI3K/AKT signaling to promote apoptosis and inhibit the proliferation of granulosa cells. Exp Cell Res, 2022. **412**(1): p. 113002.

195. Nera, K.P., et al., Loss of Pax5 promotes plasma cell differentiation. Immunity, 2006. **24**(3): p. 283-93.

196. Nera, K.P. and O. Lassila, Pax5--a critical inhibitor of plasma cell fate. Scand J Immunol, 2006. **64**(3): p. 190-9.

197. Sandova, V., et al., IL4-STAT6 signaling induces CD20 in chronic lymphocytic leukemia and this axis is repressed by PI3Kδ inhibitor idelalisib. Haematologica, 2021. **106**(11): p. 2995-2999.

198. Denzin, L.K., et al., Negative Regulation by HLA-DO of MHC Class II-Restricted Antigen Processing. Science, 1997. **278**(5335): p. 106-109.

199. Liljedahl, M., et al., HLA-DO is a lysosomal resident which requires association with HLA-DM for efficient intracellular transport. Embo j, 1996. **15**(18): p. 4817-24.

200. van Ham, S.M., et al., HLA-DO is a negative modulator of HLA-DM-mediated MHC class II peptide loading. Curr Biol, 1997. **7**(12): p. 950-7.

201. Green, M.R., et al., Mutations in early follicular lymphoma progenitors are associated with suppressed antigen presentation. Proc Natl Acad Sci U S A, 2015. **112**(10): p. E1116-25.

202. Klein, U., et al., Transcription factor IRF4 controls plasma cell differentiation and class-switch recombination. Nat Immunol, 2006. **7**(7): p. 773-82.

203. Soh, K.T., et al., CD319 (SLAMF7) an alternative marker for detecting plasma cells in the presence of daratumumab or elotuzumab. Cytometry B Clin Cytom, 2021. **100**(4): p. 497-508.

204. Ou, X., S. Xu, and K.P. Lam, Deficiency in TNFRSF13B (TACI) expands T-follicular helper and germinal center B cells via increased ICOS-ligand expression but impairs plasma cell survival. Proc Natl Acad Sci U S A, 2012. **109**(38): p. 15401-6.

205. Higashioka, K., et al., Association of circulating SLAMF7+Tfh1 cells with IgG4 levels in patients with IgG4-related disease. BMC Immunology, 2020. **21**(1): p. 31.

206. O'Connell, P., et al., SLAMF7 Signaling Reprograms T Cells toward Exhaustion in the Tumor Microenvironment. J Immunol, 2021. **206**(1): p. 193-205.

207. Wang, J., et al., The Role of CXCL11 and its Receptors in Cancer: Prospective but Challenging Clinical Targets. Cancer Control, 2024. **31**: p. 10732748241241162.

208. Guan, X., et al., Perforin 1 in Cancer: Mechanisms, Therapy, and Outlook. Biomolecules, 2024. **14**(8).

209. Nguyen, H.-M., et al., Interferon stimulated gene 15 (ISG15) in cancer: An update. Cancer Letters, 2023. **556**: p. 216080.

210. Hilchey, S.P., et al., Human Follicular Lymphoma CD39+-Infiltrating T Cells Contribute to Adenosine-Mediated T Cell Hyporesponsiveness1. The Journal of Immunology, 2009. **183**(10): p. 6157-6166.

211. Roider, T., et al., Multimodal and spatially resolved profiling identifies distinct patterns of T cell infiltration in nodal B cell lymphoma entities. Nature Cell Biology, 2024. **26**(3): p. 478-489.

212. Robson, S.C., J. Sévigny, and H. Zimmermann, The E-NTPDase family of ectonucleotidases: structure function relationships and pathophysiological significance. Purinergic signalling, 2006. **2**(2): p. 409-430.

213. Allard, B., et al., The ectonucleotidases CD 39 and CD 73: novel checkpoint inhibitor targets. Immunological reviews, 2017. **276**(1): p. 121-144.

214. de Andrade Mello, P., R. Coutinho-Silva, and L.E.B. Savio, Multifaceted effects of extracellular adenosine triphosphate and adenosine in the tumor–host interaction and therapeutic perspectives. Frontiers in immunology, 2017. **8**: p. 1526.

215. Maruhashi, T., et al., Binding of LAG-3 to stable peptide-MHC class II limits T cell function and suppresses autoimmunity and anti-cancer immunity. Immunity, 2022. **55**(5): p. 912-924.e8.

216. Yazawa, N., et al., CD19 regulates innate immunity by the toll-like receptor RP105 signaling in B lymphocytes. Blood, 2003. **102**(4): p. 1374-1380.

217. Mestrallet, F., et al., CD180 overexpression in follicular lymphoma is restricted to the lymph node compartment. Cytometry B Clin Cytom, 2016. **90**(5): p. 433-9.

218. Ndacayisaba, L.J., et al., Characterization of BCMA Expression in Circulating Rare Single Cells of Patients with Plasma Cell Neoplasms. Int J Mol Sci, 2022. **23**(21).

219. Rinaldi, I., et al., Role of Anti-B-Cell Maturation Antigen (BCMA) in the Management of Multiple Myeloma. Cancers (Basel), 2022. **14**(14).

220. Low, M.S.Y., et al., IRF4 Activity Is Required in Established Plasma Cells to Regulate Gene Transcription and Mitochondrial Homeostasis. Cell Rep, 2019. **29**(9): p. 2634-2645.e5.

221. Fillatreau, S., Natural regulatory plasma cells. Current Opinion in Immunology, 2018. **55**: p. 62-66.

222. Endo, T.A., et al., A new protein containing an SH2 domain that inhibits JAK kinases. Nature, 1997. **387**(6636): p. 921-924.

223. Reshetnikova, E.S., et al., Differential expression of FCRLA in naïve and activated mouse B cells. Cellular Immunology, 2012. **272**(2): p. 182-192.

224. Fernández, S., et al., JAK/STAT blockade reverses the malignant phenotype of Hodgkin and Reed-Sternberg cells. Blood Adv, 2023. **7**(15): p. 4135-4147.

225. Reddy, A., et al., Genetic and Functional Drivers of Diffuse Large B Cell Lymphoma. Cell, 2017. **171**(2): p. 481-494.e15.

226. Zak, J., et al., JAK inhibition enhances checkpoint blockade immunotherapy in patients with Hodgkin lymphoma. Science, 2024. **384**(6702): p. eade8520.

227. Cannon, L., E.C. Academia, and A.E. Glode, A Review of PI3K Inhibitors in B-Cell Malignancies. J Adv Pract Oncol, 2019. **10**(7): p. 715-725.

# A. Appendix

**Immunohistochemical staining**

CD23 IHC was performed was following: „Paraffin“ followed by „Entparaffinierung“ was selected on the instrument. Slide temperature was increased from 72 °C to middle temperature („Entparaffinierung“). Pre-treatment was selected. Ultra CC1 was selected. Slide was heated to 100 °C and incubated for 4 min (cell conditioner no 1). CC1 was selected for 8 min, 16 min, 24 min and 32 min. Pre-primary peroxidase blocker was selected. Primary antibody was selected. Primary antibody temperature was selected. Slides were heated to 37 °C (primary antibody). Select antibody titration. Hand apply (primary antibody), incubate for 32 min. Select Optiview HQ linker. Select Optiview HQ Universal Linker. Apply one drop of OV HQ UNIV LINKR to coverslip, incubate for 8 min. Select Optiview HRP Multimer. Select HRP Multimer incubation time. Apply one drop of OV HRP MULTIMER to cover slip, incubate for 8 min. Select counterstaining. Apply 1 drop of HEMATOXYLIN (counterstaining), apply LCS, incubate for 20 min. Select post-counterstaining. Apply one drop of BLUING REAGENT (post-counterstaining), apply LCS, incubate for 8 min.

**Mutation Analysis protocol:**

**Library preparation**

- Prepare 2X Primer-Pool (**26**)
- Vortex and centrifuge
- Perform PCR using thermocycler
    - 99 °C 2 min
    - 99 °C 15 sec
    - 60 °C 4 min
    - 24 cycles
- Store samples at 10 °C over night and proceed or store at -20 °C for longer storage duration

**Table 26: Preparation of 2X primer pool**

| | **Volume per sample [µL]** |
|---|---|
| 5X Ion AmpliSeq HiFi Mix | 4 |
| 2X Ion Ampliseq Primer Pool | 10 |
| 10 ng DNA | ≤ 6 |
| $ddH_2O$ | Adjust to 20 |

**Primer digestion**

- Add 2 µL FuPa reagent to each sample
- Perform digestion using following PCR program:
    - 50 °C 10 min
    - 55 °C 10 min
    - 60 °C 20 min
    - 10 °C up to 1 h

**Adapter ligation**

- Prepare barcode mix (per sample):
    - 2 µL Ion P1 Adapter
    - 2 µL Ion Express Barcode X (1 – 16)
    - dd$H_2O$ (adjust to 8 µL total volume)
- Mix Switch Solution, Barcode mix, DNA ligase and digested amplicons (per sample)
    - 4 µL Switch Solution
    - 2 µL Barcode Mix
    - 2 µL DNA Ligase
    - 22 µL digested amplicons
- Perform ligation PCR
    - 22 °C 30 min
    - 72 °C 10 min
    - 10 °C up to 1 h
- PCR products can be stored at -20 °C

**Purification of samples**

- Vortex AMPure beads, centrifuge and add 54 µL AMPure beads per sample directly to the PCR tubes
- Vortex and centrifuge
- Incubate for 5 min at room temperature
- Incubate tubes on a magnetic rack, open lids and incubate for 2 min
- Remove supernatant
- Add 150 µL 70% ethanol per sample
- Change stripe position after 30 s to force bead cake to travel through ethanol
- Repeat 3x
- Remove supernatant and repeat cycle

- Remove supernatant and let bead cake dry
- Add 35 µL Low-TE-buffer
- Vortex and incubate for 5 min at room temperature on a normal rack
- Incubate for 2 min on a magnetic rack, open lids
- Transfer supernatant to new PCR tubes
- Repeat complete purification procedure

**Library quantification**

- Prepare *E.coli* dilution using 68 pM stock solution
    - 25 µL per sample
    - 3x 1:10 dilution (6.8 pM, 0.68 pM, 0.068 pM)
    - 6.8 pM solution: 22.5 µL $ddH_2O$ + 2.5 µL 68 pM *E.coli*
    - 0.68 pM solution: 22.5 µL $ddH_2O$ + 2.5 µL 6.8 pM *E.coli*
    - 0.068 pM solution: 22.5 µL $ddH_2O$ + 2.5 µL 0.68 pM *E.coli*
- Prepare 1:500 dilution for each library
    - 2 µL library + 998 µL $ddH_2O$
- Prepare PCR mix as follows and pipette into a 96 well PCR plate:
    - 5 µL 2X TaqMan MasterMix
    - 0.5 µL 2X Ion TaqMan Assay
- Add one of the following to the mix
    - 4.5 µL 1:500 library or *E.coli* dilution or $ddH_2O$
- Perform qPCR (40 cycles) on Light Cycler 480
    - 2 min 50 °C
    - 3 sec 95 °C
    - 30 sec 60 °C
- Calculate Cp values as follows:
    - Analysis → Abs Quant/$2^{nd}$ Derivate Max → mark samples → High sensitivity → Calculate → Export
- Sample curves should be located within *E.coli* standard curves

**Library pooling**

- Calculate (using coverage plan formulas)
    - Required $ddH_2O$ volume for sample dilution
    - Required volume of diluted samples for library pool
- Add 4 µL sample into an Eppendorf tube

- Prepare library pool
    - Add calculated sample volumes
    - Transfer calculated volume of library pool into end pool
- Prepare EA pool
    - Add 2 µL from each EA tube to EA pool
    - Transfer volume calculated with coverage plan to end pool
- Fill with $ddH_2O$

**Template preparation Ion Chef and sequencing Ion GeneStudio S5**

- Use torrent browser S5, select AmpliSeq DNA plan in templates
- Select chip based on number of amplicons and panel
- Enter number of barcodes

**Starting Ion Chef**

- Booting of Ion Chef instrument
- Add endpool tubes to position A and B f the reagent kit
- Proceed with quick start
- Add sequencing chips and required materials
- Start program with "Start check", program runs for approx. 13 h

**S5 initialization and run**

- Booting of S5 instrument and preparation of sequencing reagents
- Select "initialize" on the instrument, change washing solution bottle and S5 sequencing reagent cartridge
- Washing procedure starts
- Chip 1 is placed in S5, Chip 2 is stored in the fridge until usage
- Correct plan is selected, and run is started, if Chip 2 is usage, change after run 1
- Data upload to server occurs directly after run completion

**Table 27: Genes analyzed in FL panel**
CDS = coding DNA sequence, HS = hot spot, amplicon ranges from 125bp to 275bp

| Gene | Transcript | Position (GRCh37/hg19) | Exon(s) | Amplicon(s) |
|---|---|---|---|---|
| ***CREBBP*** | NM_004380 | chr16: 3,786,032 - 3,790,555 | 24-28 (HS) | 10 |
| ***CREBBP*** | NM_004380 | chr16: 3,781,188 - 3,781,479 | 30 (HS) | 3 |
| ***EZH2*** | NM_004456 | chr7: 148,508,712 - 148,508,817 | 16 (HS) | 1 |
| ***EP300*** | NM_001429 | chr22: 41,489,009 - 41,574,960 | CDS | 63 |
| ***FOXO1*** | NM_002015 | chr13: 41,133,660 - 41,240,349 | CDS | 10 |
| ***GNA13*** | NM_006572 | chr17: 63,010,375 - 63,052,711 | CDS | 8 |
| ***HIST1H1B*** | NM_005322 | chr6: 27,834,627 - 27,835,307 | CDS | 6 |
| ***HIST1H1C*** | NM_005319 | chr6: 26,056,015 - 26,056,656 | CDS | 6 |
| ***HIST1H1D*** | NM_005320 | chr6: 26,232,440 - 26,237,216 | CDS | 6 |
| ***HIST1H1E*** | NM_005321 | chr6: 26,156,619 - 26,157,278 | CDS | 5 |
| ***KMT2D*** | NM_003482 | chr12: 49,415,563 - 49,449,107 | CDS | 120 |
| ***MEF2B*** | NM_001145785 | chr19: 19,256,503 - 19,261,544 | CDS | 11 |
| ***TNFRSF14*** | NM_003820 | chr1: 2,488,104 - 2,494,712 | CDS | 11 |

**Table 28: Genes analyzed in FLneg panel**
CDS = coding DNA sequence, HS = hot spot, amplicon ranges from 125bp to 275bp

| Gene | Transcript | Position (GRCh37/hg19) | Exon(s) | Amplicon(s) |
|---|---|---|---|---|
| ***TNFAIP3*** | NM_001270507 | chr6: 138,192,365 – 138,202,456 | CDS | 29 |
| ***STAT6*** | NM_003153 | chr12: 57,490,355 – 57,502,061 | CDS | 42 |
| ***SOCS1*** | NM_003745 | chr16: 11,348,700 – 11,349,335 | CDS | 6 |
| ***XPO1*** | NM_003400 | chr2: 61,719,455 – 61,719,569 | 15 (HS) | 2 |
| ***NOTCH1*** | NM_017617 | chr9: 139,397,629 – 139,399,561 | 26-27 (HS) | 6 |
| ***NOTCH1*** | NM_017617 | chr9: 139,390,439 – 139,392,015 | 34 (HS) | 16 |
| ***NOTCH1*** | NM_017617 | chr9: 139,390,111 – 139,390,214 | 3'UTR | 1 |
| ***NOTCH2*** | NM_024408 | chr1: 120,457,828 – 120,459,322 | 34 (HS) | 15 |
| ***NOTCH2*** | NM_024408 | chr1: 120,454,993 – 120,455,112 | 3'UTR | 1 |
| ***MYD88*** | NM_002468 | chr3: 38,182,618 – 38,182,726 | 5 (HS) | 2 |
| ***MAP2K1*** | NM_002755 | chr15: 66,727,360 – 66,729,235 | 2-3 (HS) | 6 |

**Table 29: Genes analyzed in Oncomine Lymphoma III panel**
CDS = coding DNA sequence, HS = hot spot

| Gene | Transcript | Position (hg19) | Exon(s) | Amplicon(s) |
|---|---|---|---|---|
| ***ALK*** | NM_004304.5 | chr2: 29,430,068 - 29,445,473 | CDS (HS) | 68 |
| ***ARAF*** | NM_001654.5 | chrX: 47,424,369 - 47,428,432 | CDS (HS) | 33 |
| ***ARID1A*** | NM_006015.6 | chr1: 27,087,865 - 27,100,399 | CDS | 98 |
| ***ARID1B*** | NM_001371656.1 | chr6: 157,519,935 - 157,511,354 | CDS | 81 |
| ***ATM*** | NM_000051.3 | chr11: 108,115,505 - 108,186,648 | CDS | 196 |
| ***B2M*** | NM_004048.3 | chr15: 45,007,526 - 45,010,163 | CDS | 15 |

| | | | | |
|---|---|---|---|---|
| ***BCL10*** | NM_003921.5 | chr1: 85,736,509 - 85,742,045 | CDS | 12 |
| ***BCL11A*** | NM_022893.4 | chr2: 60,695,857 - 60,679,811 | CDS | 31 |
| ***BCL2*** | NM_000633.2 | chr18: 60,795,848 - 60,794,199 | CDS | 15 |
| ***BCL6*** | NM_001706.5 | chr3: 187,451,311 - 187,446,342 | CDS | 27 |
| ***BIRC3*** | NM_182962.3 | chr11: 102,196,187 - 102,207,843 | CDS | 28 |
| ***BRAF*** | NM_004333.6 | chr7: 140,453,142 - 140,477,875 | CDS (HS) | 67 |
| ***BTG1*** | NM_001731.3 | chr12: 92,536,944 - 92,538,029 | CDS | 13 |
| ***BTG2*** | NM_006763.3 | chr1: 203,274,725 - 203,278,198 | CDS | 12 |
| ***BTK*** | NM_000061.3 | chrX: 100,611,164 - 100,611,166 | CDS (HS) | 3 |
| ***CARD11*** | NM_032415.6 | chr7: 2,976,810 - 2,963,887 | CDS (HS) | 14 |
| ***CBL*** | NM_005188.4 | chr11: 119,148,891 - 119,149,290 | CDS (HS) | 48 |
| ***CCND1*** | NM_053056.3 | chr11: 69,457,736 - 69,456,214 | CDS (HS) | 17 |
| ***CCR4*** | NM_005508.5 | chr3: 32,994,895 - 32,996,017 | CDS | 11 |
| ***CD28*** | NM_006139.4 | chr2: 204,571,400 - 204,594,515 | CDS | 11 |
| ***CD70*** | NM_001252.5 | chr19: 6,590,156 - 6,591,023 | CDS | 14 |
| ***CD79A*** | NM_001783.4 | chr19: 42,381,355 - 42,384,825 | CDS | 12 |
| ***CD79B*** | NM_001039933.3 | chr17: 62,007,084 - 62,007,194 | CDS (HS) | 27 |
| ***CDKN2A*** | NM_001195132.1 | chr9: 21,968,704 - 21,994,340 | CDS | 16 |
| ***CHD2*** | NM_001271.4 | chr15: 93,498,643 - 93,543,880 | CDS | 99 |
| ***CREBBP*** | NM_004380.3 | chr16: 3,799,618 - 3,842,105 | CDS | 113 |
| ***CXCR4*** | NM_001008540 | chr2: 136,872,419 - 136,875,650 | CDS | 13 |
| ***DDR2*** | NM_006182.4 | chr1: 162,741,996 - 162,746,240 | CDS (HS) | 35 |
| ***EP300*** | NM_001429.4 | chr22: 41,533,647 - 41,566,585 | CDS | 94 |
| ***ETV6*** | NM_001987.5 | chr12: 11,803,042 - 12,044,000 | CDS | 23 |
| ***EZH2*** | NM_004456.5 | chr7: 148,506,392 - 148,516,789 | CDS | 54 |
| ***FAS*** | NM_000043.6 | chr10: 90,768,626 - 90,773,144 | CDS | 19 |
| ***FBXW7*** | NM_033632.3 | chr4: 153,258,944 - 153,252,030 | CDS | 43 |
| ***GATA2*** | NM_032638.5 | chr3: 128,200,720 - 128,202,743 | CDS (HS) | 23 |
| ***GNA13*** | NM_006572.6 | chr17: 63,014,361 - 63,010,957 | CDS | 15 |
| ***HIST1H1E*** | NM_005321.3 | chr6: 26,157,549 - 26,156,552 | CDS | 11 |
| ***HIST1H3B*** | NM_003537.4 | chr6: 26,032,134 - 26,032,424 | CDS (HS) | 24 |
| ***HLA-B*** | NM_005514.8 | chr6: 31,322,874 - 31,323,379 | CDS | 15 |
| ***ID3*** | NM_002167.5 | chr1: 23,884,762 - 23,885,530 | CDS | 17 |
| ***IKBKB*** | NM_001556.3 | chr8: 42,166,335 - 42,163,896 | CDS (HS) | 13 |
| ***IRF4*** | NM_002460.4 | chr6: 401,404 - 397,272 | CDS | 21 |
| ***JAK2*** | NM_004972.4 | chr9: 5,029,763 - 5,073,805 | CDS | 83 |
| ***JAK3*** | NM_000215.4 | chr19: 17,942,017 - 17,952,375 | CDS | 55 |
| ***KLF2*** | NM_016270.4 | chr19: 16,437,647 - 16,436,863 | CDS | 12 |
| ***KMT2D*** | NM_003482.4 | chr12: 49,435,690 - 49,423,029 | CDS | 202 |

| | | | | |
|---|---|---|---|---|
| ***KRAS*** | NM_033360.4 | chr12: 25,398,279 - 25,362,879 | CDS | 35 |
| ***MAP2K1*** | NM_002755.4 | chr15: 66,727,453 - 66,774,186 | CDS | 52 |
| ***MEF2B*** | NM_001145785.2 | chr19: 19,257,344 - 19,256,851 | CDS | 18 |
| ***MTOR*** | NM_004958.4 | chr1: 11,168,338 - 11,227,532 | CDS (HS) | 38 |
| ***MYC*** | NM_002467.6 | chr8: 128,750,484 - 128,748,879 | CDS | 15 |
| ***MYD88*** | NM_002468 | chr3: 38,181,327 - 38,181,515 | CDS (HS) | 28 |
| ***NFKBIA*** | NM_020529.3 | chr14: 35,871,199 - 35,873,870 | CDS | 17 |
| ***NOTCH1*** | NM_017617.5 | chr9: 139,399,115 - 139,412,754 | CDS | 106 |
| ***NOTCH2*** | NM_024408.4 | chr1: 120,467,918 - 120,572,620 | CDS | 115 |
| ***PAX5*** | NM_016734.3 | chr9: 37,015,165 - 36,923,501 | CDS (HS) | 12 |
| ***PIM1*** | NM_002648.4 | chr6: 37,138 539 - 37,140,958 | CDS | 18 |
| ***PLCG2*** | NM_002661.5 | chr16: 81,953,069 - 81,990,504 | CDS | 69 |
| ***POT1*** | NM_015450.3 | chr7: 124,532,300 - 124,499,186 | CDS | 53 |
| ***PRDM1*** | NM_001198.4 | chr6: 106,546,941 - 106,555,381 | CDS | 32 |
| ***REL*** | NM_002908.4 | chr2: 61,147,166 - 61,147,787 | CDS | 28 |
| ***RHOA*** | NM_001664.4 | chr3: 49,412,974 - 49,412,979 | CDS (HS) | 36 |
| ***SF3B1*** | NM_012433.4 | chr2: 198,266,714 - 198,267,482 | CDS (HS) | 33 |
| ***SGK1*** | NM_001143676.1 | chr6: 134,491,386 - 134,638,618 | CDS | 34 |
| ***SMARCA4*** | NM_001128849.3 | chr19: 11,095,939 - 11,137,032 | CDS | 109 |
| ***SOCS1*** | NM_003745.1 | chr16: 11,348,145 - 11,349,345 | CDS | 15 |
| ***SPEN*** | NM_015001.3 | chr1: 16,235,806 - 16,264,511 | CDS | 119 |
| ***STAT3*** | NM_139276.2 | chr17: 40,474,461 - 40,481,578 | CDS (HS) | 17 |
| ***STAT5B*** | NM_012448.4 | chr17: 40,354,727 - 40,370,950 | CDS (HS) | 13 |
| ***STAT6*** | NM_003153.5 | chr12: 57,493,530 - 57,499,402 | CDS | 45 |
| ***TCF3*** | NM_001136139.4 | chr19: 1,622,292 - 1,621,065 | CDS | 40 |
| ***TERC*** | NM_001566 | chr3: 169,482,258 - 169,482,988 | CDS | 10 |
| ***TET2*** | NM_001127208.2 | chr4: 106,163,981 - 106,183,015 | CDS | 73 |
| ***TMSB4X*** | NM_021109.4 | chrX: 12,994,232 - 12,995,316 | CDS | 17 |
| ***TNFAIP3*** | NM_001270507.2 | chr6: 138,195,972 - 138,200,498 | CDS | 29 |
| ***TNFRSF14*** | NM_003820.3 | chr1: 2,489,772 - 2,494,345 | CDS | 16 |
| ***TP53*** | NM_000546.5 | chr17: 7,577,009 - 7,579,922 | CDS | 26 |
| ***TRAF3*** | NM_003300.4 | chr14: 103,338,234 - 103,372,141 | CDS | 26 |
| ***XPO1*** | NM_003400.4 | chr2: 61,719,472 - 61,709,517 | CDS (HS) | 13 |

**Table 30: Genes analyzed in IL4R panel**
CDS = coding DNA sequence

| Gene | Transcript | Position (GRCh37/hg19) | Exon(s) | Amplicon(s) |
|---|---|---|---|---|
| ***JAK1*** | NM_002227.4 | chr1: 65,300,235 - 65,351,957 | CDS | 54 |
| ***DUSP2*** | NM_004418.4 | chr2: 96,809,552 - 96,811,103 | CDS | 14 |
| ***JAK2*** | NM_004972.4 | chr9: 5,021,978 - 5,126,801 | CDS | 55 |
| ***PTPRD*** | NM_002839.4 | chr9: 8,317,864 - 8,733,853 | CDS | 84 |
| ***IL4R*** | NM_001257406.2 | chr16: 27,351,515 - 27,375,161 | CDS | 32 |
| ***STAT3*** | NM_139276.3 | chr17: 40,467,753 - 40,500,544 | CDS | 40 |
| ***SOCS3*** | NM_003955.4 | chr17: 76,354,489 - 76,355,186 | CDS | 9 |
| ***TYK2*** | NM_003331.5 | chr19: 10,451,500 - 10,489,092 | CDS | 56 |
| ***JAK3*** | NM_000215.4 | chr19: 17,937,542 - 17,955,236 | CDS | 57 |
| ***PTPN1*** | NM_002827.4 | chr20: 49,127,055 - 49,199,262 | CDS | 22 |
| ***IL13RA1*** | NM_001560.3 | chrX: 117,861,592 - 117,925,827 | CDS | 22 |

**Table 31: List of detected gene mutations in FLneg by targeted next-generation sequencing**
AF = allele frequency, Chr = chromosome, n = 50 (modified from Nann *et al.* 2020 [60])

| Case | Gene | Chr | Position (hg19) | cDNA change | Protein change | Coverage | AF | Validation | SIFT score | SIFT | PolyPhen- 2 score | PolyPhen-2 |
|---|---|---|---|---|---|---|---|---|---|---|---|---|
| **FLneg1** | *ATM* | 11 | 108175413 | c.5511_5512del | p.F1837Lfs | 2272 | 54 | N/A | DEL | N/A | N/A | N/A |
| **FLneg1** | *B2M* | 15 | 45003813 | c.67+2T>G | p.? | 3217 | 13 | N/A | N/A | N/A | N/A | N/A |
| **FLneg1** | *TMSB4X* | X | 12994410 | c.30C>G | p.I10M | 5415 | 12 | N/A | 0.02 | damaging | 0.981 | probably damaging |
| **FLneg1** | *TMSB4X* | X | 12994403 | c.23C>T | p.A8V | 5405 | 11 | N/A | 0.05 | tolerated | 0.855 | probably damaging |
| **FLneg1** | *SGK1* | 6 | 134495655 | c.431G>A | p.C144Y | 5590 | 7 | N/A | 0 | damaging | 0.151 | possibly damaging |
| **FLneg2** | *TNFRSF14* | 1 | 2489881 | c.278G>T | p.C93F | 1628 | 13 | single amplicons | 0 | damaging | 1 | probably damaging |
| **FLneg4** | *CREBBP* | 16 | 3786794 | c.4417G>A | p.A1473T | 5057 | 24 | Sanger sequencing | 0.012 | damaging | 0.999 | probably damaging |
| **FLneg4** | *EZH2* | 7 | 148508728 | c.1936T>A | p.Y646N | 827 | 19 | single amplicons | 0 | damaging | 0.98 | probably damaging |
| **FLneg4** | *FOXO1* | 13 | 41240274 | c.76C>G | p.P26A | 1392 | 18 | Sanger sequencing | 0 | damaging | 0.884 | possibly damaging |
| **FLneg4** | *KMT2D* | 12 | 49424741 | c.13606C>T | p.R4536* | 1873 | 23 | Sanger sequencing | STOP | N/A | N/A | N/A |
| **FLneg4** | *STAT6* | 12 | 57498330 | c.1129G>A | p.E377K | 122 | 17 | single amplicons | 0.005 | damaging | 1 | probably damaging |
| **FLneg4** | *TNFAIP3* | 6 | 138195991 | c.305A>G | p.N102S | 529 | 59 | N/A | 0 | damaging | 1 | probably damaging |
| **FLneg5** | *CREBBP* | 16 | 3786773 | c.4436_4438delGGA | p.G1479del | 5878 | 60 | Sanger sequencing | DEL | N/A | N/A | N/A |
| **FLneg5** | *KMT2D* | 12 | 49425040 | c.13448delT | p.L4483fs | 614 | 22 | Sanger sequencing | DEL | N/A | N/A | N/A |
| **FLneg5** | *CXCR4* | 2 | 136875613 | c.15+3A>C | p.? | 3719 | 12 | N/A | N/A | N/A | N/A | N/A |
| **FLneg5** | *ATM* | 11 | 108165733 | c.4856G>A | p.R1619K | 2893 | 58 | N/A | 0.53 | tolerated | 0.001 | benign |
| **FLneg6** | *CREBBP* | 16 | 3786137 | c.4628A>T | p.D1543V | 114 | 56 | Sanger sequencing | 0 | damaging | 1 | probably damaging |
| **FLneg6** | *KMT2D* | 12 | 49445998 | c.1468G>T | p.E490* | 1156 | 43 | Sanger sequencing | STOP | N/A | N/A | N/A |
| **FLneg6** | *TNFRSF14* | 1 | 2489264 | c.169T>A | p.C57S | 3849 | 13 | Sanger sequencing | 0 | damaging | 1 | probably damaging |
| **FLneg7** | *CREBBP* | 16 | 3788617 | c.4337G>C | p.R1446P | 350 | 58 | Sanger sequencing | 0 | damaging | 1 | probably damaging |
| **FLneg7** | *KMT2D* | 12 | 49430938 | c.1ß201C>T | p.Q3401* | 367 | 32 | Sanger sequencing | STOP | N/A | N/A | N/A |

| | | | | | | | | | | | | |
|---|---|---|---|---|---|---|---|---|---|---|---|---|
| **FLneg7** | *STAT6* | 12 | 57496661 | c.1256A>G | p.D419G | 153 | 27 | single amplicons | 0.001 | damaging | 1 | probably damaging |
| **FLneg7** | *STAT6* | 12 | 57496701 | c.1216C>G | p.L406V | 144 | 48 | single amplicons | 0.02 | damaging | 0.948 | possibly damaging |
| **FLneg8** | *FOXO1* | 13 | 41240277 | c.73T>A | p.W25R | 993 | 18 | Sanger sequencing | 0 | damaging | 0.02 | benign |
| **FLneg8** | *STAT6* | 12 | 57496662 | c.1255G>T | p.D419Y | 122 | 29 | N/A | 0 | damaging | 1 | probably damaging |
| **FLneg9** | *TMSB4X* | X | 12994442 | c.66_67del | p.E22Dfs | 7031 | 16 | N/A | DEL | N/A | N/A | N/A |
| **FLneg9** | *IRF4* | 6 | 394888 | c.284C>A | p.T95K | 10263 | 14 | N/A | 0 | damaging | 1 | probably damaging |
| **FLneg10** | *FOXO1* | 13 | 41240288 | c.62G>A | p.R21H | 518 | 45 | Sanger sequencing | 0 | damaging | 1 | probably damaging |
| **FLneg10** | *HIST1H1D* | 6 | 26234608 | c.554A>C | p.K185T | 188 | 46 | Sanger sequencing | 0.003 | damaging | 0.891 | possibly damaging |
| **FLneg10** | *STAT6* | 12 | 57496662 | c.1255G>C | p.D419H | 149 | 41 | N/A | 0.001 | damaging | 1 | probably damaging |
| **FLneg10** | *TNFRSF14* | 1 | 2489877 | c.274A>T | p.K92* | 4562 | 71 | Sanger sequencing | STOP | N/A | N/A | N/A |
| **FLneg11** | *CREBBP* | 16 | 3781324 | c.5039_5041delTCC | p.S1680del | 1292 | 50 | Sanger sequencing | DEL | N/A | N/A | N/A |
| **FLneg11** | *EZH2* | 7 | 148508727 | c.1937A>T | p.Y646F | 910 | 15 | Sanger sequencing | 0.02 | damaging | 0.817 | possibly damaging |
| **FLneg11** | *STAT6* | 12 | 57496662 | c.1255G>A | p.D419N | 2314 | 28 | N/A | 0.01 | damaging | 1 | probably damaging |
| **FLneg11** | *TNFRSF14* | 1 | 2489166 | c.71T>A | p.V24E | 7714 | 23 | Sanger sequencing | 0.02 | damaging | 0.999 | probably damaging |
| **FLneg11** | *TNFRSF14* | 1 | 2492102 | c.500_501insC | p.P167fs | 3879 | 23 | Sanger sequencing | INS | N/A | N/A | N/A |
| **FLneg12** | *CREBBP* | 16 | 3786796 | c.4415G>T | p.W1472L | 1309 | 44 | N/A | 0 | damaging | 1 | probably damaging |
| **FLneg14** | *CREBBP* | 16 | 3788618 | c.4336C>T | p.R1446C | 802 | 41 | single amplicons | 0.007 | damaging | 1 | probably damaging |
| **FLneg14** | *KMT2D* | 12 | 49434464 | c.7088_7089insC | p.S2364fs | 541 | 19 | Sanger sequencing | INS | N/A | N/A | N/A |
| **FLneg14** | *STAT6* | 12 | 57498344 | c.1115A>C | p.E372A | 12230 | 19 | N/A | 0.01 | damaging | 0.99 | probably damaging |
| **FLneg17** | *CREBBP* | 16 | 3786715 | c.4496T>G | p.L1499R | 1679 | 3 | single amplicons | 0 | damaging | 1 | probably damaging |
| **FLneg17** | *STAT6* | 12 | 57493830 | c.1556A>T | p.D519V | 2778 | 10 | single amplicons | 0.01 | damaging * | 0.999 | probably damaging |
| **FLneg18** | *CREBBP* | 16 | 3786719 | c.4492C>T | p.R1498* | 3522 | 28 | single amplicons | STOP | N/A | N/A | N/A |
| **FLneg18** | *EP300* | 22 | 41572419 | c.4948T>C | p.S1650P | 5697 | 24 | N/A | 0 | damaging | 0.998 | probably damaging |

| | | | | | | | | | | | | |
|---|---|---|---|---|---|---|---|---|---|---|---|---|
| **FLneg18** | *STAT6* | 12 | 57496654 | c.1263T>A | p.N421K | 9931 | 29 | single amplicons | 0.003 | damaging | 1 | probably damaging |
| **FLneg18** | *STAT6* | 12 | 57496670 | c.1247G>T | p.G416V | 10651 | 29 | single amplicons | 0 | damaging | 1 | probably damaging |
| **FLneg18** | *TNFAIP3* | 6 | 138192661 | c.295+2T>G | Splice Site | 7104 | 50 | SPLICE SITE | N/A | N/A | N/A | N/A |
| **FLneg18** | *TNFRSF14* | 1 | 2489266 | c.171C>A | p.C57* | 4108 | 44 | N/A | STOP | N/A | N/A | N/A |
| **FLneg25** | *EP300* | 22 | 41523665 | c.1081G>A | p.V361M | 1450 | 50 | N/A | 0.148 | tolerated | 0.999 | probably damaging |
| **FLneg25** | *FOXO1* | 13 | 41240277 | c.73T>G | p.W25G | 1241 | 6 | single amplicons | 0 | damaging | 0.734 | possibly damaging |
| **FLneg25** | *HIST1H1B* | 6 | 27834964 | c.344C>T | p.A115V | 1277 | 37 | N/A | 0.024 | damaging | 0.281 | benign |
| **FLneg25** | *STAT6* | 12 | 57498330 | c.1129G>A | p.E377K | 7027 | 23 | N/A | 0.005 | damaging | 1 | probably damaging |
| **FLneg25** | *TNFRSF14* | 1 | 2488138 | c.35G>A | p.W12* | 1821 | 14 | single amplicons | STOP | N/A | N/A | N/A |
| **FLneg25** | *TNFRSF14* | 1 | 2492146 | c.544C>T | p.Q182* | 2319 | 24 | single amplicons | STOP | N/A | N/A | N/A |
| **FLneg26** | *NOTCH1* | 9 | 139390676 | c.7514_7515insC | p.E2506* | 26723 | 10 | single amplicons | STOP | N/A | N/A | N/A |
| **FLneg26** | *TNFAIP3* | 6 | 138196100 | c.414_417delTAAA | p.K139fs | 10360 | 10 | single amplicons | DEL | N/A | N/A | N/A |
| **FLneg26** | *TNFAIP3* | 6 | 138192656 | c.292_295+4delinsAC | Splice Site | 7965 | 13 | N/A | SPLICE SITE | N/A | N/A | N/A |
| **FLneg26** | *TNFRSF14* | 1 | 2488124 | c.21G>A | p.W7* | 3487 | 28 | single amplicons | STOP | N/A | N/A | N/A |
| **FLneg26** | *TET2* | 4 | 106180790 | c.3818G>A | p.C1273Y | 9882 | 5 | N/A | 0 | damaging | 1 | probably damaging |
| **FLneg26** | *KLFZ2* | 19 | 16437727 | c.956_976del | p.L319_K325del | 586 | 12 | N/A | DEL | N/A | N/A | N/A |
| **FLneg26** | *HLA-B* | 6 | 31324050 | c.513G>A | p.W171* | 6020 | 13 | N/A | STOP | N/A | N/A | N/A |
| **FLneg26** | *PRDM1* | 6 | 106536269 | c.236C>T | p.A79V | 6471 | 14 | N/A | 0 | damaging | 1 | probably damaging |
| **FLneg26** | *HLA-B* | 6 | 31324503 | c.305T>C | p.L102P | 3297 | 15 | N/A | 0 | damaging | 1 | probably damaging |
| **FLneg26** | *TMSB4X* | X | 12994364 | c.-16-1G>A | p.? | 6697 | 22 | N/A | N/A | N/A | N/A | N/A |
| **FLneg26** | *KLFZ2* | 19 | 16436742 | c.791G>A | p.W264* | 2473 | 17 | N/A | STOP | N/A | N/A | N/A |
| **FLneg27** | *HIST1H1D* | 6 | 26234590 | c.572C>T | p.A191V | 2148 | 7 | single amplicons | 0.685 | tolerated | 0.079 | benign |
| **FLneg27** | *SOCS1* | 16 | 11348906 | c.430T>C | p.F144L | 5526 | 10 | single amplicons | 0 | damaging | 1 | probably damaging |
| **FLneg27** | *STAT3* | 17 | 40475052 | c.1858A>T | p.T620S | 3906 | 11 | N/A | 0.01 | damaging | 0.482 | possibly damaging |
| **FLneg29** | *HIST1H1C* | 6 | 26056077 | c.580A>C | p.K194Q | 1374 | 10 | N/A | 0 | damaging | 0.999 | probably damaging |

| | | | | | | | | | | | | |
|---|---|---|---|---|---|---|---|---|---|---|---|---|
| **FLneg29** | *HIST1H1E* | 6 | 26156847 | c.229A>G | p.N77D | 3994 | 10 | single amplicons | 0.014 | damaging | 0.991 | probably damaging |
| **FLneg29** | *KMT2D* | 12 | 49439712 | c.4732A>T | p.K1578* | 1306 | 9 | single amplicons | STOP | N/A | N/A | N/A |
| **FLneg29** | *STAT6* | 12 | 57498330 | c.1129G>A | p.E377K | 11517 | 10 | single amplicons | 0.005 | damaging | 1 | probably damaging |
| **FLneg29** | *TNFRSF14* | 1 | 2489255 | c.161_162insG | p.C54fs | 3986 | 17 | single amplicons | INS | N/A | N/A | N/A |
| **FLneg30** | *EZH2* | 7 | 148508727 | c.1937A>T | p.Y646F | 4927 | 14 | single amplicons | 0.02 | damaging | 0.817 | possibly damaging |
| **FLneg30** | *HIST1H1E* | 6 | 26156854 | c.236G>A | p.R79H | 2347 | 8 | single amplicons | 0.016 | damaging | 1 | probably damaging |
| **FLneg30** | *TNFRSF14* | 1 | 2489787 | c.184C>G | p.R62G | 8292 | 10 | single amplicons | 0.085 | tolerated | 0.953 | possibly damaging |
| **FLneg30** | *TNFRSF14* | 1 | 2489848 | c.245C>T | p.T82I | 8337 | 5 | single amplicons | 0.002 | damaging | 1 | probably damaging |
| **FLneg30** | *HLA-B* | 6 | 31324484 | c.324C>G | p.Y108* | 6180 | 11 | N/A | STOP | N/A | N/A | N/A |
| **FLneg30** | *FAS* | 10 | 90773895 | c.696T>A | p.Y232* | 5445 | 11 | N/A | STOP | N/A | N/A | N/A |
| **FLneg30** | *CDH2* | 15 | 93545488 | c.4219T>A | p.S1407T | 1317 | 44 | N/A | 0.61 | tolerated | 0.118 | benign |
| **FLneg32** | *EZH2* | 7 | 148508728 | c.1936T>A | p.Y646N | 5877 | 4 | single amplicons | 0 | damaging | 0.98 | probably damaging |
| **FLneg32** | *KMT2D* | 12 | 49440413 | c.4397A>G | p.K1466R | 8880 | 44 | N/A | 0.047 | damaging | 1 | probably damaging |
| **FLneg32** | *TNFRSF14* | 1 | 2489252 | c.157T>G | p.C53G | 7418 | 4 | single amplicons | 0 | damaging | 0.995 | probably damaging |
| **FLneg32** | *TET2* | 4 | 106158498 | c.3399C>A | p.C1133* | 2588 | 6 | N/A | STOP | N/A | N/A | N/A |
| **FLneg32** | *CDKN2A* | 9 | 21971063 | c.295C>T | p.R99W | 1353 | 10 | N/A | 0 | damaging | 0.999 | probably damaging |
| **FLneg32** | *B2M* | 15 | 45003746 | c.2T>A | p.M1K | 2241 | 5 | N/A | 0 | damaging | 0.961 | probably damaging |
| **FLneg33** | *SMARCA4* | 19 | 11101907 | c.1327A>G | p.K443E | 2616 | 21 | N/A | 0 | damaging | 0.994 | probably damaging |
| **FLneg33** | *TET2* | 4 | 106196634 | c.4969del | p.D1657Ifs | 792 | 41 | N/A | DEL | N/A | N/A | N/A |
| **FLneg33** | *TET2* | 4 | 106156348 | c.1249C>T | p.Q417* | 9624 | 44 | N/A | STOP | N/A | N/A | N/A |
| **FLneg35** | *NOTCH2* | 1 | 120458120 | c.7225C>T | p.Q2409* | 6083 | 21 | N/A | STOP | N/A | N/A | N/A |
| **FLneg35** | *TP53* | 17 | 7577099 | c.839G>A | p.R280K | 3776 | 24 | N/A | 0 | damaging | 0.977 | probably damaging |
| **FLneg35** | *ATM* | 11 | 108186610 | c.6067G>A | p.G2023R | 6701 | 42 | N/A | 0.01 | damaging | 1 | probably damaging |
| **FLneg35** | *ATM* | 11 | 108216575 | c.8524C>T | p.P2842S | 3077 | 41 | N/A | 0.05 | tolerated | 1 | probably damaging |
| **FLneg35** | *KMT2D* | 12 | 49418494 | c.15922-3C>G | p.? | 3141 | 24 | N/A | N/A | N/A | N/A | N/A |

| | | | | | | | | | | | | |
|---|---|---|---|---|---|---|---|---|---|---|---|---|
| **FLneg35** | *SPEN* | 1 | 16255141 | c.2415_2418del | p.E805Dfs | 3860 | 20 | N/A | DEL | N/A | N/A | N/A |
| **FLneg35** | *MYC* | 8 | 128752960 | c.1121A>G | p.H374R | 5202 | 16 | N/A | 0 | damaging | 1 | probably damaging |
| **FLneg35** | *SGK1* | 6 | 134493362 | c.1040G>C | p.S347T | 2360 | 15 | N/A | N/A | N/A | N/A | N/A |
| **FLneg36** | *CREBBP* | 16 | 3788653 | c.4301T>C | p.L1434P | 4903 | 15 | single amplicons | 0 | damaging | 1 | probably damaging |
| **FLneg36** | *PLCG2* | 16 | 81972516 | c.3310_3313del | p.V1104Mfs | 4435 | 16 | N/A | DEL | N/A | N/A | N/A |
| **FLneg37** | *CREBBP* | 16 | 3786763 | c.4448T>A | p.I1483N | 12503 | 23 | N/A | 0 | damaging | 1 | probably damaging |
| **FLneg37** | *KMT2D* | 12 | 49432651 | c.8488C>T | p.R2830* | 10822 | 23 | N/A | STOP | N/A | N/A | N/A |
| **FLneg37** | *STAT6* | 12 | 57496661 | c.1256A>G | p.D419G | 6900 | 24 | N/A | 0.001 | damaging | 1 | probably damaging |
| **FLneg38** | *CREBBP* | 16 | 3781323 | c.5039_5041delCCT | p.S1680del | 1617 | 39 | N/A | DEL | N/A | N/A | N/A |
| **FLneg38** | *EZH2* | 7 | 148508727 | c.1937A>T | p.Y646F | 4560 | 22 | N/A | 0.02 | damaging | 0.817 | possibly damaging |
| **FLneg38** | *STAT6* | 12 | 57496661 | c.1256A>G | p.D419G | 2401 | 14 | N/A | 0.001 | damaging | 1 | probably damaging |
| **FLneg38** | *TNFAIP3* | 6 | 138202199 | c.2116C>T | p.R706* | 1264 | 17 | N/A | STOP | N/A | N/A | N/A |
| **FLneg38** | *TNFRSF14* | 1 | 2491369 | c.412T>C | p.C138R | 4529 | 40 | N/A | 0.003 | damaging | 1 | probably damaging |
| **FLneg41** | *EZH2* | 7 | 148508728 | c.1936T>A | p.Y646N | 3677 | 6 | single amplicons | 0 | damaging | 0.98 | probably damaging |
| **FLneg41** | *STAT6* | 12 | 57493818 | c.1568A>G | p.D523G | 1555 | 15 | single amplicons | 0.01 | damaging | 1 | probably damaging |
| **FLneg41** | *TNFRSF14* | 1 | 2489186 | c.92_93insCG | p.A32fs | 5722 | 13 | N/A | INS | N/A | N/A | N/A |
| **FLneg42** | *CREBBP* | 16 | 3788616 | c.4337_4338delGCinsTT | p.R1446L | 5666 | 39 | N/A | INS | N/A | 1 | probably damaging |
| **FLneg42** | *BCL6* | 3 | 187451456 | c.26T>G | p.Ile9Ser | 4348 | 16 | N/A | 0 | damaging | 1 | probably damaging |
| **FLneg42** | *JAK2* | 9 | 5044488 | c.436G>A | p.Asp146Asn | 9423 | 9 | N/A | 0 | damaging | 1 | probably damaging |
| **FLneg44** | *CREBBP* | 16 | 3781323 | c.5039_5041delTCC | p.S1680del | 2887 | 30 | N/A | DEL | N/A | N/A | N/A |
| **FLneg44** | *MEF2B* | 19 | 19256665 | c.1048C>T | p.P350S | 628 | 17 | N/A | 0.016 | damaging | 0.728 | probably damaging |
| **FLneg44** | *STAT6* | 12 | 57496661 | c.1256A>G | p.D419G | 3879 | 15 | N/A | 0.001 | damaging | 1 | probably damaging |
| **FLneg44** | *TNFRSF14* | 1 | 2491380 | c.423C>A | p.Y141* | 5707 | 30 | N/A | STOP | N/A | N/A | N/A |
| **FLneg45** | *CREBBP* | 16 | 3786761 | c.4450T>G | p.F1484V | 838 | 24 | N/A | 0.001 | damaging | 0.993 | probably damaging |
| **FLneg45** | *STAT6* | 12 | 57498330 | c.1129G>A | p.E377K | 11320 | 8 | single amplicons | 0.005 | damaging | 1 | probably damaging |
| **FLneg46** | *CREBBP* | 16 | 3786130 | c.4635G>A | p.W1545* | 243 | 14 | single amplicons | STOP | N/A | N/A | N/A |
| **FLneg46** | *CREBBP* | 16 | 3786740 | c.4471C>G | p.Q1491E | 2120 | 17 | N/A | 0.001 | damaging | 0.993 | probably damaging |

| | | | | | | | | | | | | |
|---|---|---|---|---|---|---|---|---|---|---|---|---|
| **FLneg46** | *STAT3* | 17 | 40481459 | c.1250G>C | p.Arg417Thr | 10015 | 19 | N/A | 0 | damaging | 0.901 | probably damaging |
| **FLneg63** | *STAT6* | 12 | 57496661 | c.1256A>G | p.D419G | 1301 | 14 | N/A | 0.001 | damaging | 1 | probably damaging |
| **FLneg65** | *STAT6* | 12 | 57496662 | c.1255G>C | p.D419H | 770 | 21 | N/A | 0.001 | damaging | 1 | probably damaging |
| **FLneg66** | *STAT6* | 12 | 57496671 | c.1246G>T | p.G416C | 669 | 13 | N/A | 0 | damaging | 1 | probably damaging |
| **FLneg67** | *CREBBP* | 16 | 3786124 | c.4640dup | p.N1547Kfs | 767 | 26 | N/A | DUP | N/A | N/A | N/A |
| **FLneg67** | *STAT6* | 12 | 57496661 | c.1256A>G | p.D419G | 755 | 27 | N/A | 0.001 | damaging | 1 | probably damaging |
| **FLneg67** | *SOCS1* | 16 | 11348945 | c.391C>T | p.Q131* | 1999 | 13 | N/A | STOP | N/A | N/A | N/A |
| **FLneg67** | *SOCS1* | 16 | 11349162 | c.174C>G | p.F58L | 1189 | 12 | N/A | 0.006 | damaging | 0.97 | probably damaging |
| **FLneg68** | *STAT6* | 12 | 57493830 | c.1556A>T | p.D519V | 3874 | 28 | N/A | 0.01 | damaging * | 0.999 | probably damaging * |
| **FLneg68** | *CREBBP* | 16 | 3789627 | c.4232G>A | p.Gly1411Glu | 16092 | 28 | N/A | 0 | damaging | 1 | probably damaging |
| **FLneg69** | *STAT6* | 12 | 57496662 | c.1255G>C | p.D419H | 7801 | 16 | N/A | 0 | damaging | 1 | probably damaging |
| **FLneg69** | *TNFRSF14* | 1 | 2491265 | c.311_324delGCCTGCGCGCGAGC | p.Gly104AlafsTer125 | 11363 | 28 | N/A | DEL | N/A | N/A | N/A |
| **FLneg69** | *EP300* | 22 | 41513670 | c.574A>G | p.Met192Val | 9549 | 54 | N/A | 0.01 | damaging | 0.589 | possibly damaging |
| **FLneg69** | *CREBBP* | 16 | 3786748 | c.4463C>G | p.Pro1488Arg | 20993 | 24 | N/A | 0 | damaging | 1 | probably damaging |
| **FLneg70** | *STAT6* | 12 | 57498345 | c.1114G>A | p.E372K | 9495 | 42 | N/A | 0 | damaging | 0.99 | probably damaging |
| **FLneg70** | *SOCS1* | 16 | 11349164 | c.172T>C | p.F58L | 4803 | 22 | N/A | N/A | N/A | N/A | N/A |
| **FLneg70** | *SOCS1* | 16 | 11349173 | c.163T>C | p.F55L | 4789 | 23 | N/A | N/A | N/A | N/A | N/A |
| **FLneg70** | *KMT2D* | 12 | 49440391 | c.4418+1G>A | p.? | 16448 | 28 | N/A | N/A | N/A | N/A | N/A |
| **FLneg70** | *FOXO1* | 13 | 41240288 | c.62G>C | p.Arg21Pro | 12807 | 22 | N/A | 0 | damaging | 0.999 | probably damaging |
| **FLneg71** | *SOCS1* | 16 | 11348722 | c.614G>T | p.S205I | 6709 | 13 | N/A | N/A | N/A | N/A | N/A |
| **FLneg71** | *SOCS1* | 16 | 11349301 | c.35C>G | p.A12G | 2428 | 14 | N/A | N/A | N/A | N/A | N/A |
| **FLneg71** | *SOCS1* | 16 | 11348962 | c.374G>A | p.S125N | 13254 | 14 | N/A | N/A | N/A | N/A | N/A |
| **FLneg71** | *SOCS1* | 16 | 11348918 | c.418A>C | p.S140R | 12791 | 11 | N/A | N/A | N/A | N/A | N/A |
| **FLneg71** | *FOXO1* | 13 | 41240280 | c.70A>G | p.Thr24Ala | 9432 | 4 | N/A | 0 | damaging | 0.993 | probably damaging |
| **FLneg73** | *STAT6* | 12 | 57496661 | c.1256A>G | p.D419G | 2375 | 18 | N/A | 0.001 | damaging | 1 | probably damaging |
| **FLneg73** | *SOCS1* | 16 | 11348803 | c.526_533del | p.E176Pfs | 2375 | 24 | N/A | DEL | N/A | N/A | N/A |
| **FLneg73** | *SOCS1* | 16 | 11349085 | c.251T>G | p.L84R | 2375 | 16 | N/A | N/A | N/A | N/A | N/A |
| **FLneg74** | *SOCS1* | 16 | 11349139 | c.197G>A | p.R66H | 1673 | 15 | N/A | N/A | N/A | N/A | N/A |

| | | | | | | | | | | | | |
|---|---|---|---|---|---|---|---|---|---|---|---|---|
| **FLneg74** | *TNFRSF14* | 1 | 2489785 | c.182A>C | p.Y61S | 4188 | 23 | N/A | 0.36 | tolerated | 0.978 | probably damaging |
| **FLneg74** | *KMT2D* | 12 | 49426896 | c.11592C>G | p.H3864Q | 2792 | 4 | N/A | 0.08 | tolerated | 0 | benign |
| **FLneg74** | *KMT2D* | 12 | 49427265 | c.11220_11222delGCA | p.Q3745del | 4326 | 5 | N/A | DEL | N/A | N/A | N/A |
| **FLneg74** | *FOXO1* | 13 | 41240285 | c.59_64delCGCGCT | p.R21_S22del | 3229 | 16 | N/A | DEL | N/A | N/A | N/A |
| **FLneg74** | *GNA13* | 17 | 63052467 | c.243_244delCG | p.E82GfsTer19 | 5512 | 3 | N/A | DEL | N/A | N/A | N/A |
| **FLneg75** | *STAT6* | 12 | 57498330 | c.1129G>A | p.E377K | 3741 | 17 | N/A | 0 | damaging | 1 | probably damaging |
| **FLneg75** | *SOCS1* | 16 | 11348920 | c.416G>A | p.G139D | 4152 | 42 | N/A | N/A | N/A | N/A | N/A |
| **FLneg75** | *TNFRSF14* | 1 | 2489186 | c.91G>T | p.G31* | 2321 | 20 | N/A | N/A | N/A | N/A | N/A |
| **FLneg75** | *KMT2D* | 12 | 49432047 | c.9092T>C | p.L3031P | 1955 | 21 | N/A | 0 | damaging | 1 | probably damaging |
| **FLneg75** | *KMT2D* | 12 | 49432056 | c.9083T>A | p.L3028* | 1959 | 21 | N/A | STOP | N/A | N/A | N/A |
| **FLneg75** | *KMT2D* | 12 | 49432073 | c.9066T>A | p.D3022E | 1956 | 21 | N/A | 0 | damaging | 1 | probably damaging |
| **FLneg75** | *FOXO1* | 13 | 41240274 | c.76C>T | p.P26S | 3597 | 23 | N/A | 0 | damaging | 0.964 | probably damaging |
| **FLneg76** | *STAT6* | 12 | 57496661 | c.1256A>G | p.D419G | 3333 | 5 | N/A | 0.001 | damaging | 1 | probably damaging |
| **FLneg77** | *STAT6* | 12 | 57498330 | c.1129G>A | p.E377K | 3273 | 7 | N/A | N/A | N/A | N/A | N/A |
| **FLneg77** | *SOCS1* | 16 | 11424852 | c.347G>A | p.S116N | 3273 | 15 | N/A | N/A | N/A | N/A | N/A |
| **FLneg78** | *STAT6* | 12 | 57498330 | c.1129G>A | p.Glu377Lys | 2171 | 28 | N/A | 0 | damaging | 1 | probably damaging |
| **FLneg79** | *STAT6* | 12 | 57496655 | c.1262A>G | p.Asn421Ser | 3139 | 31 | N/A | 0 | damaging | 1 | probably damaging |
| **FLneg79** | *SOCS1* | 16 | 11349040 | c.296G>A | p.Gly99Asp | 963 | 9 | N/A | N/A | N/A | N/A | N/A |
| **FLneg79** | *SOCS1* | 16 | 11349146 | c.190T>A | p.Tyr64Asn | 1589 | 19 | N/A | N/A | N/A | N/A | N/A |
| **FLneg79** | *CREBBP* | 16 | 3788618 | c.4336C>T | p.Arg1446Cys | 3313 | 46 | N/A | 0 | damaging | 1 | probably damaging |
| **FLneg79** | *FOXO1* | 13 | 41240280 | c.70A>G | p.Thr24Ala | 2709 | 44 | N/A | 0 | damaging | 0.993 | probably damaging |
| **FLneg79** | *HIST1H1C* | 6 | 26056544 | c.113C>T | p.Pro38Leu | 416 | 26 | N/A | 0.18 | tolerated | 0.997 | probably damaging |
| **FLneg79** | *EP300* | 22 | 41537051 | c.1879_1887delGCGGAATAC | p.Ala627_Tyr629del | 3626 | 21 | N/A | DEL | N/A | N/A | N/A |
| **FLneg79** | *JAK1* | 1 | 65307283 | c.2405A>G | p.Lys802Arg | 3182 | 47 | N/A | 0 | damaging | 0.999 | probably damaging |
| **FLneg80** | *STAT6* | 12 | 57496661 | c.1256A>C | p.Asp419Ala | 6334 | 30 | N/A | 0 | damaging | 0.999 | probably damaging |
| **FLneg80** | *SOCS1* | 16 | 11348986 | c.348_350delCGTinsGGA | p.[Ser116Arg;Val117Glu] | 10311 | 34 | N/A | DELINS | N/A | N/A | N/A |
| **FLneg80** | *TNFRSF14* | 1 | 2489822 | c.225_226delTG | p.Cys75Ter | 10825 | 51 | N/A | DEL | N/A | N/A | N/A |
| **FLneg80** | *HIST1H1E* | 6 | 26157111 | c.493G>T | p.Ala165Ser | 5291 | 46 | N/A | N/A | N/A | N/A | N/A |

| | | | | | | | | | | | | |
|---|---|---|---|---|---|---|---|---|---|---|---|---|
| **FLneg80** | *FOXO1* | 13 | 41240279 | c.71C>T | p.Thr24Ile | 5660 | 40 | N/A | 0 | damaging | 0.998 | probably damaging |
| **FLneg80** | *HIST1H1B* | 6 | 27835012 | c.296C>T | p.Thr99Ile | 917 | 35 | N/A | N/A | N/A | N/A | N/A |
| **FLneg81** | *NOTCH1* | 9 | 139390896 | c.7295G>A | p.Ser2432Asn | 1128 | 13 | N/A | 0.64 | tolerated | 0.001 | benign |
| **FLneg81** | *STAT6* | 12 | 57498348 | c.1111T>C | p.Cys371Arg | 2418 | 12 | N/A | 0 | damaging | 0.998 | probably damaging |
| **FLneg81** | *SOCS1* | 16 | 11348997 | c.320_335delGCCAGCGGAACTGCTT | p.Arg107LeufsTer6 | 700 | 2 | N/A | DEL | N/A | N/A | N/A |
| **FLneg81** | *TNFRSF14* | 1 | 2489243 | c.148G>T | p.Gly50Cys | 2067 | 16 | N/A | 0 | damaging | 1 | probably damaging |
| **FLneg81** | *CREBBP* | 16 | 3788606 | c.4348T>C | p.Tyr1450His | 3139 | 12 | N/A | 0 | damaging | 1 | probably damaging |
| **FLneg81** | *KMT2D* | 12 | 49432651 | c.8488C>T | p.Arg2830Ter | 10003 | 12 | N/A | N/A | N/A | N/A | N/A |
| **FLneg81** | *HIST1H1E* | 6 | 26156964 | c.346G>A | p.Ala116Thr | 4325 | 9 | N/A | N/A | N/A | N/A | N/A |
| **FLneg82** | *STAT6* | 12 | 57496661 | c.1256A>G | p.Asp419Gly | 2853 | 35 | N/A | 0 | damaging | 1 | probably damaging |
| **FLneg82** | *TNFRSF14* | 1 | 2489802 | c.201C>G | p.Cys67Trp | 9082 | 43 | N/A | 0 | damaging | 1 | probably damaging |
| **FLneg82** | *CREBBP* | 16 | 3781323 | c.5039_5041delCCT | p.Ser1680del | 1494 | 51 | N/A | DEL | N/A | N/A | N/A |
| **FLneg82** | *FOXO1* | 13 | 41240242 | c.108C>G | p.Asn36Lys | 5383 | 34 | N/A | 0.26 | tolerated | 0.02 | possibly damaging |
| **FLneg82** | *FOXO1* | 13 | 41240286 | c.64T>C | p.Ser22Pro | 5367 | 33 | N/A | 0 | damaging | 0.952 | probably damaging |
| **FLneg83** | *STAT6* | 12 | 57496661 | c.1256A>T | p.Asp419Val | 2489 | 18 | N/A | 0 | damaging | 1 | probably damaging |
| **FLneg83** | *CREBBP* | 16 | 3788651 | c.4303G>A | p.Asp1435Asn | 2954 | 43 | N/A | 0 | damaging | 0.999 | probably damaging |
| **FLneg83** | *TNFRSF14* | 1 | 2491313 | c.357_358delTG | p.Cys119TrpfsTer114 | 5317 | 22 | N/A | DEL | N/A | N/A | N/A |
| **FLneg83** | *FOXO1* | 13 | 41240289 | c.61C>T | p.Arg21Cys | 4217 | 21 | N/A | 0 | damaging | 1 | probably damaging |
| **FLneg84** | *STAT6* | 12 | 57498330 | c.1129G>A | p.Glu377Lys | 5412 | 24 | N/A | 0 | damaging | 1 | probably damaging |
| **FLneg84** | *KMT2D* | 12 | 49443616 | c.3754C>T | p.Arg1252Ter | 1846 | 30 | N/A | N/A | N/A | N/A | N/A |
| **FLneg84** | *CREBBP* | 16 | 3786733 | c.4471C>A | p.Gln1491Lys | 5121 | 17 | N/A | 0 | damaging | 0.993 | probably damaging |
| **FLneg84** | *HIST1H1C* | 6 | 26056305 | c.352C>G | p.Pro118Ala | 1173 | 40 | N/A | 0.11 | tolerated | 0.005 | benign |
| **FLneg84** | *TNFRSF14* | 1 | 2492070 | c.470_476dup | p.Asp159GlufsTer77 | 615 | 38 | N/A | DUP | N/A | N/A | N/A |

**Table 32: List of detected gene mutations in FLpos by targeted next-generation sequencing**
AF = allele frequency, Chr = chromosome, n = 24

| Case | Gene | Chr | Position (hg19) | cDNA change | Protein change | Coverage | AF | Validation | SIFT score | SIFT | PolyPhen- 2 score | PolyPhen-2 |
|---|---|---|---|---|---|---|---|---|---|---|---|---|
| **FLpos1** | *KMT2D* | 12 | 49420460 | c.15289C>T | p.R5097* | 8444 | 25 | N/A | STOP | N/A | N/A | N/A |
| **FLpos1** | *KMT2D* | 12 | 49441847 | c.4135_4136delAT | p.M1379VfsTer52 | 4491 | 43 | N/A | DEL | N/A | N/A | N/A |
| **FLpos1** | *CREBBP* | 16 | 3786715 | c.4496T>G | p.L1499R | 6101 | 30 | N/A | 0 | damaging | 1 | probably damaging |
| **FLpos2** | *STAT6* | 12 | 57496662 | c.1255G>C | p.D419H | 2614 | 10 | N/A | N/A | N/A | N/A | N/A |
| **FLpos2** | *MAP2K1* | 15 | 66679250 | c.389A>G | p.Y130C | 2614 | 8 | N/A | N/A | N/A | N/A | N/A |
| **FLpos2** | *SOCS1* | 16 | 11348962 | c.374G>C | p.S125T | 2614 | 21 | N/A | N/A | N/A | N/A | N/A |
| **FLpos2** | *SOCS1* | 16 | 11348983 | c.353A>C | p.K118T | 2614 | 20 | N/A | N/A | N/A | N/A | N/A |
| **FLpos3** | *TNFRSF14* | 1 | 2488106 | c.3G>A | p.M1? | 1419 | 30 | N/A | 0 | damaging | 0.86 | probably damaging |
| **FLpos3** | *HIST1H1D* | 6 | 26234678 | c.5039_5041delCCT | p.S1680del | 1617 | 31 | N/A | DEL | N/A | N/A | N/A |
| **FLpos3** | *CREBBP* | 16 | 3781323 | c.169G>A | p.G57S | 2049 | 14 | N/A | N/A | N/A | N/A | N/A |
| **FLpos4** | *KMT2D* | 12 | 49431262 | c.9877C>T | p.Q3293* | 5011 | 25 | N/A | STOP | N/A | N/A | N/A |
| **FLpos4** | *CREBBP* | 16 | 3788662 | c.4292T>G | p.I1431S | 2048 | 17 | N/A | 0 | damaging | 1 | probably damaging |
| **FLpos4** | *BORCS8-MEF2B* | 19 | 19260045 | c.248A>T | p.D83V | 1996 | 19 | N/A | 0 | damaging | 1 | probably damaging |
| **FLpos5** | *KMT2D* | 12 | 49432520 | c.8618delG | p.G2873VfsTer37 | 1732 | 18 | N/A | DEL | N/A | N/A | N/A |
| **FLpos5** | *KMT2D* | 12 | 49439955 | c.4586G>A | p.W1529* | 3407 | 21 | N/A | STOP | N/A | N/A | N/A |
| **FLpos5** | *FOXO1* | 13 | 41240286 | c.64T>C | p.S22P | 3634 | 9 | N/A | N/A | N/A | N/A | N/A |
| **FLpos5** | *CREBBP* | 16 | 3788618 | c.4336C>T | p.R1446C | 1678 | 39 | N/A | N/A | N/A | N/A | N/A |
| **FLpos6** | *STAT6* | 12 | 57492825 | c.1928C>T | p.P643L | 16734 | 37 | N/A | 0 | damaging | 0.954 | probably damaging |
| **FLpos7** | *SOCS1* | 16 | 11348906 | c.430T>C | p.F144L | 9541 | 10 | N/A | N/A | N/A | N/A | N/A |
| **FLpos7** | *STAT6* | 12 | 57493830 | c.1556A>T | p.D519V | 4404 | 6 | N/A | 0 | damaging | 0.999 | probably damaging |
| **FLpos8** | *STAT6* | 12 | 57496662 | c.1255G>A | p.D419N | 7120 | 36 | N/A | 0 | damaging | 1 | probably damaging |
| **FLpos8** | *KMT2D* | 12 | 49434544 | c.7009C>T | p.Q2337* | 3989 | 31 | N/A | STOP | N/A | N/A | N/A |
| **FLpos10** | *CREBBP* | 16 | 3786649 | c.4560+2T>A | p.? | 977 | 11 | N/A | N/A | N/A | N/A | N/A |
| **FLpos10** | *EZH2* | 7 | 148508728 | c.1936T>A | p.Tyr646Asn | 1014 | 22 | N/A | 0 | damaging | 0.98 | probably damaging |
| **FLpos10** | *TNFRSF14* | 1 | 2488138 | c.35G>A | p.Trp12Ter | 309 | 25 | N/A | N/A | N/A | N/A | N/A |
| **FLpos11** | *EZH2* | 7 | 148508727 | c.1937A>T | p.Tyr646Phe | 2278 | 33 | N/A | 0 | damaging | 0.817 | possibly damaging |

| | | | | | | | | | | | | |
|---|---|---|---|---|---|---|---|---|---|---|---|---|
| **FLpos11** | *TNFRSF14* | 1 | 2488174 | c.69+2T>A | p.? | 491 | 65 | N/A | N/A | N/A | N/A | N/A |
| **FLpos11** | *KMT2D* | 12 | 49430931 | c.10205_10206insT | p.Ala3403GlyfsTer20 | 2170 | 51 | N/A | INS | N/A | N/A | N/A |
| **FLpos12** | *GNA13* | 17 | 63052533 | c.179G>A | p.Gly60Asp | 9084 | 35 | N/A | 0 | damaging | 1 | probably damaging |
| **FLpos12** | *KMT2D* | 12 | 49420630 | c.15119A>G | p.Asp5040Gly | 1381 | 32 | N/A | 0 | damaging | 1 | probably damaging |
| **FLpos12** | *KMT2D* | 12 | 49433560 | c.7982_7989delTCCCAGGT | p.Leu2661HisfsTer10 | 7633 | 37 | N/A | DEL | N/A | N/A | N/A |
| **FLpos13** | *STAT6* | 12 | 57496661 | c.1256A>G | p.Asp419Gly | 5545 | 4 | N/A | N/A | N/A | N/A | N/A |
| **FLpos13** | *CREBBP* | 6 | 3781323 | c.5039_5041delCCT | p.Ser1680del | 1268 | 80 | N/A | DEL | N/A | N/A | N/A |
| **FLpos13.2** | *STAT6* | 12 | 57493831 | c.1555G>A | p.D519N | 1995 | 4 | N/A | 0.252 | tolerated * | 0.994 | probably damaging |
| **FLpos14** | *STAT6* | 12 | 57493830 | c.1556A>G | p.Asp519Gly | 2636 | 44 | N/A | 0 | damaging | 0.994 | probably damaging |
| **FLpos14** | *TNFRSF14* | 1 | 2491416 | c.460_460+1delinsTT | p.? | 1694 | 29 | N/A | DELINS | N/A | N/A | N/A |
| **FLpos14** | *GNA13* | 17 | 63010848 | c.661G>C | p.Val221Leu | 985 | 54 | N/A | 0.02 | damaging | 0.165 | possibly damaging |
| **FLpos14** | *CREBBP* | 16 | 3781323 | c.5039_5041delCCT | p.Ser1680del | 1893 | 63 | N/A | DEL | N/A | N/A | N/A |
| **FLpos15** | *EZH2* | 7 | 148508727 | c.1937A>C | p.Tyr646Ser | 802 | 18 | N/A | 0 | damaging | 0.688 | possibly damaging |
| **FLpos15** | *CREBBP* | 16 | 3790421 | c.4112T>A | p.Val1371Asp | 506 | 12 | N/A | 0 | damaging | 1 | probably damaging |
| **FLpos15** | *KMT2D* | 12 | 49426586 | c.11902C>T | p.Gln3968Ter | 12162 | 34 | N/A | N/A | N/A | N/A | N/A |
| **FLpos16** | *STAT6* | 12 | 57496661 | c.1256A>G | p.Asp419Gly | 2347 | 28 | N/A | 0 | damaging | 1 | probably damaging |
| **FLpos16** | *CREBBP* | 16 | 3781206 | c.5159G>A | p.Cys1720Tyr | 411 | 15 | N/A | 0 | damaging | 0.999 | probably damaging |
| **FLpos16** | *BORCS8-MEF2B* | 19 | 19258640 | c.260C>T | p.Thr87Met | 488 | 15 | N/A | 0 | damaging | 0.988 | probably damaging |
| **FLpos16** | *TNFRSF14* | 1 | 2492139 | c.537T>A | p.Cys179Ter | 510 | 16 | N/A | N/A | N/A | N/A | N/A |
| **FLpos17** | *EZH2* | 7 | 148508728 | c.1936T>C | p.Tyr646His | 7319 | 36 | N/A | 0 | damaging | 0.98 | probably damaging |
| **FLpos17** | *CREBBP* | 16 | 3781323 | c.5039_5041delCCT | p.Ser1680del | 1205 | 70 | N/A | DEL | N/A | N/A | N/A |
| **FLpos17** | *TNFRSF14* | 1 | 2491336 | c.379T>C | p.Cys127Arg | 2615 | 71 | N/A | 0 | damaging | 1 | probably damaging |
| **FLpos17** | *EP300* | 22 | 41525967 | c.1244T>C | p.Leu415Pro | 2202 | 33 | N/A | 0 | damaging | 1 | probably damaging |
| **FLpos18** | *SOCS1* | 16 | 11348989 | c.347G>A | p.Ser116Asn | 4521 | 11 | N/A | N/A | N/A | N/A | N/A |
| **FLpos18** | *FOXO1* | 13 | 41239803 | c.547C>G | p.Leu183Val | 571 | 7 | N/A | 0 | damaging | 0.997 | probably damaging |
| **FLpos18** | *CREBBP* | 16 | 3786704 | c.4507T>G | p.Tyr1503Asp | 6198 | 15 | N/A | 0 | damaging | 1 | probably damaging |
| **FLpos18** | *FOXO1* | 13 | 41240273 | c.77C>T | p.Pro26Leu | 4627 | 18 | N/A | 0 | damaging | 0.993 | probably damaging |
| **FLpos18** | *SOCS3* | 17 | 76354980 | c.197G>T | p.Gly66Val | 1090 | 12 | N/A | N/A | N/A | N/A | N/A |

| | | | | | | | | | | | | |
|---|---|---|---|---|---|---|---|---|---|---|---|---|
| **FLpos18** | *SOCS3* | 17 | 76355077 | c.99_100insCGAGTACCAGCTG | p.Val34ArgfsTer69 | 3993 | 8 | N/A | INS | N/A | N/A | N/A |
| **FLpos18** | *SOCS3* | 17 | 76355100 | c.77G>C | p.Ser26Thr | 2910 | 11 | N/A | N/A | N/A | N/A | N/A |
| **FLpos18** | *TYK2* | 19 | 10473075 | c.1534G>A | p.Gly512Arg | 5114 | 53 | N/A | 0.04 | damaging | 0.131 | benign |
| **FLpos19** | *TNFRSF14* | 1 | 2491418 | c.460+1G>A | p.? | 1967 | 42 | N/A | N/A | N/A | N/A | N/A |
| **FLpos19** | *HIST1H1B* | 6 | 27834947 | c.361C>T | p.Pro121Ser | 1061 | 42 | N/A | N/A | N/A | N/A | N/A |
| **FLpos19** | *EZH2* | 7 | 148508728 | c.1936T>A | p.Tyr646Asn | 1643 | 52 | N/A | 0 | damaging | 0.98 | probably damaging |
| **FLpos19** | *CREBBP* | 16 | 3786803 | c.4404_4405delAG | p.Gly1469AlafsTer9 | 4106 | 61 | N/A | DEL | N/A | N/A | N/A |
| **FLpos20** | *SOCS1* | 16 | 11349202 | c.133G>A | p.Val45Ile | 3638 | 23 | N/A | N/A | N/A | N/A | N/A |
| **FLpos22** | *HIST1H1E* | 6 | 26156811 | c.193G>C | p.Ala65Pro | 296 | 27 | N/A | N/A | N/A | N/A | N/A |
| **FLpos22** | *EZH2* | 7 | 148508728 | c.1936T>C | p.Tyr646His | 1405 | 35 | N/A | 0 | damaging | 0.98 | probably damaging |
| **FLpos23** | *KMT2D* | 12 | 49434419 | c.7134T>A | p.Tyr2378Ter | 1643 | 30 | N/A | N/A | N/A | N/A | N/A |
| **FLpos23** | *TNFRSF14* | 1 | 2489220 | c.125G>A | p.Cys42Tyr | 1750 | 33 | N/A | 0 | damaging | 0.999 | probably damaging |
| **FLpos23** | *CREBBP* | 16 | 3788653 | c.4301T>A | p.Leu1434Gln | 4246 | 46 | N/A | 0 | damaging | 1 | probably damaging |
| **FLpos39** | *STAT6* | 12 | 57493561 | c.1733G>A | p.R578Q | 2508 | 59 | N/A | 0.1 | tolerated | 0.992 | probably damaging |
| **FLpos39** | *SOCS1* | 16 | 11348706 | c.630G>C | p.Q210H | 2783 | 52 | N/A | N/A | N/A | N/A | N/A |
| **FLpos39** | *SOCS1* | 16 | 11348709 | c.627C>A | p.F209L | 2784 | 13 | N/A | N/A | N/A | N/A | N/A |
| **FLpos39** | *HIST1H1E* | 6 | 26156750 | c.132T>G | p.I44M | 1864 | 16 | N/A | N/A | N/A | N/A | N/A |
| **FLpos39** | *KMT2D* | 12 | 49435737 | c.6146G>A | p.W2049* | 4744 | 21 | N/A | STOP | N/A | N/A | N/A |
| **FLpos39** | *FOXO1* | 13 | 41240294 | c.56G>C | p.R19P | 2205 | 12 | N/A | 0 | damaging | 0.988 | probably damaging |
| **FLpos39** | *CREBBP* | 16 | 3786738 | c.4473A>C | p.Q1491H | 11163 | 11 | N/A | 0 | damaging | 0.999 | probably damaging |
| **FLpos40** | *CREBBP* | 16 | 3786704 | c.4507T>G | p.Y1503D | 6329 | 12 | N/A | 0 | damaging | 1 | probably damaging |
| **FLpos40** | *CREBBP* | 16 | 3781323 | c.5039_5041delCCT | p.S1680del | 636 | 12 | N/A | DEL | N/A | N/A | N/A |
| **FLpos40** | *STAT6* | 12 | 57496661 | c.1256A>C | p.D419A | 4797 | 18 | N/A | 0.01 | damaging | 0.999 | probably damaging |
| **FLpos40** | *TNFRSF14* | 1 | 2489235 | c.140A>G | p.Y47C | 2265 | 23 | N/A | 0.001 | damaging | 1 | probably damaging |

**Table 33: Shared genes across both HTG Precision Immuno-Oncology panel and NanoString Immune Profiling panel as well as genes that were unique for the respective panel**

| NanoString panel genes | Shared genes | HTG panel genes |
|---|---|---|
| *AIRE* | *A2M* | *AADAT* |
| *AMBP* | *ABCB1* | *ABCB11* |
| *AMICA1* | *ABL1* | *ABCC2* |
| *ATG10* | *ADA* | *ABCC6* |
| *BST1* | *ADORA2A* | *ABCF1* |
| *C1QBP* | *AICDA* | *ABCG2* |
| *C1R* | *AKT3* | *ABHD1* |
| *C1S* | *ALCAM* | *ABL2* |
| *C2* | *ANP32B* | *ACKR3* |
| *C4B* | *ANXA1* | *ACP6* |
| *C4BPA* | *APOE* | *ACTG2* |
| *C6* | *APP* | *ACTR3B* |
| *C7* | *ARG1* | *ADAM17* |
| *C8A* | *ARG2* | *ADCY1* |
| *C8B* | *ATF1* | *ADD2* |
| *C8G* | *ATF2* | *ADGRE5* |
| *C9* | *ATG12* | *ADORA2B* |
| *CARD9* | *ATG16L1* | *ADRB2* |
| *CCL3L1* | *ATG5* | *AGER* |
| *CD164* | *ATG7* | *AHR* |
| *CD207* | *ATM* | *AIF1* |
| *CD36* | *AXL* | *AKT1* |
| *CD3EAP* | *BAGE* | *ALOX15B* |
| *CD46* | *BATF* | *ALOX5* |
| *CD81* | *BAX* | *ANAPC1* |
| *CD9* | *BCL10* | *ANKRD30A* |
| *CD97* | *BCL2* | *ANLN* |
| *CFB* | *BCL2L1* | *ANPEP* |
| *CFD* | *BCL6* | *APAF1* |
| *CFI* | *BID* | *APC2* |
| *CFP* | *BIRC5* | *ARHGAP11A* |
| *CLU* | *BLK* | *ARHGAP11B* |

| | | |
|---|---|---|
| *COLEC12* | *BLNK* | *ARHGDIB* |
| *CT45A1* | *BMI1* | *ARHGEF26* |
| *CTAG1B* | *BST2* | *ARMCX6* |
| *CTAGE1* | *BTK* | *AS3MT* |
| *CTCFL* | *BTLA* | *ASCL1* |
| *CTSW* | *C1QA* | *ASF1A* |
| *CYFIP2* | *C1QB* | *ASF1B* |
| *DDX43* | *C3* | *ASPM* |
| *ECSIT* | *C3AR1* | *ASRGL1* |
| *ELANE* | *C5* | *ATF3_activating* |
| *F12* | *CAMP* | *ATF3_repressing* |
| *FCER1A* | *CARD11* | *ATOH1* |
| *FCGR1A* | *CASP1* | *ATP5F1* |
| *FCGR2A* | *CASP10* | *ATXN1* |
| *FCGR3A* | *CASP3* | *AUNIP* |
| *FUT7* | *CASP8* | *AURKA* |
| *GAGE1* | *CCL1* | *AURKB* |
| *HAMP* | *CCL11* | *AXIN1* |
| *HCK* | *CCL13* | *AXIN2* |
| *HLA-DRB3* | *CCL14* | *B3GAT1* |
| *HLA-DRB4* | *CCL15* | *BAGE_family* |
| *IFNA1* | *CCL16* | *BAGE2_BAGE3* |
| *IFNA17* | *CCL17* | *BAGE4_BAGE5* |
| *IFNA2* | *CCL18* | *BATF2* |
| *IFNA7* | *CCL19* | *BCL2L11* |
| *IFNA8* | *CCL2* | *BEX1* |
| *IGLL1* | *CCL20* | *BEX2* |
| *IKBKE* | *CCL21* | *BMP6* |
| *IL18RAP* | *CCL22* | *BMP7* |
| *IL1RAPL2* | *CCL23* | *BNC1* |
| *IL22* | *CCL24* | *BORA* |
| *IL8* | *CCL25* | *BRCA1* |
| *ILF3* | *CCL26* | *BRCA2* |
| *INPP5D* | *CCL27* | *BRIP1* |

| | | |
|---|---|---|
| *ITCH* | *CCL28* | *BRMS1L* |
| *ITGA2B* | *CCL3* | *BUB1* |
| *JAM3* | *CCL4* | *BUB1B* |
| *KIR_Activating_Subgroup_1* | *CCL5* | *C11orf71* |
| *KIR_Activating_Subgroup_2* | *CCL7* | *C17orf80* |
| *KIR_Inhibiting_Subgroup_1* | *CCL8* | *C19orf66* |
| *KIR_Inhibiting_Subgroup_2* | *CCND3* | *C1orf56* |
| *KLRC1* | *CCR1* | *C20orf24* |
| *KLRC2* | *CCR2* | *C4A_C4B* |
| *LAMP2* | *CCR3* | *CA4* |
| *LBP* | *CCR4* | *CALML3* |
| *LILRA1* | *CCR5* | *CASP4* |
| *LILRA5* | *CCR6* | *CASP5* |
| *LILRB3* | *CCR7* | *CAV1* |
| *LRRN3* | *CCR9* | *CBLB* |
| *LTF* | *CCRL2* | *CCDC138* |
| *MAGEA3* | *CD14* | *CCNA2* |
| *MAP4K2* | *CD160* | *CCNB1* |
| *MASP1* | *CD163* | *CCNB2* |
| *MASP2* | *CD180* | *CCND1* |
| *MAVS* | *CD19* | *CCNE1* |
| *MCAM* | *CD1A* | *CCNE2* |
| *MEFV* | *CD1B* | *CCNF* |
| *MFGE8* | *CD1C* | *CCR10* |
| *MNX1* | *CD1D* | *CCR8* |
| *NCF4* | *CD1E* | *CCT5* |
| *NFATC2* | *CD2* | *CD226* |
| *NOS2A* | *CD200* | *CD52* |
| *PASD1* | *CD209* | *CD5L* |
| *PIN1* | *CD22* | *CD69* |
| *PLA2G1B* | *CD24* | *CD72* |
| *PNMA1* | *CD244* | *CDC20* |
| *PRM1* | *CD247* | *CDC25A* |
| *ROPN1* | *CD27* | *CDC25C* |

| | | |
|---|---|---|
| *RORA* | *CD274* | *CDC45* |
| *S100A7* | *CD276* | *CDC6* |
| *SAA1* | *CD28* | *CDC7* |
| *SBNO2* | *CD33* | *CDCA2* |
| *SEMG1* | *CD34* | *CDCA3* |
| *SERPING1* | *CD37* | *CDCA5* |
| *SH2B2* | *CD38* | *CDCA8* |
| *SIGLEC1* | *CD3D* | *CDH15* |
| *SPA17* | *CD3E* | *CDK4* |
| *SPACA3* | *CD3G* | *CDK6* |
| *SPO11* | *CD4* | *CDKN1B* |
| *SSX4* | *CD40* | *CDKN2A* |
| *TANK* | *CD40LG* | *CDKN3* |
| *TFE3* | *CD44* | *CDT1* |
| *TFEB* | *CD47* | *CEACAM5* |
| *TMEFF2* | *CD48* | *CENPA* |
| *TPTE* | *CD5* | *CENPE* |
| *TXK* | *CD53* | *CENPF* |
| *UBC* | *CD55* | *CENPH* |
| *ULBP2* | *CD58* | *CENPI* |
| *USP9Y* | *CD59* | *CENPL* |
| *XCL2* | *CD6* | *CENPU* |
| *YTHDF2* | *CD63* | *CENPW* |
| | *CD68* | *CEP250* |
| | *CD7* | *CEP55* |
| | *CD70* | *CES1* |
| | *CD74* | *CGREF1* |
| | *CD79A* | *CHDH* |
| | *CD79B* | *CHGA* |
| | *CD80* | *CHMP4B* |
| | *CD83* | *CHRM2* |
| | *CD84* | *CHRM3* |
| | *CD86* | *CHST10* |
| | *CD8A* | *CIITA* |

| | | |
|---|---|---|
| | *CD8B* | *CIP2A* |
| | *CD96* | *CKAP2* |
| | *CD99* | *CKAP2L* |
| | *CDH1* | *CLCA2* |
| | *CDH5* | *CLDN3* |
| | *CDK1* | *CLEC12A* |
| | *CDKN1A* | *CLEC2B* |
| | *CEACAM1* | *CLEC9A* |
| | *CEACAM6* | *CLSPN* |
| | *CEACAM8* | *CNNM1* |
| | *CEBPB* | *CNTLN* |
| | *CHIT1* | *COCH* |
| | *CHUK* | *COL1A1* |
| | *CKLF* | *COL1A2* |
| | *CLEC4A* | *CORO1A* |
| | *CLEC4C* | *CPA3* |
| | *CLEC5A* | *CPE* |
| | *CLEC6A* | *CRISPLD1* |
| | *CLEC7A* | *CRMP1* |
| | *CMA1* | *CRTAM* |
| | *CMKLR1* | *CSF2RA* |
| | *COL3A1* | *CSK* |
| | *CR1* | *CT45_family* |
| | *CR2* | *CT47_family* |
| | *CREB1* | *CTAG1A_1B* |
| | *CREB5* | *CTAG2* |
| | *CREBBP* | *CTBP1* |
| | *CRP* | *CTNNB1* |
| | *CSF1* | *CTRC* |
| | *CSF1R* | *CXCL8* |
| | *CSF2* | *CYP27A1* |
| | *CSF2RB* | *DAPK2* |
| | *CSF3* | *DAPL1* |
| | *CSF3R* | *DBF4* |

| | | |
|---|---|---|
| | *CTLA4* | *DCLRE1A* |
| | *CTSG* | *DCN* |
| | *CTSH* | *DDIAS* |
| | *CTSL* | *DDX5* |
| | *CTSS* | *DEPDC1* |
| | *CX3CL1* | *DGAT2* |
| | *CX3CR1* | *DGKA* |
| | *CXCL1* | *DHX40* |
| | *CXCL10* | *DIAPH3* |
| | *CXCL11* | *DLAT* |
| | *CXCL12* | *DLD* |
| | *CXCL13* | *DLGAP5* |
| | *CXCL14* | *DLX6* |
| | *CXCL16* | *DNAH14* |
| | *CXCL2* | *DNMT1* |
| | *CXCL3* | *DONSON* |
| | *CXCL5* | *DPYSL4* |
| | *CXCL6* | *DSC3* |
| | *CXCL9* | *DSE* |
| | *CXCR1* | *DSG3* |
| | *CXCR2* | *DST* |
| | *CXCR3* | *DTL* |
| | *CXCR4* | *E2F2* |
| | *CXCR5* | *E2F7* |
| | *CXCR6* | *EBF4* |
| | *CYBB* | *ECT2* |
| | *CYLD* | *EEF1G* |
| | *DDX58* | *EEF2* |
| | *DEFB1* | *EFNA4* |
| | *DMBT1* | *EFNB3* |
| | *DOCK9* | *EGFR* |
| | *DPP4* | *EGR3* |
| | *DUSP4* | *EHD2* |
| | *DUSP6* | *EIF2A* |

| | | |
|---|---|---|
| | *EBI3* | *EIF2AK2* |
| | *EGR1* | *ELL3* |
| | *EGR2* | *EME1* |
| | *ELK1* | *EMP1* |
| | *ENG* | *EMX2* |
| | *ENTPD1* | *ENO1* |
| | *EOMES* | *EPHX3* |
| | *EP300* | *EPSTI1* |
| | *EPCAM* | *ERBB2* |
| | *ETS1* | *ERBB3* |
| | *EWSR1* | *ERCC6L* |
| | *F13A1* | *ESCO2* |
| | *F2RL1* | *ESPL1* |
| | *FADD* | *ESYT2* |
| | *FAS* | *ETS2* |
| | *FCER1G* | *ETV1* |
| | *FCER2* | *ETV4* |
| | *FCGR2B* | *EXO1* |
| | *FEZ1* | *EYS* |
| | *FLT3* | *EZH2* |
| | *FLT3LG* | *FABP4* |
| | *FN1* | *FAM111B* |
| | *FOS* | *FAM122B* |
| | *FOXJ1* | *FAM161A* |
| | *FOXP3* | *FAM222A* |
| | *FPR2* | *FAM69B* |
| | *FUT5* | *FAM72_family* |
| | *FYN* | *FAM83B* |
| | *GATA3* | *FANCA* |
| | *GNLY* | *FANCD2* |
| | *GPI* | *FANCI* |
| | *GTF3C1* | *FAP* |
| | *GZMA* | *FASLG* |
| | *GZMB* | *FBLN1* |

| | | |
|---|---|---|
| | *GZMH* | *FCAR* |
| | *GZMK* | *FCGR1A_FCGR1B* |
| | *GZMM* | *FCGR2A_2C* |
| | *HAVCR2* | *FCGR3A_3B* |
| | *HLA-A* | *FCMR* |
| | *HLA-B* | *FCRL2* |
| | *HLA-C* | *FCRLA* |
| | *HLA-DMA* | *FEN1* |
| | *HLA-DMB* | *FGD6* |
| | *HLA-DOB* | *FGFR3* |
| | *HLA-DPA1* | *FICD* |
| | *HLA-DPB1* | *FLI1* |
| | *HLA-DQA1* | *FLT1* |
| | *HLA-DQB1* | *FLVCR1* |
| | *HLA-DRA* | *FMO5* |
| | *HLA-E* | *FOLH1* |
| | *HLA-G* | *FOXA1* |
| | *HMGB1* | *FOXG1* |
| | *HRAS* | *FOXM1* |
| | *HSD11B1* | *FOXO1* |
| | *ICAM1* | *FOXP1* |
| | *ICAM2* | *FOXRED2* |
| | *ICAM3* | *FPR1* |
| | *ICAM4* | *FRYL* |
| | *ICOS* | *FUT4* |
| | *ICOSLG* | *FXYD5* |
| | *IDO1* | *FYB1* |
| | *IFI16* | *FZD3* |
| | *IFI27* | *G6PD* |
| | *IFI35* | *GABRA5* |
| | *IFIH1* | *GAD1* |
| | *IFIT1* | *GADD45GIP1* |
| | *IFIT2* | *GAGE_family* |
| | *IFITM1* | *GATA2* |

| | | |
|---|---|---|
| | *IFITM2* | *GBP1* |
| | *IFNAR1* | *GBP5* |
| | *IFNAR2* | *GCK* |
| | *IFNB1* | *GCK_liver* |
| | *IFNG* | *GCK_Pan* |
| | *IFNGR1* | *GDF15* |
| | *IFNL1* | *GGT7* |
| | *IFNL2* | *GINS4* |
| | *IGF1R* | *GLB1L2* |
| | *IGF2R* | *GLIPR1* |
| | *IKBKB* | *GPR18* |
| | *IKBKG* | *GPR19* |
| | *IL10* | *GPRIN1* |
| | *IL10RA* | *GRAP2* |
| | *IL11* | *GSDME* |
| | *IL11RA* | *GTSE1* |
| | *IL12A* | *GUSB* |
| | *IL12B* | *H2AFZ* |
| | *IL12RB1* | *HASPIN* |
| | *IL12RB2* | *HCAR1* |
| | *IL13* | *HCAR2* |
| | *IL13RA1* | *HDC* |
| | *IL13RA2* | *HELLS* |
| | *IL15* | *HERC6* |
| | *IL15RA* | *HES1* |
| | *IL16* | *HES5* |
| | *IL17A* | *HEXIM2* |
| | *IL17B* | *HEY1* |
| | *IL17F* | *HEY2* |
| | *IL17RA* | *HEYL* |
| | *IL17RB* | *HGF* |
| | *IL18* | *HHLA2* |
| | *IL18R1* | *HIF1A* |
| | *IL19* | *HIST1H2BH* |

| | | |
|---|---|---|
| | *IL1A* | *HJURP* |
| | *IL1B* | *HK1* |
| | *IL1R1* | *HK2* |
| | *IL1R2* | *HLA-DOA* |
| | *IL1RAP* | *HLA-DQA2* |
| | *IL1RL1* | *HLA-DQB2* |
| | *IL1RL2* | *HLA-DRB1* |
| | *IL1RN* | *HLA-F* |
| | *IL2* | *HLF* |
| | *IL21* | *HMBS* |
| | *IL21R* | *HMGCS2* |
| | *IL22RA1* | *HMMR* |
| | *IL22RA2* | *HMOX1* |
| | *IL23A* | *HMX2* |
| | *IL23R* | *HNF1A* |
| | *IL24* | *HNF1B* |
| | *IL25* | *HORMAD1* |
| | *IL26* | *HORMAD2* |
| | *IL27* | *HPDL* |
| | *IL2RA* | *HPN* |
| | *IL2RB* | *HSP90B1* |
| | *IL2RG* | *HSPA1A* |
| | *IL3* | *IBSP* |
| | *IL32* | *ID2* |
| | *IL34* | *ID3* |
| | *IL3RA* | *ID4* |
| | *IL4* | *IDH1* |
| | *IL4R* | *IDH2* |
| | *IL5* | *IDO2* |
| | *IL5RA* | *IFI44L* |
| | *IL6* | *IFI6* |
| | *IL6R* | *IFIT3* |
| | *IL6ST* | *IFIT5* |
| | *IL7* | *IFITM3* |

| | | |
|---|---|---|
| | *IL7R* | *IFNA_Family* |
| | *IL9* | *IFNL3* |
| | *IRAK1* | *IFNL4* |
| | *IRAK2* | *IFNLR1* |
| | *IRAK4* | *IGFBP3* |
| | *IRF1* | *IGSF6* |
| | *IRF2* | *IHH* |
| | *IRF3* | *IKZF1* |
| | *IRF4* | *IKZF2* |
| | *IRF5* | *IKZF3* |
| | *IRF7* | *IKZF4* |
| | *IRF8* | *IL10RB* |
| | *IRGM* | *IL17C* |
| | *ISG15* | *IL17D* |
| | *ISG20* | *IL18BP* |
| | *ITGA1* | *IL20* |
| | *ITGA2* | *IL20RA* |
| | *ITGA4* | *IL20RB* |
| | *ITGA5* | *IL31* |
| | *ITGA6* | *IL33* |
| | *ITGAE* | *IL9R* |
| | *ITGAL* | *IMPG2* |
| | *ITGAM* | *INSM1* |
| | *ITGAX* | *IQGAP3* |
| | *ITGB1* | *IRAK3* |
| | *ITGB2* | *IRF9* |
| | *ITGB3* | *IRS1* |
| | *ITGB4* | *ITGA3* |
| | *ITK* | *ITGB7* |
| | *JAK1* | *ITLN2* |
| | *JAK2* | *ITPKC* |
| | *JAK3* | *JAKMIP3* |
| | *KIR3DL1* | *JAML* |
| | *KIR3DL2* | *JCHAIN* |

| | | |
|---|---|---|
| | *KIR3DL3* | *KCNA1* |
| | *KIT* | *KCNH2* |
| | *KLRB1* | *KCNK5* |
| | *KLRD1* | *KDM5B* |
| | *KLRF1* | *KDR* |
| | *KLRG1* | *KHDRBS2* |
| | *KLRK1* | *KHK* |
| | *LAG3* | *KIF14* |
| | *LAIR2* | *KIF15* |
| | *LAMP1* | *KIF18B* |
| | *LAMP3* | *KIF20A* |
| | *LCK* | *KIF23* |
| | *LCN2* | *KIF2C* |
| | *LCP1* | *KIF4A* |
| | *LGALS3* | *KIF5C* |
| | *LIF* | *KIFC1* |
| | *LILRA4* | *KIR2DL1* |
| | *LILRB1* | *KIR2DL1_2DL2* |
| | *LILRB2* | *KIR2DL3* |
| | *LRP1* | *KIR2DL4* |
| | *LTA* | *KIR2DL5A_5B* |
| | *LTB* | *KIR2DS2_2DS4* |
| | *LTBR* | *KIR2DS4* |
| | *LTK* | *KIR2DSx* |
| | *LY86* | *KIR3DS1* |
| | *LY9* | *KIR-panL* |
| | *LY96* | *KIR-panS* |
| | *LYN* | *KLF2* |
| | *MAF* | *KLHDC9* |
| | *MAGEA1* | *KNL1* |
| | *MAGEA12* | *KPNA2* |
| | *MAGEA4* | *KREMEN1* |
| | *MAGEB2* | *KRT13* |
| | *MAGEC1* | *KRT16* |

| | | |
|---|---|---|
| | *MAGEC2* | *KRT17* |
| | *MAP2K1* | *KRT18* |
| | *MAP2K2* | *KRT19* |
| | *MAP2K4* | *KRT34* |
| | *MAP3K1* | *KRT5* |
| | *MAP3K5* | *KRT6A* |
| | *MAP3K7* | *KRT7* |
| | *MAPK1* | *KRT8* |
| | *MAPK11* | *KRTCAP3* |
| | *MAPK14* | *KSR2* |
| | *MAPK3* | *L1CAM* |
| | *MAPK8* | *LAMC3* |
| | *MAPKAPK2* | *LAPTM5* |
| | *MARCO* | *LAT* |
| | *MBL2* | *LEXM* |
| | *MEF2C* | *LGALS1* |
| | *MERTK* | *LGALS9* |
| | *MICA* | *LGSN* |
| | *MICB* | *LIMA1* |
| | *MIF* | *LIPE* |
| | *MME* | *LMNA* |
| | *MPPED1* | *LMNB1* |
| | *MR1* | *LOXL1* |
| | *MRC1* | *LOXL2* |
| | *MS4A1* | *LRBA* |
| | *MS4A2* | *LRG1* |
| | *MSR1* | *LST1* |
| | *MST1R* | *LTB4R* |
| | *MUC1* | *LTBP1* |
| | *MX1* | *LYVE1* |
| | *MYD88* | *LYZ* |
| | *NCAM1* | *M6PR* |
| | *NCR1* | *MAB21L2* |
| | *NEFL* | *MAD2L1* |

| | | |
|---|---|---|
| | *NFATC1* | *MADCAM1* |
| | *NFATC3* | *MAGEA10* |
| | *NFATC4* | *MAGEA3_A6* |
| | *NFKB1* | *MAP2K6* |
| | *NFKB2* | *MAP2K7* |
| | *NFKBIA* | *MAP4* |
| | *NLRC5* | *MAP4K1* |
| | *NLRP3* | *MCM10* |
| | *NOD1* | *MCM2* |
| | *NOD2* | *MCM6* |
| | *NOTCH1* | *MCM7* |
| | *NRP1* | *MECOM* |
| | *NT5E* | *MELK* |
| | *NUP107* | *MGA* |
| | *OAS3* | *MKI67* |
| | *OSM* | *MLANA* |
| | *PAX5* | *MLF1* |
| | *PBK* | *MMP11* |
| | *PDCD1* | *MMP12* |
| | *PDCD1LG2* | *MMP2* |
| | *PDGFC* | *MMP9* |
| | *PDGFRB* | *MND1* |
| | *PECAM1* | *MNDA* |
| | *PIK3CD* | *MOB3A* |
| | *PIK3CG* | *MPO* |
| | *PLA2G6* | *MRAP2* |
| | *PLAU* | *MS4A4A* |
| | *PLAUR* | *MSH2* |
| | *PMCH* | *MSH3* |
| | *POU2AF1* | *MSH4* |
| | *POU2F2* | *MSH5* |
| | *PPARG* | *MSH6* |
| | *PPBP* | *MT2A* |
| | *PRAME* | *MTDH* |

| | | |
|---|---|---|
| | *PRF1* | *MTFR2* |
| | *PRG2* | *MTOR* |
| | *PRKCD* | *MXD3* |
| | *PRKCE* | *MYBL2* |
| | *PSEN1* | *MYC* |
| | *PSEN2* | *MYH10* |
| | *PSMB10* | *MYH11* |
| | *PSMB7* | *MYH9* |
| | *PSMB8* | *MYO1B* |
| | *PSMB9* | *MYO5C* |
| | *PSMD7* | *MYOCD* |
| | *PTGDR2* | *MYOF* |
| | *PTGS2* | *NCAPG* |
| | *PTPRC* | *NCAPG2* |
| | *PVR* | *NCAPH* |
| | *PYCARD* | *NCF1* |
| | *RAG1* | *NCK1* |
| | *REL* | *NCL* |
| | *RELA* | *NCR3* |
| | *RELB* | *NCR3LG1* |
| | *REPS1* | *NDC1* |
| | *RIPK2* | *NDC80* |
| | *RORC* | *NECTIN2* |
| | *RPS6* | *NEIL3* |
| | *RRAD* | *NEK2* |
| | *RUNX1* | *NGFR* |
| | *RUNX3* | *NKG7* |
| | *S100A12* | *NKX2-1* |
| | *S100A8* | *NMRAL1* |
| | *S100B* | *NOS2* |
| | *SELE* | *NOS3* |
| | *SELL* | *NOTCH3* |
| | *SELPLG* | *NOX1* |
| | *SERPINB2* | *NPM1* |

| | | |
|---|---|---|
| | *SH2D1A* | *NPR3* |
| | *SH2D1B* | *NRL* |
| | *SIGIRR* | *NTN3* |
| | *SLAMF1* | *NTRK2* |
| | *SLAMF6* | *NUDT1* |
| | *SLAMF7* | *NUF2* |
| | *SLC11A1* | *NUSAP1* |
| | *SMAD2* | *OAS1* |
| | *SMAD3* | *OAS2* |
| | *SMPD3* | *OAZ1* |
| | *SOCS1* | *OCLN* |
| | *SPANXB1* | *OIP5* |
| | *SPINK5* | *OLR1* |
| | *SPN* | *OPTN* |
| | *SPP1* | *ORC1* |
| | *SSX1* | *ORC6* |
| | *ST6GAL1* | *PAGE1* |
| | *STAT1* | *PAGE2_PAGE5* |
| | *STAT2* | *PAGE3* |
| | *STAT3* | *PAGE4* |
| | *STAT4* | *PAGE5* |
| | *STAT5B* | *PATZ1* |
| | *STAT6* | *PBX1* |
| | *SYCP1* | *PCLAF* |
| | *SYK* | *PCNA* |
| | *SYT17* | *PDHA1* |
| | *TAB1* | *PDHA2* |
| | *TAL1* | *PDHB* |
| | *TAP1* | *PDHX* |
| | *TAP2* | *PDK1* |
| | *TAPBP* | *PDK2* |
| | *TARP* | *PDK3* |
| | *TBK1* | *PDK4* |
| | *TBX21* | *PDLIM1* |

| | | |
|---|---|---|
| | *TCF7* | *PDLIM3* |
| | *TFRC* | *PDP1* |
| | *TGFB1* | *PF4* |
| | *TGFB2* | *PFKFB3* |
| | *THBD* | *PFKFB4* |
| | *THBS1* | *PGF* |
| | *THY1* | *PHF10* |
| | *TICAM1* | *PIF1* |
| | *TICAM2* | *PIK3CA* |
| | *TIGIT* | *PIMREG* |
| | *TIRAP* | *PKLR* |
| | *TLR1* | *PKM* |
| | *TLR10* | *PKMYT1* |
| | *TLR2* | *PKP1* |
| | *TLR3* | *PLA2G7* |
| | *TLR4* | *PLEKHG4* |
| | *TLR5* | *PLEKHG6* |
| | *TLR6* | *PLK1* |
| | *TLR7* | *PLK4* |
| | *TLR8* | *PMEL* |
| | *TLR9* | *PML* |
| | *TNF* | *PNOC* |
| | *TNFAIP3* | *POC1A* |
| | *TNFRSF10B* | *PODXL2* |
| | *TNFRSF10C* | *POLQ* |
| | *TNFRSF11A* | *POLR2A* |
| | *TNFRSF11B* | *POU5F1_1B* |
| | *TNFRSF12A* | *PPARD* |
| | *TNFRSF13B* | *PPIA* |
| | *TNFRSF13C* | *PPM1E* |
| | *TNFRSF14* | *PRC1* |
| | *TNFRSF17* | *PRDM1* |
| | *TNFRSF18* | *PRDM6* |
| | *TNFRSF1A* | *PRR11* |

| | | |
|---|---|---|
| | *TNFRSF1B* | *PRR15L* |
| | *TNFRSF4* | *PSMB5* |
| | *TNFRSF8* | *PSMB6* |
| | *TNFRSF9* | *PSRC1* |
| | *TNFSF10* | *PTEN* |
| | *TNFSF11* | *PTGER1* |
| | *TNFSF12* | *PTGER2* |
| | *TNFSF13* | *PTGER3* |
| | *TNFSF13B* | *PTGER4* |
| | *TNFSF14* | *PTGS1* |
| | *TNFSF15* | *PTK7* |
| | *TNFSF18* | *PTPN11* |
| | *TNFSF4* | *PTPN6* |
| | *TNFSF8* | *PTPN7* |
| | *TOLLIP* | *PTPRCAP* |
| | *TP53* | *PVT1* |
| | *TPSAB1* | *PXYLP1* |
| | *TRAF2* | *PYCR1* |
| | *TRAF3* | *PYGL* |
| | *TRAF6* | *RAC1* |
| | *TREM1* | *RACGAP1* |
| | *TREM2* | *RAD51* |
| | *TTK* | *RAD51AP1* |
| | *TXNIP* | *RAD54L* |
| | *TYK2* | *RB1* |
| | *VCAM1* | *RBM24* |
| | *VEGFA* | *RBX1* |
| | *VEGFC* | *RDM1* |
| | *XCR1* | *REV3L* |
| | *ZAP70* | *RFC4* |
| | *ZNF205* | *RGS20* |
| | | *RHOG* |
| | | *RIC8A* |
| | | *RMI2* |

| | | |
|---|---|---|
| | | *RNASEH2A* |
| | | *RND2* |
| | | *RNF149* |
| | | *RNF4* |
| | | *RNFT2* |
| | | *ROR2* |
| | | *RPL38* |
| | | *RPL6* |
| | | *RPS19* |
| | | *RPS7* |
| | | *RPSA* |
| | | *RRAS2* |
| | | *RRM1* |
| | | *RRM2* |
| | | *RTN1* |
| | | *S100A9* |
| | | *SALL2* |
| | | *SAMD12* |
| | | *SAMD9* |
| | | *SAMHD1* |
| | | *SCAMP5* |
| | | *SCG3* |
| | | *SDHA* |
| | | *SEMA4D* |
| | | *SERINC2* |
| | | *SERPINA1* |
| | | *SERPINB5* |
| | | *SERPINB7* |
| | | *SERPINE1* |
| | | *SGO1* |
| | | *SGO2* |
| | | *SHCBP1* |
| | | *SIGLEC5* |
| | | *SIT1* |

| | | |
|---|---|---|
| | | *SKA1* |
| | | *SKA3* |
| | | *SKAP2* |
| | | *SKP2* |
| | | *SLAMF8* |
| | | *SLC25A3* |
| | | *SLC25A5-AS1* |
| | | *SLC27A2* |
| | | *SLC2A1* |
| | | *SLC31A2* |
| | | *SLC35B1* |
| | | *SLFN11* |
| | | *SMAD7* |
| | | *SMPDL3B* |
| | | *SNAI1* |
| | | *SNAI2* |
| | | *SOCS3* |
| | | *SOCS5* |
| | | *SOD1* |
| | | *SOX2* |
| | | *SOX9* |
| | | *SP100* |
| | | *SP110* |
| | | *SPANXACD* |
| | | *SPANXN1* |
| | | *SPANXN3* |
| | | *SPANXN4* |
| | | *SPANXN5* |
| | | *SPC24* |
| | | *SPC25* |
| | | *SPDL1* |
| | | *SPI1* |
| | | *SPIB* |
| | | *SPIN4* |

| | | |
|---|---|---|
| | | *SPINK1* |
| | | *SPOP* |
| | | *SPTLC3* |
| | | *SRGN* |
| | | *SSX2_2B* |
| | | *STAT5A* |
| | | *STIL* |
| | | *STK32A* |
| | | *STOX2* |
| | | *SUSD3* |
| | | *SUZ12* |
| | | *SV2A* |
| | | *SVIL* |
| | | *SYT4* |
| | | *TACC3* |
| | | *TACSTD2* |
| | | *TAGAP* |
| | | *TAGLN* |
| | | *TAGLN3* |
| | | *TCF12* |
| | | *TCF19* |
| | | *TCL1A* |
| | | *TCL1B* |
| | | *TDO2* |
| | | *TEDC2* |
| | | *TEK* |
| | | *TESC* |
| | | *TEX14* |
| | | *TFF1* |
| | | *TGFBI* |
| | | *TGFBR1* |
| | | *TGFBR2* |
| | | *TGIF2* |
| | | *THAP11* |

| | | |
|---|---|---|
| | | *TIMP1* |
| | | *TK1* |
| | | *TLDC1* |
| | | *TMBIM1* |
| | | *TMEM173* |
| | | *TMEM246* |
| | | *TMPO* |
| | | *TNFAIP8* |
| | | *TNFRSF10A* |
| | | *TNFRSF10D* |
| | | *TNFRSF19* |
| | | *TNFRSF21* |
| | | *TNFRSF25* |
| | | *TNFSF9* |
| | | *TOP2A* |
| | | *TP63* |
| | | *TPX2* |
| | | *TRABD2A* |
| | | *TRAP1* |
| | | *TRAT1* |
| | | *TRIM21* |
| | | *TRIM22* |
| | | *TRIM29* |
| | | *TRIM59* |
| | | *TRIP13* |
| | | *TROAP* |
| | | *TSG101* |
| | | *TUBB* |
| | | *TWIST1* |
| | | *TWIST2* |
| | | *TXLNA* |
| | | *TYMS* |
| | | *TYROBP* |
| | | *UBA6* |

| | | |
|---|---|---|
| | | *UBE2C* |
| | | *UBE2T* |
| | | *UBE3A* |
| | | *UHRF1* |
| | | *ULBP1* |
| | | *UNC5D* |
| | | *UPK2* |
| | | *UPK3A* |
| | | *VAV1* |
| | | *VSIR* |
| | | *VSNL1* |
| | | *VTCN1* |
| | | *VWDE* |
| | | *VWF* |
| | | *WARS* |
| | | *WASHC4* |
| | | *WDHD1* |
| | | *WDR60* |
| | | *WDR76* |
| | | *WNK2* |
| | | *WNT5A* |
| | | *WNT7B* |
| | | *XAF1* |
| | | *XAGE1B_1E* |
| | | *XAGE2* |
| | | *XAGE3* |
| | | *XAGE5* |
| | | *XCL1* |
| | | *XCL1_XCL2* |
| | | *YWHAZ* |
| | | *ZBTB46* |
| | | *ZEB1* |
| | | *ZIC5* |
| | | *ZNF14* |

| | | |
|---|---|---|
| | | *ZNF74* |
| | | *ZWILCH* |
| | | *ZYX* |

**Table 34: Differentially expressed genes between FLneg$^{m}$ and FLneg$^{wt}$ using HTG technology**
Genes with FC +/- 1.5, p-adj. ≤ 0.05 were considered as significant. 40 DEGs were identified

| Genes | log2FoldChange | Fold Change | padj |
|---|---|---|---|
| *FCER2* | 2.310822977 | 5.0 | 0.00 |
| *IL4R* | 1.618089627 | 3.1 | 0.00 |
| *CCL17* | 1.160086305 | 2.2 | 0.05 |
| *CD83* | 1.150176513 | 2.2 | 0.00 |
| *ALOX5* | 1.087141431 | 2.1 | 0.00 |
| *IL17RB* | 1.036229768 | 2.1 | 0.04 |
| *MME* | 1.028606315 | 2.0 | 0.01 |
| *ELL3* | 0.998817017 | 2.0 | 0.03 |
| *CD40* | 0.94512678 | 1.9 | 0.00 |
| *GPR18* | 0.93243143 | 1.9 | 0.00 |
| *NCF1* | 0.927937872 | 1.9 | 0.03 |
| *CD22* | 0.888839956 | 1.9 | 0.01 |
| *MS4A1* | 0.858704053 | 1.8 | 0.03 |
| *HLA-DOB* | 0.828739579 | 1.8 | 0.01 |
| *CD180* | 0.824001375 | 1.8 | 0.01 |
| *CIITA* | 0.794765932 | 1.7 | 0.01 |
| *LTB* | 0.734671166 | 1.7 | 0.04 |
| *HLA-DMB* | 0.727434439 | 1.7 | 0.02 |
| *CLEC4A* | 0.716367751 | 1.6 | 0.00 |
| *PIK3CG* | 0.67362849 | 1.6 | 0.01 |
| *SELL* | 0.670650995 | 1.6 | 0.03 |
| *PAX5* | 0.641313364 | 1.6 | 0.03 |
| *TNFRSF17* | 0.626577245 | 1.5 | 0.03 |
| *IL13RA1* | 0.573361633 | 1.5 | 0.03 |
| *WASHC4* | 0.570023354 | 1.5 | 0.02 |
| *CCDC138* | 0.569599659 | 1.5 | 0.03 |
| *ENTPD1* | -0.590407972 | -1.5 | 0.04 |
| *CCL4* | -0.692930078 | -1.6 | 0.01 |
| *FCGR3A_3B* | -0.702175704 | -1.6 | 0.02 |
| *S100A8* | -0.734991285 | -1.7 | 0.03 |
| *LAG3* | -0.774113586 | -1.7 | 0.02 |
| *IRF4* | -0.776111375 | -1.7 | 0.04 |
| *MNDA* | -0.815157675 | -1.8 | 0.00 |
| *FCGR1A_FCGR1B* | -0.872795331 | -1.8 | 0.04 |
| *CXCL10* | -0.930667302 | -1.9 | 0.04 |
| *C1QB* | -0.977362395 | -2.0 | 0.03 |
| *FCGR2B* | -1.048768946 | -2.1 | 0.00 |
| *TNFRSF13B* | -1.151701649 | -2.2 | 0.00 |
| *FCRLA* | -1.194851168 | -2.3 | 0.01 |
| *SLAMF7* | -1.564909571 | -3.0 | 0.00 |

**Table 35: Differentially expressed genes between FLneg$^{m}$ and FLneg$^{wt}$ using NanoString technology**
Genes with FC +/- 1.5, p-adj. < 0.05. were considered as significant. 71 DEGs were identified

| Genes | log2FoldChange | Fold Change | padj |
|---|---|---|---|
| *LTF* | 2.325482526 | 5.01 | 0.00 |
| *FCER2* | 2.1901257 | 4.56 | 0.00 |
| *CCL17* | 2.13668735 | 4.40 | 0.00 |
| *IL17RB* | 1.814213163 | 3.52 | 0.00 |
| *IL4R* | 1.61043966 | 3.05 | 0.00 |
| *MME* | 1.287332902 | 2.44 | 0.00 |
| *LY86* | 1.201558605 | 2.30 | 0.00 |
| *C3* | 1.094035611 | 2.13 | 0.01 |
| *TNFRSF17* | 0.991052044 | 1.99 | 0.00 |
| *CLEC4A* | 0.990664851 | 1.99 | 0.00 |
| *SYT17* | 0.962455633 | 1.95 | 0.04 |
| *LILRB1* | 0.935907402 | 1.91 | 0.00 |
| *HLA-DOB* | 0.919487243 | 1.89 | 0.00 |
| *IL3RA* | 0.884762418 | 1.85 | 0.02 |
| *CD83* | 0.84292592 | 1.79 | 0.01 |
| *CD180* | 0.817719953 | 1.76 | 0.00 |
| *S100B* | 0.777798566 | 1.71 | 0.03 |
| *CD40* | 0.759401837 | 1.69 | 0.00 |
| *IRAK2* | 0.747722617 | 1.68 | 0.01 |
| *THY1* | 0.743836613 | 1.67 | 0.00 |
| *SELL* | 0.695416881 | 1.62 | 0.00 |
| *SH2B2* | 0.692557486 | 1.62 | 0.00 |
| *MEF2C* | 0.691637732 | 1.62 | 0.02 |
| *CD9* | 0.642805166 | 1.56 | 0.03 |
| *IRF8* | 0.595356731 | 1.51 | 0.02 |
| *CCL19* | 0.593118705 | 1.51 | 0.04 |
| *HLA-DMB* | 0.587736552 | 1.50 | 0.00 |
| *MAP2K1* | 0.570931394 | 1.49 | 0.00 |
| *IL13RA1* | 0.546146852 | 1.46 | 0.00 |
| *NLRC5* | -0.539110416 | -1.45 | 0.00 |
| *CCRL2* | -0.549993763 | -1.46 | 0.01 |
| *CD274* | -0.567411141 | -1.48 | 0.00 |
| *C4B* | -0.582776221 | -1.50 | 0.05 |
| *CXCR3* | -0.599385974 | -1.52 | 0.01 |
| *CSF3R* | -0.609329427 | -1.53 | 0.04 |
| *CCL5* | -0.611667247 | -1.53 | 0.04 |
| *GATA3* | -0.638136629 | -1.56 | 0.03 |
| *SLAMF7* | -0.667124767 | -1.59 | 0.02 |
| *ISG15* | -0.681383691 | -1.60 | 0.03 |
| *GZMK* | -0.690150988 | -1.61 | 0.04 |
| *CXCR6* | -0.714938841 | -1.64 | 0.02 |
| *PRF1* | -0.742602091 | -1.67 | 0.01 |
| *CCR1* | -0.754161683 | -1.69 | 0.03 |
| *CCL3* | -0.757253129 | -1.69 | 0.00 |
| *DUSP4* | -0.767775682 | -1.70 | 0.01 |
| *FCER1G* | -0.783731387 | -1.72 | 0.00 |
| *EOMES* | -0.831593118 | -1.78 | 0.02 |
| *HCK* | -0.848289401 | -1.80 | 0.00 |
| *CCR5* | -0.860322034 | -1.82 | 0.01 |
| *CD70* | -0.867609976 | -1.82 | 0.02 |
| *IL10* | -0.872422424 | -1.83 | 0.00 |
| *CD1D* | -0.875718774 | -1.83 | 0.02 |
| *ENTPD1* | -0.904062034 | -1.87 | 0.00 |
| *HSD11B1* | -0.917879318 | -1.89 | 0.03 |
| *EBI3* | -0.983695898 | -1.98 | 0.01 |
| *GZMH* | -0.987889409 | -1.98 | 0.02 |
| *IRF4* | -0.997940713 | -2.00 | 0.00 |
| *LAG3* | -1.050032262 | -2.07 | 0.00 |
| *ITGB4* | -1.053147497 | -2.08 | 0.01 |
| *IL12A* | -1.056530982 | -2.08 | 0.00 |
| *TBX21* | -1.103486421 | -2.15 | 0.00 |
| *C1QA* | -1.146900989 | -2.21 | 0.00 |
| *IL1R2* | -1.14842642 | -2.22 | 0.01 |
| *CXCL10* | -1.155547626 | -2.23 | 0.04 |
| *CXCL11* | -1.160419162 | -2.24 | 0.03 |
| *LILRB3* | -1.332241473 | -2.52 | 0.02 |
| *IFNG* | -1.335610641 | -2.52 | 0.00 |
| *C1QB* | -1.393575455 | -2.63 | 0.00 |
| *TNFRSF13B* | -1.580013084 | -2.99 | 0.00 |
| *SLC11A1* | -1.604288783 | -3.04 | 0.03 |
| *FCGR3A* | -1.832328349 | -3.56 | 0.00 |
| *FCGR2B* | -1.881363425 | -3.68 | 0.00 |
| *CHIT1* | -2.696025991 | -6.48 | 0.00 |
| *CEACAM6* | -2.914701569 | -7.54 | 0.00 |